

Conceptual Design of the agri-PV demonstrators



Horizon Europe EU project
Grant Agreement No. 101096352



Views and opinions expressed are however those of the author(s) only and do not necessarily reflect those of the European Union or CINEA. Neither the European Union nor the granting authority can be held responsible for them.

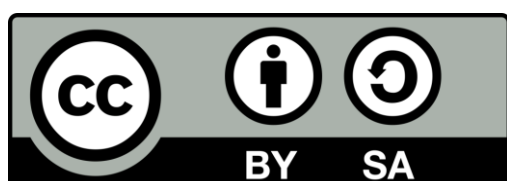
Document control sheet

Project SYMBIOSYST – Create a Symbiosis where PV and agriculture can have a mutually beneficial relationship

Topic identifier	HORIZON-CL5-2022-D3-01-06
Grant Agreement N°	101096352
Coordinator	ACCADEMIA EUROPEA DI BOLZANO (EURAC)
Duration	01/01/2023 – 31/12/2026
Work package N°	WP5
Work package title	Demonstration of novel agri-PV solutions
Work package leader	EF SOLARE ITALIA
Task n°	5.2
Task leader	LUCISUN
Document title	Conceptual Design of the agri-PV demonstrators
Lead Beneficiary	LUCISUN
Dissemination level	PUBLIC
Authors	S Prithivi Rajan, Jesus Robledo, Jonathan Leloux, Christian A. Gueymard, Angelo Pignatelli, Giovanni Borz, David Moser, Ismail Kaaya, Shu-Ngwa Asaa, Alexandros Katsikogiannis, Martin Thalheimer, Walter Guerra, Marcel Macarulla, Irma Roig, Gil Gorchs, Niels Groen, James MacDonald, Giuseppe Demofonti, Cinja Seick, Giacomo Bosco
Contributors	
Reviewer(s)	David Moser, Angelo Pignatelli, Jonathan Leloux
Issue date	13/02/2024

History of versions

Version	Date	Author - Beneficiary	Comments
V1.0	13/02/2024	Jonathan Leloux - LuciSun	Final Draft
V2.0	13/02/2024	David Moser - Eurac	Final review



This work is licensed under a Creative Common Attribution-ShareAlike 4.0 International License (CC BY-SA 4.0)

Acknowledgements

The work described in this publication has received funding from the European Union Horizon Europe research and innovation programme under grant agreement N° 101096352.

Disclaimer

This document reflects only the authors' view and not those of the European Commission or CINEA. This work may rely on data from sources external to the members of the SYMBIOSYST project Consortium. Members of the Consortium do not accept liability for loss or damage suffered by any third party as a result of errors or inaccuracies in such data. The information in this document is provided "as is" and no guarantee or warranty is given that the information is fit for any particular purpose. The user there of uses the information at its sole risk and neither the European Commission, CINEA nor any member of the SYMBIOSYST Consortium is liable for any use that may be made of the information.

Executive Summary

The SYMBIOSYST project, supported by the EC Horizon Europe Programme, aims to bridge the gap between solar energy production and agriculture by developing tailored photovoltaic (PV) solutions for both greenhouse and open-field agriculture across diverse climatic conditions in three nations. The initiative includes the creation of several agri-PV demonstrators, encompassing scenarios from vegetable farming under adjustable tracking systems to fruit cultivation with traditional and Guyot training systems. An initial task was the development of technical specifications to serve as a comprehensive guide for these demonstrators, highlighting innovations in PV module integration, environmental considerations like anti-ice features and rainwater harvesting, and monitoring systems.

Early efforts in specifying the demonstrators leveraged advanced modelling tools developed within the project, facilitating the seamless integration of photovoltaic systems into agricultural settings for mutual benefit. This involved the use of 3D simulation tools for detailed analysis of PV layout spatial arrangements, crop configurations, and support infrastructures. Techniques such as ray tracing and GPU-based 3D simulations were employed for a temporal analysis of light distribution over crops and PV modules, aiming to evaluate bifacial gains, shading impacts, and overall system efficiency comprehensively. The modelling covered both open agri-PV systems for crop and fruit production and closed systems for greenhouse agriculture, focusing on optimizing PV array placement and height on both fixed and tracker systems to encourage optimal crop growth alongside efficient energy production, and adapting PV module integration for both new and existing agricultural frameworks.

This work sets out to create a cohesive relationship between solar energy and agricultural processes, aiming to develop a model for sustainable, nearly zero-energy agricultural systems through the strategic development and demonstration of innovative PV solutions adapted to various agricultural environments. The approach involves detailed modelling to inform the design of agrivoltaic systems that are effective in diverse agricultural settings. Through analysing light distribution, crop shading, and energy efficiency, the project guides the creation of PV solutions aimed at boosting crop yields while maximizing renewable energy production. The goal is to foster sustainable, energy-efficient agricultural practices through precise design and modelling efforts.

The project's scientific contribution lies in its novel modelling and design approach to agrivoltaic systems, ensuring optimal solar photovoltaic integration with a range of agricultural practices. By employing comprehensive 3D simulations, ray tracing, and environmental analyses to maximize solar energy capture and enhance crop production, the project addresses key sustainability challenges, offering scalable energy-efficient agricultural solutions.

Preliminary results from the SYMBIOSYST project underscore the effectiveness of combining photovoltaic systems with agricultural practices. Through advanced modelling and simulation, increases in crop yields and enhanced renewable energy generation were observed. The project successfully identified optimal configurations for agrivoltaic systems across different agricultural scenarios, showcasing significant strides in energy efficiency and sustainability. These findings provide a scalable model for sustainable energy and farming practices, contributing to the advancement of renewable energy and agricultural technology sectors.

In essence, the SYMBIOSYST project undertakes a detailed exploration of integrating solar energy production with agricultural practices, through innovative modelling and design. The initiative's focus on optimizing agrivoltaic systems has revealed the potential to improve crop yields and solar energy efficiency, offering a model for sustainable agricultural and energy solutions on a global scale.

Table of Contents

Document control sheet	2
Acknowledgements	3
Disclaimer	3
Executive Summary	4
Table of Contents	5
1. INTRODUCTION	6
1.1. DESCRIPTION OF THE DELIVERABLE CONTENTS	6
1.2. ABBREVIATION LIST	7
2. AGRIVOLTAIC DEMONSTRATOR 1 - BOLZANO	8
2.1. TECHNICAL SPECIFICATIONS	8
2.2. MODELLING	16
2.2.1. OVERVIEW	16
2.2.2. MODELLING BY LUCISUN	16
2.2.3. MODELLING BY IMEC	39
2.2.4. MODELLING BY DELFT UNIVERSITY OF TECHNOLOGY (TU DELFT)	48
2.3. CONCLUSION AND DISCUSSION	53
3. AGRIVOLTAIC DEMONSTRATOR 2 – BARCELONA	54
3.1. TECHNICAL SPECIFICATIONS	54
3.2. MODELLING BY LUCISUN	55
3.3. CONCLUSION AND DISCUSSION	93
4. AGRIVOLTAIC DEMONSTRATOR 3 - NETHERLANDS	94
4.1. TECHNICAL SPECIFICATIONS	94
4.2. CONCLUSION AND DISCUSSION	102
5. AGRIVOLTAIC DEMONSTRATOR 4 - SCALEA	103
5.1. TECHNICAL SPECIFICATIONS	103
5.2. CONCLUSION AND DISCUSSION	110
6. REFERENCES	111

1. INTRODUCTION

1.1. DESCRIPTION OF THE DELIVERABLE CONTENTS

SYMBIOSYST covers both open and closed agri-PV. The focus of the project is on specific archetypes depending on the level of integration:

- For open agri-PV, solutions are developed to bring an increase in PV-crop synergies and optimise yield with a targeted electricity production. The selected demo sites are designed to demonstrate the difference between working on new (where the design of PV and crops can be fully integrated together with auxiliary systems such as irrigation, water catchment, crop protection, etc) or existing crops (where compromises and adaptation will be needed).
- For closed agri-PV, similarly, solutions are studied to be fully integrated in new greenhouses (the greenhouses structure can be modified to accommodate standard size PV modules) or adapted for existing greenhouses. The aim is to drive the development towards nearly zero energy greenhouses.

In SYMBIOSYST, the analysed scenarios for demonstration are:

Open agri-PV Scenario, for:

- Production of vegetables or horticultural crops characterized by a limited vertical development. The height of the tracker system in horizontal configuration needs to consider optimised crop yield, prevent human injury, and ensure free movement of semi-automatic agricultural devices. The ideal height is 3.5 m for different herbaceous crops (e.g., trellised tomatoes) and tall equipment. A lower height of 2-2.5 m will allow for low herbaceous crops (e.g., lettuce, beans, etc.) and low height equipment.
- Production of fruit trees (apples, pears, citrons, lemons, ...) in a "Classic" configuration: tree growth in a 3D configuration, maximum height < 4 m, inter-row spacing of about 3.00 - 3.50 m.
- Apple production according to a "Guyot" system: tree growth in a 2D configuration, maximum height < 3.5 m, inter-row spacing < 2.5 m. This system is also of interest for grape production.

Closed agri-PV Scenario, for:

- Production of vegetables or horticultural crops in Venlo type greenhouses which are used for crops like tomatoes, cucumbers, peppers, but also for cut flowers like roses and many others and pot plants. These are characterized by glass spans of 3.2 m and gutter heights about 4-6 m to accommodate for high wire planting system, thermal screens, and supplementary lighting.

The scope of this deliverable is to report the status of the Technical Specification and the Conceptual Design of the agri-PV demonstrators after 1 year of project implementation.

The deliverable contains details on the process for the definition of the draft Technical Specifications for the demos yet to be built:

- Bolzano, Italy. Open agri-PV. Apple tree orchards.
- Barcelona, Spain. Open agri-PV. Tomatoes, onions, fava beans, lettuce.
- Netherlands. Closed agri-PV. Greenhouse. Tomatoes.

For the demos yet to be built, each section reports on the results of the tools developed in WP2 and applied on the demonstrators.

The deliverable also contains the Technical Specification of one existing Demo site, also used as demo driver:

- Scalea, Italy. Open agri-PV. Citrus fruits.

In this report the Technical Specification and the Conceptual Design of the agri-PV demonstrators are defined by reporting on the results of the tools developed in WP2 and applied on the demonstrators.

1.2. ABBREVIATION LIST

Table 1: Abbreviation list.

Abbreviation	Meaning
1P	PV layout with 1 row of PV modules installed in Portrait mode
AC	Alternating current
Agri-PV/ AV	Agrivoltaics
BEG	Bifacial energy gain
DC	Direct current
DHI	Diffused horizontal irradiance
DLI	Daily light integral
DNI	Direct normal irradiance
E-W	East-West
EOT	Electrical, optical and thermal
FS	Full sun
G_{AV}	Global irradiance for the agrivoltaic system
GCR	Ground cover ratio
GHI	Global horizontal irradiance
GPU	Graphics Processing Unit
G_{ref}	Global irradiance for the reference system
GTI	Global tilted irradiance
HSAT	Horizontal Single-Axis Tracker
kWh/m^2	Kilowatt-hour per square metre
MWh/m^2	Megawatt-hour per square metre
N-S	North-South
PAR	Photosynthetically active radiation
POA	Plane of array
PV	Photovoltaics
T_a	Air temperature
W/m^2	Watts per meter square
Wp	Watt peak
W_s	Wind speed

2. AGRIVOLTAIC DEMONSTRATOR 1 - BOLZANO

2.1. TECHNICAL SPECIFICATIONS

Table 2 describes the envisioned features of the demo of Bolzano and the updates in terms of Technical Specifications at M12 of the project.

Table 2: Envisioned features of the demo of Bolzano and the updates in terms of Technical Specifications at M12 of the project.

Use case 1	Bolzano orchard of the future
Unique Value Proposition	Solution for the Apple Orchard of the future that can integrate irrigation, antifreeze, hail and insect protection, resistant to chemical products keeping the height < 3.5 m for 2D plant growth. Trackers will be installed every other row.
Location	<p>Province of South Tyrol</p> <p>Update M12: The coordinates where the prototype will be located are as follows (nearby the existing demo driver):</p> <ul style="list-style-type: none"> • 46°20'38.94"N; 11°16'40.82"E; 
Replication potential	70 ha of Guyot apple tree, 600 ha/y of renewed apple fields in South Tyrol that could be converted to 2D plant growth. Application extended to any type of guyot cultivation. Can be applied to vineyards and pears already in 2D configuration. 2500 ha per year worldwide [1].
Crop	<p>The Bolzano demo will be focused on apple trees, N-S orientation, Guyot (< 3/3.5 m, 2D growth, <2.5 m interrow). Classical tall slender spindle will be studied but not considered for the field demo (4 m height with 3D growth, 3-3.5 m interrow).</p> <p>Update M12: In Bolzano the final height of the rotation axis will be at 4.7 m. The selected site is designated for the cultivation of fruit trees, more specifically, the Ipador (Giga) apple variety.</p>

<p>Solutions implemented in the demo and demo details</p>	<p>200 m of CONVERT multifunctional trackers with height between 3 and 3.5 m (exact height to be determined depending on how the hail system is integrated) to ensure free movement of semi-automatic agricultural devices. Weathering steel will be used to manufacture the trackers, as a low environmental and visual impact in an agri-PV field. It is proposed to develop a crop + PV smart tracking algorithm for this project focused on the needs of Bolzano’s side.</p> <p>The site will be divided into (i) reference field with no PV system, (ii) trackers installed on existing fields (100 m of trackers), (iii) trackers installed together with new apple trees to allow for full integration and optimization. In total, the size of the PV system will be around 60 kWp (around 180 modules with various levels of semitransparency).</p> <p>UPDATE M12: The plan is for 240 m of trackers divided into 2 portions (4 + 6 trackers) with a total of 240 modules (to be discussed how many can be provided by ALEO using 2 levels of semitransparency). The nominal power will be around 90 kWp.</p>
<p>Water catchment / irrigation</p>	<p>Water collected by the tracking system is comparable to a roof without gutter. Water will be conveyed to avoid issues to the plants below. Irrigation comes from sprinklers used also as antifreeze systems.</p> <p>UPDATE M12: Sprinklers are redesigned as actual sprinklers are at a height which is higher than the foreseen structures.</p>
<p>Health & Safety</p>	<p>At the moment, there are no specific norms for agri-PV (grounding, etc). Rapid shutdown as from roof/facade systems will be studied. The use of pesticides which could reach the PV modules will also be considered.</p>
<p>System integration</p>	<p>70% of crops in South Tyrol covered by hail protection systems. Agri-PV needs to be integrated. Nets against insects are also becoming a new demand.</p> <p>UPDATE M12: Reuse of existing hail protection system for the existing section. New hail net will be fixed to the tracker structures for new Agri-PV section.</p>
<p>Use of electricity</p>	<p>LAIMBURG has identified several sites for the installation. The final choice will also depend on the existing availability of electricity connection, and we will create the conditions to electrify water pumps for irrigation to create an infrastructure for the charging of electrical tools.</p> <p>UPDATE M12: see above under “location”.</p>

The location of the demonstrator along with the agri-PV taxonomy are displayed in Figure 1.

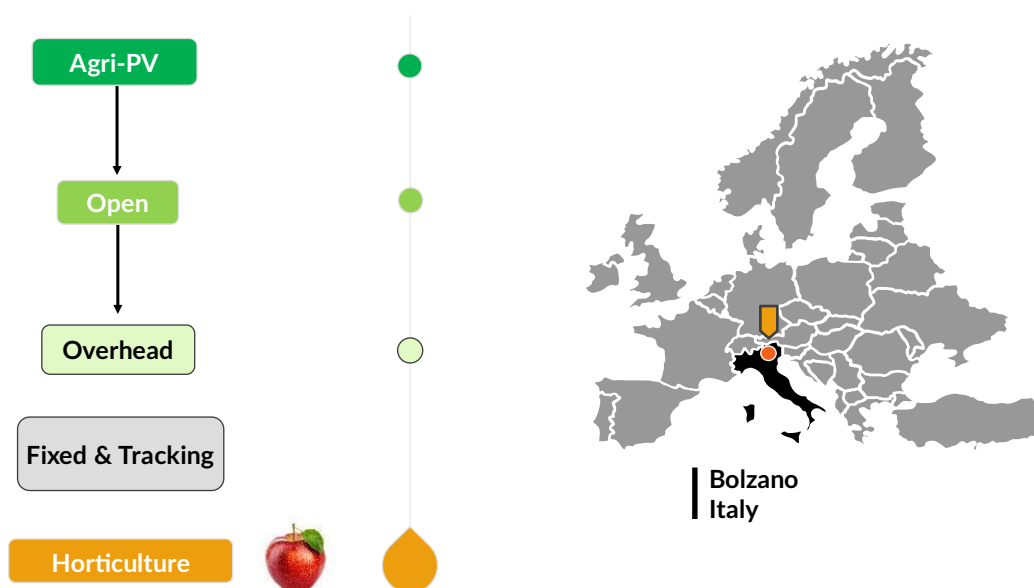


Figure 1: Agri-PV taxonomy and demonstrator location.

The apple orchard with the adopted tree training configuration along with the 2D representation for modelling are illustrated in Figure 2.



Figure 2: Apple orchard tree training configuration and 2D representation for modelling.

In this study we focused on the new plant. The main parameters that specify orchard design are the pitch and height, which are based on the training system. With Guyot training, the orchard can be modelled as a thin wall, or more specifically a translucent glass enabling a 2D analysis.

Each orchard row consists of four groups of apple plants, with each group containing two apple trees. In other words, two apple trees under one group of 6 PV modules. Figure 3 provides a side view of an orchard row, showcasing the layout and height of the crops.

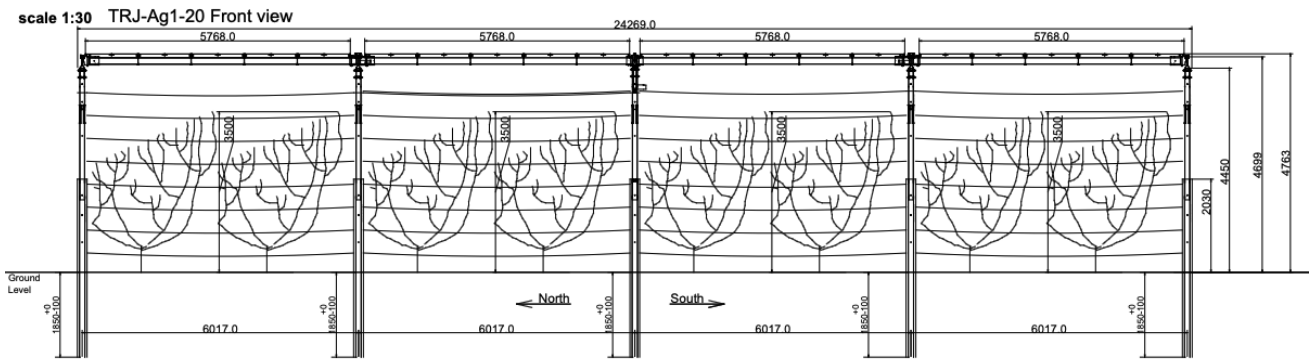


Figure 3: Front view of an apple orchard row.

In the preliminary phase, 11 different scenarios were considered, each with a different installation solution. The various scenarios taken into account are summarized in Table 3.

Table 3: Envisioned Summary of the 11 different scenarios considered in the preliminary phase.

Name	Optimised Height	Tracker	On Existing Orchard	On New Orchard	Description	Every Row in the Orchard	Every Other Row in the Orchard
Traditional	N	Y	X		PV-System installed over a traditional orchard, without changing the pre-existing system		X
L1.E	N	Y	X		1 row of PV modules in landscape mode	X	
L1.N	Y	Y		X	1 row of PV modules in landscape mode	X	
L2.E	N	Y	X		2 rows of PV modules in landscape mode		X
L2.N	Y	Y		X	2 rows of PV modules in landscape mode		X
P1.E	N	Y	X		1 row of PV modules in portrait mode		X
P1.N	Y	Y		X	1 row of PV modules in portrait mode		X
P1.Fixed	Y	N		X	1 row of PV modules in portrait mode - FIXED		X
L1.Fixed	Y	N		X	1 row of PV modules in landscape mode - FIXED	X	
L2.Fixed	Y	N		X	2 rows of PV modules in landscape mode - FIXED		X
V2.Fixed	Y	N		X	PV modules mounted in a V shape - FIXED		X

After conducting a comparative analysis, the solution featuring an elevated tracker with PV modules in a 1P configuration was confirmed as the optimal choice, striking a favourable balance among economic investment (CAPEX), anticipated producibility, and geometric regularity—offering the best integration with the orchard.

The Bolzano demo will consist of two distinct parts:

- The first portion, designated as "A," consists of four separate rows of trackers, each containing 24 modules. This portion will be installed on agricultural land where apple trees are already present.
- The second portion, designated as "B," consists of a 2 x 3 matrix of trackers, each with 24 modules. It will be installed on agricultural land where, concurrently, a new section of the existing apple orchard will be established. This new section will differ in terms of the spacing between the rows of trees.

The photovoltaic modules will be mounted on horizontal single-axis trackers (HSAT) aligned along the NNE-SSW axis (roll trackers). In the northern Italian climate, this type of single-axis solar tracking structure enhances energy production by 15-20% compared to a fixed system with equivalent capacity [2][3]. This improvement is achieved by optimizing the capture of direct solar irradiance on the PV module's surface throughout the day.

Moreover, the tracking system incorporates a backtracking algorithm, which effectively prevents mutual shading among modules on adjacent trackers during periods of low solar declination (early and late hours of the day). Consequently, a PV field equipped with trackers featuring this algorithm generates more energy than those lacking it. Additionally, the algorithm can be customized to meet specific crop-related requirements.

Each tracker is designed to accommodate 24 modules, organized into groups of 6 modules per span (across 4 spans), and allows for a maximum rotation of $\pm 55^\circ$ for the PV modules. These 24 modules are arranged in 4 groups of 6 modules each, with each group separated by 0.15 meters. In portion A, the trackers will be spaced with a pitch of 6.4 m to align with the current orchard spacing of 3.2 m. For portion B, the pitch is set at 5 m, corresponding to an orchard spacing of 2.5 m. In both cases, the rotation axis is positioned at an elevation of approximately 4.7 m, and the modules are configured in a 1P (Portrait 1) arrangement for optimal efficiency.

The top of view of the complete Agri-PV plant can be seen in Figure 4, which further elucidates the placement of the crops.

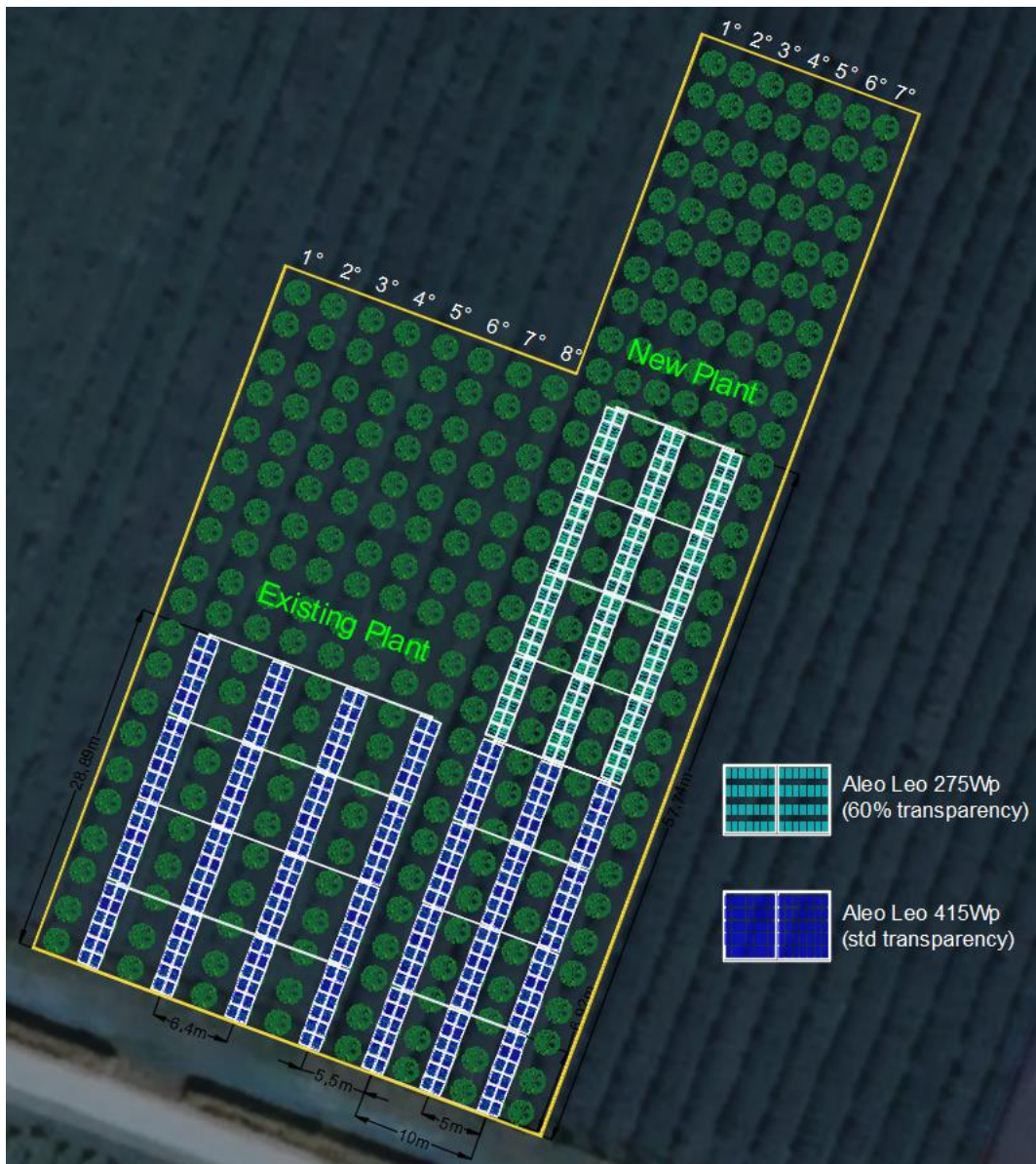


Figure 4: Top view of the complete Agri-PV system.

The structure as a whole is statically indeterminate (hyperstatic) due to the presence of beams perpendicular to the tracker axis, resulting in a truss-type structure.

The photovoltaic generator will consist of two different types of photovoltaic modules:

- Aleo Leo 415 Wp bifacial, standard transparency;
- Aleo Leo 275 Wp (estimated) bifacial, with a higher transparency factor than the standard.

Figure 5 provides the main technical information about the PV modules of Aleo.

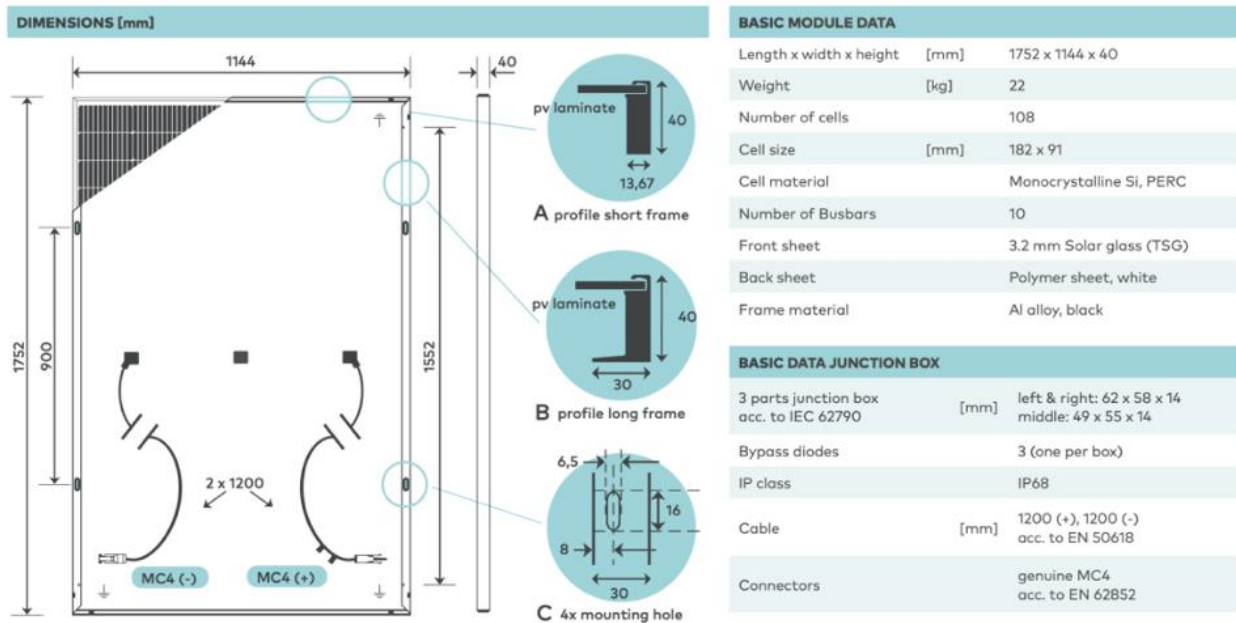


Figure 5: Main technical information about the PV modules of Aleo.

The four different solutions proposed by the PV module manufacturer are shown in Figure 6, corresponding to different semi-transparency levels.

Possible Designs of PV-modules

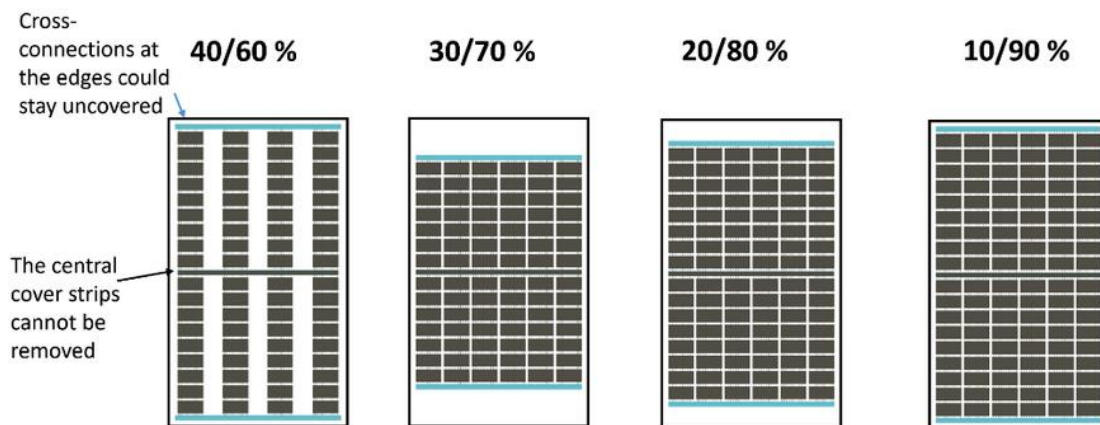


Figure 6: Overview of the four different solutions proposed by the PV module manufacturer, Aleo.

At present, the solution considered to be of most interest and therefore considered is the one with 40/60% transparency and the 10/90% solution (standard transparency).

Specifically:

- The A portion of the demo should consist of No. 96 standard modules (No. 4 trackers);
- The B portion of the demo should consist of No. 72 standard modules and No. 72 modules with increased transparency, for a total of No. 144 modules (No. 6 trackers).

Discussion is ongoing regarding the final number of PV modules to be provided by Aleo (as the number exceeds what was initially foreseen).

Figure 7 provides an overview of the layout of the PV arrays over the orchards.

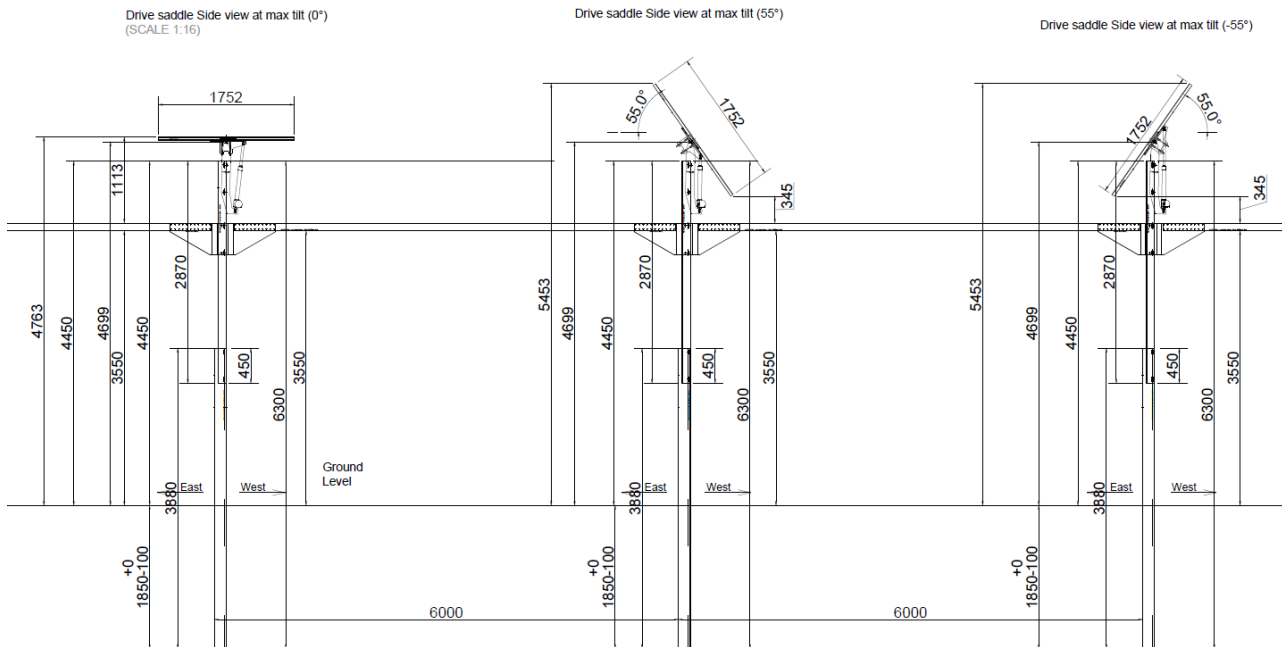


Figure 7: overview of the layout of the PV arrays over the orchards.

Several additional considerations have been taken into account or are currently being discussed:

- **Anti-ice system**

The sprinklers are used for irrigation and for anti-ice system during cold nights in spring in the flowering season and are installed at a height which is not compatible with the mounting structures. A new system will be installed with dedicated sprinklers for each tree / plant. This could potentially be used for treatments against pests / fungi, etc.

- **Hail-Net**

The existing hail protection system will be reused for portion A while in portion B will be newly installed. For both cases discussion is ongoing on the integration and compatibility with the trackers' mounting structure.

- **Rainwater collection systems**

The analysis of a rainwater collection system, for tracker structures instead of fixed ones, highlighted the difficulties to identify a solution without considerably increasing the amount of iron in structure to gather the water at the extremes of the PV panels. The works to identify a solution is still ongoing.

- **Monitoring and sensors**

The project will consider three distinct monitoring systems working together:

- a fixed system of sensors mounted directly on trackers
- a system of sensors mounted on a robot guided by 3D-LIDAR sensors
- a system of sensors mounted on a drone

A series of parameters will be monitored, evaluating both the photovoltaic and agricultural parts of the agri-voltaic system.

On the agricultural side, parameters will be monitored to help assess the health of the plant, its vigour, and crop yield, as well as environmental and soil conditions. PAR radiation will also be monitored.

For the photovoltaic part, a meteo station will be set up to measure classic parameters such as air temperature and humidity, wind speed and direction. POA irradiance and Albedo will also be measured. The condition of the modules and their possible damages will also be monitored through Aerial Thermography and Electroluminescence.

Discussion is ongoing to:

- identify a solution for rainwater collection system
- identify the exact position of the sprinkler
- identify the exact position of the fixed sensors
- identify the exact level of transparency of portion B2.

2.2. MODELLING

2.2.1. OVERVIEW

The primary goal of this preliminary investigation is to effectively apply the specialized frameworks of several partners (LuciSun, Imec, TUD) to a horticulture-centric agri-PV system and derive meaningful insights to inform the design phase. The study is meant to contribute to the following key objectives:

1. What is the maximum crop yield reduction, if any?
2. Do we have to meet any specific electrical yield or energy yield requirements?
3. Any other objective that could guide the optimization process?

2.2.2. MODELLING BY LUCISUN

1) Layout

The Agri-PV plant proposal comprises two sections: Section 1, denoted as the 'Existing Plant,' situated on the west side, and Section 2, referred to as the 'New Plant,' positioned on the east side. The primary distinction between the two sections in LuSim's simulation lies in the transparency of the PV modules. While both sections incorporate modules with standard transparency, the new plant uniquely features modules with 60% transparency.

In the initial phase (Phase 1), our focus is on modelling the existing plant.

From a modelling perspective in LuSim, the Agri-PV plant is segmented into three components:

- The PV modules support structure
- The PV system layout
- The crop layout

For the frames, a fundamental gantry system is utilized, as depicted in Figure 8. It is illustrated with beams in the x-direction (indicated by the red line in the image), aligning with the N-S direction and spaced 6.4 meters apart in the y-direction (indicated by the green line), corresponding to the E-W direction. These beams support a single grouping of 6 PV modules arranged in portrait mode. The length of one beam in the x-direction is 7.225 meters; therefore, when four such frames are positioned adjacent to each other, they collectively cover a length of 28.89 meters in the N-S direction.



Figure 8: Frame design for the Agri-PV plant is Bolzano.

We aim to model apple orchards, encompassing both the planting and harvesting phases. There are a total of eight orchard rows. However, from the perspective of modeling and simulation in LuSim, the westernmost orchard row is excluded. This exclusion is due to its insignificance in influencing the simulation or the target object, a detailed explanation of which will be provided in the subsequent Objective and Methodology section.

Currently, the investigation focuses on both the 'Existing Plant' and the 'New Plant' concerning the illumination reaching the surface of the 3D-modeled envelope of the apple crop and the corresponding percentage of shading loss caused by the PV system. The key distinction considered between the existing and new plants is that the 'new' plant incorporates Aleo PV modules with a semi-transparency factor of 40 percent.

In the realm of 3D modelling, several key questions arise regarding how to best represent plants and define these zones of interest. For plant shapes, it is possible to select either simple shapes, which approximate the outer boundaries of the crops, or more intricate shapes, which attempt to faithfully replicate the geometry of plant organs and leaves in detail. Basic geometric shapes, such as parallelepipeds, cylinders, spheres, or cones, can be employed to represent the outer envelopes, whereas shapes of varying complexity between the simplest and most detailed forms are also viable options. Each approach comes with its own set of advantages and disadvantages.

Complex geometries attempt to realistically represent the shape of crops. They facilitate the utilization of more intricate models used to evaluate crop photosynthesis and good estimates of the 3D optical porosity. This approach, however not a limiting factor, demands significantly higher computational resources because of the concomitant substantial increase in required spatial resolution and of the number of points where irradiance must be assessed. It also restricts the use of simpler agronomic models that have been developed based on a preliminary evaluation of the irradiance incident on the external canopy envelope. Figure 9 illustrates the 3D modelling of the agri-PV demonstrator ("Existing plant") in LuSim using complex shapes.

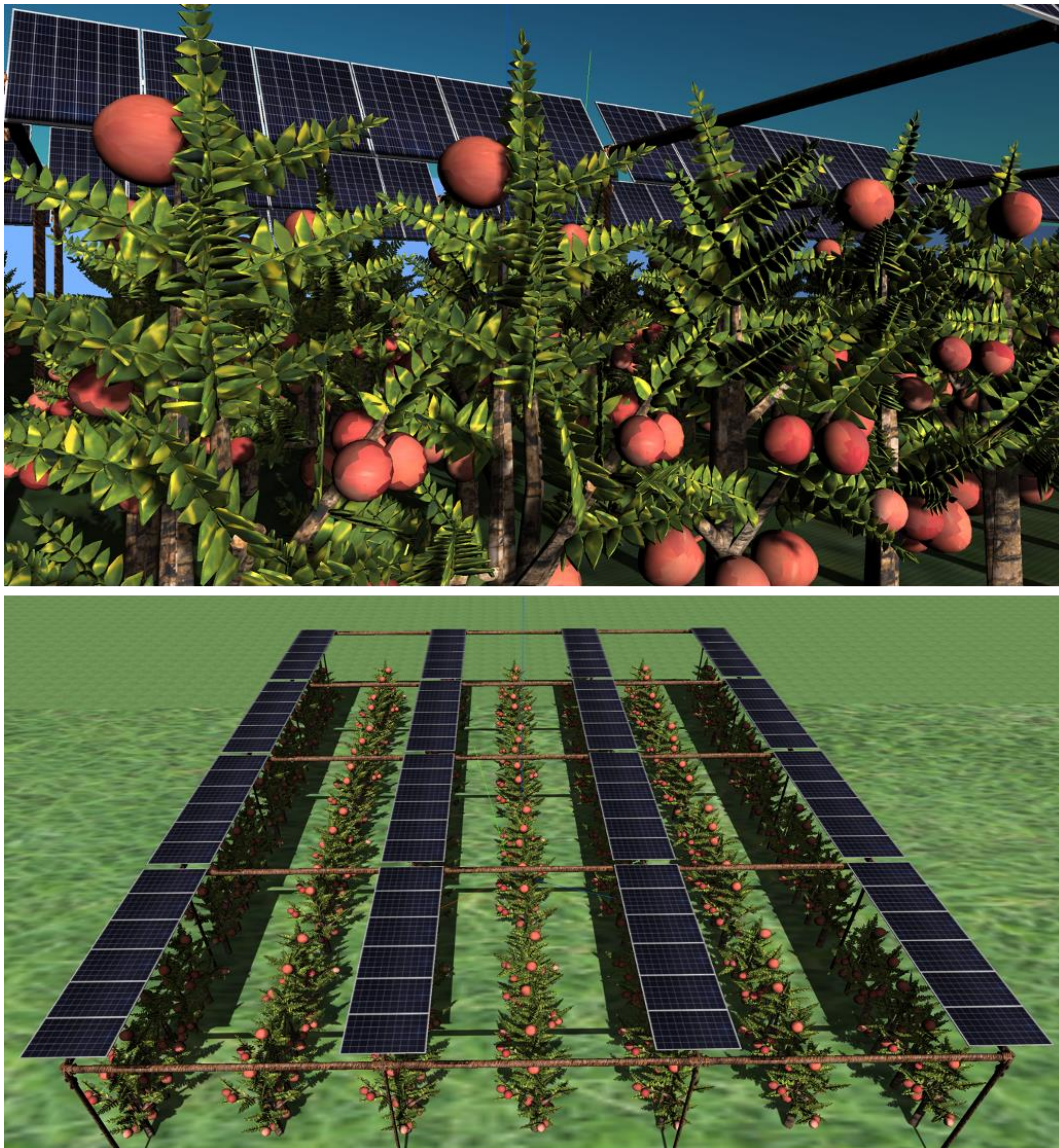


Figure 9: 3D modelling of the agri-PV demonstrator (“Existing plant”) in LuSim using complex shapes.

In contrast, the use of basic shapes that depict the external envelope of crops not only reduces the computational complexity significantly by reducing the number of points where irradiance calculations are necessary, but the approach also facilitates the direct utilization of parametric models that assess photosynthesis in the canopy based on the solar irradiation reaching its outer envelope. When employing these straightforward models, optical properties including optical porosity cannot be directly modelled, but must be incorporated through a parametric model attached to the object's texture. In most agrivoltaic applications modelled using LuSim, experience has favoured the use of basic geometric shapes alongside parameterized optical properties. If necessary, the optical porosity can be initially modelled using a high-resolution 3D representation of the plant under scrutiny, and the results can then be applied to all simple shapes employed in modelling the entire agrivoltaic system.

For these reasons, going for a simplified shape representing the outer envelope of the crop is considered at this phase. In LuSim, a parallelepiped is considered to represent 2 apple trees or one fourth of the complete orchard row, with an assumed width (E-W direction) of 0.7 m and length of 6.8 m (N-S direction). Height is considered as 3.5 m.

Figure 10 illustrates the 3D modelling of the agri-PV demonstrator on the “Existing plant” in LuSim using simple shapes. Full PV modules without added semi-transparency are used. In turn, Figure 11 illustrates the 3D modelling of the agri-PV demonstrator on the “New plant” in LuSim using simple shapes. PV modules with 40% semi-transparency are used.

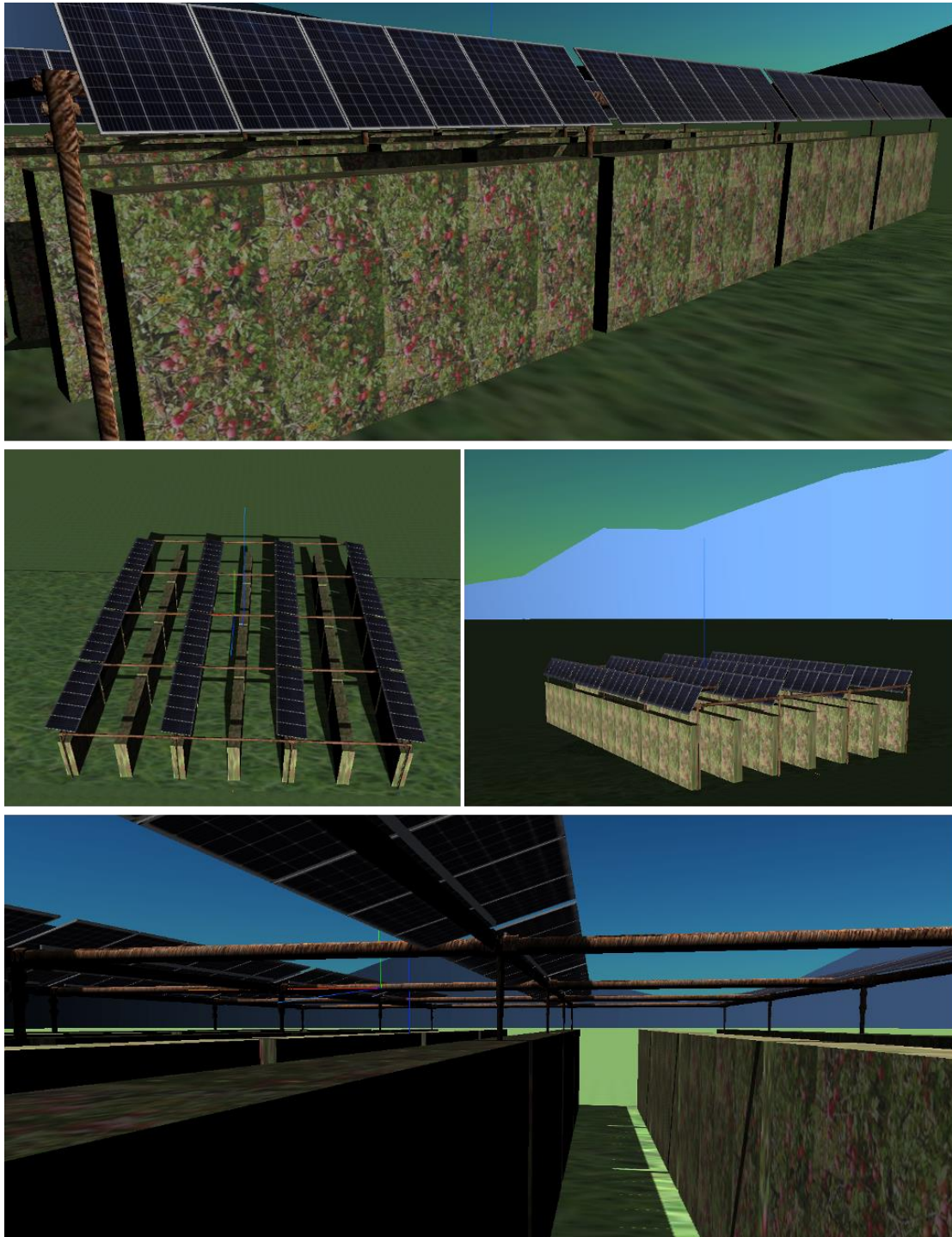


Figure 10: 3D modelling of the agri-PV demonstrator (“Existing plant”) in LuSim using simple shapes (full PV modules; no added semi-transparency).

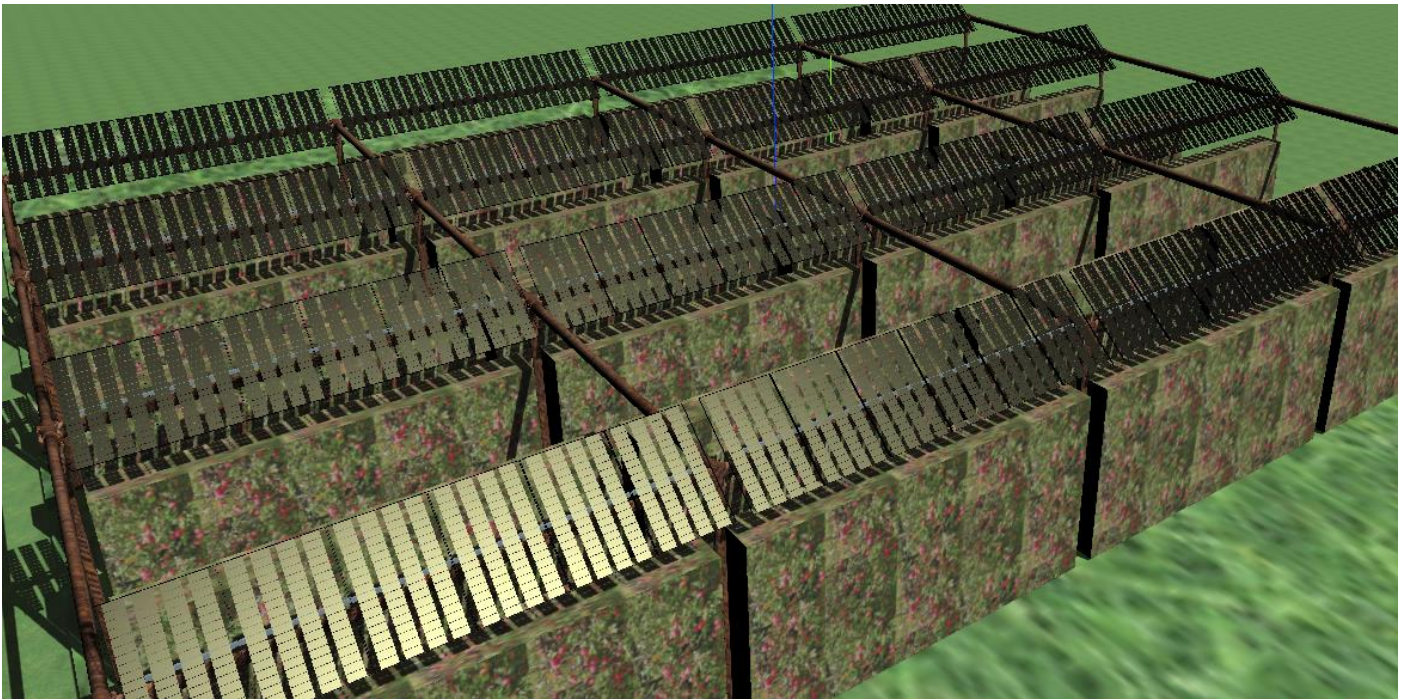


Figure 11: 3D modelling of the agri-PV demonstrator (“New plant”) in LuSim using simple shapes (PV modules with 40% semi-transparency).

2) Methodology

The assessment of shading profiles affecting both vegetation and PV modules, along with the calculation of bifacial energy gain (BEG), is conducted using the LuSim simulation tool. This tool leverages cutting-edge 3D evaluation libraries integrated into the Graphic Processor Units (GPUs) found in modern computers. Although initially developed for the video game industry, these libraries offer several compelling advantages in the context of bifacial PV applications. The achievable spatial resolution rivals that of backward ray-tracing techniques but demands only a fraction of the latter's simulation time. The methodology followed to employ GPUs in solar energy applications has been detailed in previous contributions, such as for the assessment of intricate shading issues [4] bifacial irradiance [5] the energy simulation of vertical bifacial PV systems in agrivoltaics [6], the assessment of the PV energy yield in agrivoltaic greenhouses with bifacial PV modules [7] or the 3D-modelling of light-sharing agrivoltaic systems for orchards, vineyards and berries [8]. The irradiance distribution profiles are assessed at high spatial resolution, either at the leaf scale or the PV cell level, and with a relatively high temporal resolution of 10 minutes. The 3D view-field method is employed for the comprehensive evaluation of the irradiance field, both incident and reflected, that involves the ground and PV modules on a component-by-component basis. The incident irradiance profile for each PV cell comprising the PV system is obtained at 10-minute intervals throughout the year. Then, this irradiance data time series is transformed into electrical power using a PV simulation model that accounts for conversion losses within the entire system. In most cases, conventional simulation routines, such as those contained in pvlib [9] are sufficient to model these energy losses.

To assess the impact of the actual solar resource on crop yields, each configuration is compared to a reference model. The latter is intentionally designed to closely resemble the base case, where trees are planted in rows, and vertical structures support protective nets. However, in this base case, neither PV panels nor their supporting structures are present.

The objective is to calculate the light reaching the surface of the crop's envelope, i.e., the total incident irradiance, along with the corresponding shading percentage loss due to the presence of the PV system. To achieve this, the first step involves selecting a target object that is representative of similar objects within the 3D scene. In this case, the

target object is the outer envelope of the crop, representing two apple crops, as specified in the 'Inputs' section. It is crucial to choose specific envelopes that accurately represent other crop envelopes in the scene and are unaffected by the 'border effect' or 'edge effect.'

Two envelopes or target objects are primarily selected, each representing a different case that is reflective of the entire scene. The first is the envelope located directly under the PV modules, referred to as the 'Under PV' crop. The second envelope is positioned in the free space without any PV modules or between two rows of PV modules, termed the 'Free' crop. For these two cases, the shading loss percentage is calculated and presented, defined as the difference in light reaching the specific selected target objects between the configuration with no PV system (reference case) and the Agri-PV system (test case), divided by the reference case. This reference case is crucial for determining obstructed light, calculated as the difference between the reference and test cases, and subsequently, quantifying the percentage loss. The test case is depicted in Figure 12, showcasing the two target objects highlighted in white and appropriately marked in the 3D scene. The reference case is shown in Figure 13.

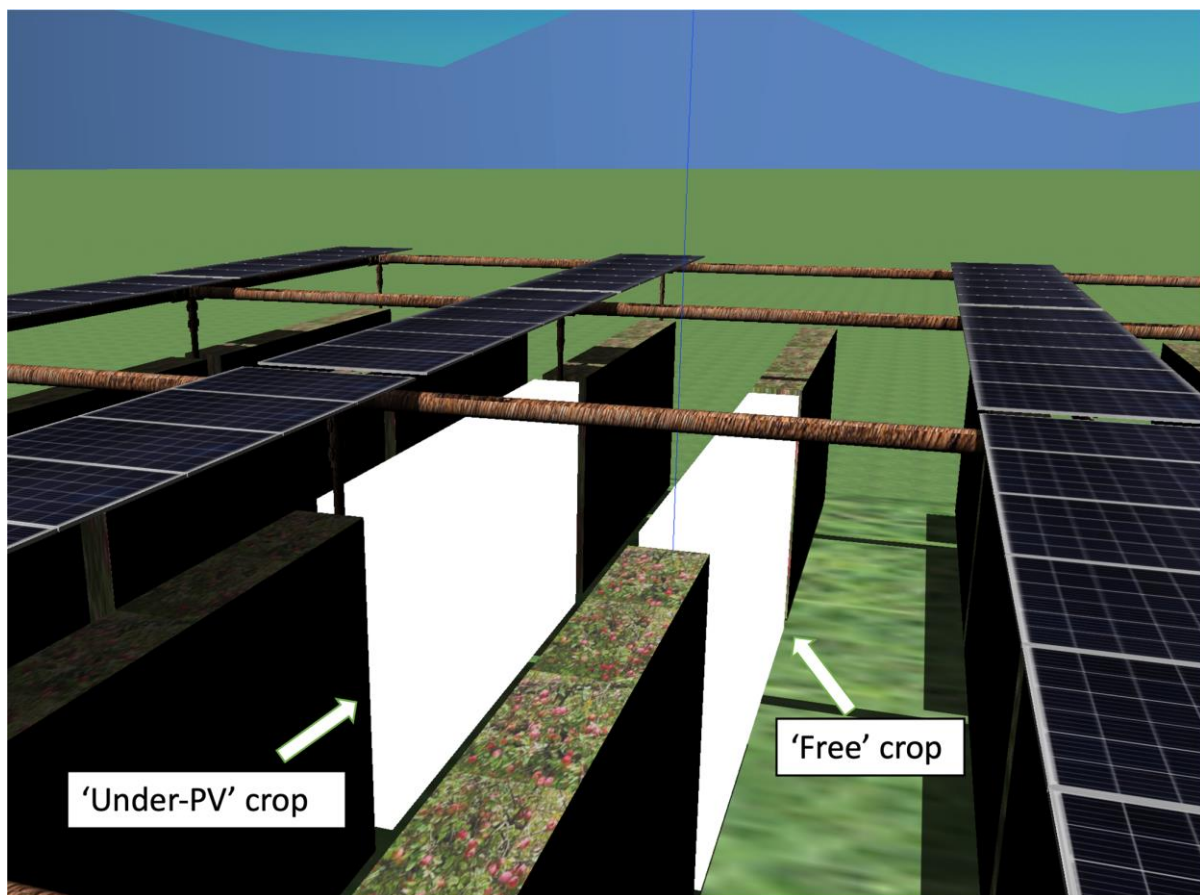


Figure 12: Test case for Bolzano's existing section of the agri-PV systems, with crops indicated as target objects for the simulations.

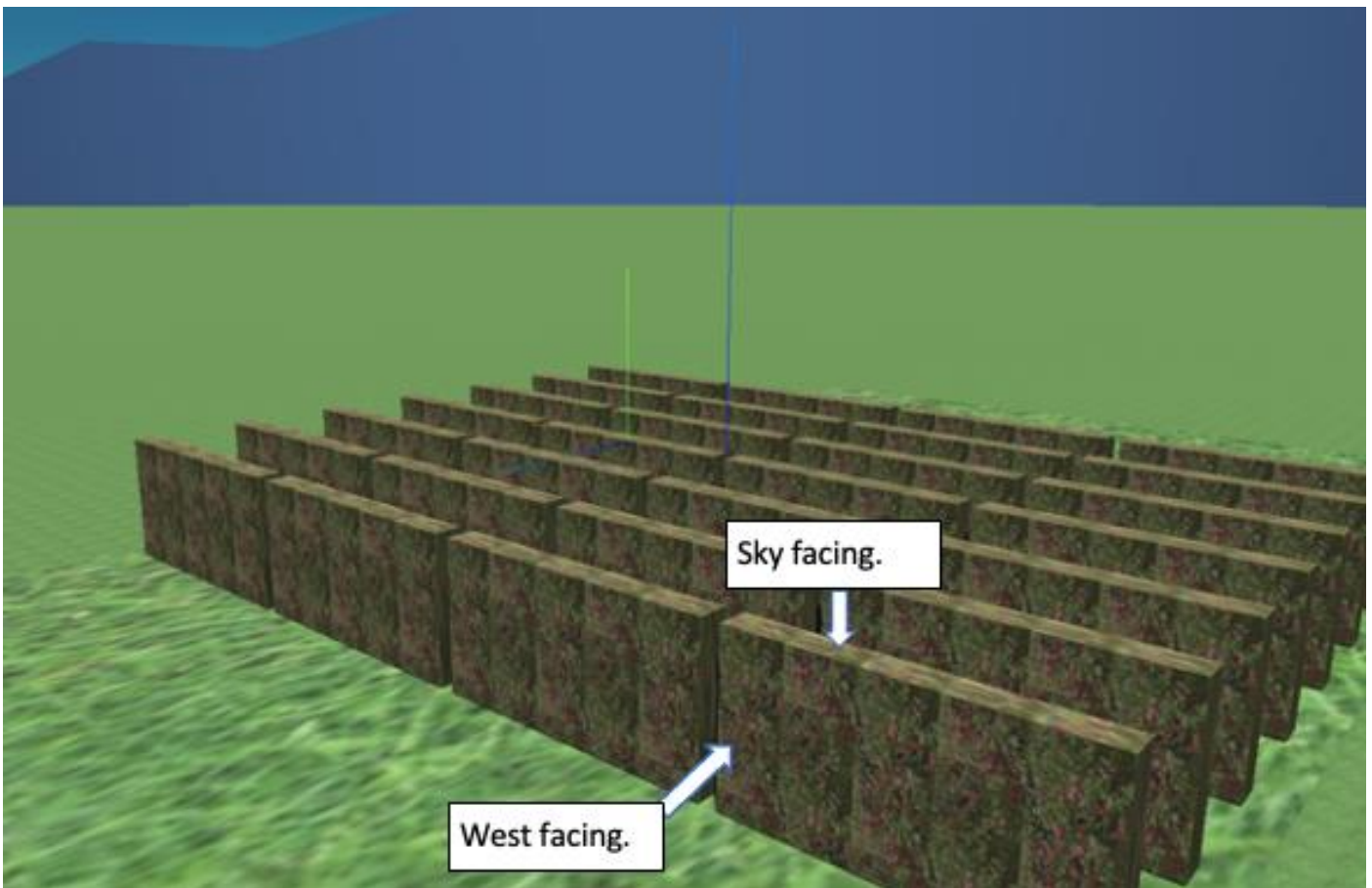


Figure 13: Reference case for Bolzano's existing section of the agri-PV systems.

When assessing the light reaching the crops and the corresponding shading loss percentage, the vertical surface of the modelled crop's envelope takes precedence. The effective surface for converting sunlight in the process of photosynthesis is significantly greater on the vertical sides of the canopy compared to the top part.

The vertical sides of the crop are divided into three zones based on their height from the ground. Zone 1 represents the bottommost segment, spanning from 0 to 1.16 meters. Zone 2 covers the middle segment, ranging from 1.16 meters to 2.32 meters. Likewise, Zone 3 represents the topmost segment, encompassing the height between 2.32 meters and 3.5 meters. Essentially, the vertical faces are evenly split into three equal zones. Figure 14 illustrates this zone separation, with the west and sky-facing sides indicated. There are three distinct zones for each one of the sides of the crops, so there are 3 zones on the eastern side, and 3 zones on the western side. In addition, there is also an additional zone representing the top horizontal part of the crops. This amounts to 7 different zones when the solar irradiance reaching the crops is evaluated. The southern and northern sides are not evaluated because the length of the rows of crops is considered to be long enough so that the impact of these zones can be considered as negligible.

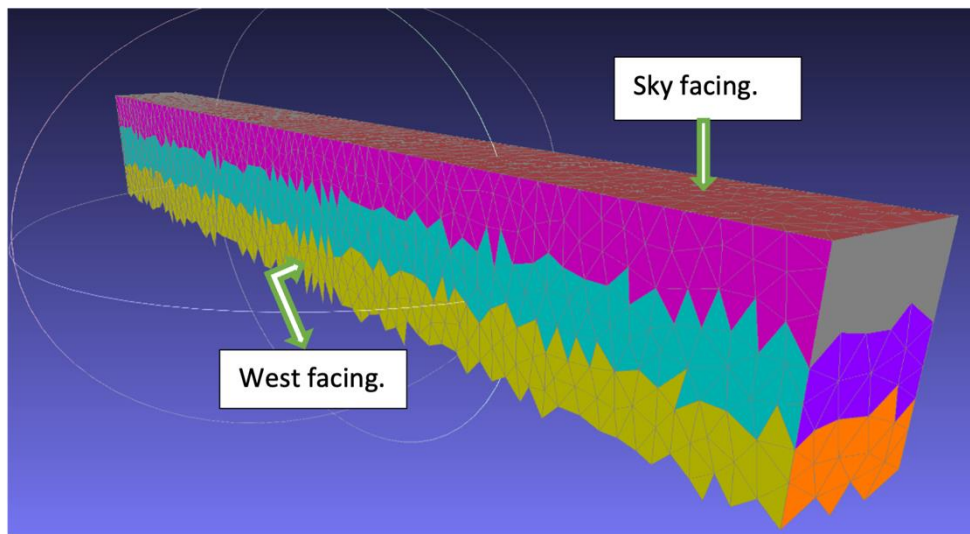


Figure 14: Zone separation for the apple crops as seen from the east side.

Subsequently, each object is assigned a texture containing its optical properties. A mesh associated with these textures defines the spatial resolution used in irradiance modelling.

Once the 3D mesh model of the agrivoltaic system has been completed, the irradiance simulations are carried out at each instant and for each radiation component (direct, isotropic sky diffuse, circumsolar sky diffuse, and ground reflected). The irradiance values are then aggregated into areas of interest within the 3D scenario, as well as over periods of time that are relevant to the crop yield to be evaluated. Those periods depend on the type of crop and the corresponding growth and harvest seasons. These integrations are typically done on a daily, monthly, or yearly basis, depending on what needs to be evaluated.

Based on the coordinates provided in Table 2, a Typical Meteorological Year (TMY) dataset coming from PVGIS-SARAH2 has been used for modelling. This dataset contains the solar resource data as well as the meteorological data corresponding to the specified location.

Other variables obtained from the PVGIS-SARAH2 are air temperature, wind speed, wind direction and relative humidity.

Table 4 shows a monthly summary of the most relevant solar resource and weather data used in the PV energy yield evaluation. GHI corresponds to Global Horizontal Irradiation, DHI corresponds to Diffuse Horizontal Irradiation, W_s to the wind speed and T_a to air temperature.

Table 4: Monthly summary of the most relevant solar resource and weather data used in the crop and PV yield evaluation.

Month	GHI [kWh/m ²]	DHI [kWh/m ²]	T_a [°C]	W_s [m/s]
Jan.	51.06	18.34	-1.31	0.66
Feb.	61.73	24.56	-2.34	0.54
Mar.	118.06	44.41	2.94	0.73
Apr.	170.85	51.1	9.33	0.73
May	142.38	71.23	8.58	0.87
June	179.95	77.98	15.22	0.71

July	212.71	67.18	19.73	0.65
Aug.	167.08	65.06	18.12	0.62
Sep.	117.61	51.75	13.24	0.62
Oct.	59.34	37.98	9.52	0.66
Nov.	44.08	22.84	3.16	0.79
Dec.	41.33	14.64	1.38	0.66
Year	1366.18	547.07	8.13	0.7

3) Results

This section presents the results depicting the total incident irradiation on the crops, accompanied by the corresponding shading loss percentages. A comparative analysis is conducted among various zones for each crop or target object. Additionally, specific zones from diverse target objects are juxtaposed to evaluate their shading loss percentages. To streamline the presentation and manage the visual data, the comparison is currently limited to the top and middle zones on the west side and the sky-facing side across different target objects. The target objects under consideration include 'under PV' and 'free crops'.

Figure 15 shows the evolution of the global irradiance over all the sides of the 'under-PV' crop and the individual respective zones for a clear-sky day of summer, the 18th of July (TMY). Notably, irradiance undergoes a significant reduction around solar noon, with this diminished light persisting longer on the side of the canopy facing the sky. This phenomenon results from the shadow cast by the overhead PV modules. Conversely, during early morning and late afternoon, irradiance increases on the eastern and western vertical sides of the canopy, especially at the higher sections less affected by shading. The irradiance on the northern and southern sides is minimal. These observations stem from the geometry of agrivoltaic systems, where sunlight predominantly strikes the crops at an angle. Consequently, the western and eastern sides, having a larger effective surface area for sunlight absorption, play a crucial role in photosynthesis.

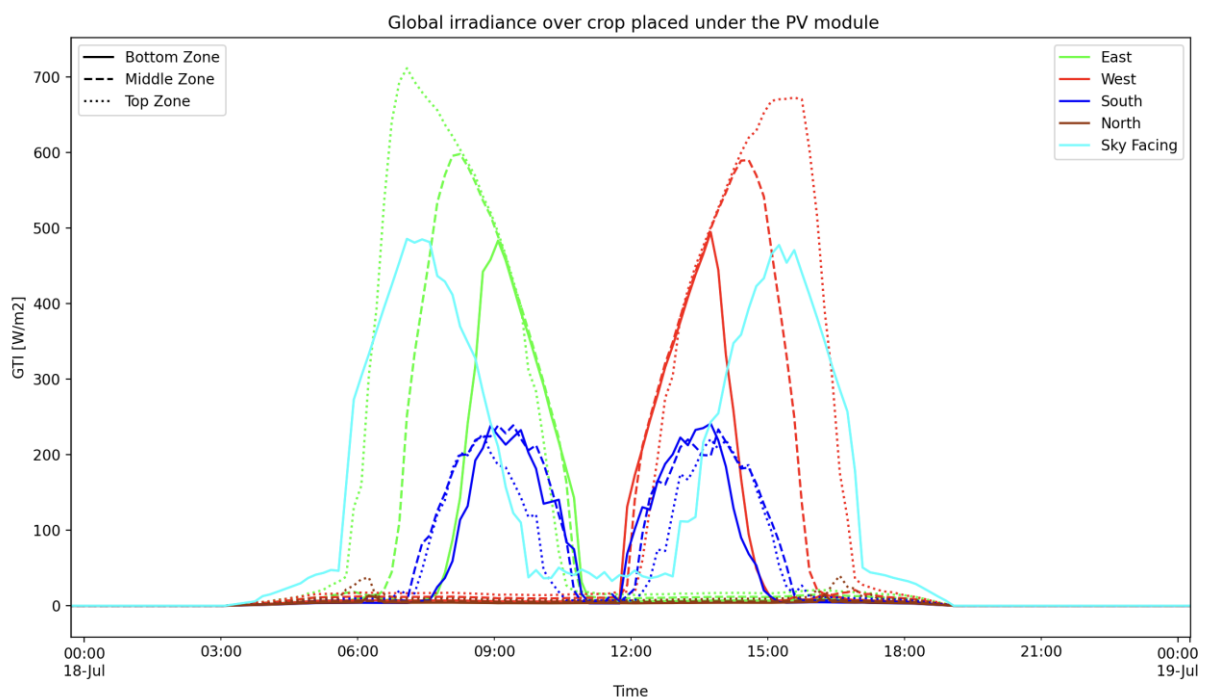


Figure 15: Global irradiance on 18th of July (TMY) for the crop under PV modules.

Figure 16 depicts the percentage of shading loss observed throughout the day, highlighting the alternating periods of shade and direct sunlight. This pattern is a direct consequence of the agrivoltaic (agri-PV) system's design, which consists of sequential rows of crops interspersed with photovoltaic (PV) panel arrays.

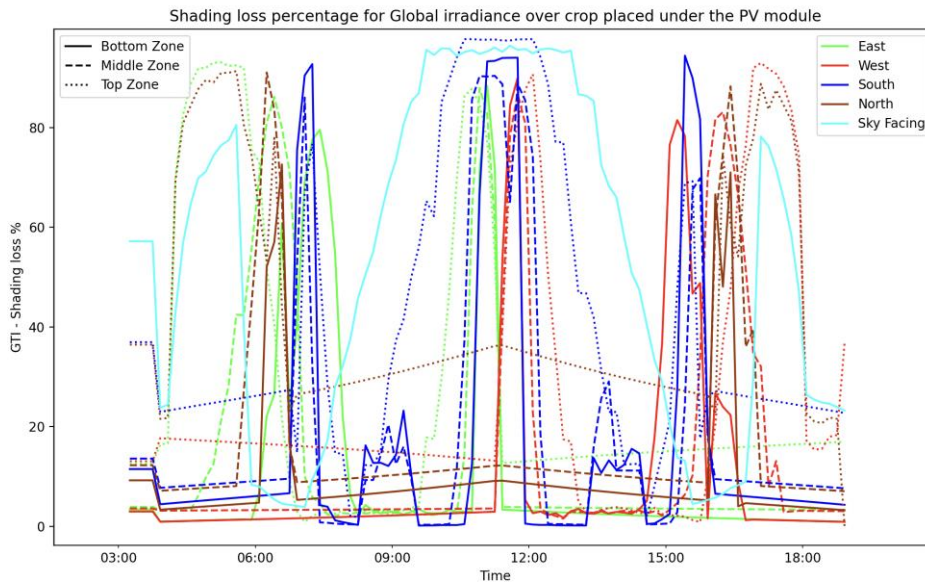


Figure 16: Shading loss percentage on the global irradiance for the 18th of July (TMY) for the crop under PV modules.

Figure 17 presents a heatmap that visualizes the daily distribution of global irradiation on the eastern side of the crop situated beneath PV modules, specifically for July 18th (TMY). This heatmap focuses on a specific area of interest within the larger context of the agrivoltaic system. It reveals that the irradiance levels at the uppermost part of the canopy are higher compared to those at the bottom. This variation is attributed to the mutual shading occurring among the different crop rows.

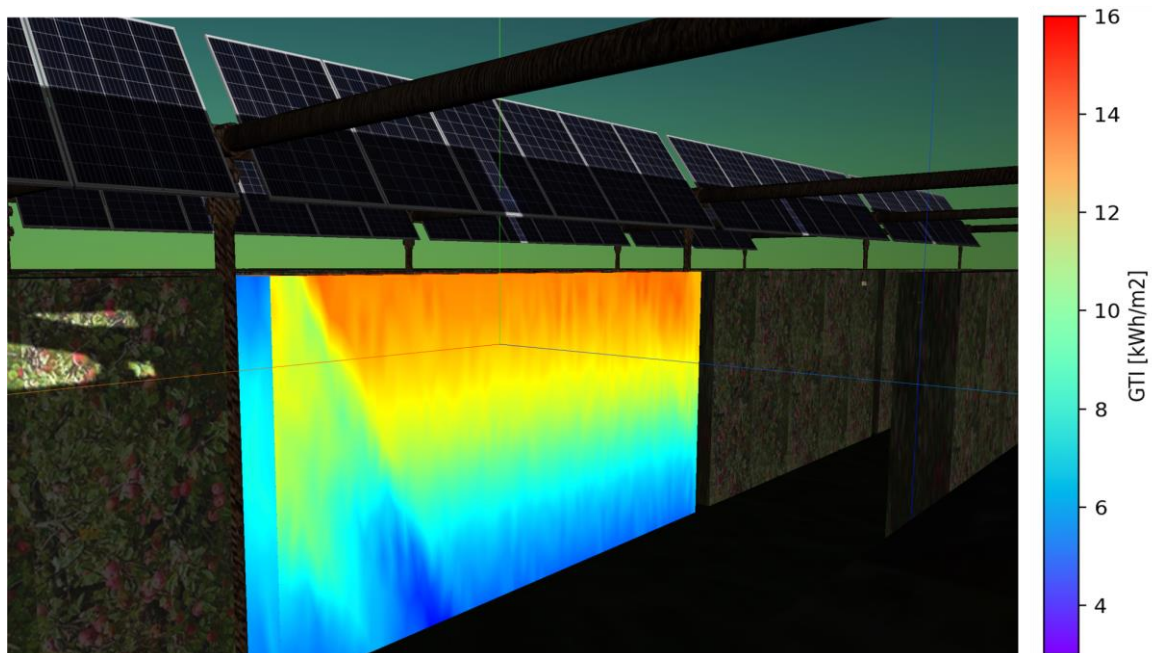


Figure 17: Heatmap showcasing daily global irradiation for 18th of July (TMY) over the east facing side of the crop under PV modules.

Similarly to the case of the crops under the PV modules shown previously, Figure 18 shows the evolution of global irradiance over all the sides of the ‘Free’ crop and the individual respective zones. In contrast to the areas beneath the crops shaded by PV modules, the part of the canopy facing the sky receives the highest amount of irradiance, especially around solar noon. This peak irradiance coincides with the sun's zenith, when it shines directly overhead, and the angle of incidence on horizontal surfaces is minimal. The vertical eastern and western sides of the canopy, however, absorb significantly less irradiance per unit area. This reduction is primarily due to the oblique shadows cast by the PV modules mounted above adjacent rows. Despite receiving less irradiance per unit surface, these vertical portions of the canopy still play a crucial role in overall photosynthesis. Their contribution is significant because the total surface area they encompass is considerably larger.

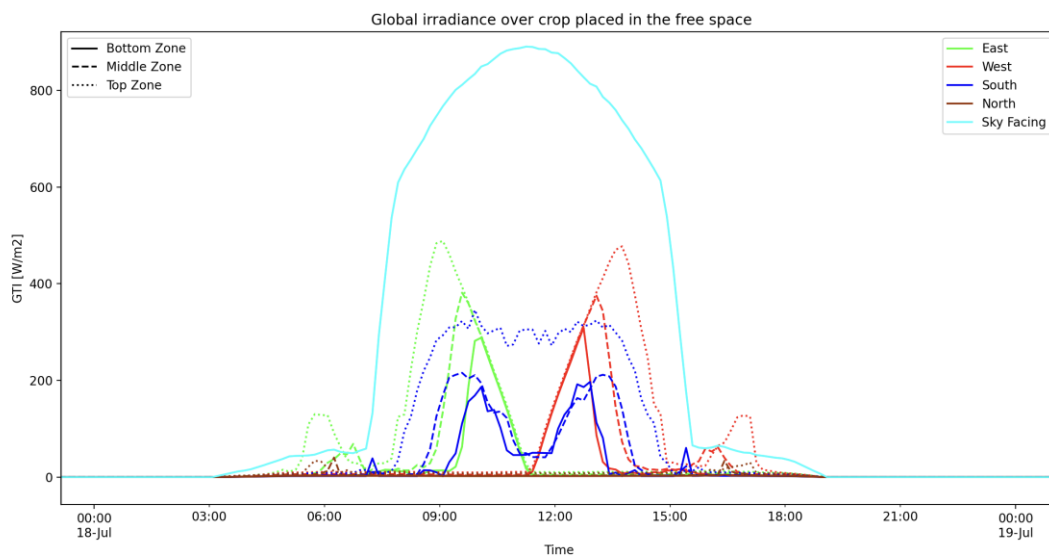


Figure 18: Global irradiance on 18th of July (TMY) for the crop under free space.

Figure 19 displays the percentage of shading loss experienced by the global irradiance. Notably, shading on the side of the canopy facing the sky is minimal around solar noon and maintains low levels for extended periods. In contrast, the vertical sides of the canopy suffer more significant reductions in solar irradiance. This is due to the oblique shadows cast by the structures, which persist and impact these areas for longer durations.

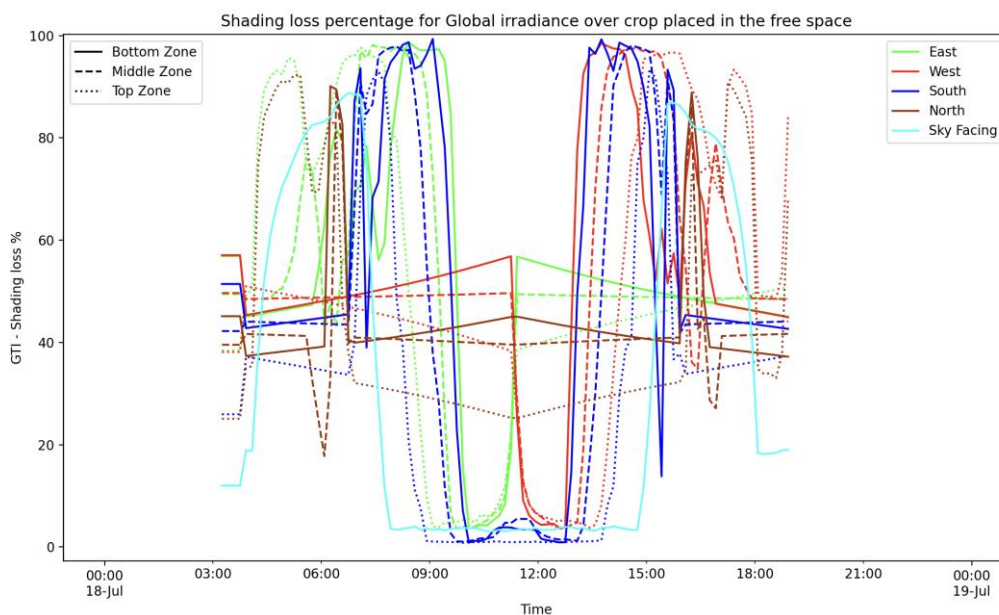


Figure 19: Shading loss percentage on the global irradiance for the 18th of July (TMY) for the crop under free space.

Figure 20 presents a heatmap that visualizes the daily distribution of global irradiation on the eastern side of the crop situated under free space (no PV modules over it), specifically for July 18th (TMY). This heatmap focuses on a specific area of interest within the larger context of the agrivoltaic system. It reveals that the irradiance levels at the uppermost part of the canopy are higher compared to those at the bottom. This variation is mainly attributed to the mutual shading occurring among the different crop rows.

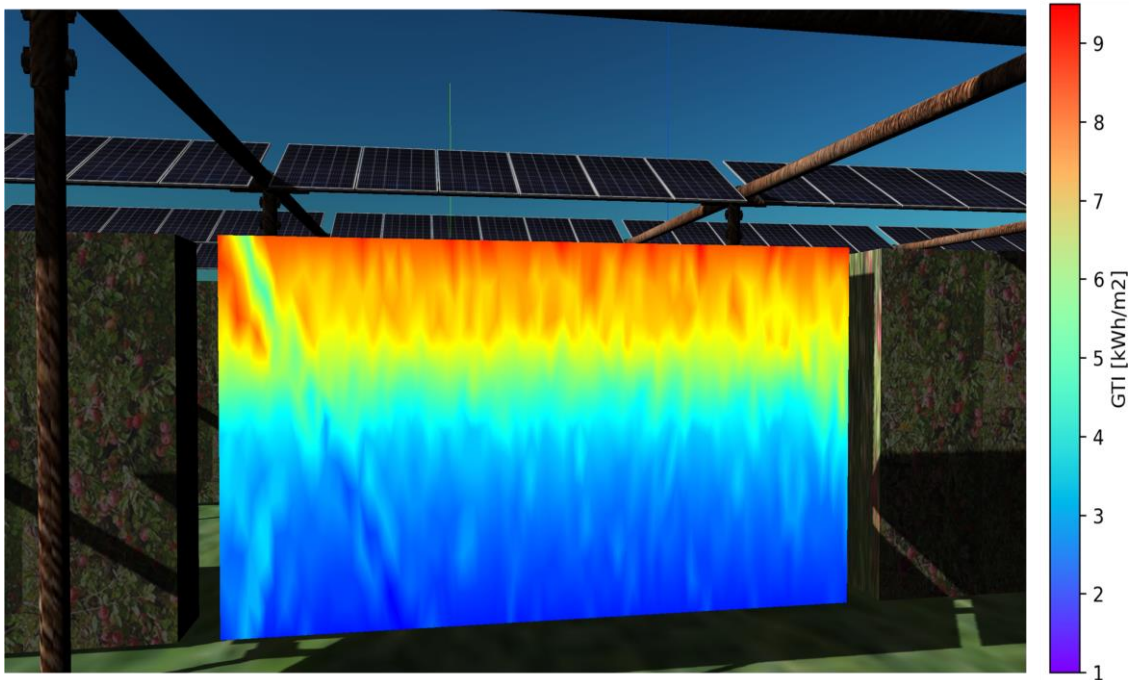


Figure 20: Heatmap showcasing total global irradiation for 18th of July (TMY) over the east facing side of the crop under free space.

Two types of crops situation respect to the agri-PV system were selected as focal points to represent the comprehensive scenario of shading effects on crops within agrivoltaic systems. The analysis has yielded significant findings, elucidating the effects of shading on these designated crops, termed 'under-PV' and 'free' crops. These insights underscore the importance of selecting specific crops for detailed examination. Focusing on a particular area, the top zone on the west-facing side. Figure 21 shows the shading loss percentage on July 18th for both 'under-PV' and 'free' crops. This comparison illustrates the influence of the agrivoltaic system's shading on each crop's sunlight exposure, determined by its height and position within the field.

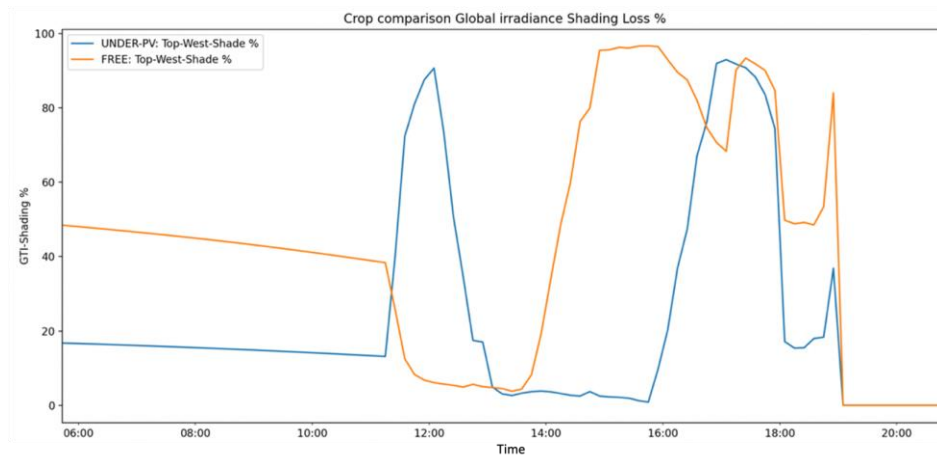


Figure 21: Shading loss percentage for 18th of July comparison for the top zone of west facing side.

To enhance understanding of the observed shading trends and to validate the findings, LuSim allows for the visualization of shading patterns at any selected moment in time. For a clear comparison of the shading impact on the designated target crops, two instances are illustrated: the shading observed at 12:00 (Figure 22) and 16:00 (Figure 23), both through realistic views and corresponding heatmaps for those times. Additionally, the specific zones targeted on these crops are marked to emphasize the differences in shading patterns.

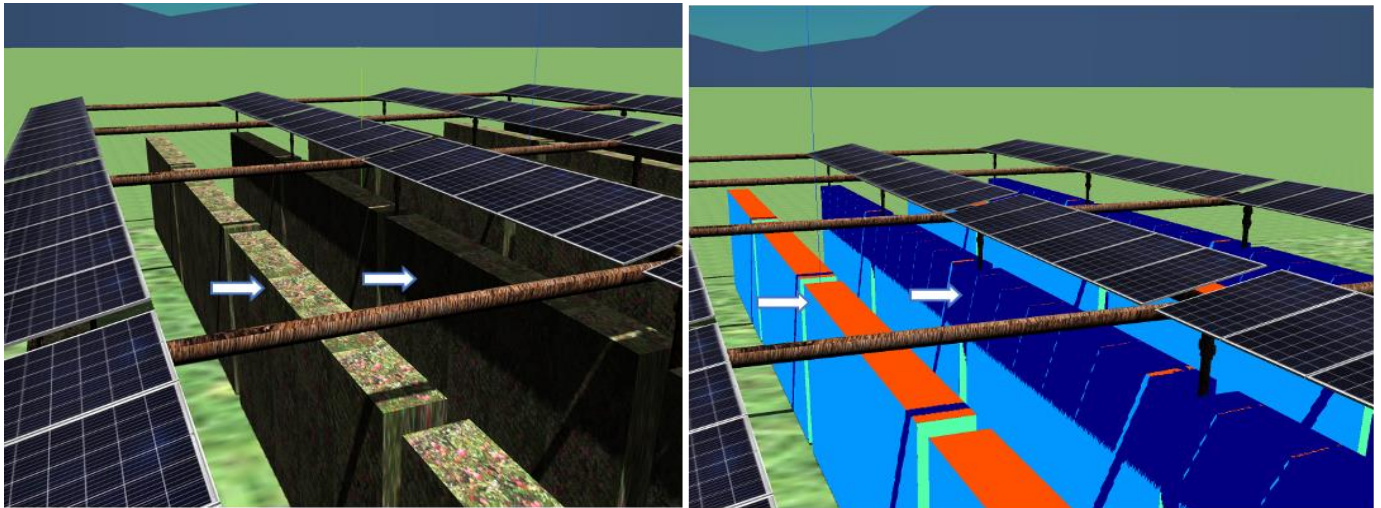


Figure 22: Realistic shading (left) and the corresponding heatmap (right) in 3D space at 12:00 on 18th July (TMY) for the top zone of west facing side.

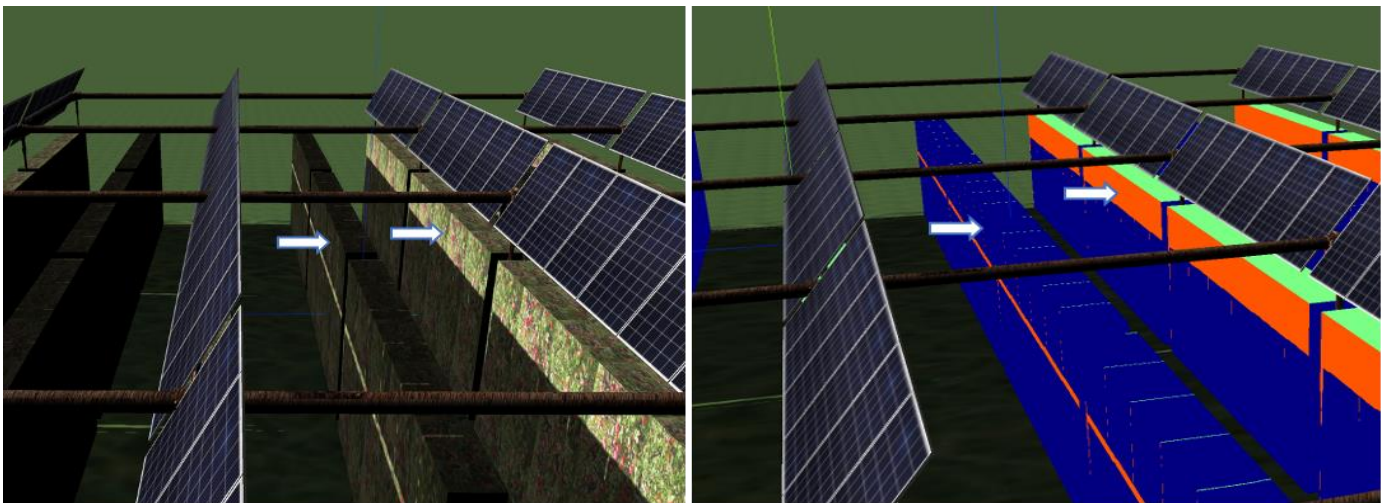


Figure 23: Realistic shading (left) and the corresponding heatmap (right) in 3D space at 16:00 on 18th July (TMY) for the top zone of west facing side.

The variation in shading patterns throughout the day becomes notably significant when aggregated over daily and monthly periods, as shown in Figure 24 for daily aggregation and Figure 25 for monthly aggregation. Therefore, the positioning of crops relative to the photovoltaic (PV) system plays a crucial role in managing shading losses and substantially affects the availability of solar resources for the crops.

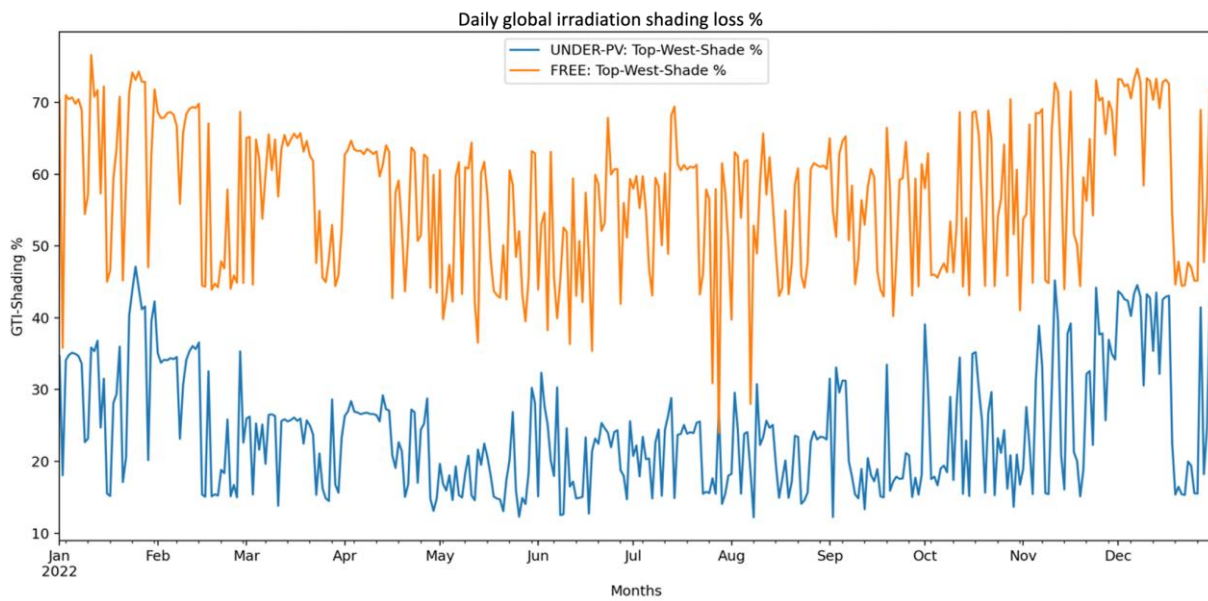


Figure 24: Daily GTI shading loss percentage comparison for the top zone of west facing side.

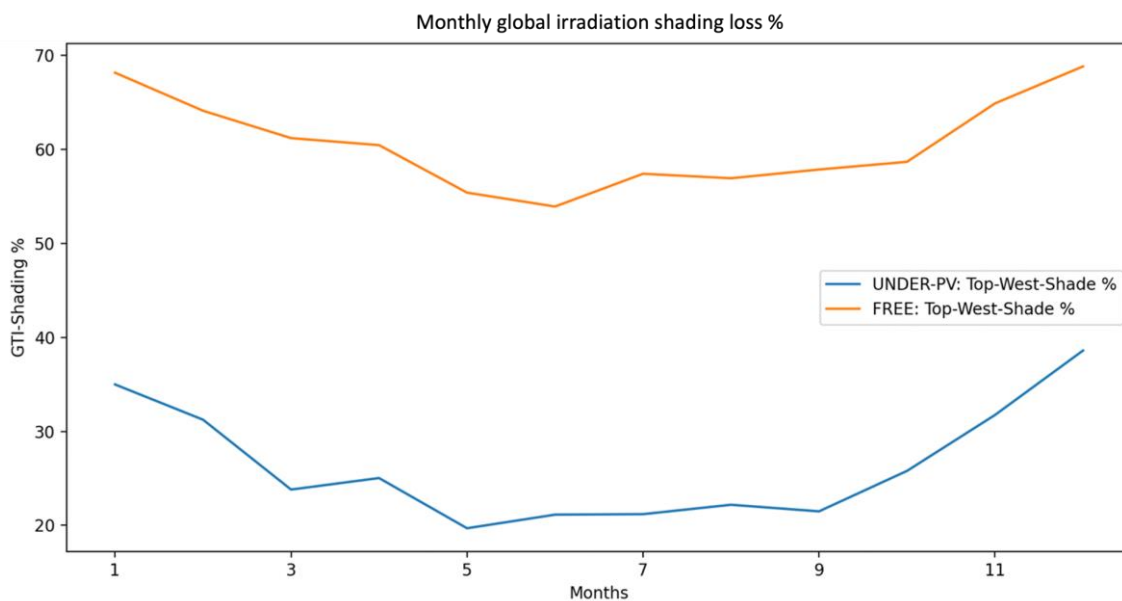


Figure 25: Monthly GTI shading loss percentage comparison for the top zone of west facing side.

The observed differences in shading trends between 'Under-PV' and 'Free' crops, as shown in the daily and monthly plots, also extend across various zones along the vertical faces of the crops' cuboidal envelopes. Contrarily, when examining the sky-facing side of the crops, the trend reverses. This contrasting shading pattern trend is depicted in Figure 26 for a clear-sky day on July 18th of the Typical Meteorological Year (TMY) series.

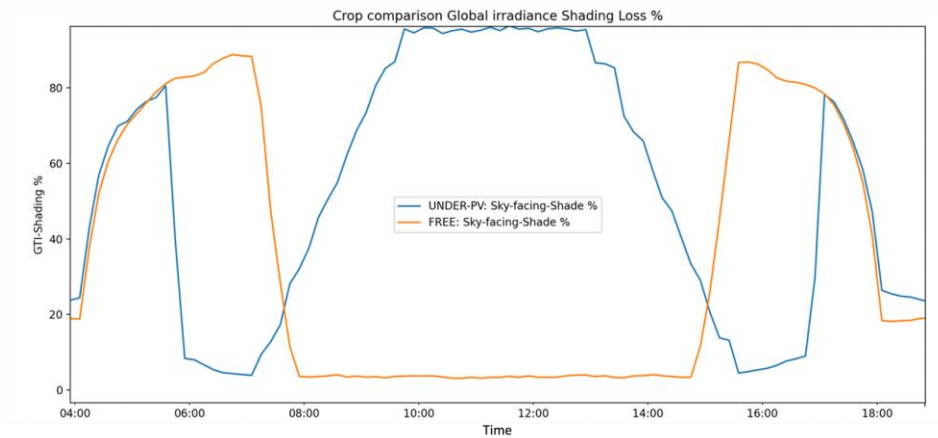


Figure 26: Shading loss percentage for 18th of July comparison for the sky facing side.

To visualize the shading pattern differences, the realistic shade on the sky-facing sides of the selected crop is depicted alongside its heatmap at different times. The shade at 7:00 is captured in Figure 27, while the situation at 12:00 is shown in Figure 28.

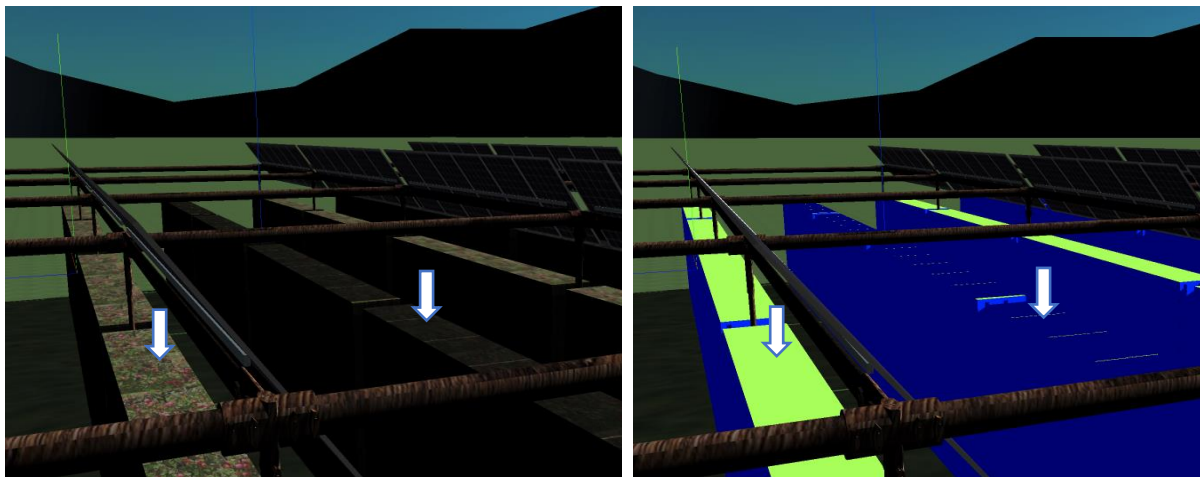


Figure 27: Realistic shading (left) and the corresponding heatmap (right) in 3D space at 7:00 on 18th July (TMY) for the sky facing side.

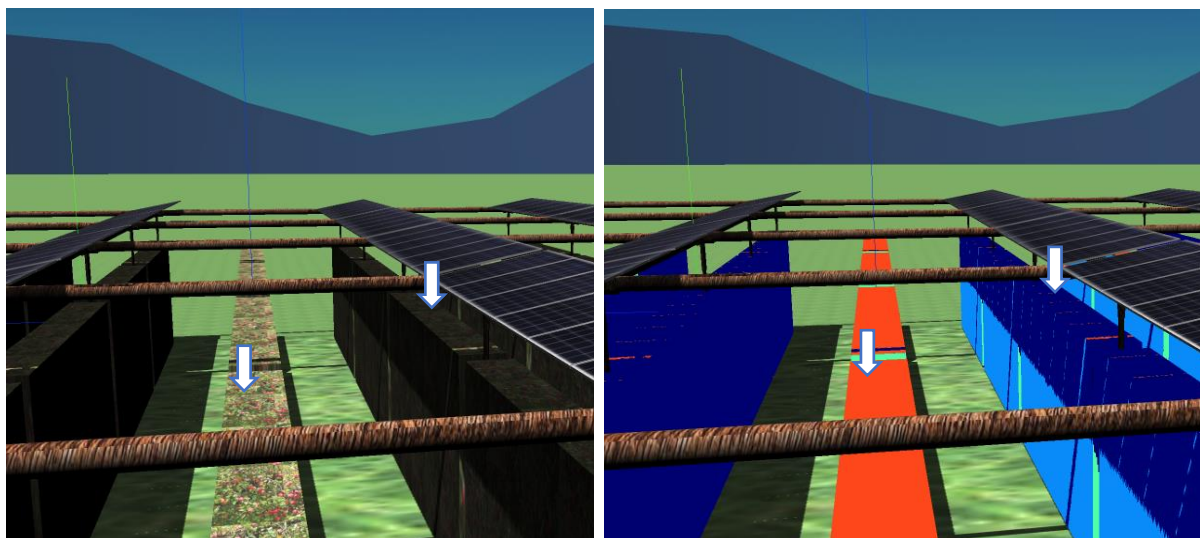


Figure 28: Realistic shading (left) and the corresponding heatmap (right) in 3D space at 12:00 on 18th July (TMY) for the sky facing side.

Aggregation of data on daily (Figure 29) and monthly (Figure 30) scales reveals that the sky-facing side of 'free' crops, which are not situated directly beneath PV modules, receives a notably higher level of irradiance compared to crops located under the modules. This contrast is distinct from the trends observed for the vertical sides of the crops' envelope. Furthermore, shading losses are higher during the summer season due to the sun's elevated position, leading to increased shading from the modules on the crops directly beneath them. In contrast, the winter season sees a lower solar trajectory, allowing more sunlight to reach the top of the horizontal, sky-facing part of the crops. This area is less affected by mutual shading between crop rows, resulting in improved sunlight exposure.

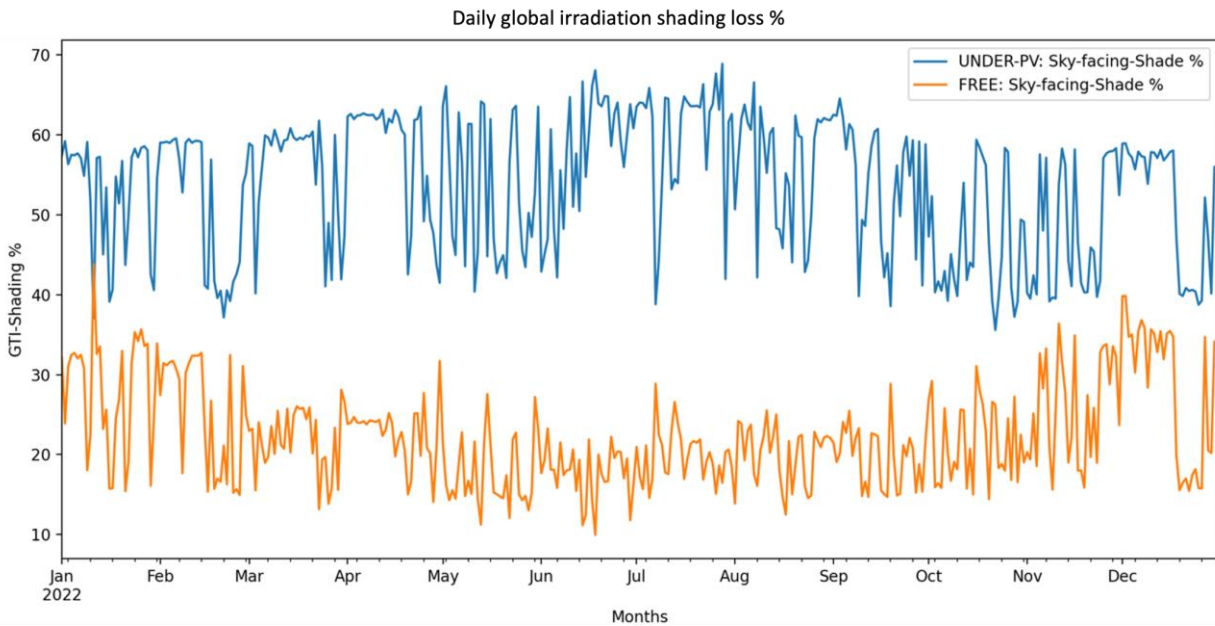


Figure 29: Daily shading loss percentage comparison for the sky facing side.

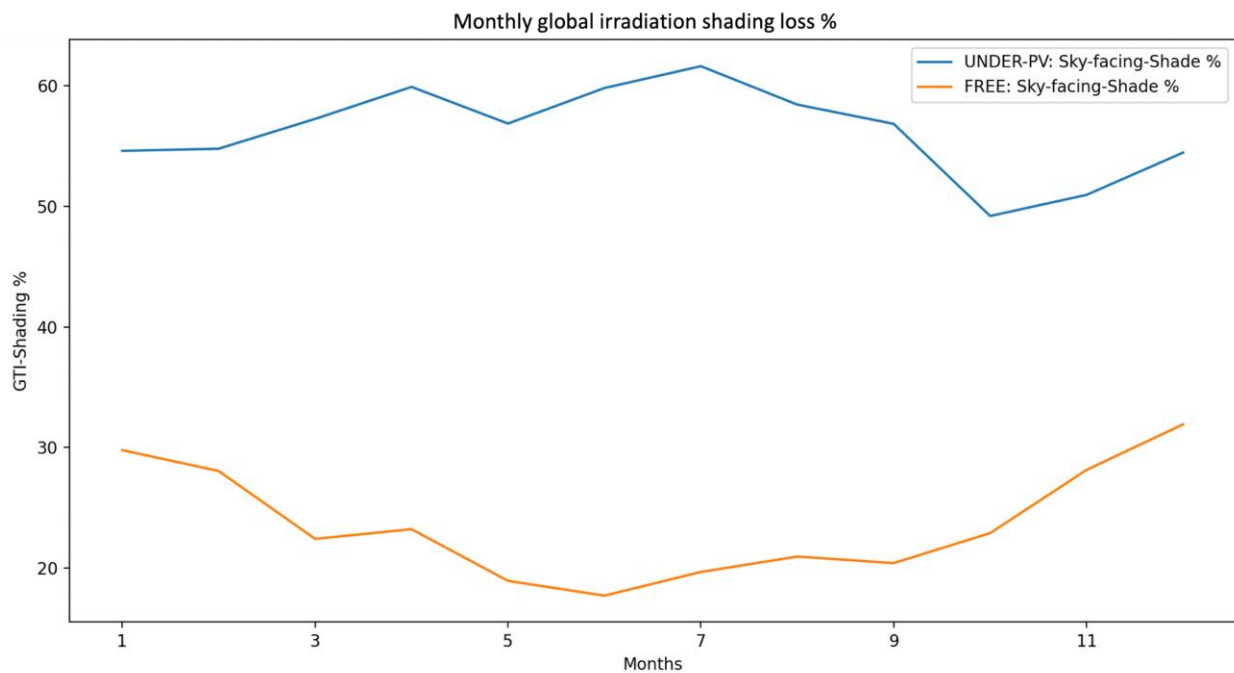


Figure 30: Monthly shading loss percentage comparison for the sky facing side.

The Following section presents the results for the 'New' plant in the similar fashion as above.

Figure 31 shows the evolution of global irradiance and the corresponding the shading loss percentage over all the sides of the 'Under-PV' crop and the individual respective zones, and Figure 32 shows the corresponding shading losses.

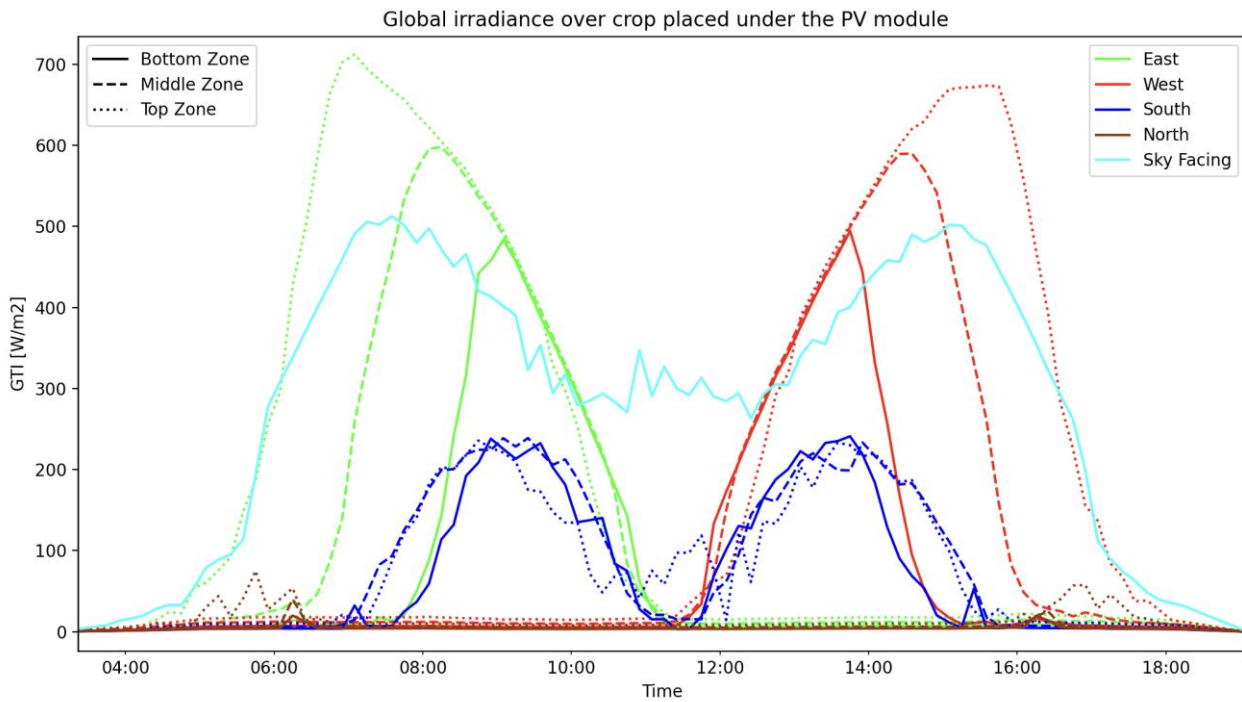


Figure 31: Global irradiance on 18th of July (TMY) for the crop under PV panels.

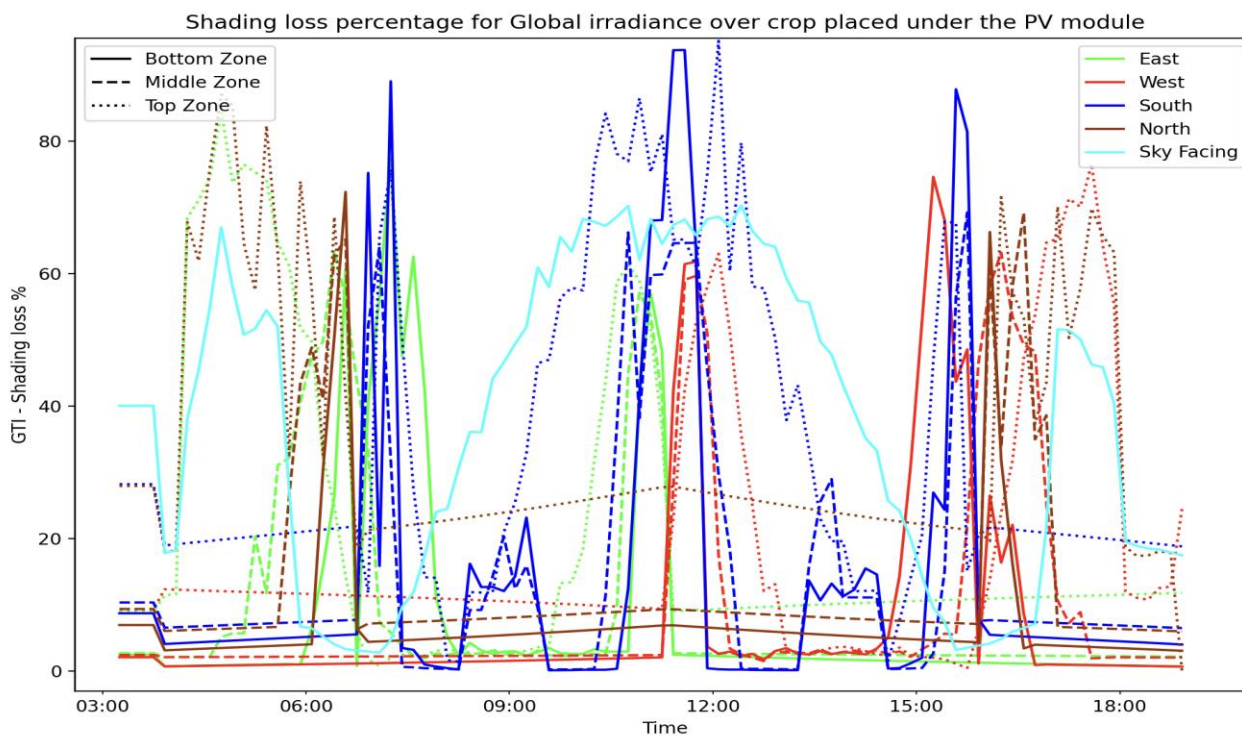


Figure 32: Shading loss percentage on the global irradiance for the 18th of July (TMY) for the crop under PV panels.

Figure 33 features a heatmap illustrating the daily pattern of global irradiance on the eastern side of the crop located beneath PV modules, for July 18th according to the Typical Meteorological Year (TMY) data. This heatmap zooms in on a designated area of interest within the broader agrivoltaic system setup. It highlights that irradiance is more intense at the top of the canopy than at the bottom, a disparity primarily due to the mutual shading effect among various crop rows. This phenomenon mirrors observations previously noted for crops situated in open areas without PV module coverage.

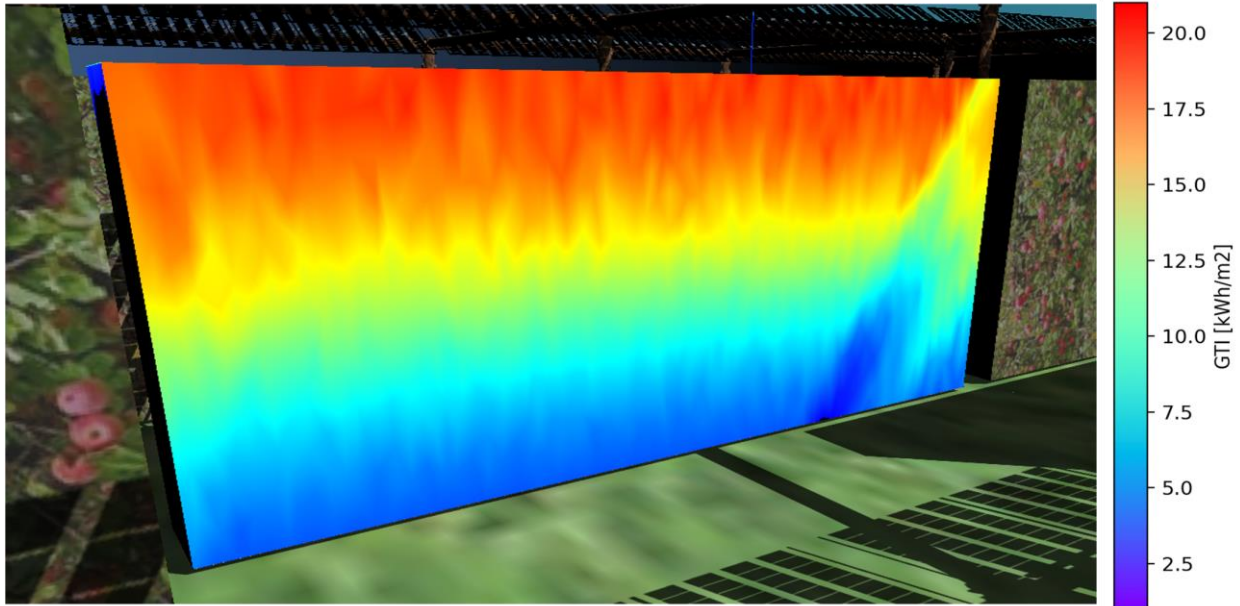


Figure 33: Heatmap showcasing total global irradiation for 18th of July (TMY) over the east facing side of the crop under PV modules.

Figure 34 and Figure 35 shows the evolution of global irradiance and the corresponding the shading loss percentage over all the sides of the 'Free' crop and the individual respective zones.

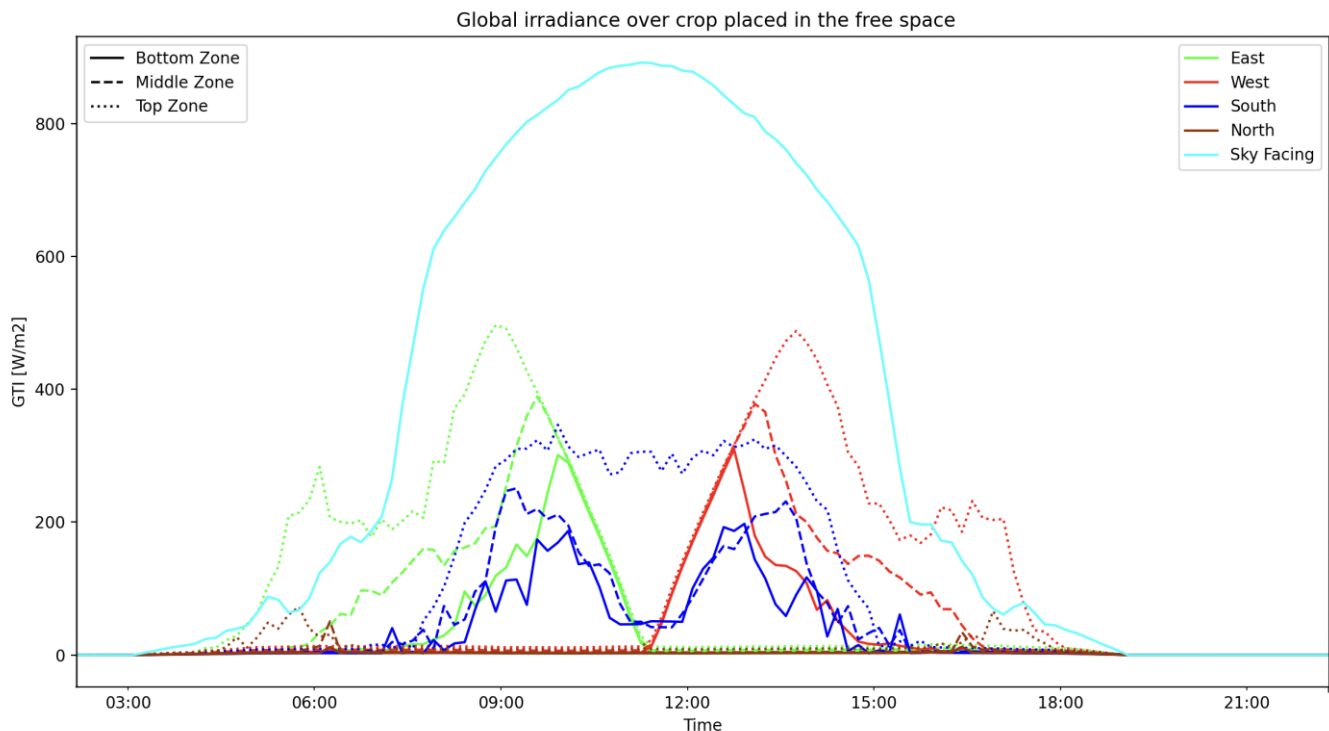


Figure 34: Global irradiance on 18th of July (TMY) for the crop under free space.

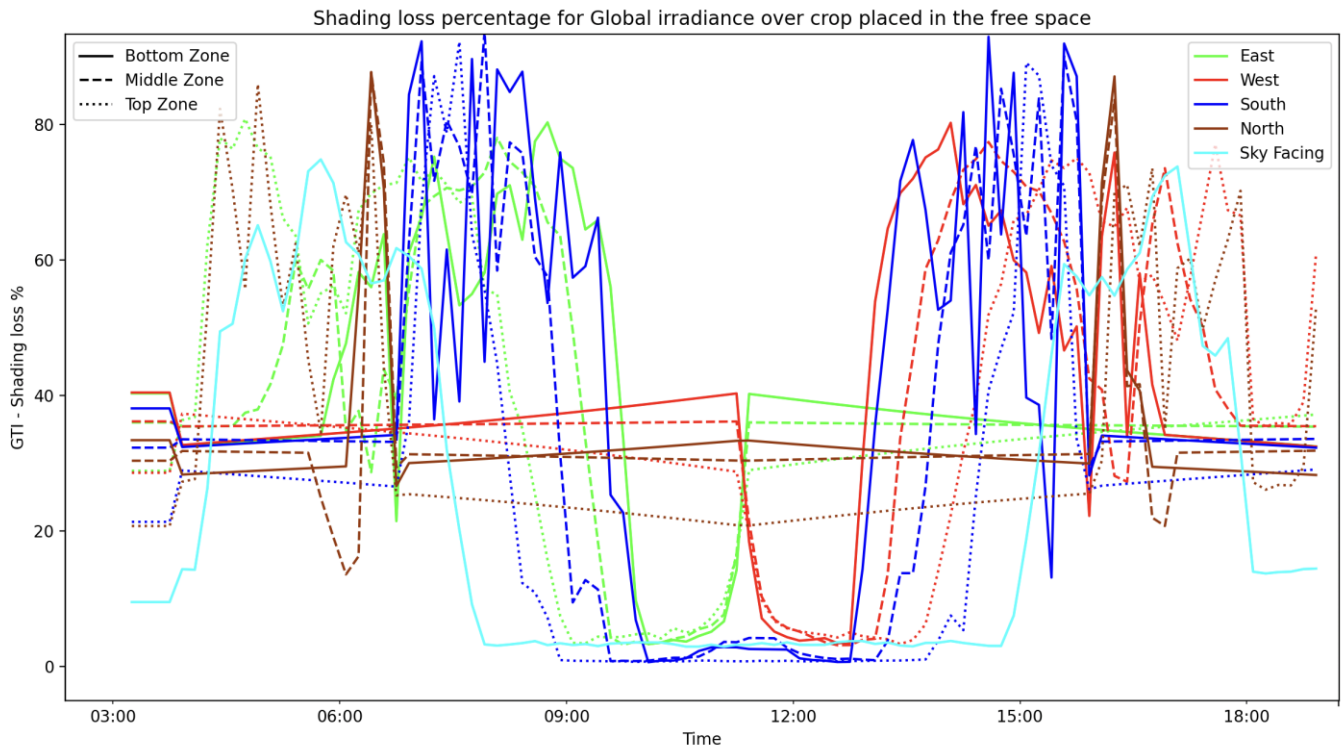


Figure 35: Shading loss percentage on the global irradiance for the 18th of July (TMY) for the crop under free space.

Figure 36 presents a heatmap that illustrates the daily pattern of global irradiance on the eastern side of the crop, which is situated beneath no PV modules, for July 18th, according to Typical Meteorological Year (TMY) data. This heatmap focuses on a specific area of interest within the larger context of the agrivoltaic system setup. It emphasizes that the irradiance is more intense at the top of the canopy than at the bottom. This variation is mainly attributed to the mutual shading effect among the different rows of crops.

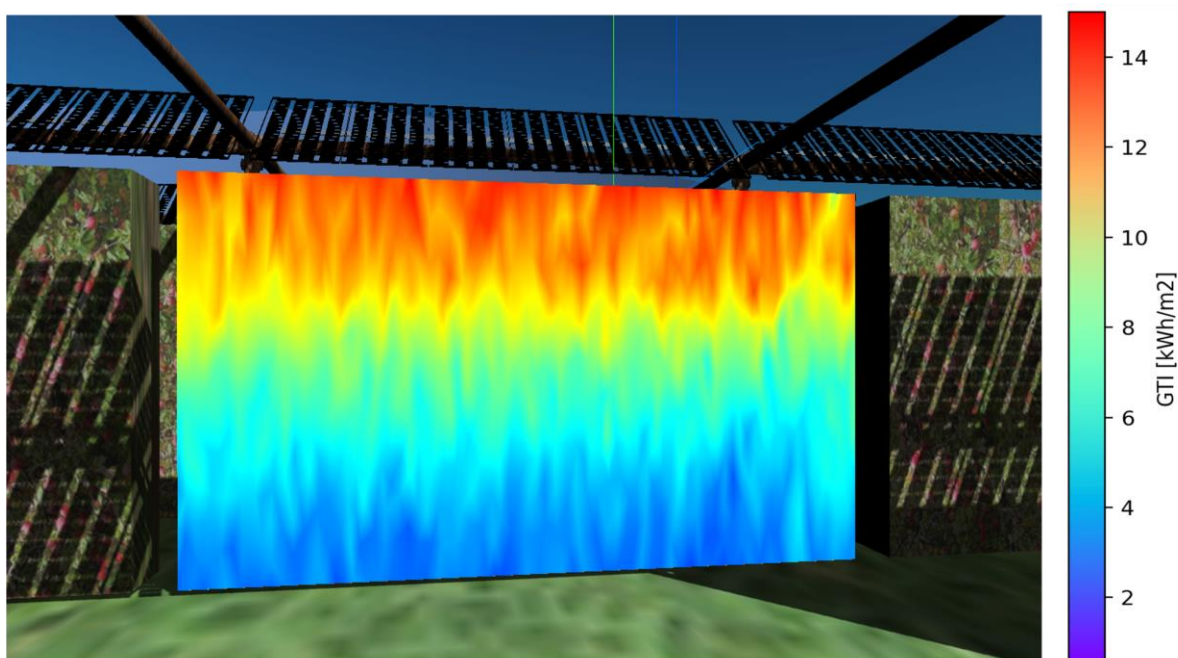


Figure 36: Heatmap showcasing total global irradiation for 18th of July (TMY) over the east facing side of the crop under free space.

For the 'Existing' plant the trend between the vertical face of the envelope and the sky facing horizontal surface has been evaluated, thus here the sky facing horizontal surface of both target's crop cuboidal envelope will be compared for the shading trend. In the similar fashion as above, Figure 37 shows the shading pattern on the two selected target crops' envelope's sky facing horizontal surface for a clear sky day on 18th July of the TMY time series.

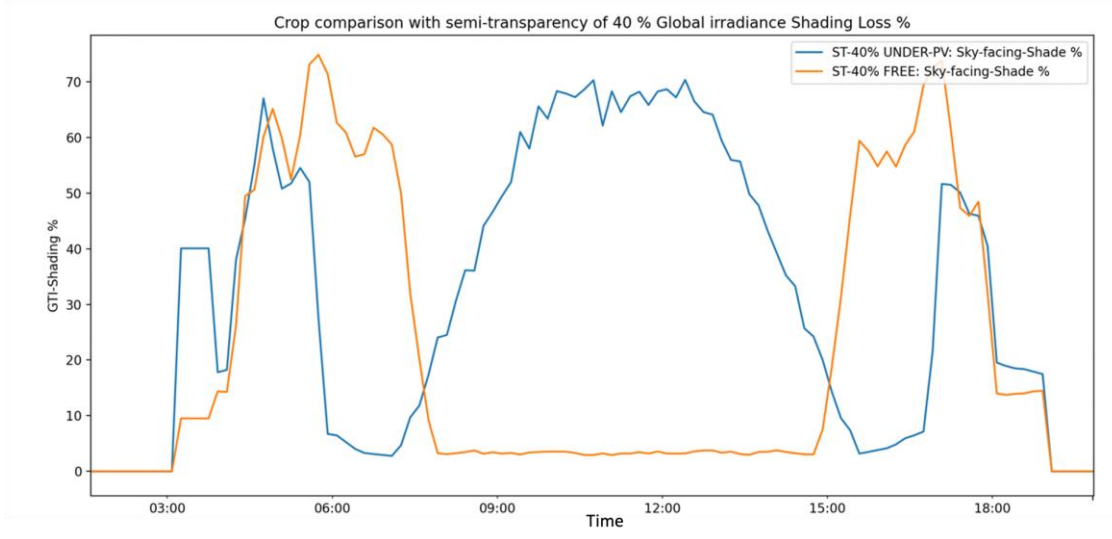


Figure 37: Shading loss percentage for 18th of July comparison for the sky facing side with PV modules of semi-transparency 40%.

To illustrate the differences in shading patterns, Figure 38 depicts the realistic image of shadows cast on the sky-facing side along with the corresponding heatmap for the timestamp 6:30 AM, while Figure 39 shows the same for the timestamp 12:00 PM.

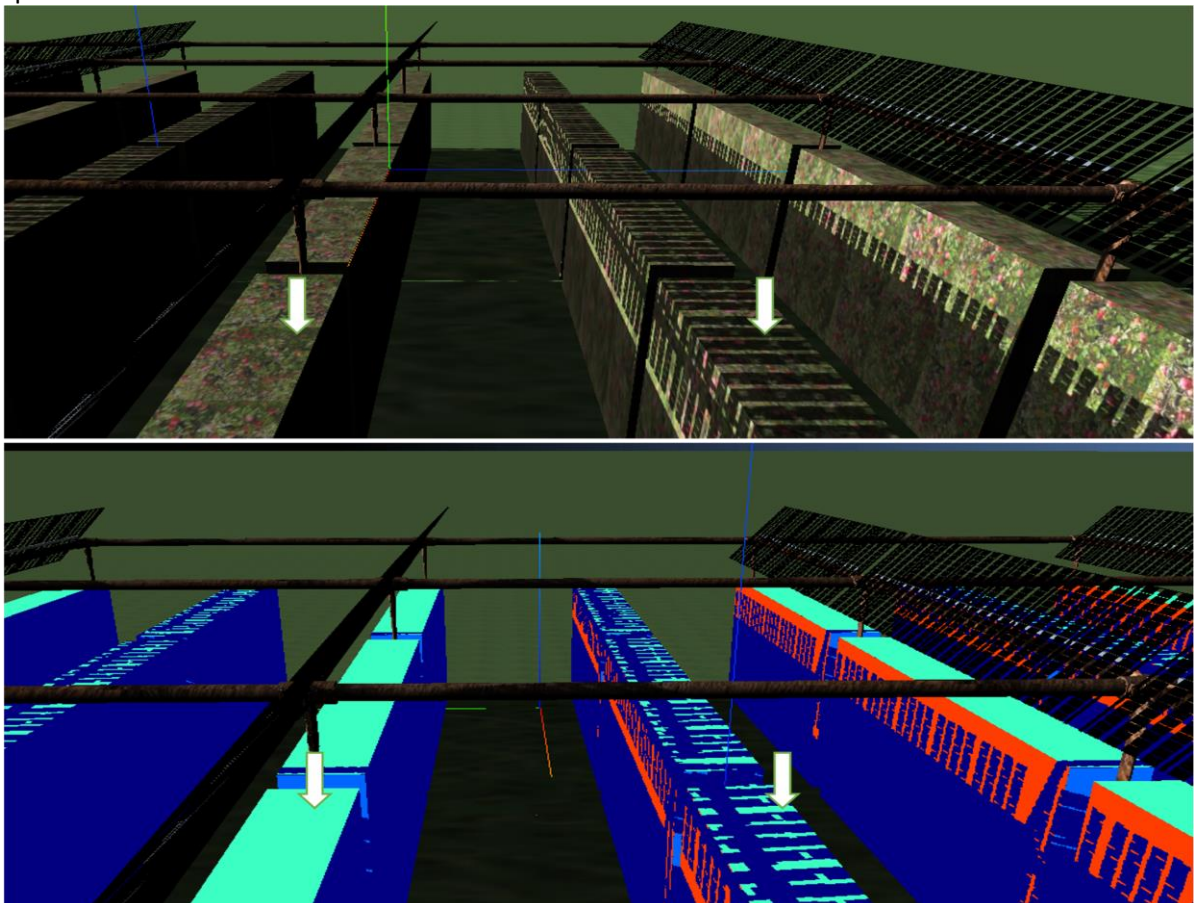


Figure 38: Realistic shading (above) and the corresponding heatmap (below) in 3D space at 6:30 on 18th July (TMY) for the sky facing side.

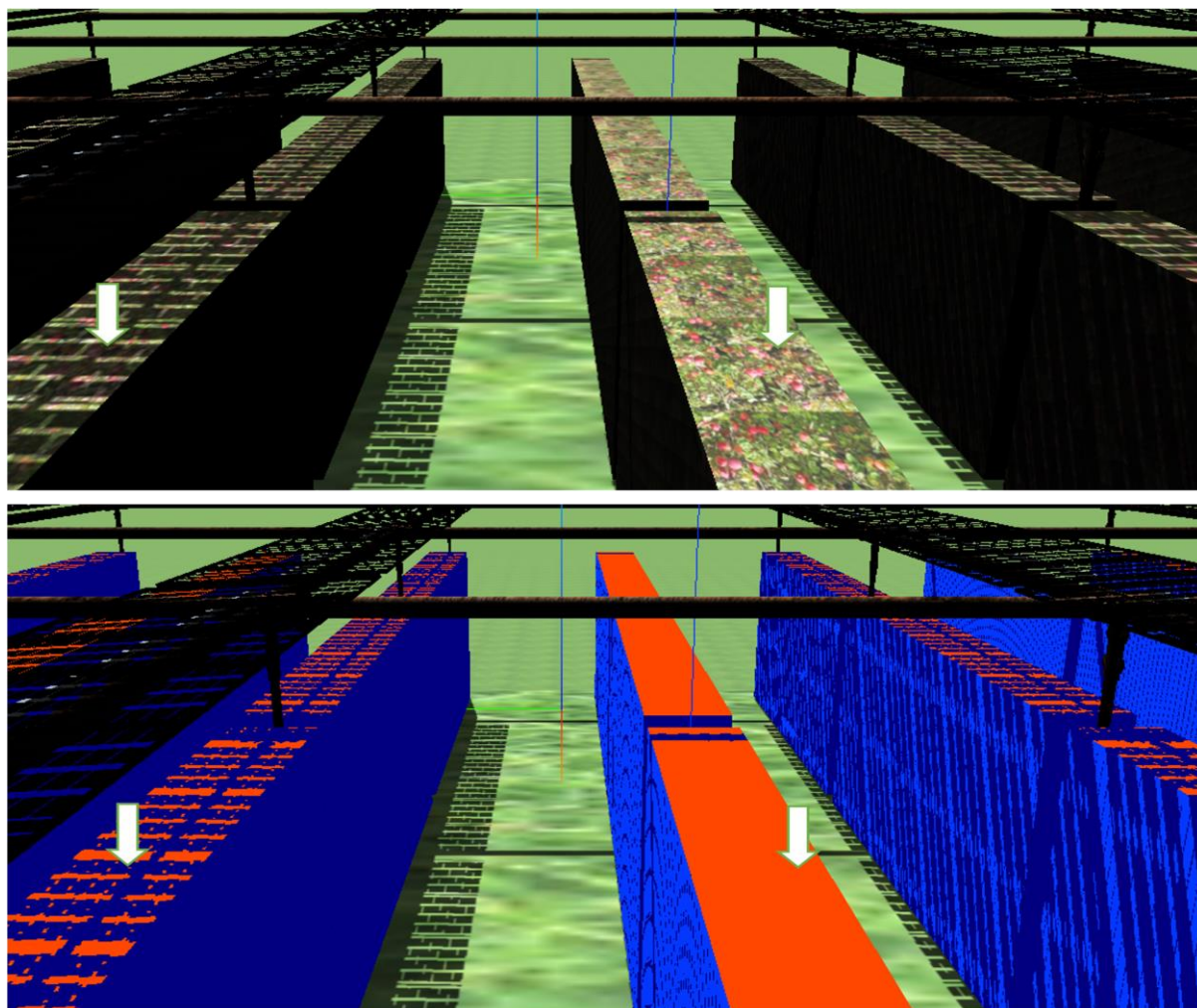


Figure 39: Realistic shading (above) and the corresponding heatmap (below) in 3D space at 12:00 on 18th July (TMY) for the sky facing side.

Aggregation of data on daily (Figure 40) and monthly (Figure 41 for semi-transparency 40% and **Figure 30** for semi-transparency 10%) scales reveals that the sky-facing side of 'free' crops, which are not situated directly beneath PV modules, receives a notably higher level of irradiance compared to crops located under the modules. This contrast is distinct from the trends observed for the vertical sides of the crops' envelope. Furthermore, shading losses are higher during the summer season due to the sun's elevated position, leading to increased shading from the modules on the crops directly beneath them. In contrast, the winter season sees a lower solar trajectory, allowing more sunlight to reach the top of the horizontal, sky-facing part of the crops. This area is less affected by mutual shading between crop rows, resulting in improved sunlight exposure.

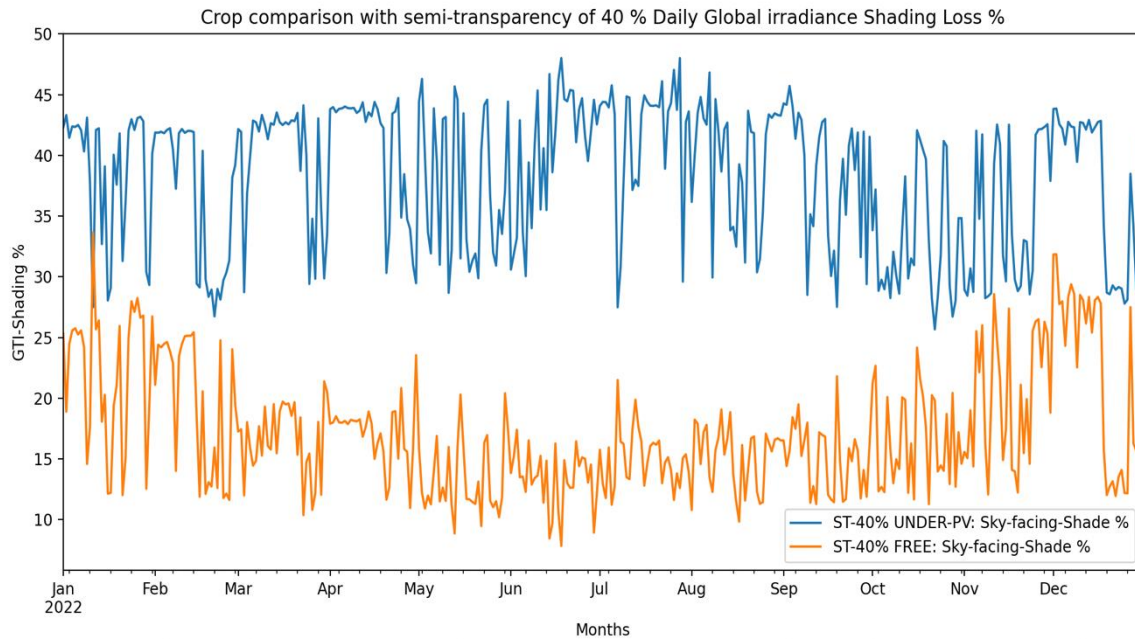


Figure 40: Daily shading loss percentage comparison for the sky facing side with PV modules of semi-transparency 40%.

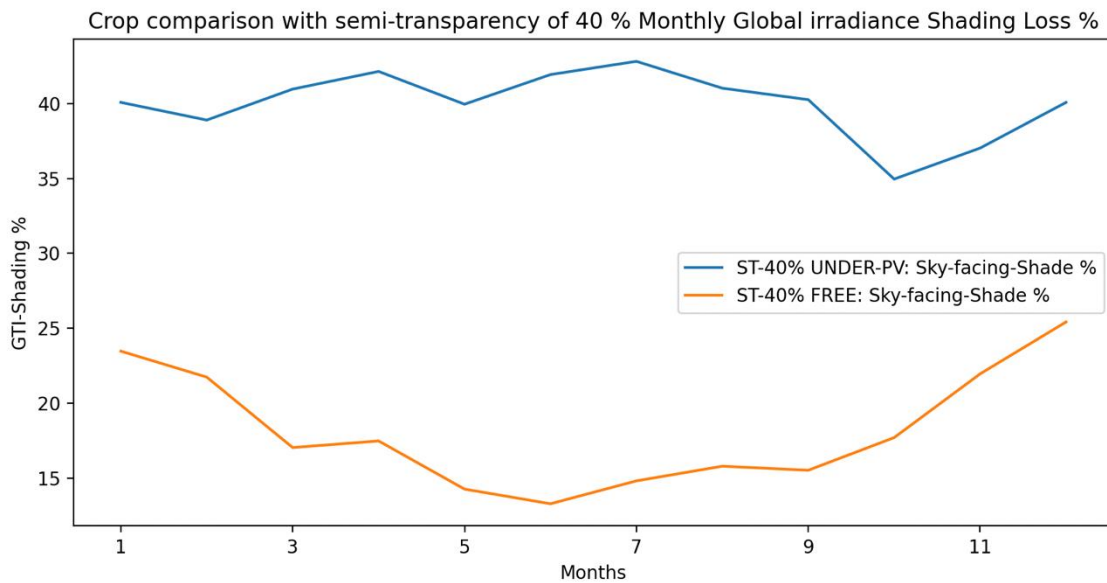


Figure 41: Monthly shading loss percentage comparison for the sky facing side with PV modules of semi-transparency 40%.

Figure 42 showcases a yearly shading loss comparison for crops under PV panels within both the 'Existing plant' and the 'New plant'. In contrast, Figure 43 illustrates the comparison for crops in free space. Observations reveal that crops beneath PV panels experience reduced shading losses, especially when attention is given to the vertical sides of the crop's envelope, which are pivotal for light absorption. This advantage is more noticeable in systems outfitted with semi-transparent PV modules as opposed to those with standard transparency modules. However, for the sky-facing horizontal side of the crop's envelope, crops placed in free space demonstrate improved outcomes, particularly when the system includes semi-transparent modules.

Crucially, the vertical sides of the crops are the primary drivers of photosynthesis due to their substantially larger effective collecting surface area for light. This makes the vertical orientation significantly more effective for photosynthesis than the horizontal surfaces, underscoring why optimal design often involves placing crops under PV modules. Besides enhancing photosynthesis, this arrangement also provides protective benefits against environmental threats such as hail, rain, and freeze, making it a highly advantageous setup for crop growth and protection.

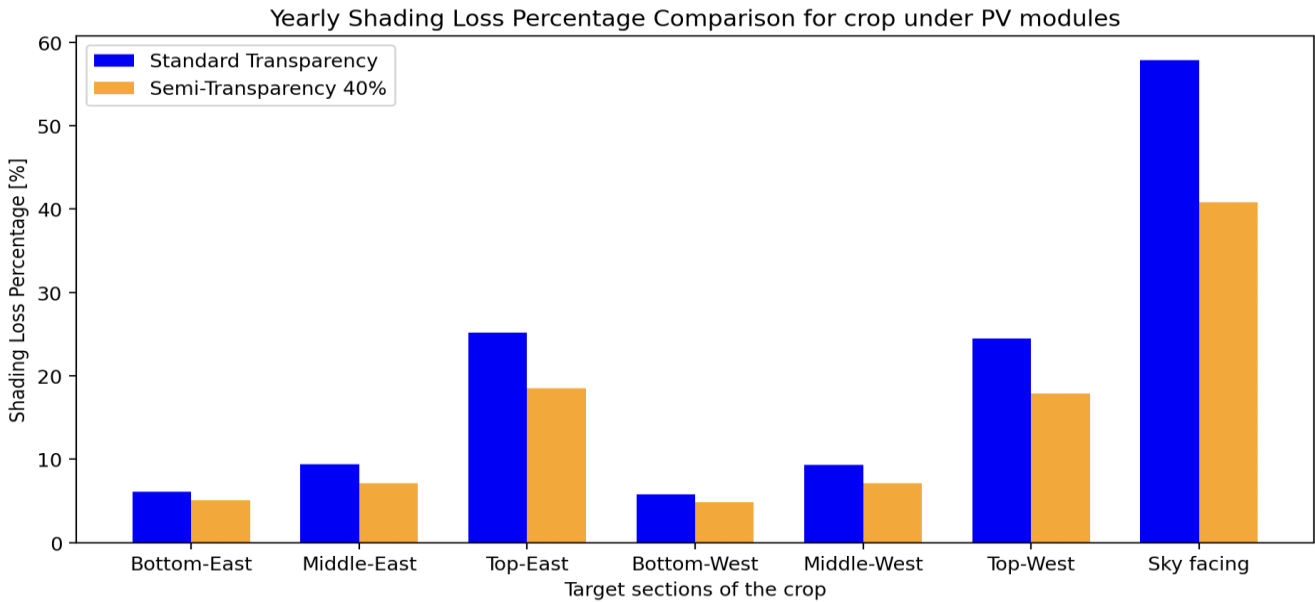


Figure 42: Yearly shading loss percentage for crop under PV modules in 'existing' and 'new plant'.

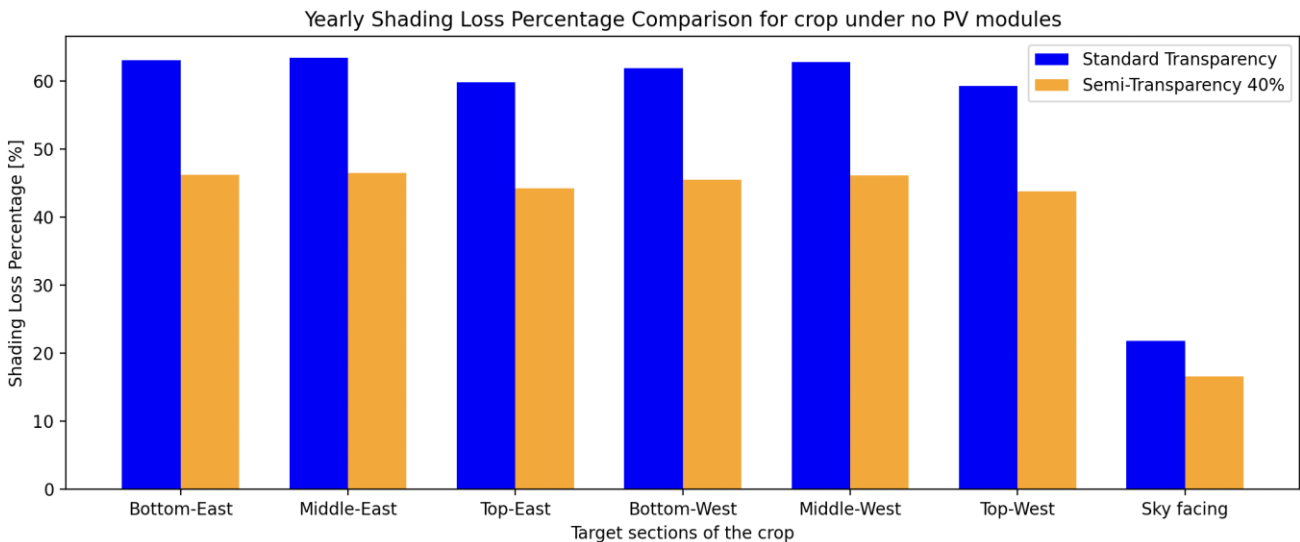


Figure 43: Yearly shading loss percentage for crop under no PV Modules in 'existing' and 'new plant'.

2.2.3. MODELLING BY IMEC

1. Methodology

1.1. Modelling approach

The geometric model of the crop (apple tree) is created using SketchUp Pro. A scene generator script in Python is then used to generate copies and the entire orchard based on the design specifications. Two apple trees representing a fourth of an orchard row are modelled with a length of 6.8 m in the N-S direction and a thickness of 0.7 m in the east-west direction. The height of each tree is 3.5 m. The vertical side of each crop/tree is divided into three equal sections: the bottom, middle and top zones. Given a tree height of 3.5 m, each section therefore has a length of 1.166 m. Figure 44 shows the design parameters of the apple orchard and the geometric model of the apple orchard trees.

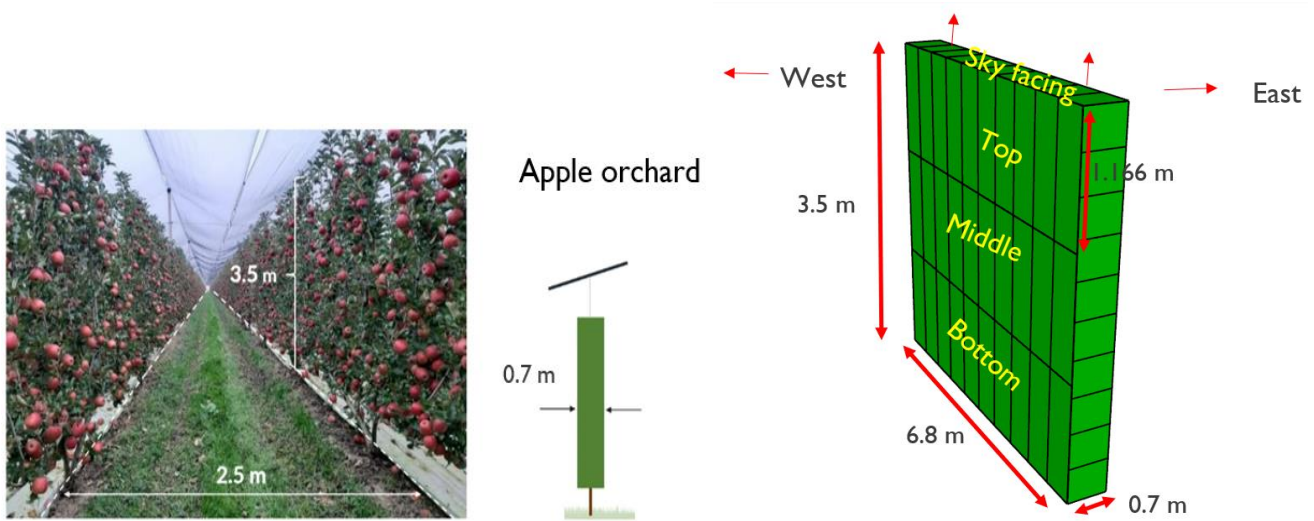


Figure 44: Left: Example of apple orchard used as guide in modelling. Right: Geometric model of apple tree created with SketchUp Pro. Crop model shows 4 zones (sky-facing, top, middle, and bottom of east and west sides) used to study the irradiance distribution.

To assess the shading on the different faces of interest, the shading loss percentage is also calculated for the “free crop” and crop under PV. The shading loss percentage is calculated as:

$$\text{Shading loss percentage} = \frac{G_{ref} - G_{AV}}{G_{ref}} \times 100$$

Where G_{ref} is the irradiance on the reference system (with no PV system) and G_{AV} is the irradiance in the agrivoltaic system. The reference system is vital for understanding the amount of light blocked by the PV modules and hence the percentage loss. Figure 45 shows the geometric model of the AV system.

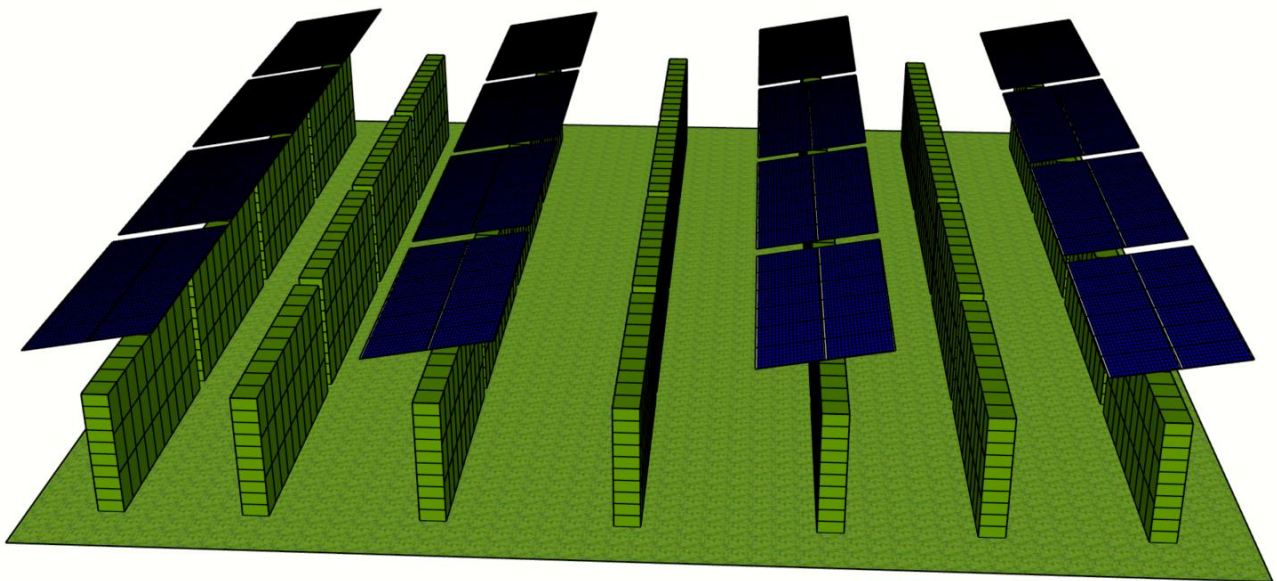


Figure 45: Layout of the AV orchard modelled in this work. Model is representative of the existing Bolzano system.

The irradiance on the two selected crop envelopes is determined for the sky facing side and the *top*, *middle* and *bottom* of the *west* and *east* sides of the two crop envelopes selected. The east and west sides (vertical sides) of the crop envelope take priority in the irradiance calculations because they are more effective in the photosynthesis process compared to the sky-facing part. Also, each crop row is considered to be long enough such that the impact of the north and south faces is considered to be insignificant. There are therefore 3 zones on the east side, 3 on the west side and the sky-facing side, amounting to 7 different zones per crop envelope where the total irradiance is calculated. Figure 46 shows the crop under PV module and the “free crop” (crop between rows of PV modules) used in the irradiance distribution calculations.

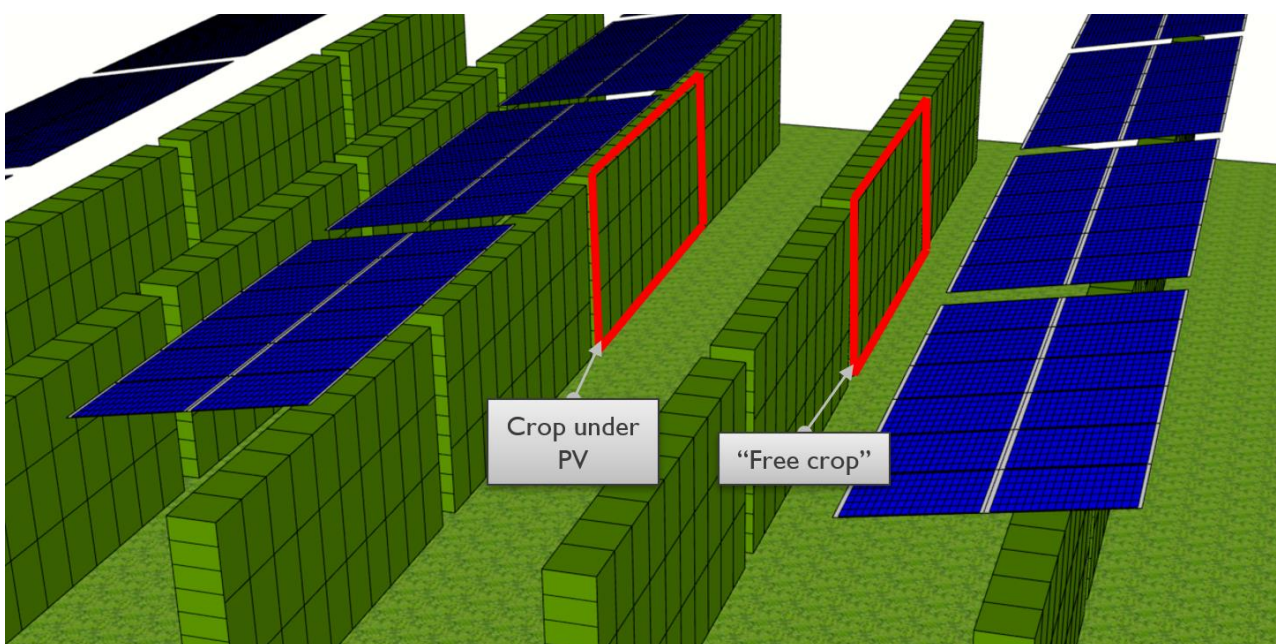


Figure 46: Illustration of crops used as targets for the irradiance distribution analyses.

1.2. Imec’s Framework

Figure 47 illustrates imec’s energy yield modelling framework, employing a rigorous bottom-up physics-based approach. This framework integrates precise irradiance and energy generation modelling, accommodating spatial and temporal variations. The coupled Electrical, Optical and Thermal (EOT) modelling framework requires first, measured meteorological data: ambient temperature, irradiance, wind speed and direction; second, material properties: optical, thermal, and electrical constants, thicknesses of each layer in the module; third, cell and module technology parameters such as electrical behavior of the cell, temperature coefficients, External Quantum Efficiency, module/cell interconnect layout serve also as input.

The Ray-tracing model uses the weather data to calculate the plane-of-array irradiation (GPOA) on all PV elements. The electrical model and thermal model use the cell, module, and array characteristics along with their thermal properties to derive the IV characteristics of the system.

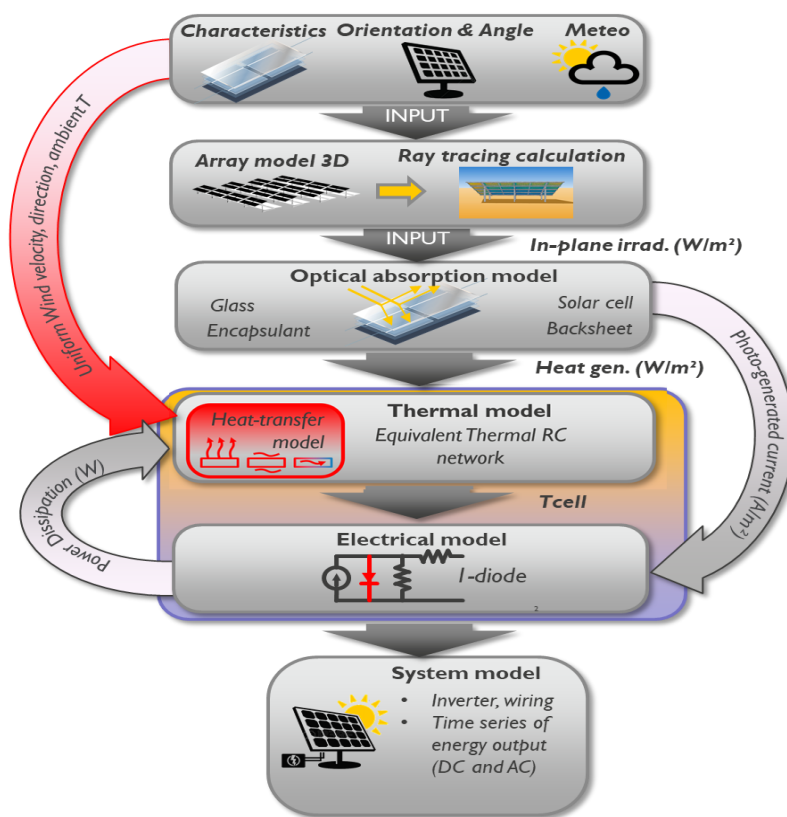


Figure 47: Imec’s energy yield simulation framework.

2. Results

The results presented here are the total irradiance on the crop envelopes and the shading loss percentage. For each of the crops studied (“free crop” and crop under PV), the total yearly irradiance on each of the 7 zones (sky-facing and the top, middle and bottom the east and west sides) is calculated and presented. Imec’s simulation framework can also be used to visualize the irradiance distribution on the different surfaces of interest such as the PV modules, the crops and ground. Figure 48 shows the total yearly irradiation on the different faces of the crop canopy for the open/reference AV system. It can be seen that the highest irradiation is recorded for the sky facing part of the open field, followed by the top, middle and bottom parts. The east side also receives more irradiation compared to the west side for each crop row.

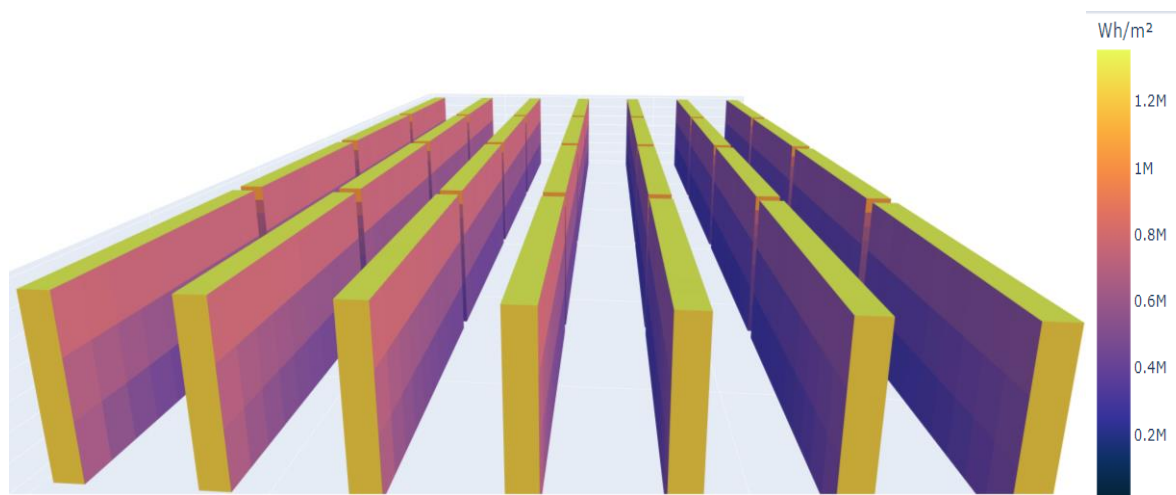


Figure 48: Total yearly Irradiation distribution for the open (reference) system.

The calculated values from the simulations for the reference system are shown in Figure 49.

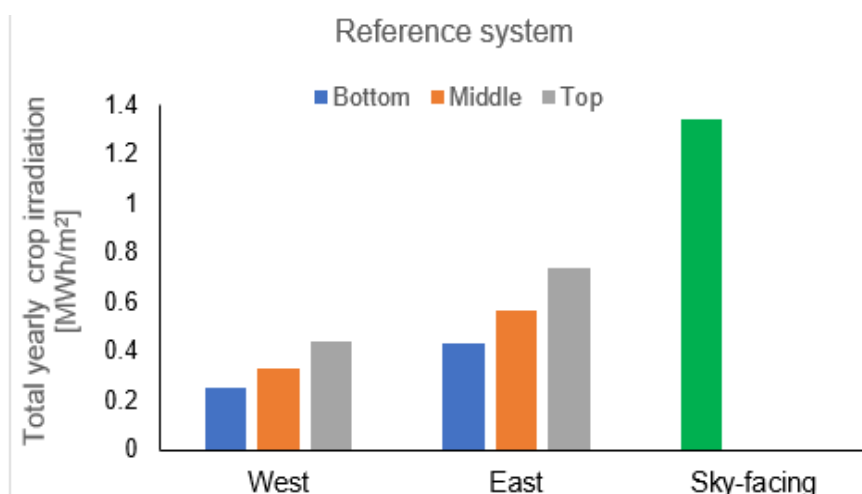


Figure 49: Calculated total yearly irradiation for the different faces of the crop canopy for the reference system.

Figure 50 shows the total yearly irradiation (MWh/m²) for the sky-facing and the top, middle and bottom of the east and west sides for the crop under the PV modules and the “free crop”.

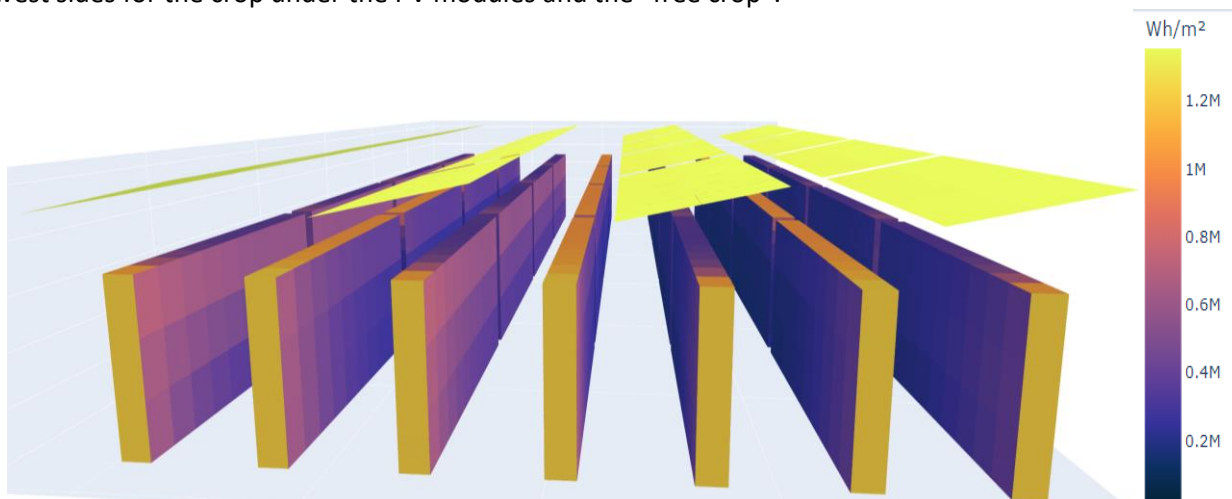


Figure 50: Total yearly Irradiation distribution on the crops and PV modules in the AV system.

On both the east and west sides, the top, middle and bottom of the crop under the PV module receive more irradiation than the “free crop” as seen in Figure 51. This is because the “free crop receives more shading from the neighbouring PV rows during sunrise and sunset periods. However, around solar noon, the “free crop” is not shaded and hence, its sky-facing part receives higher irradiation than the crop under PV module. It can also be seen that for both east and west sides of the “free crop” and crop under PV, the top zone receives the highest irradiance followed by the middle and the bottom zones.

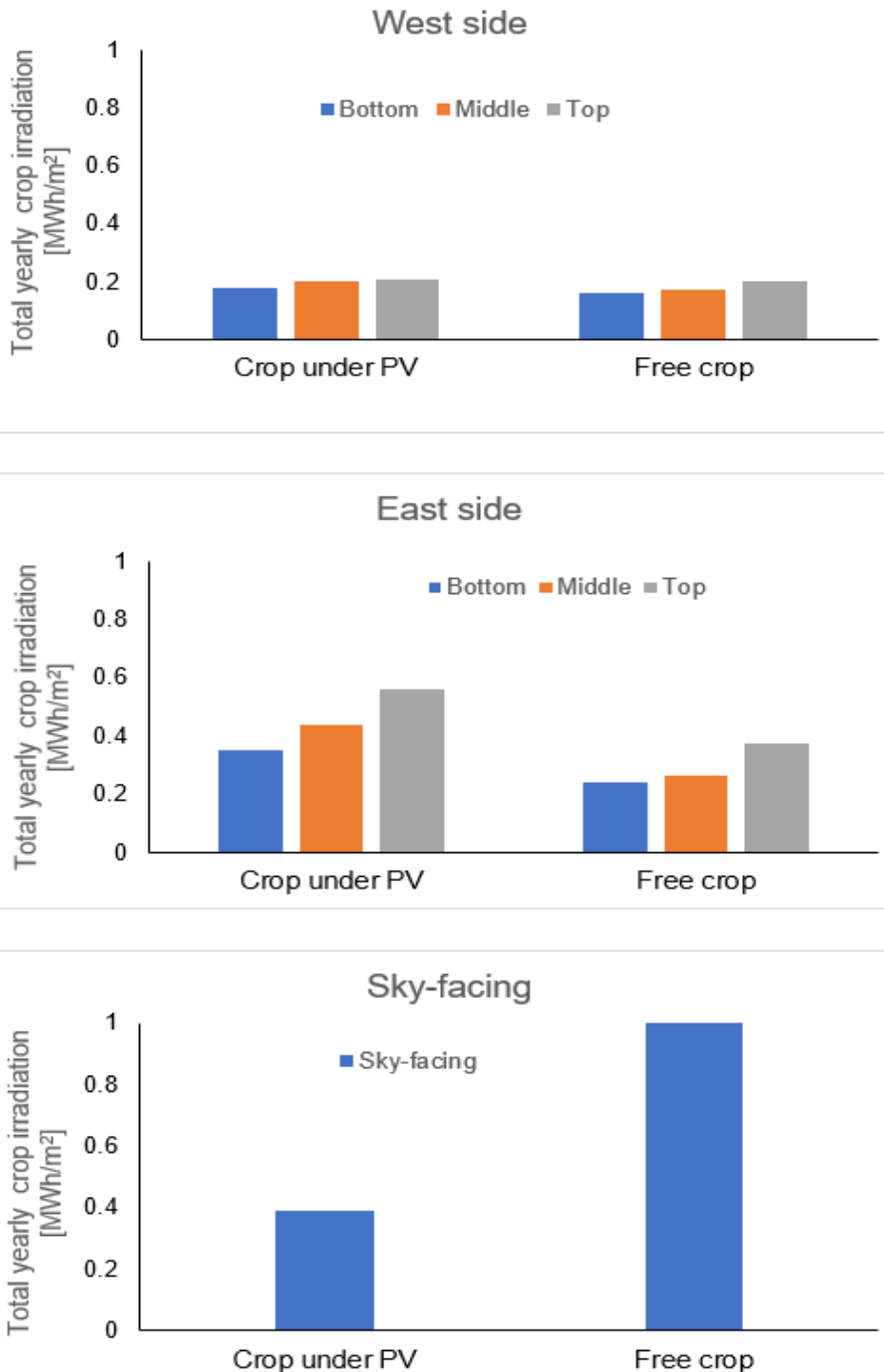


Figure 51: Calculated total yearly irradiation on the different faces of the AV system.

The visualization of the total daily irradiation for a clear sky day (July 18th) is shown in Figure 52. The straight lines represent the crop under PV modules while the dotted lines illustrate the “free crop”. It illustrates the higher irradiance received during the morning (east side) compared to the sunset periods (west side). We also see the highest irradiance for the sky-facing zone of the “free crop”.

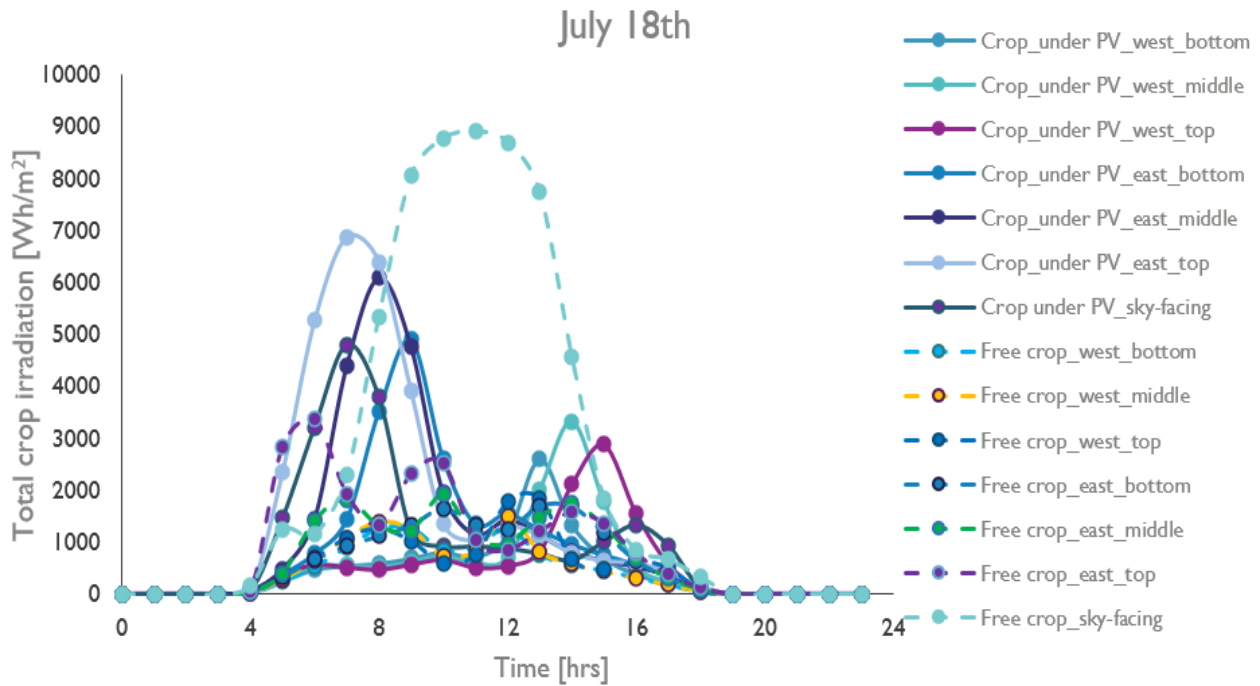


Figure 52: Crop canopy irradiation distribution for a clear sky day in July.

The yearly percentage of shading induced by the PV modules compared to a reference (open field) is calculated and presented for the different surfaces as shown in Figure 53. The installation of PV modules above crops leads to shading of the crops. The shading loss percentage therefore tells us how much of the crop incident light is lost due to the presence of the PV modules. On both the east and west sides, the “free crop” experienced more shading loss than the crop under PV. On the west side, the bottom zone experienced the least shading loss followed by the middle and the top for both the crop under PV and the “free crop”. The sky-facing zone of the crop under PV had the highest shading loss of about 71%.

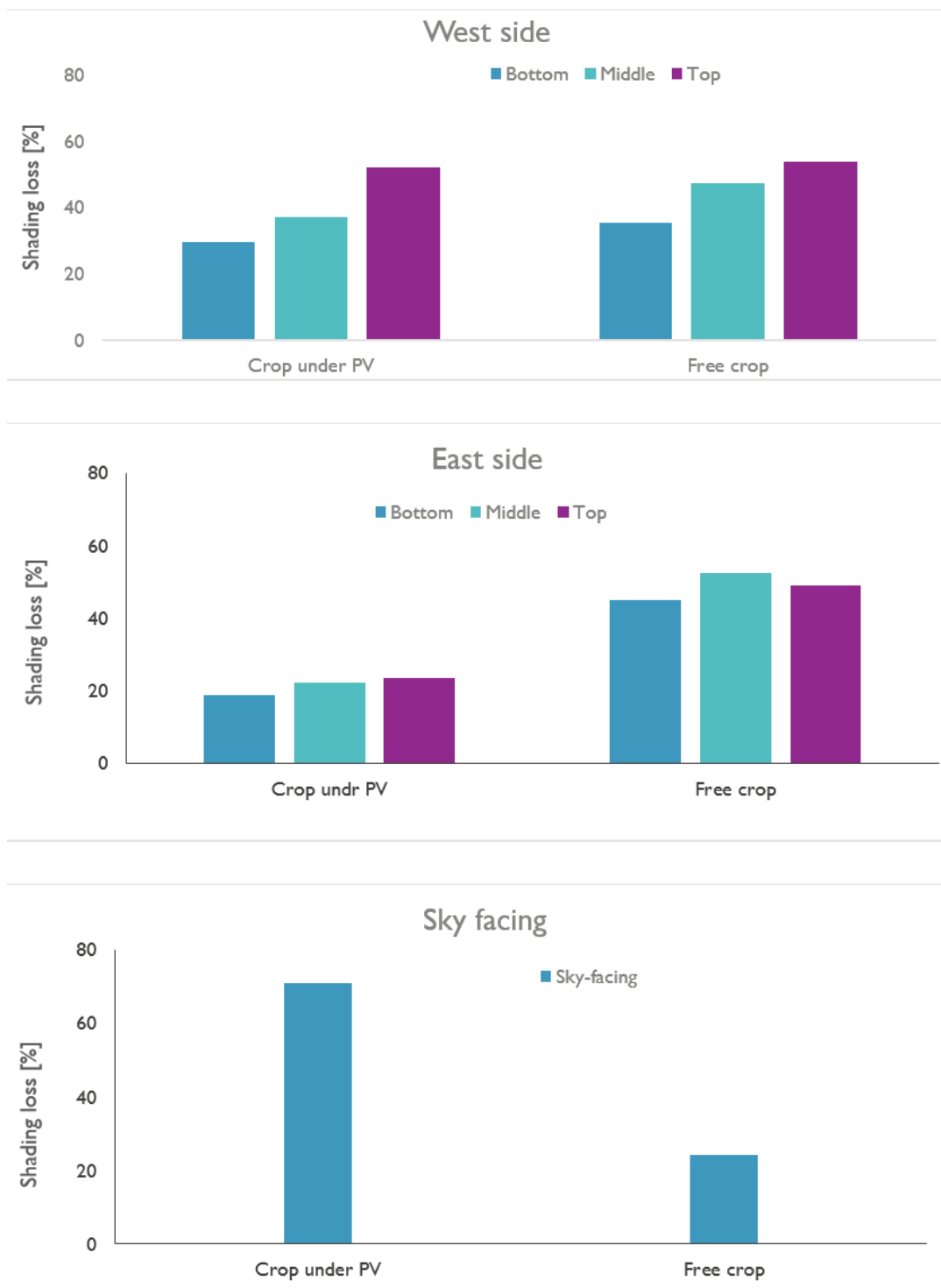


Figure 53: Shading loss for the different zones of the crop canopy.

3. Energy yield: Modelling parameters

During the geometric modelling, optical material properties were assigned to the different geometric components in the AV system. The PV cell is considered opaque with a low reflectivity value of 0.03. The glass is considered transparent with a normal transmittance of 98% and refractive index of 1.53. The PV module aluminium frame is also considered opaque. The ground component of the system is given a standard albedo similar to grassland or bare soil, with a value of 0.22. Table 5 shows a summary of the optical and radiance parameters for the different components.

Table 5: Optical material properties of geometric components.

<i>Geometric component</i>	<i>Optical properties</i>	<i>Radiance material properties</i>					
<i>PV cell</i>	<i>0.03 normal reflectivity</i>	<i>Plastic</i>	<i>0.05</i>	<i>0.05</i>	<i>0.05</i>	<i>0</i>	<i>0</i>
<i>Glass</i>	<i>1.53 refractive index 98% transmittance</i>	<i>glazing</i>	<i>0.9</i>	<i>0.9</i>	<i>0.9</i>	<i>0</i>	<i>0</i>
<i>Frame</i>	<i>opaque</i>	<i>Metal</i>	<i>0.5176</i>	<i>0.5294</i>	<i>0.5373</i>	<i>0.8</i>	<i>0.1</i>
<i>Soil</i>	<i>0.22 albedo</i>	<i>-</i>	<i>-</i>	<i>-</i>	<i>-</i>	<i>-</i>	<i>-</i>

The PV module electrical performance parameters are obtained from the data sheet of the LEO 415W PV module as shown in The V_{OC} temperature coefficient is -0.26 %/K.

Table 6: Electrical datasheet of LEO 415 W PV module used in energy yield simulations.

ELECTRICAL DATA (STC)			LEO L64S400	LEO L64S405	LEO L64S410	LEO L64S415
Rated power	P_{MPP}	[W]	400	405	410	415
Rated voltage	V_{MPP}	[V]	31.14	31.34	31.53	31.72
Rated current	I_{MPP}	[A]	12.84	12.92	13.00	13.08
Open-circuit voltage	V_{OC}	[V]	37.08	37.20	37.32	37.44
Short-circuit current	I_{SC}	[A]	13.46	13.55	13.63	13.71
Efficiency	η	[%]	20.0	20.2	20.5	20.7

Electrical values measured under standard test conditions (STC): 1000 W/m²; 25 °C; AM 1.5

To maintain the accuracy of the simulation while reducing the computational time, the resolution of the sky using the Reinhart patch subdivision was kept at 1. The simulation was also performed at module level and for a monofacial module, only the front side was targeted. Table 7 shows the radiance and simulation parameters.

Table 7: Radiance and simulation parameters used in this work.

<i>Points per surface</i>	<i>25</i>
<i>Reinhart_skypatch_subdivision</i>	<i>1</i>
<i>Ray tracing_level</i>	<i>Module</i>
<i>Granularity</i>	<i>Module</i>
<i>Simulated side</i>	<i>Front</i>

4. Power curves and energy yield

The power curve for a clear sky day (July 18th) is shown in Figure 54 below. The power curve has a uniform round, bell-shape as the output increases during the morning, peaks around midday and gradually reduces in the afternoon to sunset.

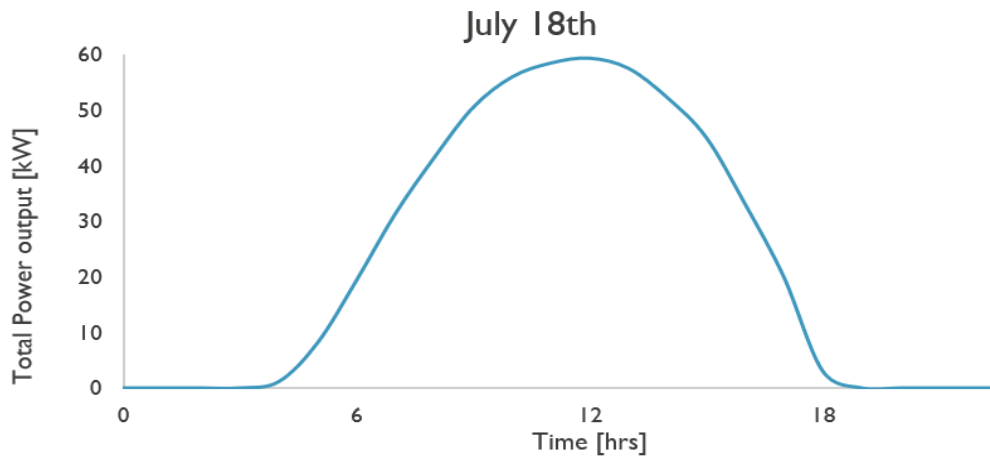


Figure 54: Power output for a clear sky day in July.

For the AC energy yield, an inverter conversion efficiency of 97% is used in the calculations. Losses due to soiling are neglected. However, the soiling rate in AV systems is generally higher than ground-mounted PV systems due to agricultural activity such as tilling and harvesting. In the simulated system with a low tilt angle of 10°, the soiling rate is expected to be much higher. Mismatch losses are also neglected. Figure 55 shows the total monthly energy yield for the AV system.

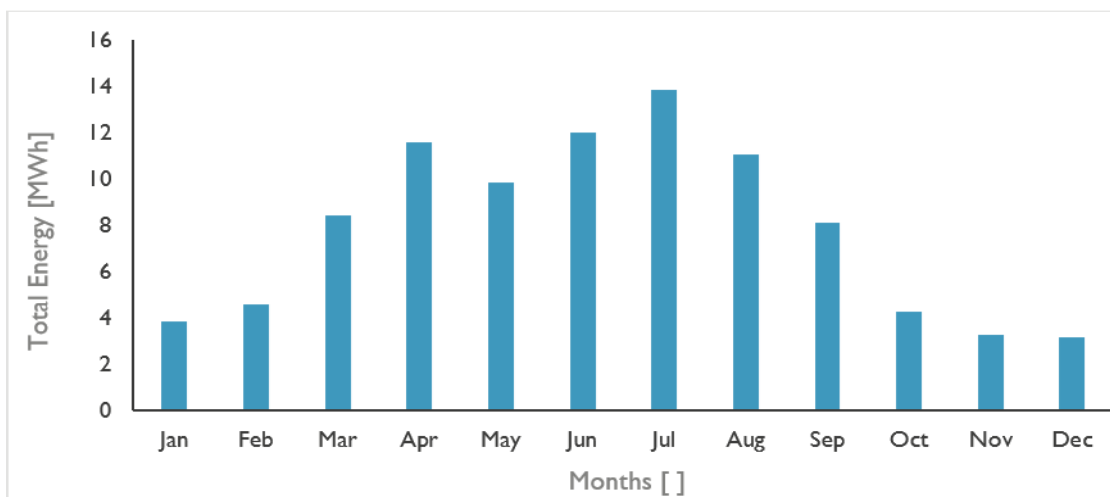


Figure 55: Monthly energy yield for the AV system.

2.2.4. MODELLING BY DELFT UNIVERSITY OF TECHNOLOGY (TU DELFT)

1) Methodology

An apple orchard is composed of multiple strips of trees trained to grow in a specific manner, optimizing light interception. The Guyot training system, illustrated in Figure 56, effectively reduces the width of each strip, enabling a two-dimensional (2D) analysis by modelling the surface as a thin, dielectric, which we call translucent virtual canopy. Optical properties were estimated based on individual leaf characteristics, with transmittance adjusted by the canopy’s gap percentage (fraction of the total surface area not covered by leaves). The virtual canopy was divided into three sections each with its own transmittance, capable of reflecting the decreasing leaf density towards the top.

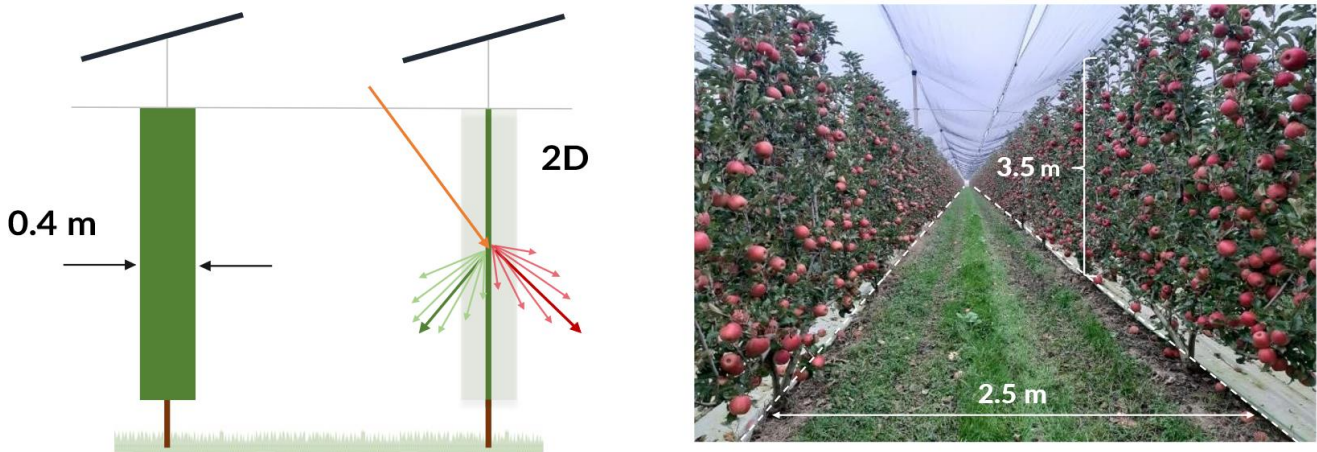


Figure 56: Cross-section of the apple orchard with Guyot tree training. The default pitch and maximum tree height are shown on the right.

Modelling fruit crop agri-PV systems can be challenging due to complex geometries and materials with non-Lambertian optical properties. Raytracing, and the algorithms of *Radiance* [10] addresses these challenges. Its functionalities have been extended to Windows through a Python wrapper, called *bifacial_radiance*, developed by NREL [11] TU Delft tailored the tool for agri-PV applications and optimization workflows, as depicted in Figure 57, outlining the essential steps for such simulations. At first, the scene is set which includes the 3D geometries and their optical properties (both specular and diffuse). Following, the sky is discretised, and each sky patch is assigned with a radiance value. This information is organised and stored allowing Radiance to quickly determine how light interacts with each surface. The simulation accuracy and resolution are then defined allowing raytracing to be initiated. Finally, irradiance can be further processed to determine yields or other key performance indicators. Computational time scales almost linearly with simulation resolution (number of irradiance scan points). Therefore, the results presented here describe the irradiance distribution within an apple tree at the centre of a farm consisting of 15 strips. In other words, border effects are omitted, which is a reasonable simplification.

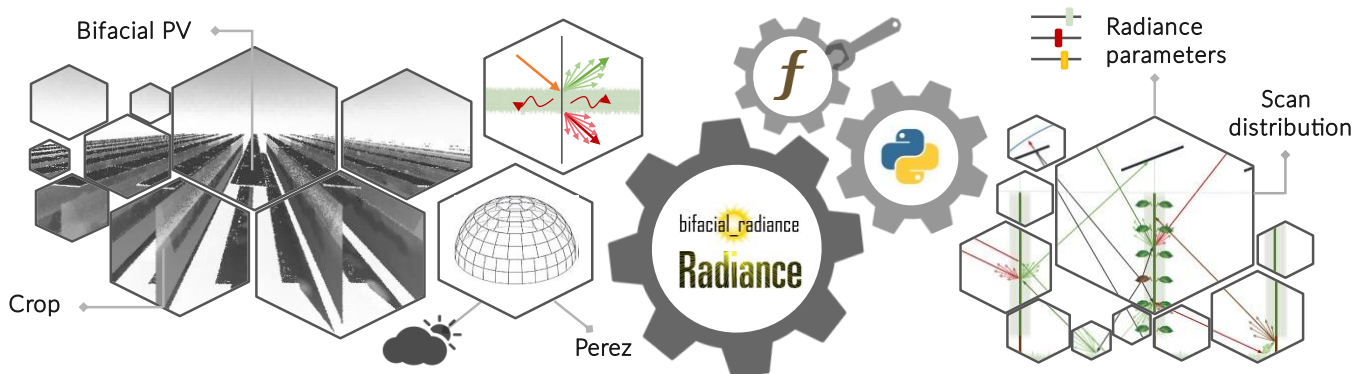


Figure 57: Simulation framework overview.

2) Modelling inputs

Table 8 provides a summary of the modelling inputs taken into account for the agri-PV simulations

Table 8: Summary of the modelling inputs taken into account for the agri-PV simulations.

Weather file

Local weather file received from EURAC with right labelled data. The DIRINT DNI decomposition was utilized and hours with GHI below 30 W/m² were filtered¹ to reduce computational burden.

Land parcel

Latitude and longitude of 46.38°, 11.29°, respectively. Dimensions of existing plant (22.4 m x 28.9 m), and new (15 m x 57.7 m) with a deviation in the N-S axis by 20.3° clockwise.

Orchard

The simulation period is from March to September which represents the growing season. The canopy was assumed to be fully developed with a 2D multi-leader (Guyot) tree training system.

Max tree height: 3.5 m

Default # of strips: 15

Default strip pitch: existing - 3.2 m, new plant - 2.5 m

PV system

Module width x length:	1.13 m x 1.76 m
Number of cells:	144 (half-cut)
Active module area:	1.75 m ²
Hub height:	1 landscape 4 m, 1 portrait 4.5 m
Pitch:	2.5 – 6.4 m
Tracker limit angles:	± 60°
Tracking algorithm:	True & backtracking
Bifaciality factor:	80%

Optical properties

Aggregated spectral resolution (broadband) with a range from 300 to 2800 nm. Average annual albedo of 21.6%; however, monthly values were utilized. Typical leaf reflectance of 21.4%. Estimated virtual canopy transmittance 38-87% f(z).

Glass transmittance: 90%^{2,3}

Aluminium frame reflectance: 56.8%²

Galvanized steel reflectance: 32.7%²

PV cell reflectance: 10%

Sampling points

Distributed around the central tree of the farm and placed horizontally. 7 sensors in total: 3 per side, and 1 at the top. In POA irradiance calculations one sensor was placed at the center of each PV module side.

Modelling additional

Faiman (modified) was used as the temperature model. The Schlick IAM model was adopted for the front side, and the Martin & Ruiz for the back. Soiling losses were ignored.

Mismatch losses: 1%⁴

MPPT, cabling losses: 1%

Inverter losses: 5%

¹ When these hours were filtered, the annual AC yield reduced by 0.3%. We expect similar reductions with crop yield as light utilization of plants is much lower than that of PV modules.

² Directional 10° hemispherical reflectance or transmittance.

³ The front and rear PV glass was omitted from crop irradiance simulations.

⁴ This is the mismatch loss within a module. Border effects are not considered here.

3) Results and discussion

3.1) Crop irradiance under an open field (full sun)

First, it is essential to acquire information about the natural light levels within the farm under an open field, also known as Full Sun (FS) condition. The heatmap in Figure 58 illustrates this variation in annual irradiation throughout the farm, excluding the shading caused by the PV array. As expected, the outer strips (S1 and S15) were exposed to more light, while the inner strips (S2-S14) experienced row-to-row shading. Consequently, light penetration from the sides is limited to at most 2 strips. In other words, not all rows need to be analyzed but rather focus on the central one only. Edge-effects were also present along the length; however, after a few meters, the variation was negligible. On the other hand, light gradients along the height of the canopy were significant. This was a result of the higher density of leaves in the lower canopy, while at the top, there were only a few branches. For each strip, the variation in irradiation is shown along the length (y-axis) and along the height of the orchard (x-axis) for both west and east facing sides. Going through S1 from left to right, one can observe the rise in irradiation along the height of its west-facing side with light levels peaking at the top of the canopy. Light levels decreased sharply along the height of the east-facing side as it experienced shading caused by neighbouring rows.

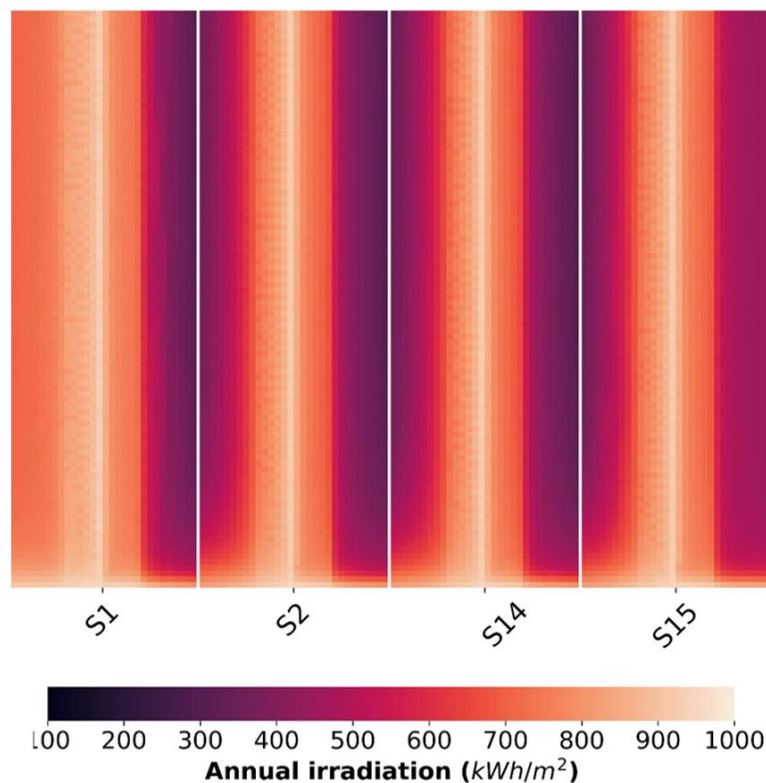


Figure 58: Average light distribution within a year throughout the farm in open-field condition. S1 to S15 represent the crop strip number from west to east.

3.2) Crop irradiance under the agri-PV array

Various agri-PV setups, including fixed and tracking systems were explored. Our analysis revealed that tracking systems performed better than fixed ones in the given climate conditions. Consequently, the two scenarios depicted in Figure 59 involve different east-west (E-W) tracking configurations. To evaluate performance, we compared the average crop irradiance under these scenarios with other light-related parameters. Although the entire growing season was

simulated, Figure 60 focuses solely on two specific days with clear skies. In existing literature, Global Horizontal Irradiance (GHI) has often been used as a proxy for open-field conditions. However, GHI does not accurately represent actual light conditions, particularly when crops with tall canopies cause significant row-to-row shading. There is also a misconception that shading, if it occurs, should happen in the afternoon. While afternoon shading can be beneficial in summer, as seen in the dip in the photo-saturation region, it is not ideal during spring when higher crop temperatures promote growth and light absorption.

Both scenarios, illustrated in Figure 59, provide adequate light for growth. Scenario 1 established a more suitable shading schedule, whereas Scenario 2 with alternating rows of modules resulted in undesirable effects such as light unevenness. Areas without modules received no protection at noon and experienced heavy shading in the morning and afternoon, potentially reducing daylight hours. Despite maintaining default tree density and having a cost-effective PV design, Scenario 2 did not support crop growth effectively.

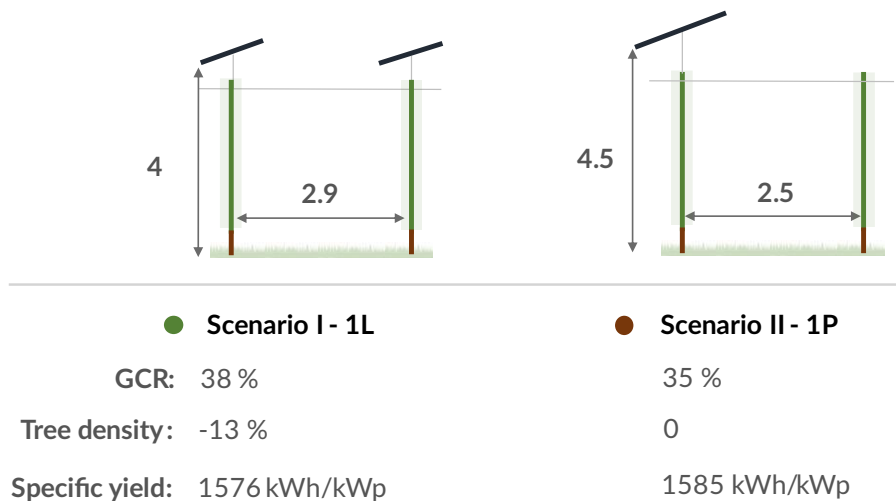


Figure 59: Specifications of the selected scenarios (dimensions in meters). Scenario 1 with modules placed on every strip in landscape, Scenario 2 with modules placed on every other strip in portrait. Other specifications: Ground Cover Ratio (GCR), tree density loss due to the increased strip pitch, and electrical specific yield.

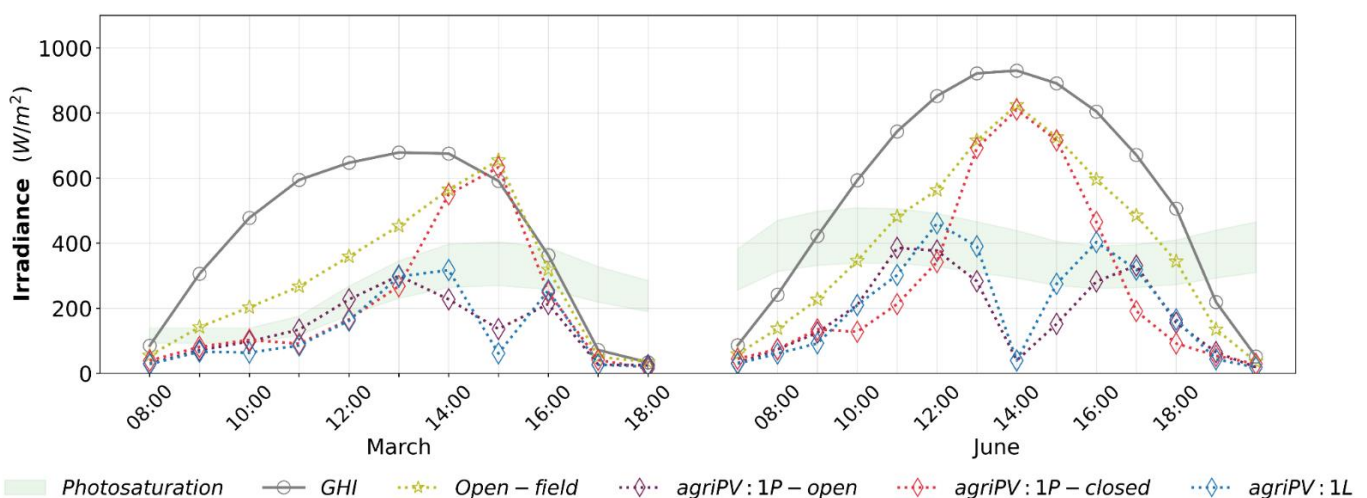


Figure 60: Daily crop irradiance variation under an open-field and under the agri-PV array of scenarios 1 and 2. For Scenario 2, “closed” and “open” refer to strips with and without modules, respectively. Each crop irradiance marker represents the mean of 7 sensors distributed throughout the central tree of the farm.

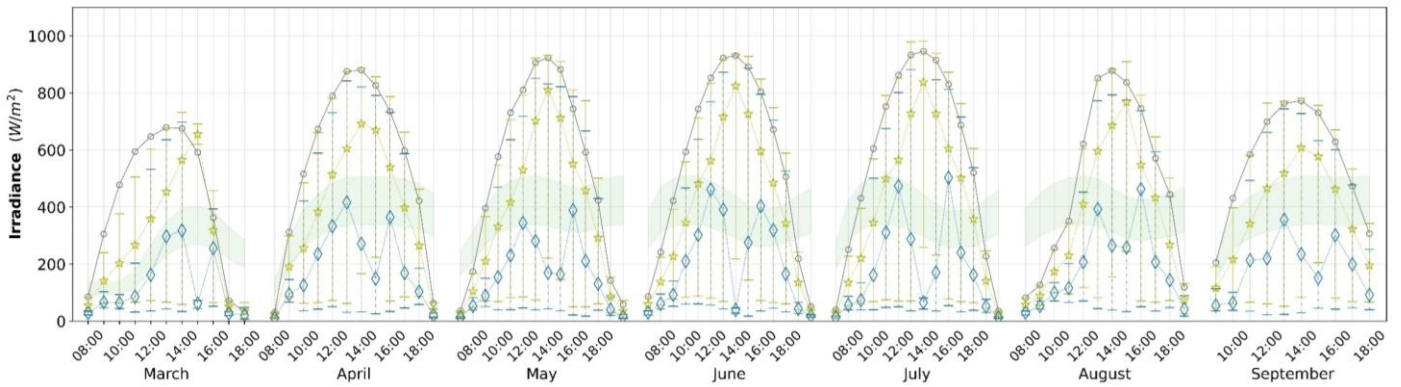


Figure 61: Mean daily crop irradiance variation throughout the growing season under an open-field and under the agri-PV array of Scenario 1.

The seasonal performance of Scenario 1 was further analysed as shown in Figure 62. Introducing PV modules not only decreased mean irradiation but also created a significant mismatch between the two sides. This discrepancy persisted throughout the growing season, except in June, underscoring the importance of mitigation strategies like adjustments in the tracking algorithm or the use of diffusers. Successfully addressing these challenges will facilitate the adoption of agri-PV systems for crops with tall canopies. The insights derived here can guide the design phase of other fruit orchards, ultimately promoting the use of agri-PV in horticulture-based systems.

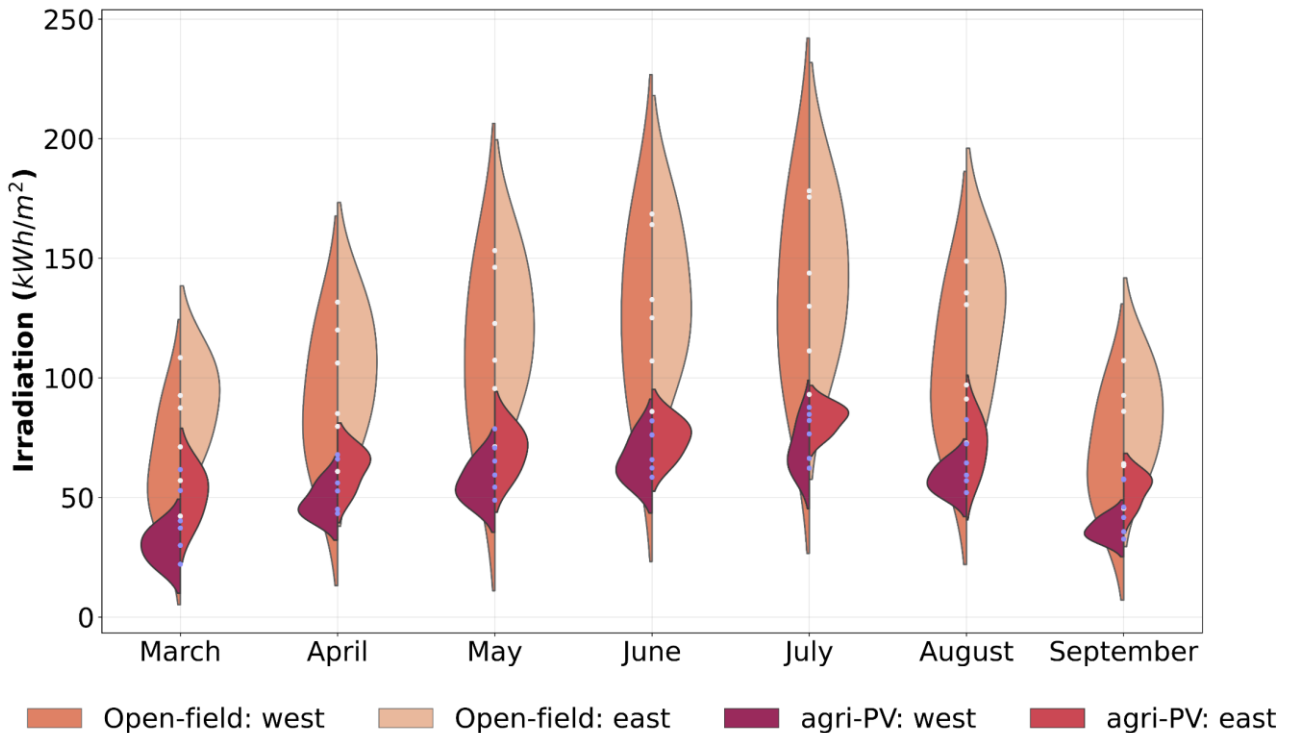


Figure 62: Accumulated crop irradiation per month throughout the growing season. This includes the magnitude and distribution (spread) of irradiation across the central tree in the field. Moreover, irradiation received under an open-field and under the shade of the agri-PV array of Scenario 1 are displayed for both west and east facing strip sides.

2.3. CONCLUSION AND DISCUSSION

The Demonstrator 1 - Bolzano project within the SYMBIOSYST initiative represents a pioneering endeavor in the integration of PV systems with agriculture, focusing specifically on the cultivation of apple trees. This comprehensive study involves the collaboration of multiple partners, each bringing unique methodologies to the table to explore the viability and benefits of agrivoltaic systems. The project's primary objective is to enhance crop yield while simultaneously generating renewable energy, thereby contributing to sustainable agricultural practices.

The Bolzano demo site has been meticulously planned to cater to the cultivation of the Ipador (Giga) apple variety, employing a dual-part setup that includes both existing and newly planted orchards. This setup is optimized for the N-S orientation and employs the Guyot training system for apple trees, ensuring efficient space utilization and maximum light exposure. The integration of Convert multifunctional trackers, manufactured from weathering steel to minimize environmental and visual impact, highlights the project's commitment to sustainability. These trackers, adjustable in height, are designed to accommodate semi-automatic agricultural devices, underscoring the project's emphasis on innovation and technological integration.

The project further differentiates between areas with and without PV systems, including trackers installed on existing fields and alongside new apple trees. This approach allows for a comprehensive analysis of the PV system's impact on crop growth and energy production, with the system's nominal power planned around 90 kWp, accommodating 240 modules of varying levels of semitransparency.

Partners LuciSun, Imec, and TU Delft have employed advanced 3D modeling techniques to simulate the agrivoltaic system's performance. These models assess the shading profiles, energy gain, and the potential impact on crop yield. The methodologies vary from complex geometric representations of plant structures to simplified models that reduce computational demands while still providing valuable insights into photosynthesis and crop growth under agrivoltaic systems.

Key findings from the project underscore the importance of the vertical sides of crops, which serve as the primary drivers of photosynthesis due to their larger effective collecting surface area for light. Semi-transparent PV modules have been identified as beneficial in reducing shading losses, a critical factor in maintaining or enhancing crop yield. However, the project's investigations also reveal significant variances in results attributed to the different simulation tools, methodologies, and assumptions employed by the partners. These differences highlight the complexity of modeling agrivoltaic systems and the need for further research to refine these models.

Looking ahead, the project plans to undertake a comprehensive comparison and benchmarking of the various models developed by the partners. This phase aims to identify the pros and cons of each approach and explore how they might be combined to achieve an optimal agrivoltaic system design. The ultimate goal is to develop a model that accurately predicts the system's performance, balancing energy production with agricultural productivity. This effort will not only contribute to the sustainability of apple cultivation under changing climatic conditions but also offer insights that could be applied to other crops and agrivoltaic system configurations.

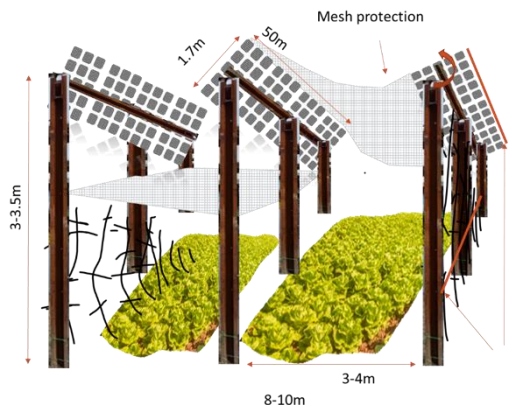
The Demonstrator 1 - Bolzano project represents a significant step forward in the development of sustainable agrivoltaic systems. By leveraging the expertise of multiple partners and employing innovative technologies and methodologies, the project aims to pave the way for the broader adoption of agrivoltaics in agriculture. The insights gained from this study will be invaluable in guiding future research and development efforts, ultimately contributing to the realization of sustainable and productive agricultural practices that are harmonized with renewable energy generation.

3. AGRIVOLTAIC DEMONSTRATOR 2 – BARCELONA

3.1. TECHNICAL SPECIFICATIONS

Table 9 describes the envisioned features of the demo of Barcelona and the updates in terms of Technical Specifications at M12 of the project.

Table 9: Envisioned features of the demo of Barcelona and the updates in terms of Technical Specifications at M12 of the project.

Use case 3	AGRIVOLTOPOLIS	
Unique Value Proposition	Solution for the vegetable crops of the future that can integrate bird and insect protection, resistant to chemical products keeping the height up to 3 m for 2D.	
Location	Barcelona province (Baix Llobregat Area).	
Replication potential	The Baix Llobregat area has 859 ha and Barcelona province has 4153 ha of vegetable crops. Application could be extended to other open field vegetable cultivation and seasonal field crops.	
Crop	The demonstrator in Barcelona, Spain, will be aimed at the production of short-stature and trellised seasonal vegetables (tomatoes, melon, lettuce, and fava beans) cultivated in rows between & under the trackers. This choice is particularly useful for the project, as it is complementary to the demonstrator planned in the Bolzano area (apple tree) and Scalea (citrus).	
Solutions implemented in the demo	 <p>Area field: 10m x 50m = 500 m²</p> <p>Area PV modules: 1.7 x 50 x 3 = 255 m²</p> <p>GCR: 0.5</p> <p>Transparency: 5-35%</p> <p>Nominal power: 410-270 W</p> <p>No. of PV modules: 132</p> <p>Max nominal power: 45 kW</p> <p>Water catchment system Integrated irrigation system</p>	<p>To ensure free movement of semi-automatic agricultural devices, the module's low point should exceed 2 meters to avoid human injury, optimized for various crops like tomatoes. Without perennial cultures, steel pile driving is viable, similar to PV projects. Locally sourced wood will construct the tracker piles' visible parts, with steel for the rest. Convert will utilize weathering steel for tracker manufacturing to minimize environmental and visual impact. A smart tracking algorithm integrating crop and PV data will be developed. UPC will design an autonomous robot for real-time weather data collection and tracker communication, offering a more efficient alternative to numerous fixed sensors, especially with seasonal vegetables. Convert, EURAC, and 3E will oversee the algorithm's development.</p>
Water catchment / irrigation	Water will be conveyed to avoid issues to the plants below. The water will be collected and redirected to the already available rainwater reservoir to later be used for drip irrigation.	
Health & Safety	At the moment there are no specific norms for agri-PV (grounding, etc). Rapid/emergency shutdown will be studied. The use of pesticides and other chemical products will be done by following the safety rules and their possible harmful effect on the PV modules will also be considered.	
System integration	In this Use Case, the biggest problem against vegetables are insects and birds. Therefore, the use of nets (that do not block excessively the sun) is suggested, to be tied to tracker posts.	
Use of electricity	There is already an existing electrical installation. The PV modules could be directly connected to it, and the electricity could be later used in the irrigation system as well as to facilitate the charge of electrical tools and vehicles.	

The proposed Agri-PV plant has two sections, Section 1 corresponding to West side and Section 2 to the East side, respectively. For the Agri-PV part, section 1 of the plant will be first modelled in this study. Figure 63 shows the overall 2D top-view representation of the plant.

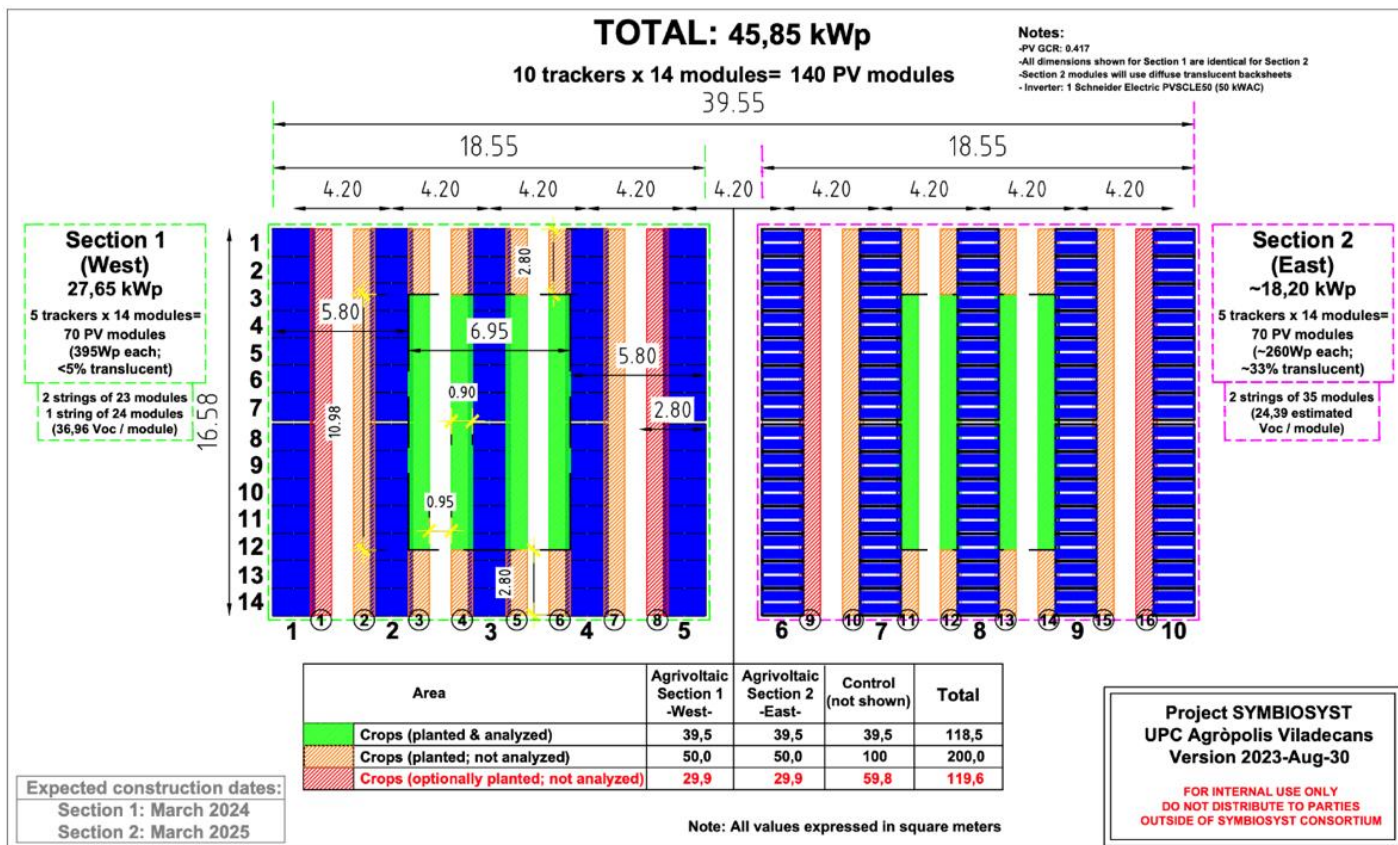


Figure 63: Layout for the Agri-PV system in Barcelona.

3.2. MODELLING BY LUCISUN

1) Layout

From a modelling perspective in LuSim, the Agri-PV plant is segmented into three components:

- a) The PV modules support structure
- b) The PV system layout
- c) The crop layout

a) The PV modules support structure

For Section 1, the design of the supporting structures for PV modules can be observed in Figure 64, which is a 3D model created for and integrated into LuSim’s 3D space. As depicted in the image, to support one row of the PV array, a simple U-framed structure grouped in three along a row, or North-South direction, is utilized, as indicated by the red line pointing towards the South. One row consists of a set of three U-frames, with dimensions along the North-South direction of 5.768 m, 4.612 m, and 5.768 m, respectively. The dimensions of one complete row are outlined in Figure 65. This row is then replicated in consecutive rows with a pitch of 4.20m, along the East-West direction (as indicated by the green line pointing towards the East), with the height of the top-most part of the frame from the ground set at 2.888 m and a total length of 17.096 m. Similar frames and dimensions are employed for Section 2B, except the height is set to 4.23 m, as depicted in Figure 66. For Section 2A, the dimensions of the support structures are kept the same as those in Section 1.

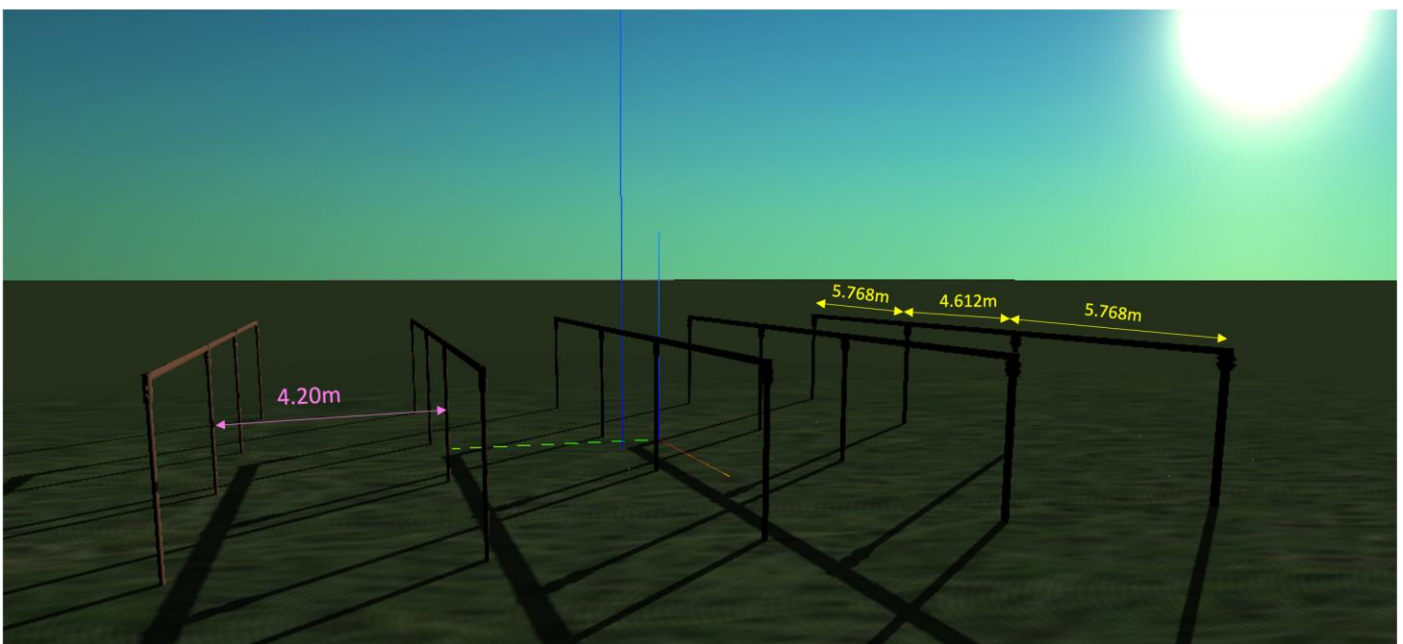


Figure 64: Support structures modelled and incorporated in LuSim’s 3D space.

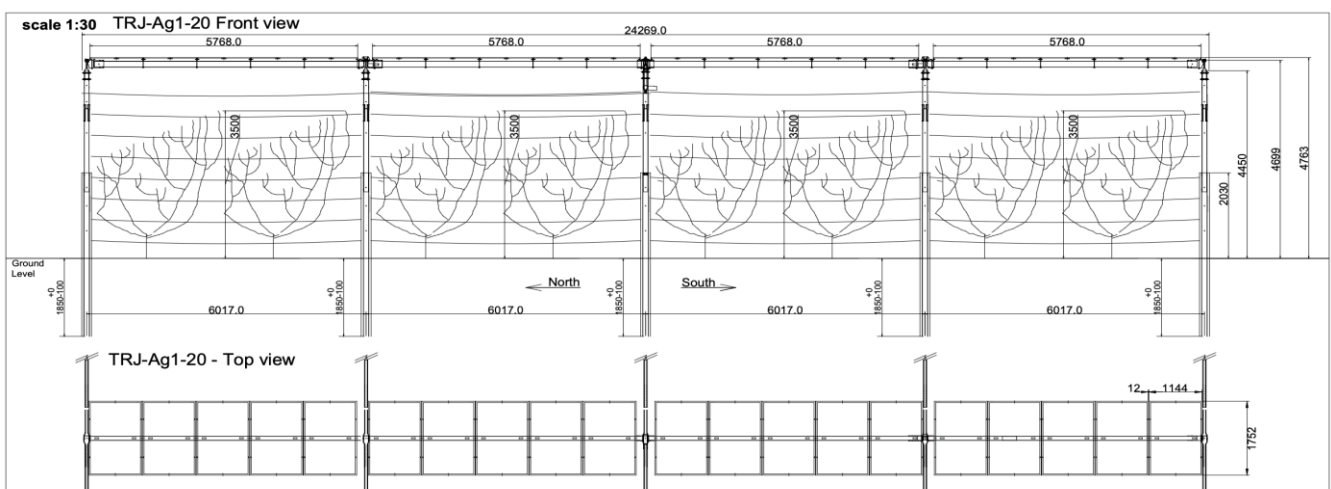
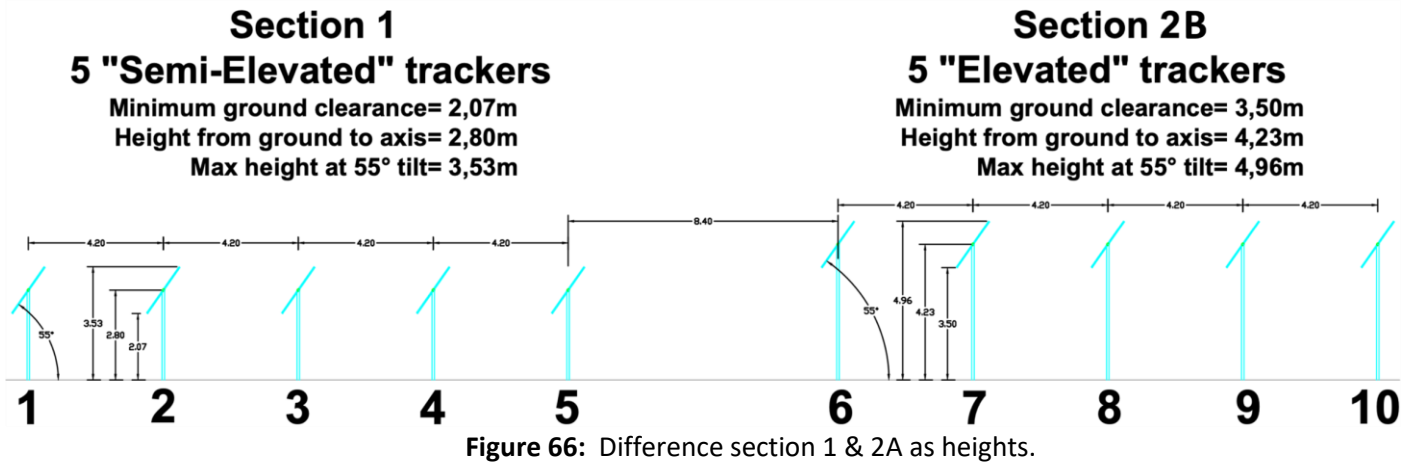


Figure 65: Frame dimensions for section 1.



b) The PV system Layout

Each section consists of 5 rows of tracking PV modules with a pitch of 4.20 meters, with each row containing 14 bifacial PV modules arranged in portrait fashion with a gap of 0.01m among them.

Figure 67 and Figure 68 detail dimensions and different possible transparencies of the PV modules considered.

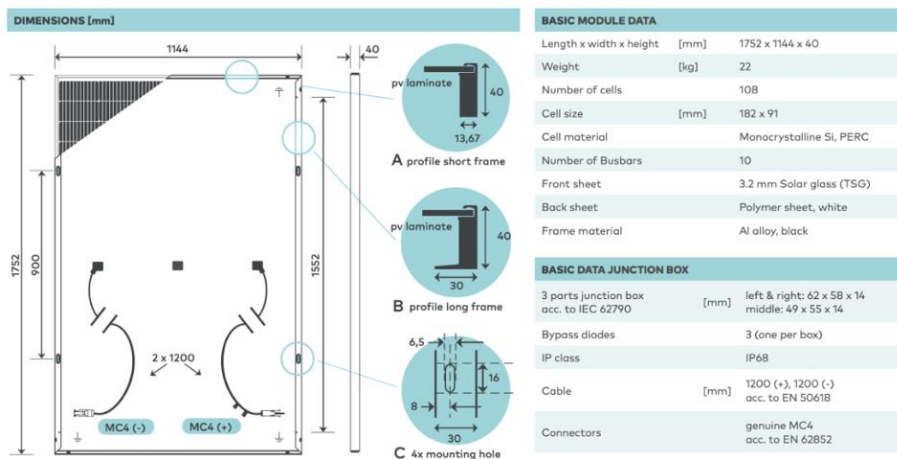
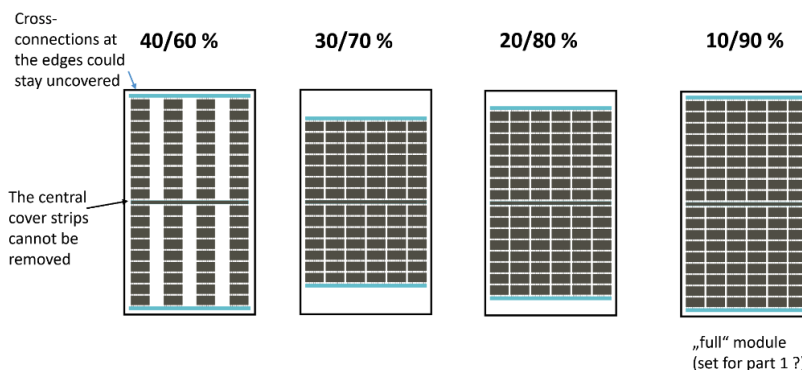


Figure 67: PV module dimensions.



Furthermore, Figure 69 shows the arrangement and layout of the PV modules in Section 1 as modelled in LuSim.

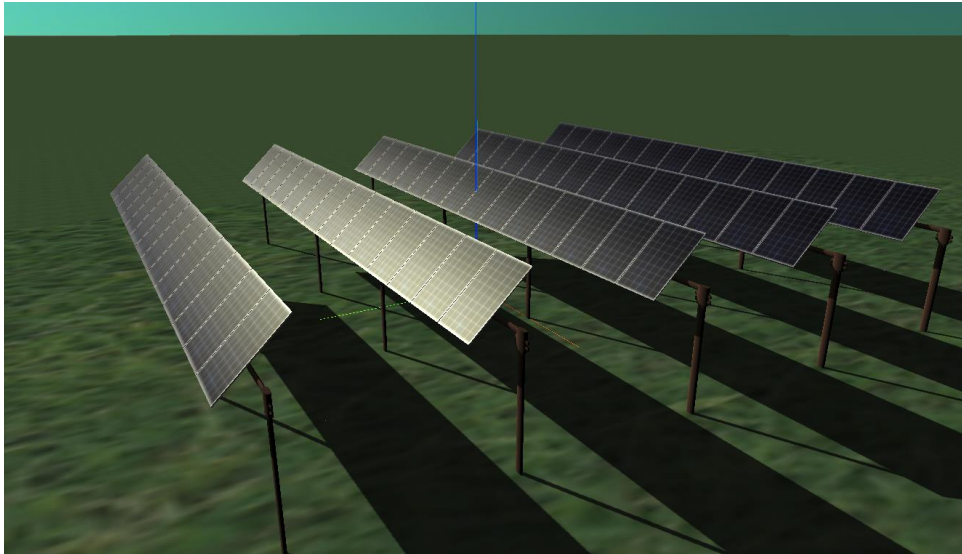


Figure 69: PV layout modelled in LuSim for Section 1.

c) Crop Layout

Four distinct kinds of crops are to be used, namely Lettuce, Fava beans, Onions and Tomato.

The crops will be studied for two years' time, and more precisely for two seasons in each year, where two crops will be studied for each season in each year. Thus, it is required to model four scenarios for each season in each year using two crops at a time. Specifically, for the first fiscal year 2025, the first season, i.e. Autumn-winter, in the period November 2024 - March 2025 will contain Fava beans and lettuce.

When assessing plant growth, the incident irradiance must be integrated separately for specific plant zones. In the realm of 3D modelling, several key questions arise regarding how to best represent plants and define these zones of interest. For plant shapes, it is possible to select either simple shapes, which approximate the outer boundaries of the crops, or more intricate shapes, which attempt to faithfully replicate the geometry of plant organs and leaves in detail. Basic geometric shapes, such as parallelepipeds, cylinders, spheres, or cones, can be employed to represent the outer envelopes, whereas shapes of varying complexity between the simplest and most detailed forms are also viable options. Each approach comes with its own set of advantages and disadvantages. Complex geometries attempt to realistically represent the shape of crops. They facilitate the utilization of more intricate models used to evaluate crop photosynthesis and good estimates of the 3D optical porosity.

However, this approach demands significantly higher computational resources because of the concomitant substantial increase in required spatial resolution and of the number of points where irradiance must be assessed. It also restricts the use of simpler agronomic models that have been developed based on a preliminary evaluation of the irradiance incident on the external canopy envelope. In contrast, the use of basic shapes that depict the external envelope of crops reduces the computational complexity significantly by reducing the number of points where irradiance calculations are necessary. This approach also facilitates the direct utilization of parametric models that assess photosynthesis in the canopy based on the solar radiation reaching its outer envelope. When employing these straightforward models, optical properties including optical porosity cannot be directly modelled, but must be incorporated through a parametric model attached to the object's texture. In most agrivoltaic applications modelled using LuSim, experience has favoured the use of basic geometric shapes alongside parameterized optical properties. If necessary, the optical porosity can be initially modelled using a high-resolution 3D representation of the plant under scrutiny, and the results can then be applied to all simple shapes employed in modelling the entire agrivoltaic system.

Figure 70 and Figure 71 provide the crop layout specific to the sections and the seasons.

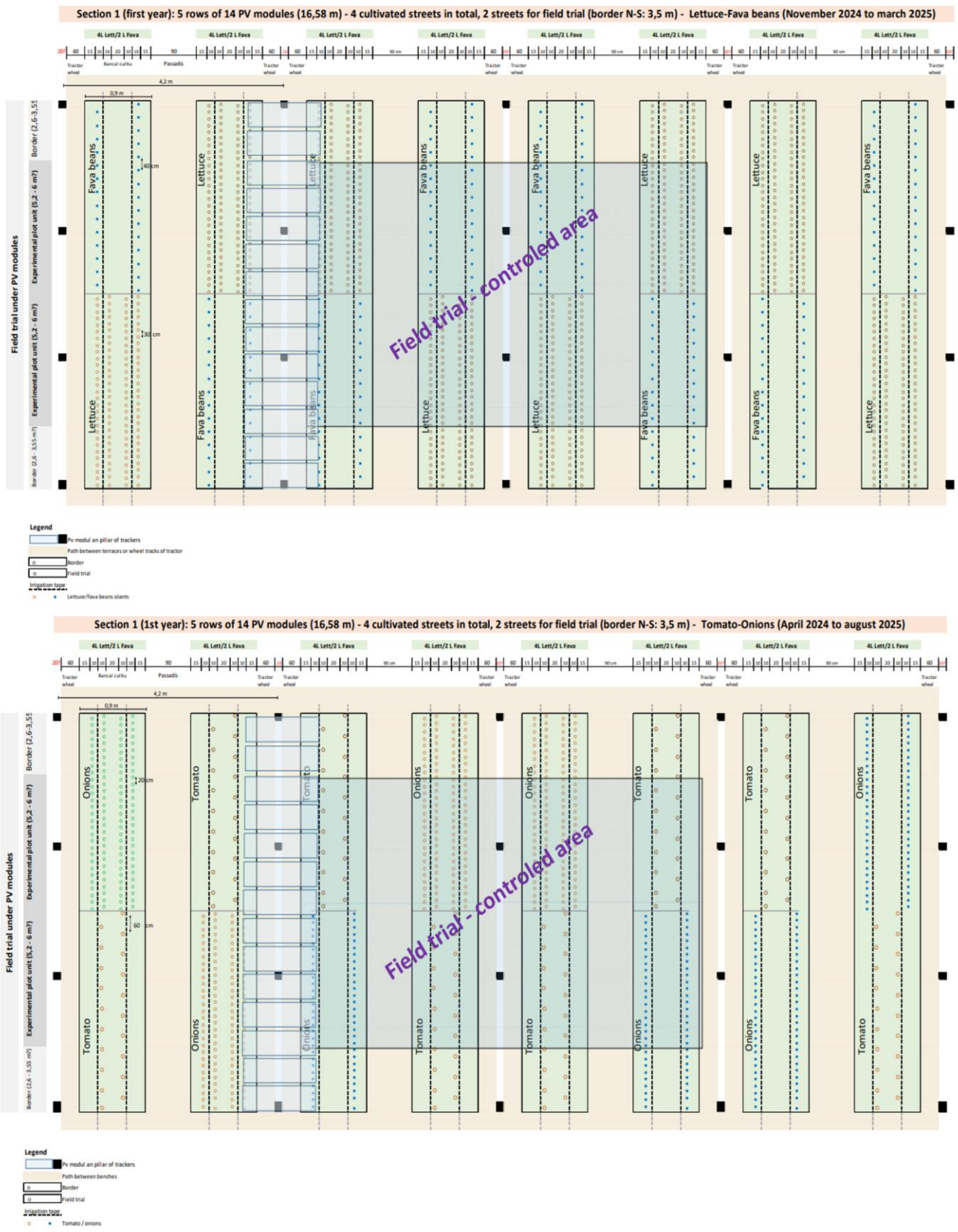


Figure 70: Crop arrangements specific to sections and crops.

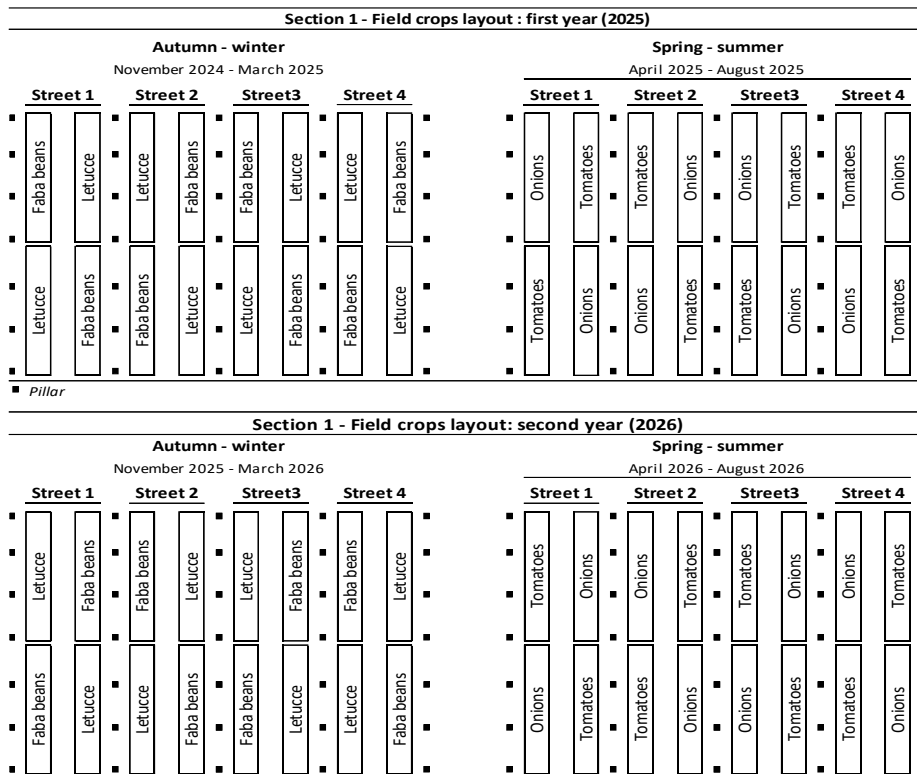


Figure 71: Crop arrangement specific to the seasons and the sections.

As mentioned above, it is possible to model the crops encompassing the intricate details and making it representative of the real crop as much as possible. As the focus will be primarily on the lettuce and tomato crop in this modelling phase of the demonstrator, Figure 72 shows a detailed modelling of complex structures of lettuce (right) and tomato (left).



Figure 72: Complex models of lettuce (left) and tomatoes (right).

The following section discusses the details on the simplified approach for crop modelling for lettuce and tomato while detailing the layout information of all the four crops.

1. Lettuce

The shape of the external envelope, representing each lettuce, is assumed to be a hemisphere with a radius of 10 cm. The spacing between rows, or pitch, is set at 20 cm. Figure 70 illustrates that there are four rows of lettuce, organized into two groups with each group containing two rows. This arrangement means that two rows are positioned in close proximity to each other, followed by a larger gap, and then another two rows are positioned at the same distance as the first two rows. The gap between the two groups of rows is specified as 20 cm. However, given the shape and dimensions of the envelope, accommodating four rows of lettuce on a single terrace is not feasible if this gap is to be maintained. Specifically, the total width available on the strip for crop planting is 90 cm, and with the lettuce radius assumed to be 10 cm, a total of 80 cm is required to fit four rows of lettuce. This arrangement leaves no space within the rows and only a 5 cm width from the edge on either side of the crop cultivation land strip, as depicted in Figure 73, which presents a section of the terrace containing lettuce, where the arrangement of lettuce rows is shown to accommodate four rows within a terrace.



Figure 73: Lettuce arrangement in the agricultural land.

2. Fava beans

A total of 2 rows of fava beans will be planted in a terrace with 0.6 cm pitch between two rows of fava beans and the pitch among fava beans within the row is 0.4 cm.

3. Tomato

As shown in Table 10, the height of the tomato plant is listed as 0.7 m, although agronomists at this demonstration site note that the majority of tomato crops do not exceed 0.5 m in height. For the purpose of this study, the size of the tomato crop is represented by a rectangular cuboid, encapsulating a complete row of tomato plants within that section. The dimensions of this cuboid are a height of 0.7 m, a width of 0.7 m, and a length of either 8.4 m or 5.6 m, depending on the specific terrace section, as illustrated in Figure 74. Unlike other demonstration sites or the typical dimensions observed for tomato crops, the plants at this site in Barcelona exhibit unique characteristics in terms of vertical growth. Here, the crops grow without the use of tutoring or support structures, causing them to spread across the ground similar to melon crops, with a maximum height ranging from 0.5 m to 0.7 m.

Despite the actual growth form of the crops, for the initial phase of this study, the crop’s envelope is considered to be a rectangular cuboid with a height of 2m and a width of 0.7m. This approach is adopted to facilitate the assessment of light distribution under the photovoltaic (PV) system and to analyse the evolution of shading loss at various heights above the ground. Furthermore, this study investigates the impact of shading by the PV system on the light reaching the ground or crop plantation area. Given that all crops, with the exception of fava beans, maintain a height within the 0.5m to 0.7m range as per Table 10, the findings from the ground level analysis are applicable to these crops due to their low stature.

In subsequent phases of the study, a more representative envelope will be modelled for the tomato crops, and the results will be compared with the initial ground level analysis. According to the planting arrangement, two rows of tomatoes are planned, with a 30 cm pitch distance between rows and a 0.6 m spacing between individual plants within the rows. Currently, the tomatoes are modelled as a single cuboid representing both rows, with the specified length and a height of 2 m. Therefore, in the visual representation, only one cuboid block representing the tomato crops is visible on each terrace.

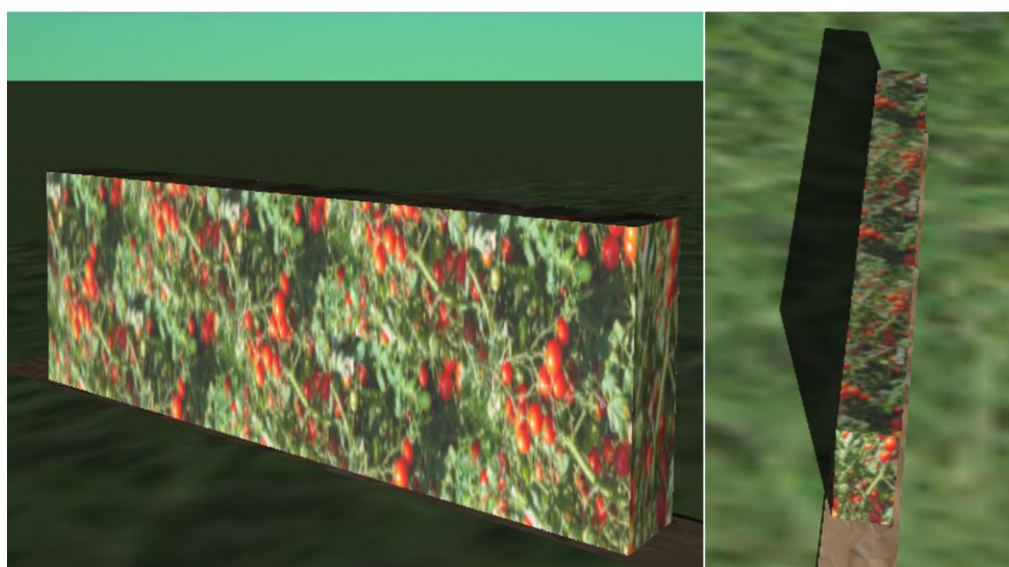


Figure 74: Tomato arrangement in the crop plantation land/strip.

4. Onions

In a terrace, a total of four rows of onions are planned for planting, organized into two groups with each group consisting of two rows. The gap between the two groups of rows is specified as 20 cm. Additionally, the spacing between individual onions within each row, also known as the pitch, is set at 20 cm. This arrangement allows for efficient use of space while ensuring adequate room for the growth and maintenance of the onion crops.

Table 10 shows the crop growth cycle and the cultivation system for the above-mentioned crops.

Table 10: Crop growth cycle and cultivation system.

Season	Crop	Growth cycle - Dates		Cultivation system			Estimated maximum plant height (cm)	Drip irrigation lines*
		Plant or seeding	Harvest	Rows of crop/terrace	Between Rows (cm)	Between plants (cm)		
Autumn - winter	Lettuce	15-30/1	30/3-5/4	4, quincunx	20	30	50	2
	Fava beans	1-15/11	1-10/4	2	60	40	150	2
Spring – summer	Tomatoes	1-15/4	15/7 – 15/8	2, quincunx.	40	60	70	2
	Onions	1-15/4	1-15/7	4, quincunx.	20	20	60	2

* Installed under plastic film mulch

2) Objective

In the proposed agricultural Agri-PV system in Barcelona, understanding the impact of the PV system on the crops is crucial. The initial step involves estimating the light that reaches the agricultural field—specifically, the land designated for crop planting—as influenced by the PV system. This study introduces an Agri-PV system with predefined layouts and dimensions for the crops, agricultural land, and the PV system. These specifications are detailed in Figure 75, which offers various perspectives of the arrangement. This approach ensures a comprehensive analysis of how the PV system affects light availability for the crops, an essential factor for optimizing both energy production and agricultural yield.

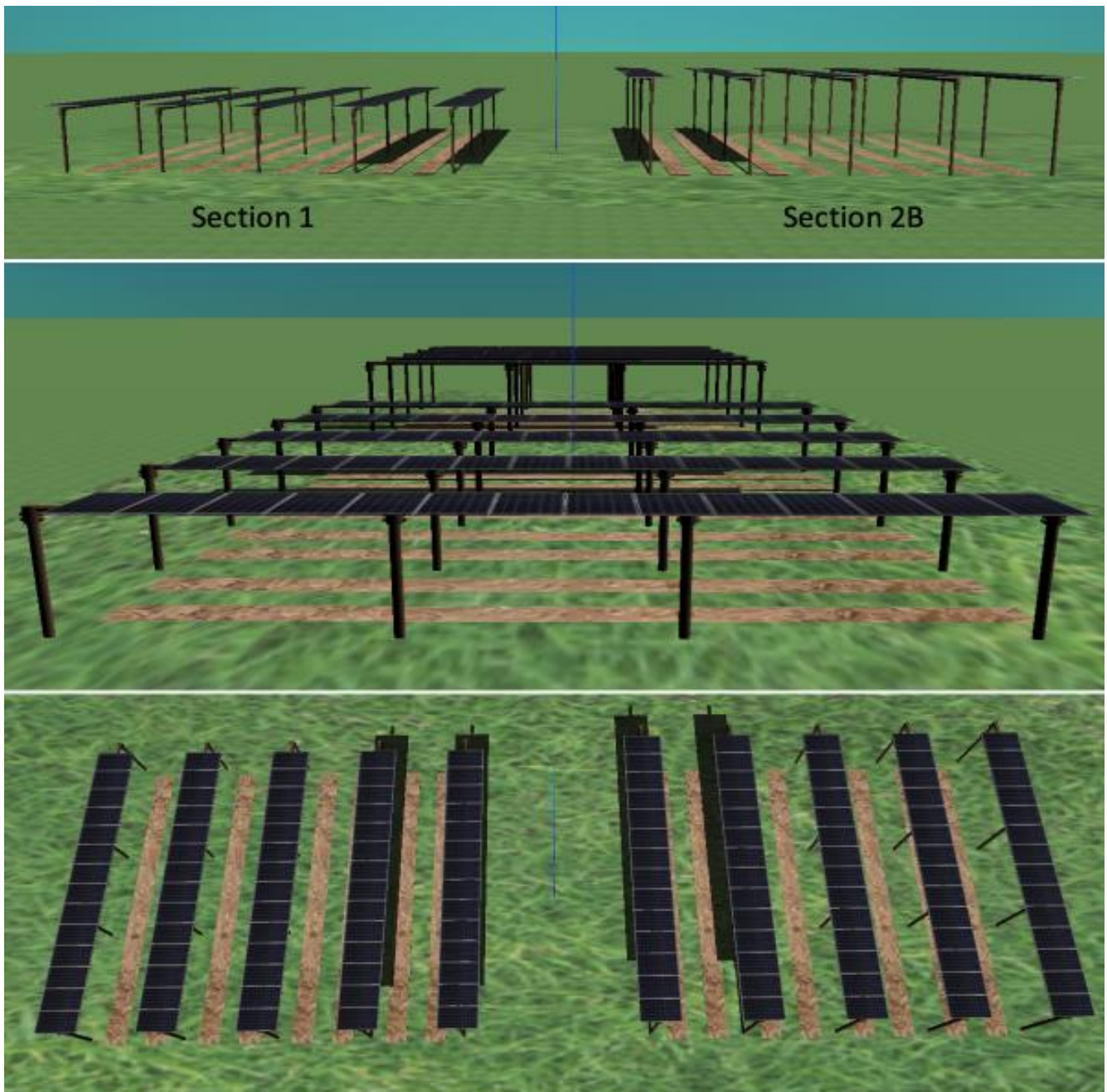


Figure 75: Different views of section 1 – 2B with the agriculture land and PV system.

3) Methodology

In this study, the focus is on estimating the light that reaches the ground as influenced by the proposed photovoltaic (PV) system. Specifically, the shading loss percentage is calculated. This metric represents the difference in light levels between a scenario without any PV system (referred to as the reference case) and one with the Agri-PV system in place (referred to as the test case), normalized by the light levels in the reference case. The test case is illustrated in Figure 75, which displays various views of the system, highlighting two distinct sections: Section 1 (west side) and Section 2B (east side). These sections are separated by an 8.4 m distance, maintaining a pitch distance of 4.2 m or a ground coverage ratio (GCR) of 41.7%.

Further analysis includes comparisons between Section 1 and two configurations within Section 2: 2A and 2B. Section 2A shares the same layout as Section 1 but utilizes Aleo PV modules with 40% semi-transparency. In contrast, Section 2B employs the same Aleo modules but differs in the height of the frame supporting the PV system, as depicted in Figure 75.

The area designated for crop planting and harvesting, marked by a brown patch in the figure, is the focal point for estimating total incident irradiance. To mitigate edge effects, this patch is defined as 0.9 m x 0.9 m, as shown in Figure 76, over which incident irradiance is calculated. Figure 77 presents one of these areas with a mesh overlay on the objects of interest for light estimation. The vertices visible through the mesh are the specific points at which incident irradiance is measured. The average of these measurements represents the irradiance at a particular point in time for the object under the mesh. This data can be integrated over various time resolutions—hourly, daily, monthly, or yearly—to determine the irradiation levels. This methodology allows for the estimation of incident light on any chosen object with adjustable spatial resolution, by altering the mesh size, and at any desired time resolution.

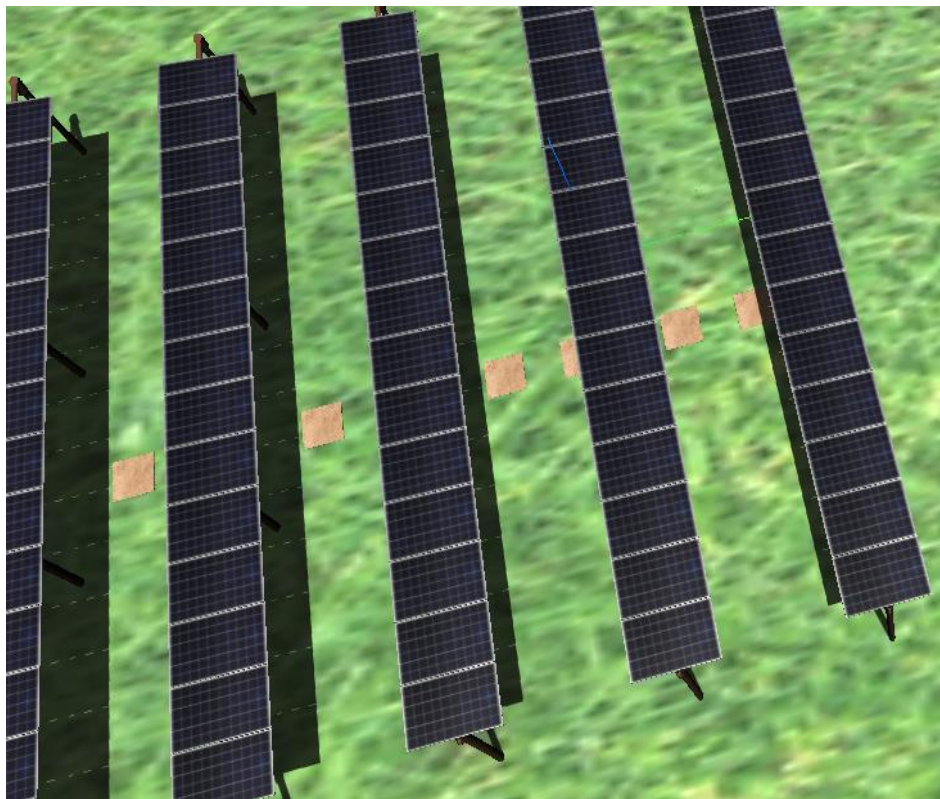


Figure 76: Agriculture land taken as a 0.9 m x 0.9 m patch.



Figure 77: Mesh showcasing the light capture points.

Figure 78 serves as the reference case for the scenario previously described, providing a baseline measurement of light levels without the influence of the photovoltaic (PV) system. By comparing the light levels between this reference case and the test case (which includes the Agri-PV system as illustrated in Figure 75), it is possible to determine the amount of light obstructed by the PV system. From this comparison, the percentage loss of light due to the PV system can be calculated. This approach allows for a precise quantification of the shading impact of the PV system on the agricultural land, offering valuable insights into how the introduction of an Agri-PV system affects the light availability for crops planted beneath or around the PV structures. This comparison is essential for understanding the trade-offs between energy production and agricultural productivity in the implementation of Agri-PV systems.



Figure 78: Reference case to get the shading loss percentage for the patches in section 1-2B.

When this project commenced, the exact coordinates of the demonstrator's location were unknown. Therefore, approximate coordinates, specifically 41.387, 2.169, were selected for the simulations. However, for the upcoming phase of simulations, precise coordinates specific to the demonstrator's location will be utilized. This slight difference in coordinates, potentially spanning a few kilometers, is not expected to significantly influence the simulation results. Based on the provided coordinates, a Typical Meteorological Year (TMY) dataset sourced from PVGIS-SARAH2 was employed for modeling purposes. This dataset comprises solar resource and meteorological data tailored to the specified location. Other variables obtained from the PVGIS-SARAH2 are air temperature, wind speed, wind direction and relative humidity.

Table 11 shows a monthly summary of the most relevant solar resource and weather data used in the PV energy yield evaluation. GHI corresponds to Global Horizontal Irradiation, DHI corresponds to Diffuse Horizontal Irradiation, W_s to wind speed, T_a to air temperature.

Table 11: Monthly summary of the most relevant solar resource and weather data used in the crop and PV yield evaluation.

Month	GHI [kWh/m ²]	DHI [kWh/m ²]	T_a [°C]	W_s [m/s]
Jan.	73.96	155.31	19.89	10.26
Feb.	84.17	118.32	30.95	11.18
Mar.	130.76	146.7	49.72	11.24
Apr.	170.74	194.55	49	13.56
May	216.1	221.2	65.75	18.01
June	219.28	210.68	70.39	21.22
July	226.62	231.01	65.6	23.06
Aug.	197.84	207.95	60.53	24.4
Sep.	138.93	151.46	50.77	20.44
Oct.	108.74	138.96	41.87	16.37
Nov.	66.53	105.68	28	11.07
Dec.	53.94	96.34	22.04	8.22
Year	1687.61	1978.16	554.51	15.7525

4) Results

The following section presents the simulation results and analysis, and it explains the terminology used for the target objects, particularly the agricultural or crop cultivation land, upon which the light is captured. As depicted in Figure 76, this land is situated at different orientations relative to the position of the PV modules, resulting in varying degrees of shading caused by the PV system. Consequently, the land positioned in different directions is treated as distinct target objects for both Section 1 and Section 2B, resulting in a total of four target objects for analysis. In Figure 79, the target objects, labeled as 'left soil' and 'right soil' for each section, are highlighted in white. Similar distinctions can be applied to Section 2A, as illustrated in Figure 86.

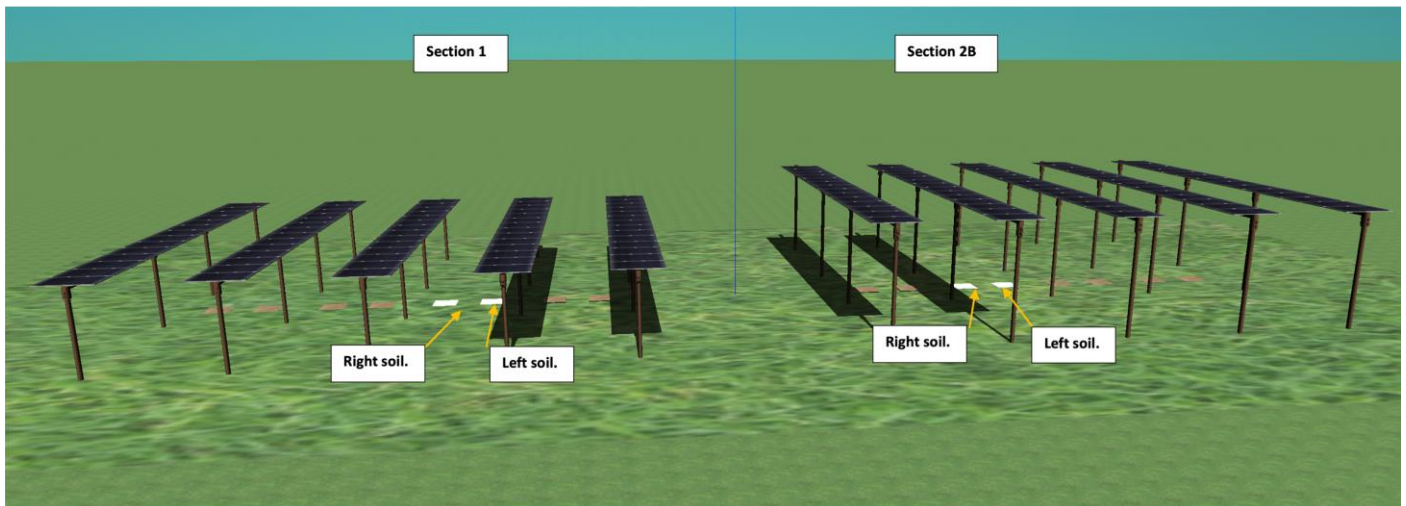


Figure 79: Section 1-2B marked with target objects.

Figure 80 and Figure 81 show the global incident irradiance and the corresponding shading loss percentage for the left and right soil of section 1 and section 2B on a clear sky day of 18th July of the TMY time series in 10 minutes time resolution.

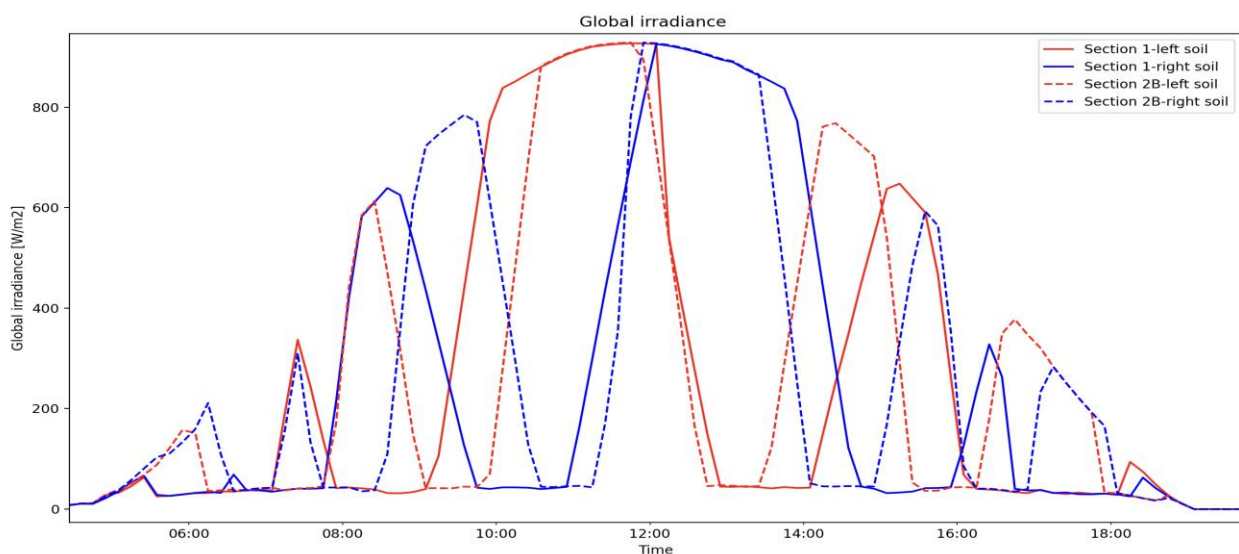


Figure 80: Global irradiance comparison on 18th July (TMY).

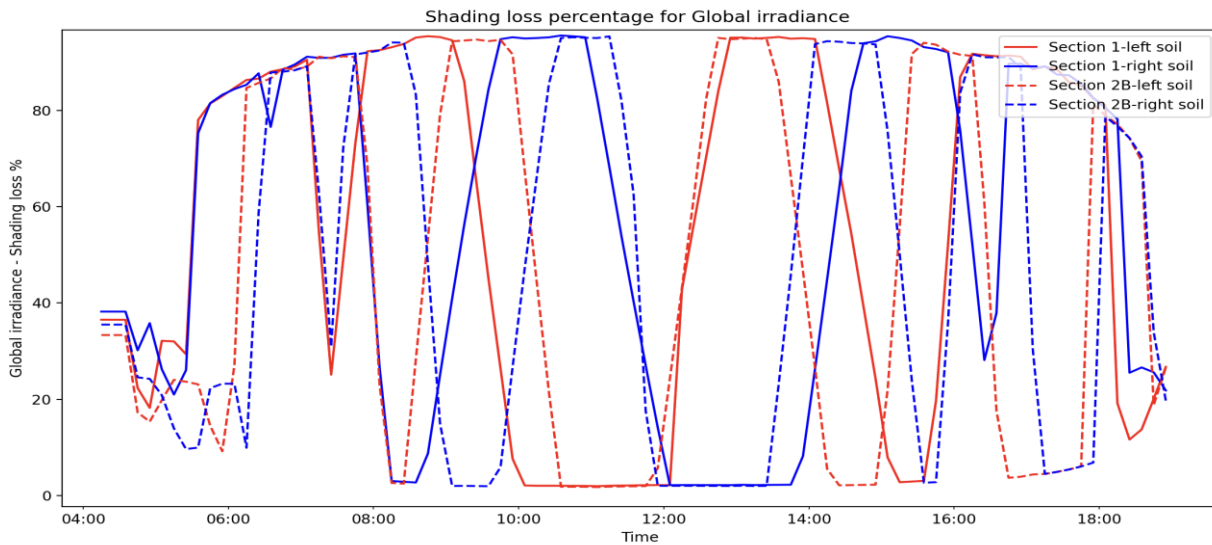


Figure 81: Shading loss percentage comparison for global irradiance on 18th July (TMY).

The shading patterns for both Section 1 and 2B exhibit notable differences. To provide a clearer visualization of the impact of the height disparity between the two sections on the shading patterns, realistic images depicting the shading caused by the PV system in both Section 1 and Section 2B at a specific moment in time have been presented. Figure 82 showcases the shading pattern for Section 1 at 11:00, highlighting the distinct shading contrasts between its 'left soil' and 'right soil'. Similarly, Figure 83 displays the shading pattern for Section 2B at 9:00, emphasizing the variation in shading patterns between its 'left soil' and 'right soil'.

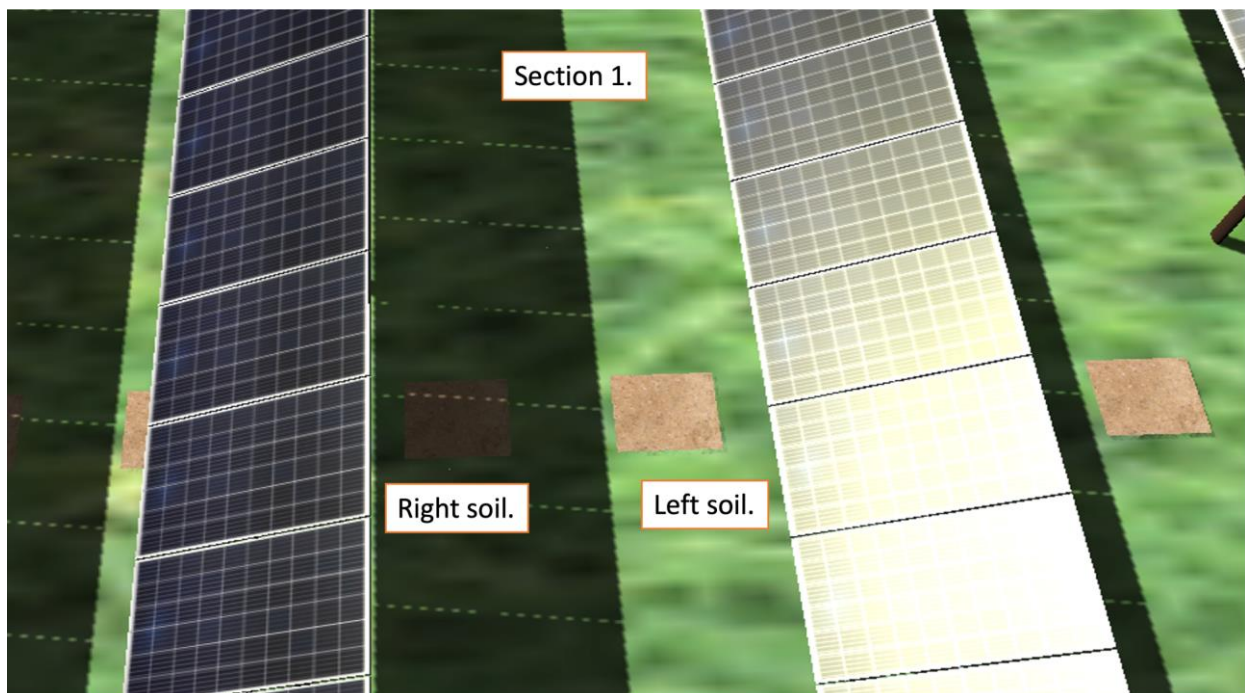


Figure 82: Shading pattern comparison for Section 1 at 11:00 AM on 18th July (TMY).

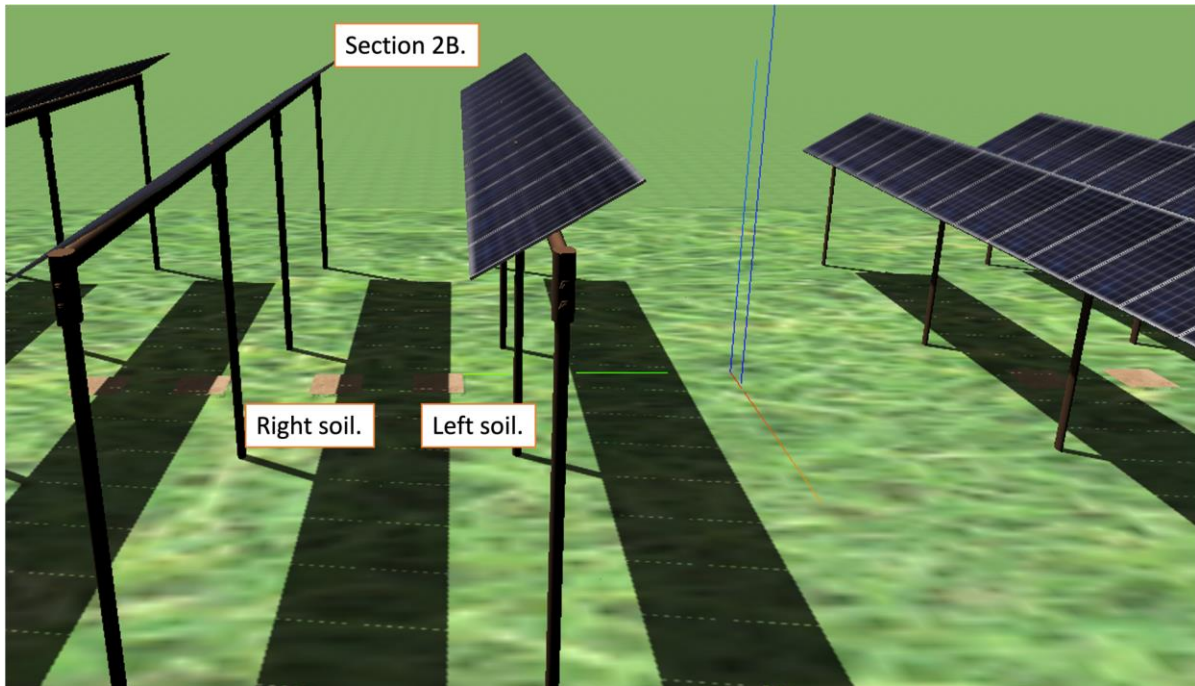


Figure 83: Shading pattern comparison for section 2B at 9:00 AM on 18th July (TMY).

However, the effect of the height difference can be seen when the irradiance values are integrated over daily and monthly time resolutions. Figure 84 shows the daily shading loss percentage comparison for global irradiation for the summer months June and July. Similarly, Figure 85 shows the monthly loss percentage comparison for global irradiation.

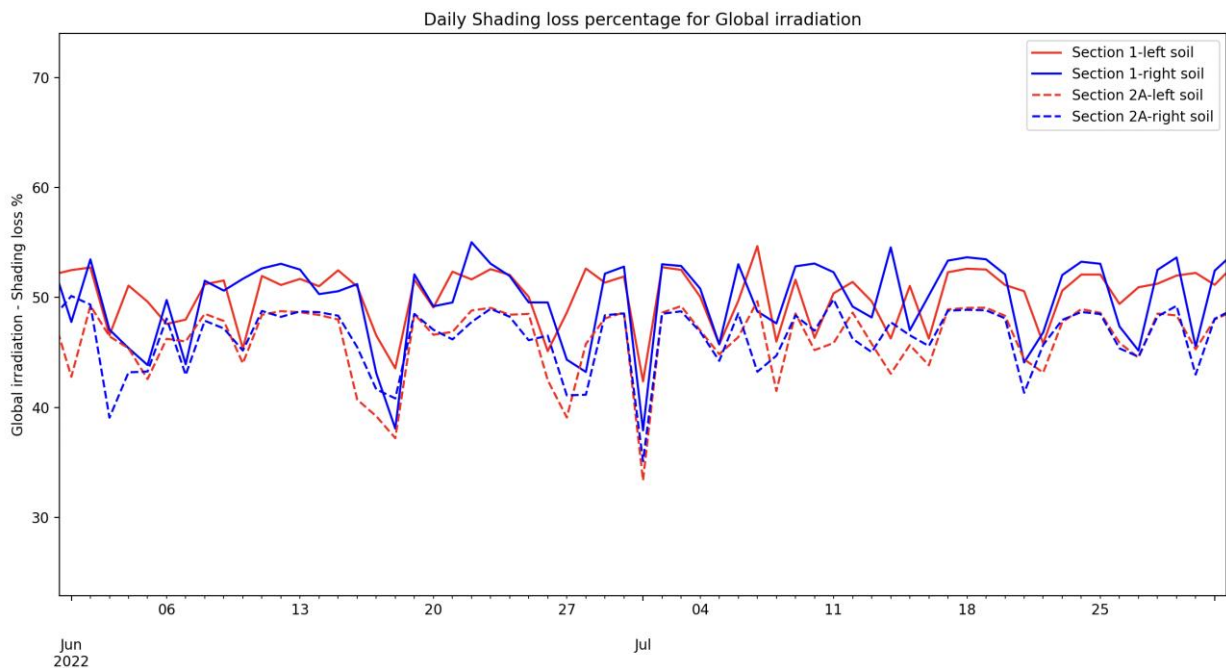


Figure 84: Daily shading loss percentage comparison for the month of June and July

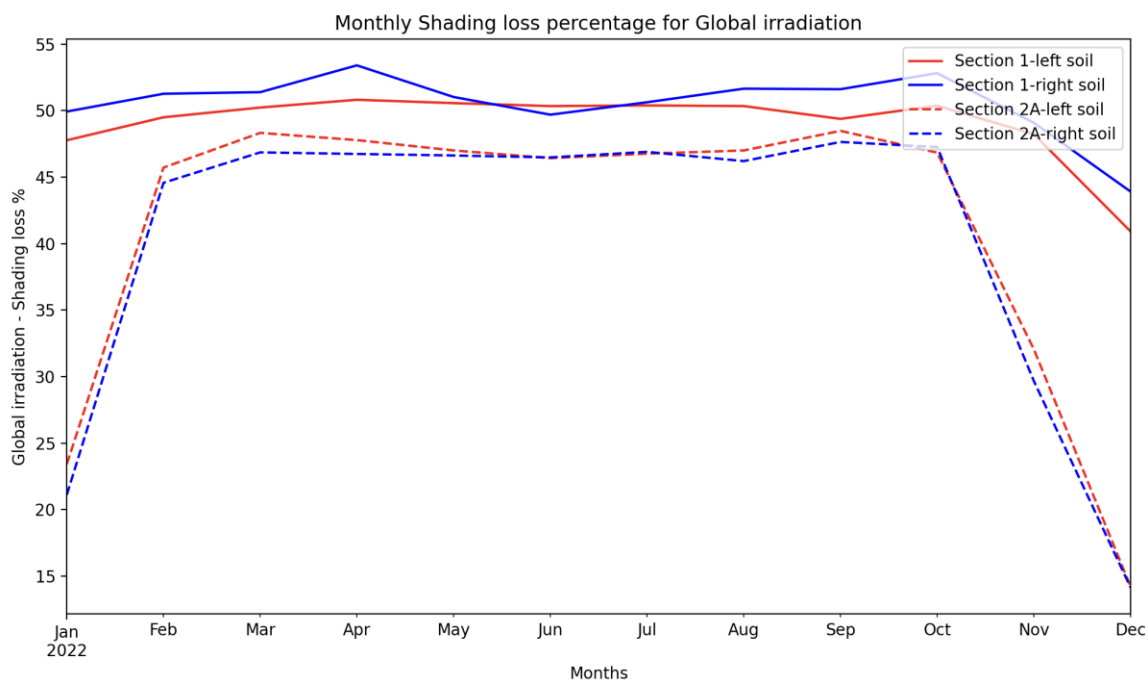


Figure 85: Monthly shading loss percentage comparison for global irradiation.

The following section contains a comparison between Section 1 and Section 2A. Figure 86 illustrates Section 2A, featuring Aleo modules with a semi-transparency of 40 percent. Additionally, the figure identifies target objects, labeled as 'left soil' and 'right soil', akin to Section 1 and Section 2B. These designations allow for consistent analysis and comparison of shading patterns across different sections within the study area.

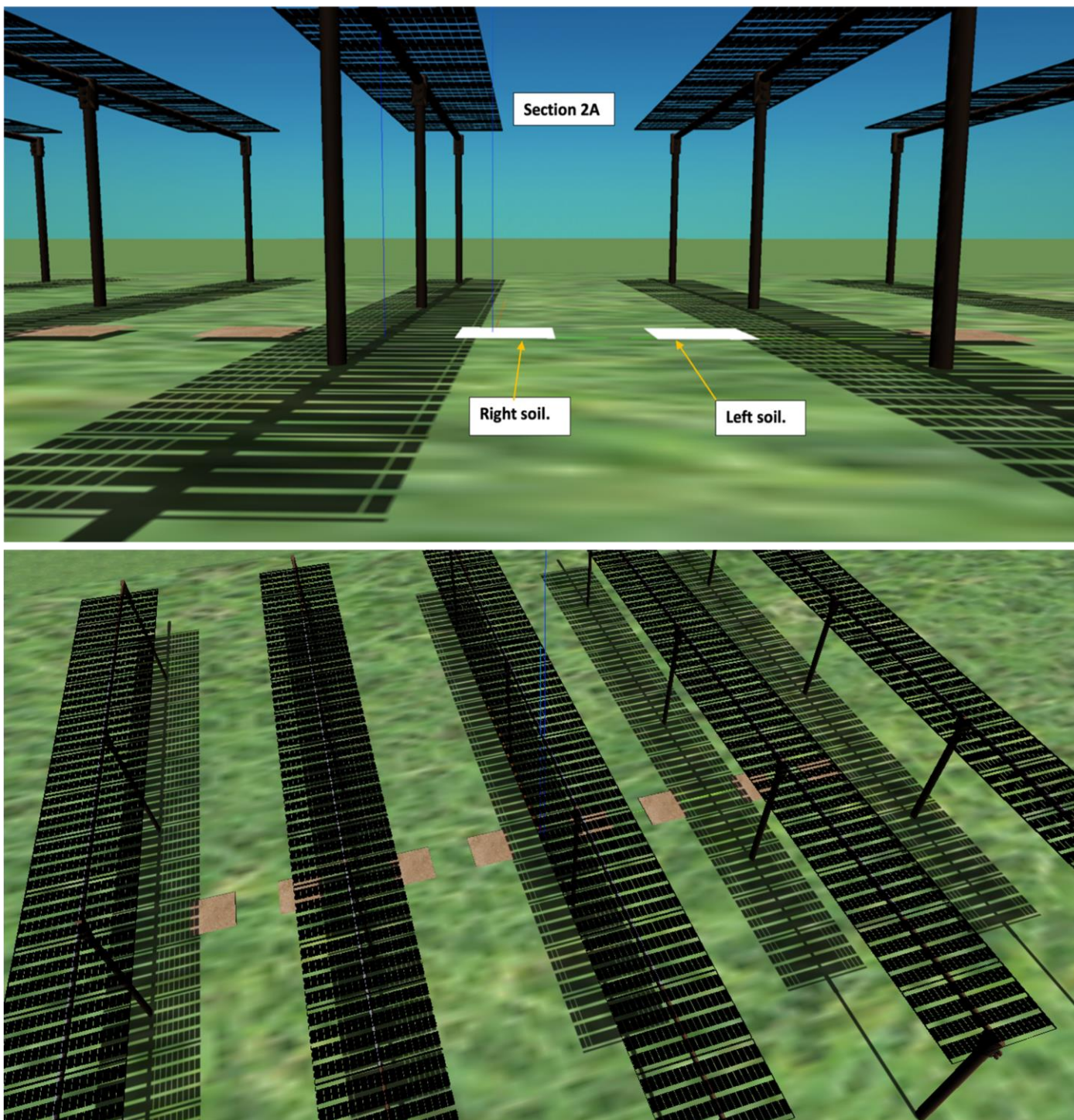


Figure 86: Section 2A showcasing semi-transparent modules.

Figure 87 and Figure 88 depict the global incident irradiance and the corresponding shading loss percentage for the left and right soil of Section 1 and Section 2A, respectively, on a clear sky day of July 18th in the Typical Meteorological Year (TMY) time series. The data is presented at a 10-minute time resolution, offering insights into how shading impacts vary over time across different sections within the study area. These figures facilitate a detailed examination of the effects of shading on incident irradiance, aiding in the assessment of the performance and efficiency of the Agri-PV system under varying conditions.

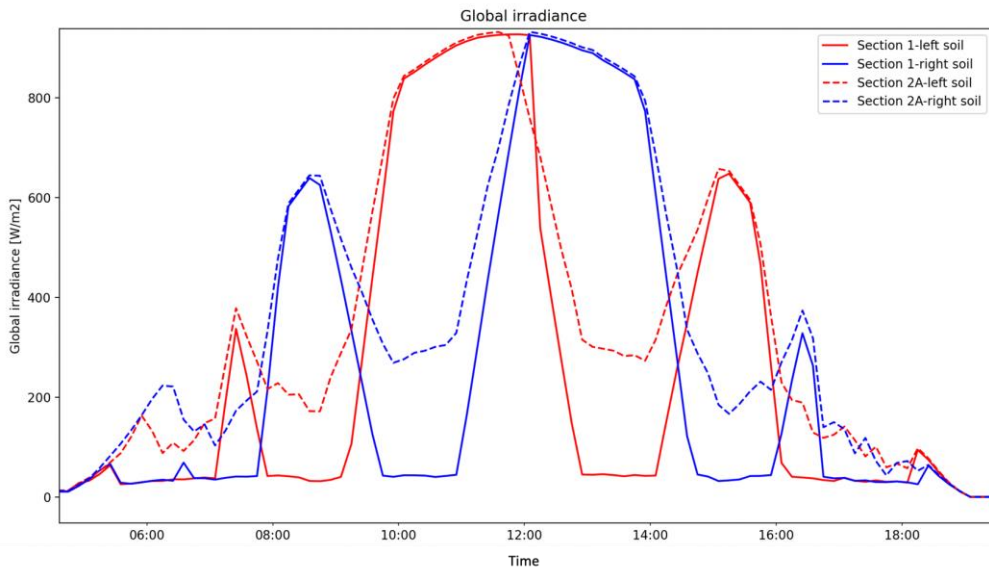


Figure 87: Global irradiance comparison for section 1 and 2A, on 18th of July.

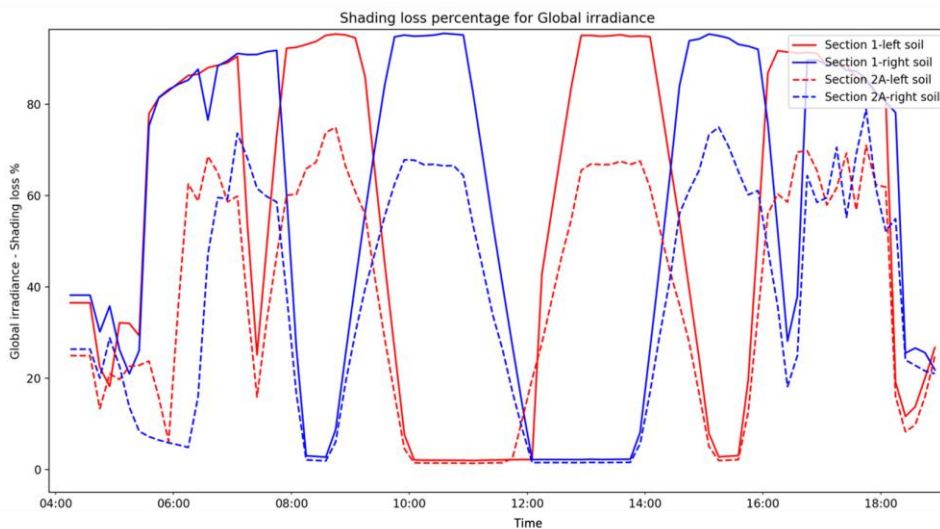


Figure 88: Shading loss comparison for global irradiance for section 1 and 2A, on 18th of July.

The sole distinction between Section 1 and 2A in the light simulation conducted using LuSim is the variation in PV panels utilized in each section. Specifically, Section 2A employs PV panels with 40% transparency, while Section 1 utilizes panels with standard transparency. Consequently, it is of considerable interest to visually compare different realistic instances in 3D, illustrating the shading effects caused by the PV panels in both sections. This is particularly relevant for understanding the shading pattern resulting from the semi-transparent modules in Section 2A.

Figure 89 and Figure 90 showcase realistic images generated by LuSim, depicting shading in 3D space caused by the PV panels in Section 1 and Section 2A, respectively. These images capture the shading patterns at the same moment in time, specifically 11:00 on July 18th, as per the TMY time series. Such visualizations provide valuable insights into the spatial distribution and intensity of shading caused by the PV panels in different sections, aiding in the comprehensive analysis of the Agri-PV system's performance under varying conditions.



Figure 89: Shading on 'left soil' and 'right soil' in section 1 at 11:00 on 18th July (TMY).

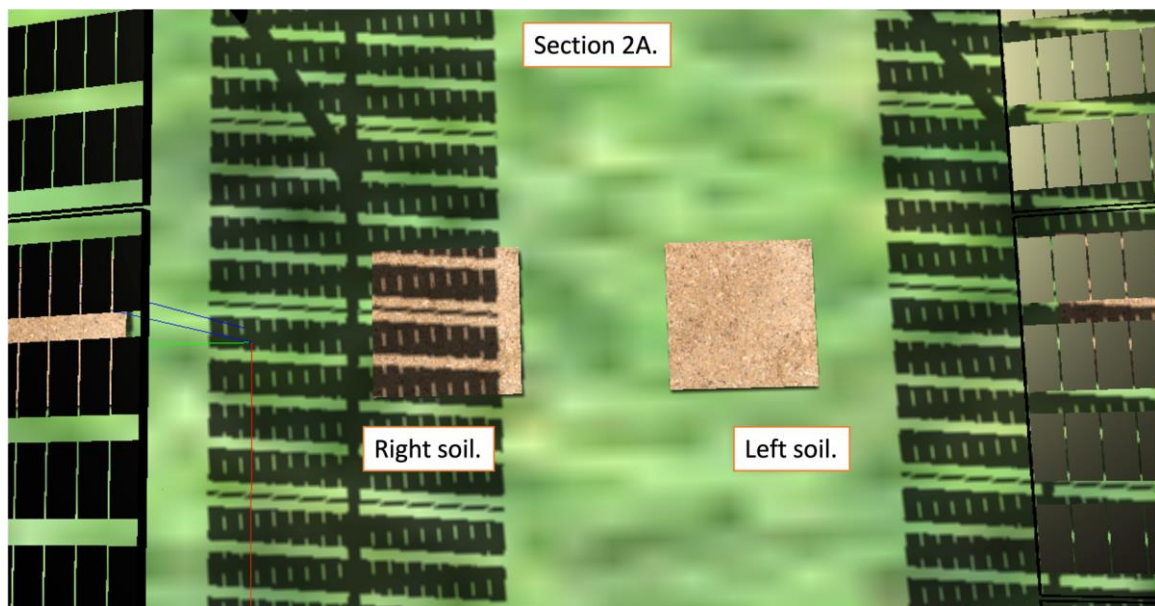


Figure 90: Shading on 'left soil' and 'right soil' in section 2A at 11:00 on 18th July (TMY).

The effect of 40% semi-transparency on shading losses can be better observed when the losses on global irradiation are accumulated over daily, monthly and yearly time periods. Figure 91 shows daily shading losses for the summer months of June and July, and Figure 92 shows monthly shading losses. Here, significance of 40% semi-transparency on shading losses can be observed when compared with the losses caused by standard transparency.

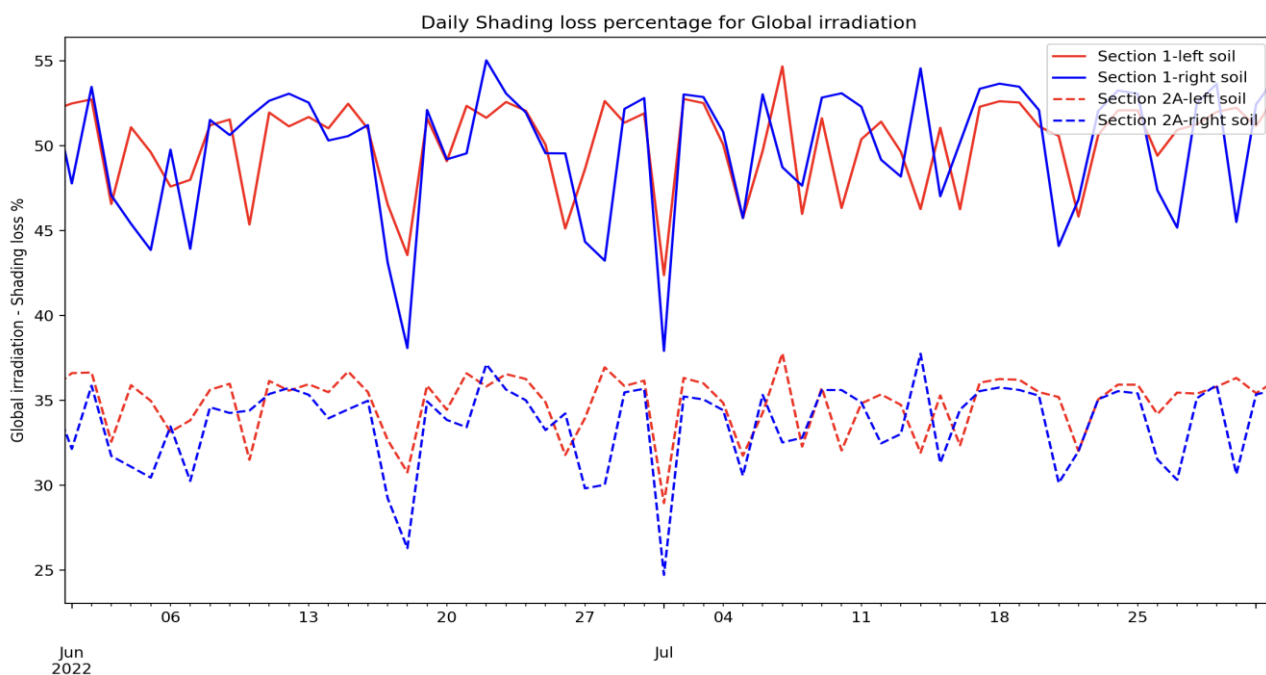


Figure 91: Daily shading losses for global irradiation in June and July for scenario with semi-transparency of 40%.

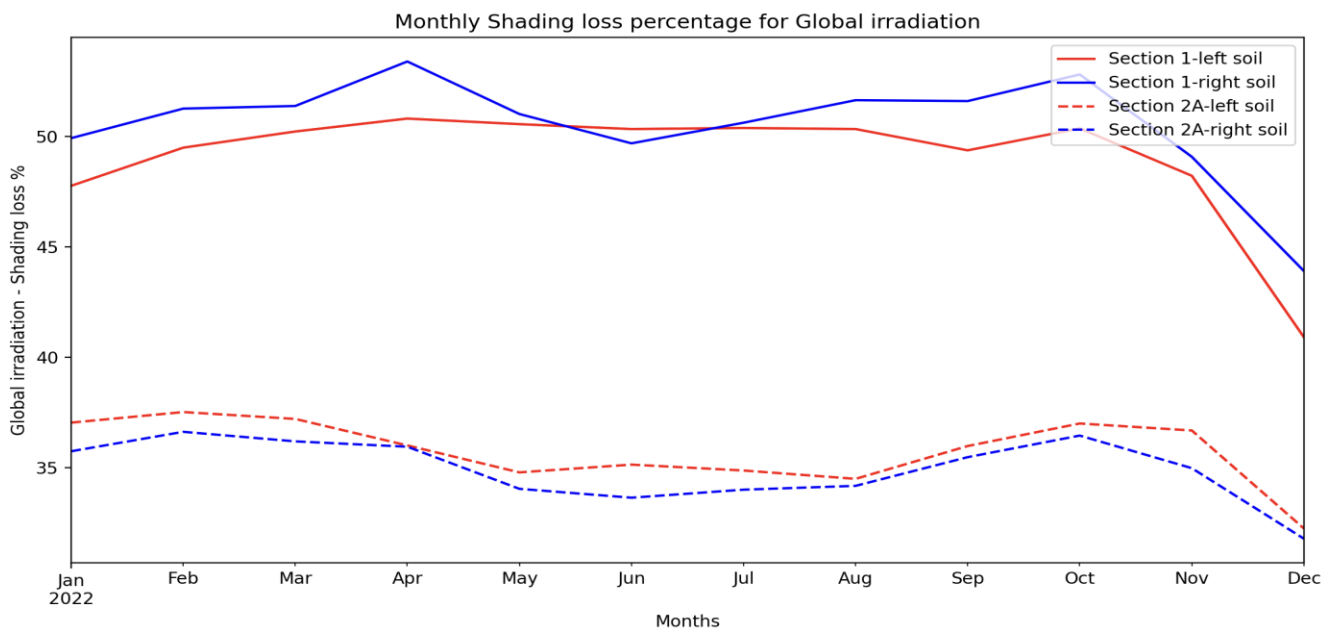


Figure 92: Monthly global irradiation and corresponding shading loss for scenario with semi-transparency of 40%.

The overall distinction between Section 1, Section 2A, and Section 2B becomes apparent when comparing their respective yearly global irradiation values and the corresponding shading loss percentages. This comparison offers a comprehensive estimate of the impact of the differences in frame height for PV panel mounting in Section 2B and the utilization of 40% semi-transparent modules in Section 2A, in contrast to Section 1.

Figure 93 presents the yearly global irradiation and the corresponding shading loss percentage comparison for Section 1, Section 2A, and Section 2B, respectively. These visualizations allow for a holistic assessment of how variations in PV panel characteristics and mounting configurations across different sections influence overall irradiation levels and shading loss percentages throughout the year. Such insights are invaluable for optimizing the design and performance of Agri-PV systems to maximize energy production while minimizing shading-induced productivity losses in agricultural settings.

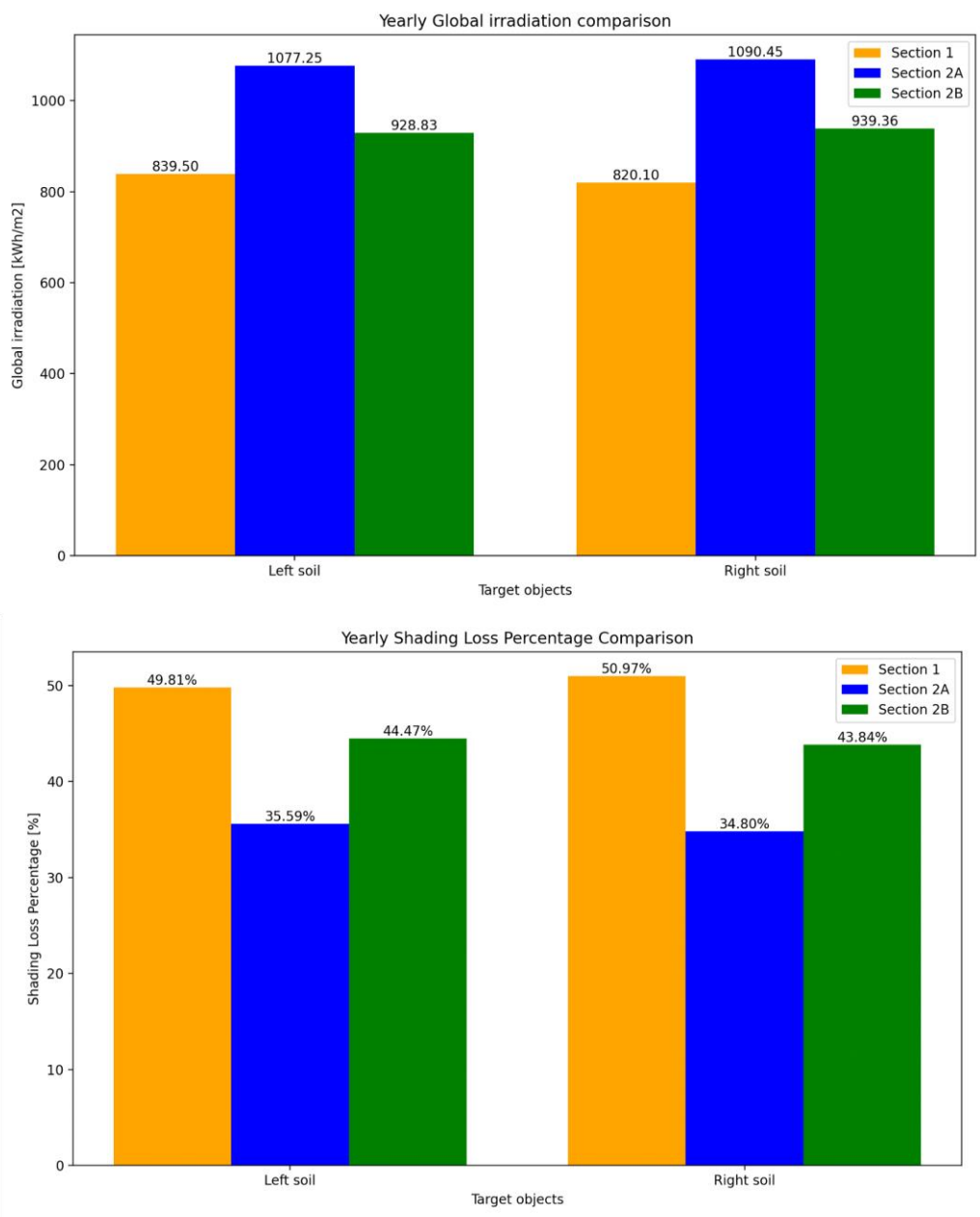


Figure 93: Yearly global irradiation and the corresponding shading loss percentage comparison.

While shading losses have been calculated for the proposed system (Section 1) along with other testing sections (2A-2B), fully understanding the impact of the proposed system's layout and associated shading pattern requires comparison with alternative configurations. Therefore, similar to the aforementioned approach, additional test cases were simulated, and corresponding shading loss percentages were obtained.

The other configurations tested include:

- Infinite shed: A configuration where an infinite shed is applied to the proposed system (Figure 94);
- Fixed-tilt: A fixed tilt system with zero-degree tilt (Figure 95);
- Fixed-tilt, Infinite-shed: A fixed tilt system with infinite sheds (Figure 96);
- Centred: A system where the agricultural land is positioned directly beneath the PV system (Figure 97)

By comparing the shading loss percentages across these different configurations, a comprehensive understanding of the optimal layout and design considerations for the Agri-PV system can be achieved. This analysis is essential for maximizing energy production while minimizing shading-induced productivity losses in agricultural settings.

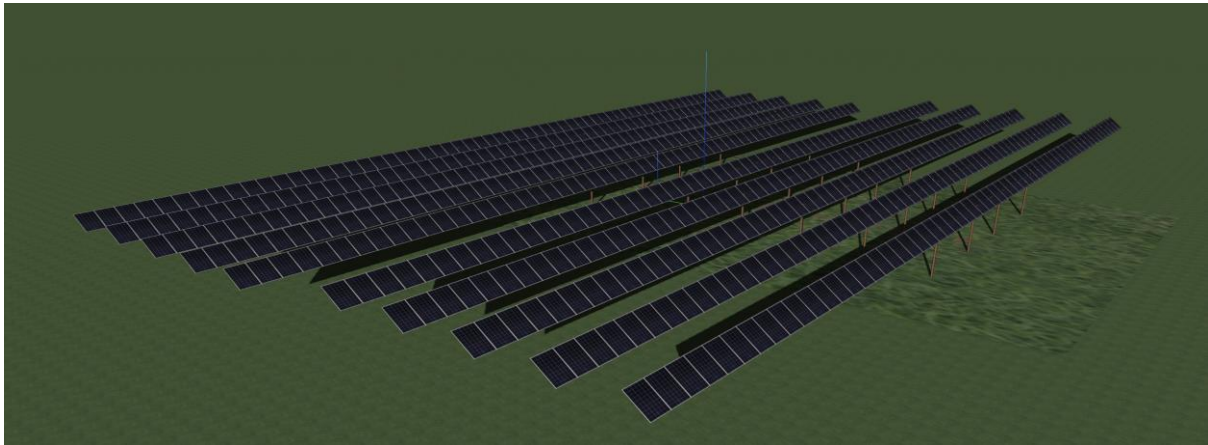


Figure 94: 'Infinite shed' applied to the 'Proposed' system.

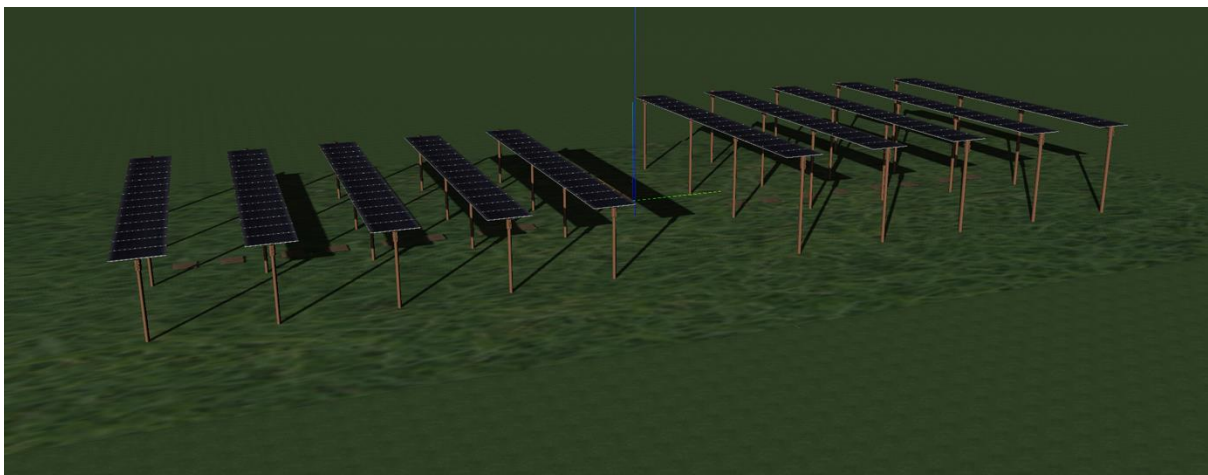


Figure 95: 'Fixed tilt' of zero degrees applied to the 'Proposed' system.

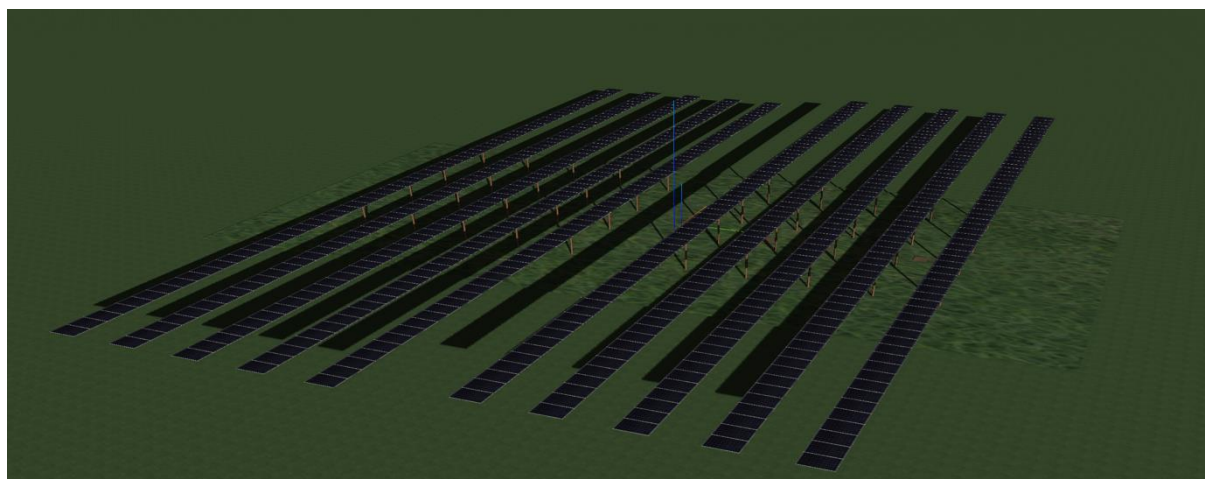


Figure 96: 'Fixed tilt, Infinite Shed' applied to the 'Proposed' system.

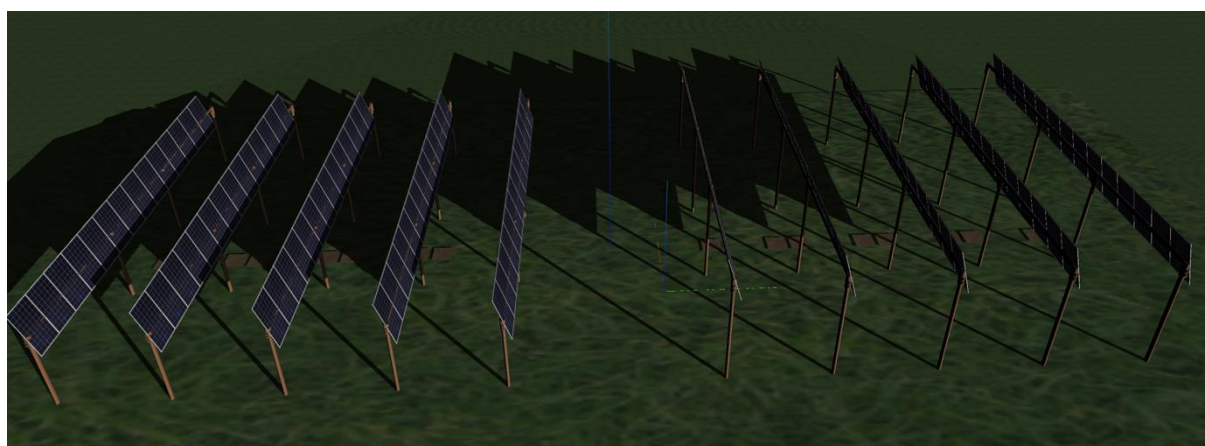


Figure 97: Agricultural land 'Centred' with respect to the PV modules in the 'Proposed' system.

The images in the following section present graphs for the left soil of Section 1 for the various configurations mentioned earlier. Figure 98 displays the global shading percentage loss over resolutions of 10 minutes, daily, monthly, and yearly, respectively. These graphs provide a comprehensive overview of how shading loss varies across different time scales for the left soil of Section 1 under different configuration scenarios. Analyzing these graphs enables a detailed assessment of the impact of configuration changes on shading-induced productivity losses, aiding in the optimization of Agri-PV system design and layout.

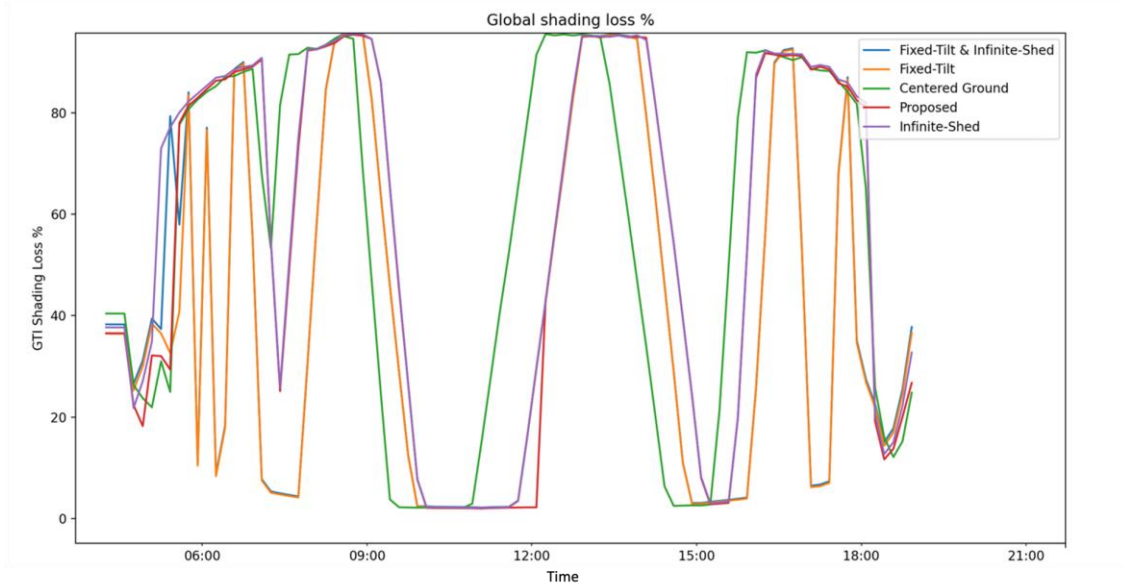


Figure 98: Global shading loss percentage for 18th of July (TMY).

The significance of these different configurations on shading losses becomes evident when the losses are integrated monthly. Figure 99 illustrates the monthly shading losses on global irradiation for the various configurations. By examining these monthly shading loss trends, one can gain valuable insights into the comparative performance of each configuration over the course of the year. This analysis facilitates the identification of optimal configuration strategies for mitigating shading-induced productivity losses in Agri-PV systems.

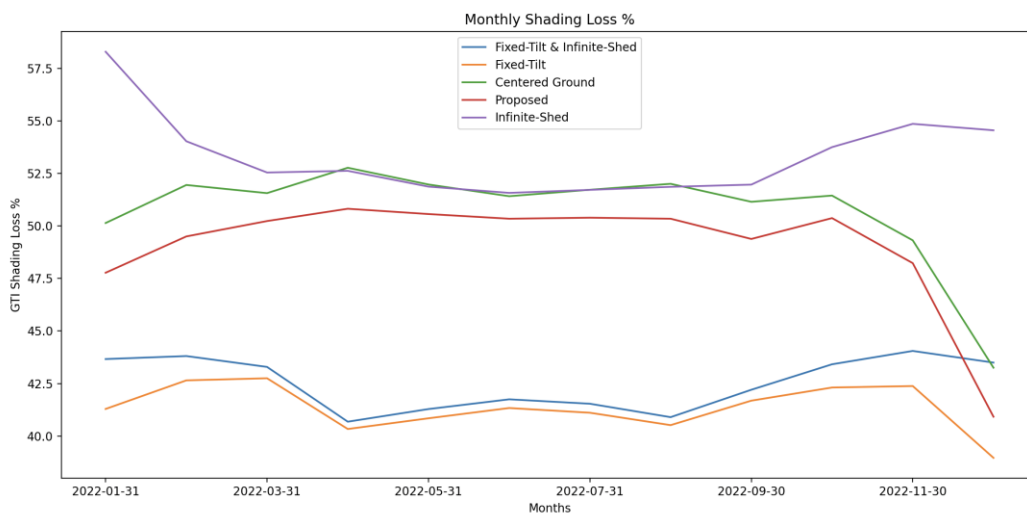


Figure 99: Monthly global shading loss percentage.

In the above graph, it can be observed that configurations with infinite sheds have higher shading losses during the winter months when the sun is at a lower altitude, compared to their non-infinite-shed counterparts. For example, when comparing the 'Proposed' system to its counterpart featuring infinite sheds, namely the 'Infinite-sheds' system, it can be noted that shading losses are significantly higher for the 'Infinite-shed' system during winter months compared to other months. This could be attributed to the fact that, since the sun is at a lower altitude during winter months, for certain time periods in the case of the proposed system, sunlight manages to reach the target object (in this case, the 'left soil') by passing under the edge of the PV array. In contrast, in the case of the 'Infinite-shed' system, even at lower altitudes, sunlight gets obstructed from reaching the same target object due to the extended length of the PV array. Figure 100 shows such a moment precisely at 15:00 on January 1st, when the sun is at a lower altitude. It can be seen that no shadow is cast on the 'left soil' for the 'Proposed' system (left) as light manages to reach it by traveling under the edge of the PV array, whereas it gets obstructed in the case of the 'Infinite-sheds' system (right) by the extended PV array, thus shading the target object.

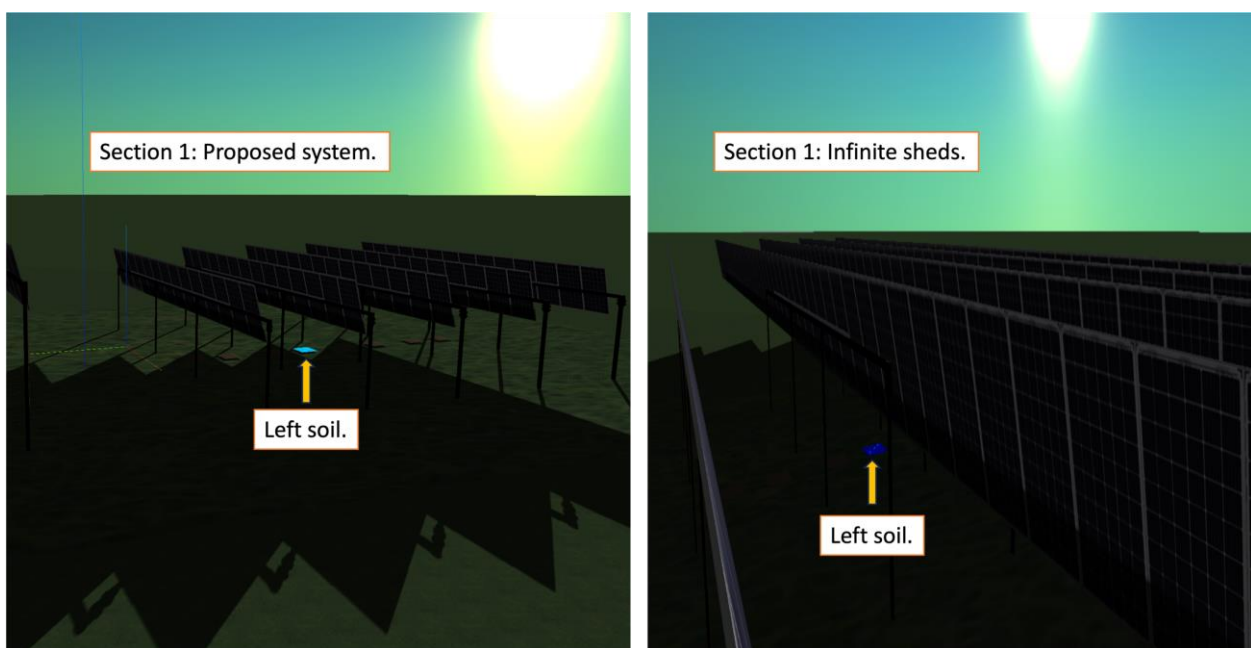


Figure 100: Comparison of edge effect for 'Proposed' system (left) and 'Infinite-shed' (right) at 15:00 on January 1st.

The overall difference between different configurations can be observed by comparing their respective yearly global irradiation shading loss percentages. This effectively provides an overall estimate of the effect of the difference in the PV layouts compared to the 'Proposed' system. Figure 101 shows the yearly global irradiation shading loss percentage comparison for all the different configurations considered.

Alternatively, the effect of shading on the vertical surface of the modeled crop's envelope is investigated, focusing on two main system configurations. The first configuration, referred to as the 'Proposed' system or 'Base case,' represents the initial setup. The second configuration involves positioning the agricultural land along with the crops directly beneath the PV modules, referred to as the 'Centred' system. By comparing these configurations, insights can be gained into how different placement strategies impact shading on the vertical surfaces of crop envelopes, providing valuable information for optimizing Agri-PV system design and layout.

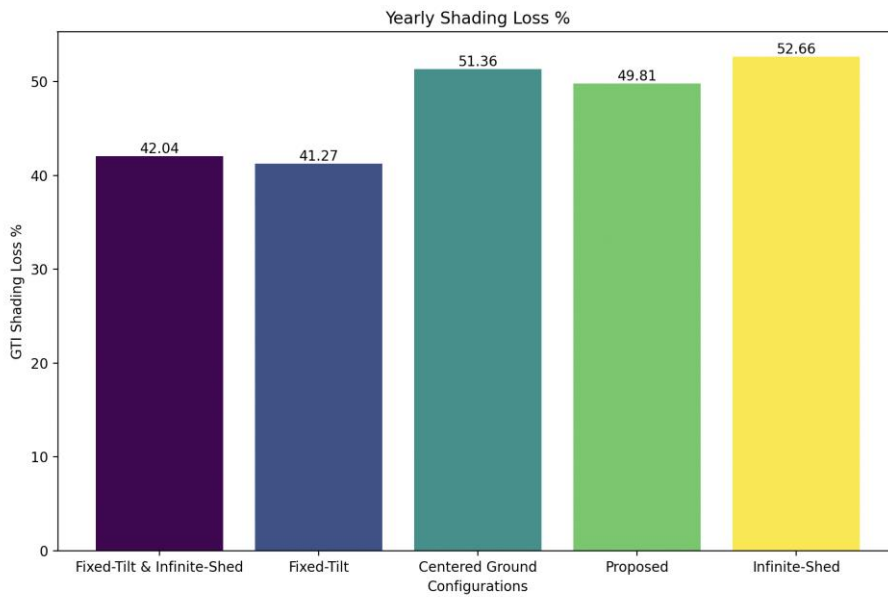


Figure 101: Yearly global shading loss percentage.

Figure 102 depicts the base Agri-PV system, with lettuce represented by light green hemispheres and tomatoes depicted by cuboids with texture of tomato crops applied, on the crop cultivation land with brown texture. The shading loss and the trend for lettuce will be similar to that of the ground, done above, hence, for the moment to estimate the shading loss over the crops, especially over the vertical part for the above-mentioned reasons, tomato crop is chosen. More specifically, the one indicated in the same figure is chosen, which will be referred as ‘left long tomato’. Alternatively, another configuration, namely ‘centred’ as depicted in Figure 103, is studied to compare and analyse it with the base case.

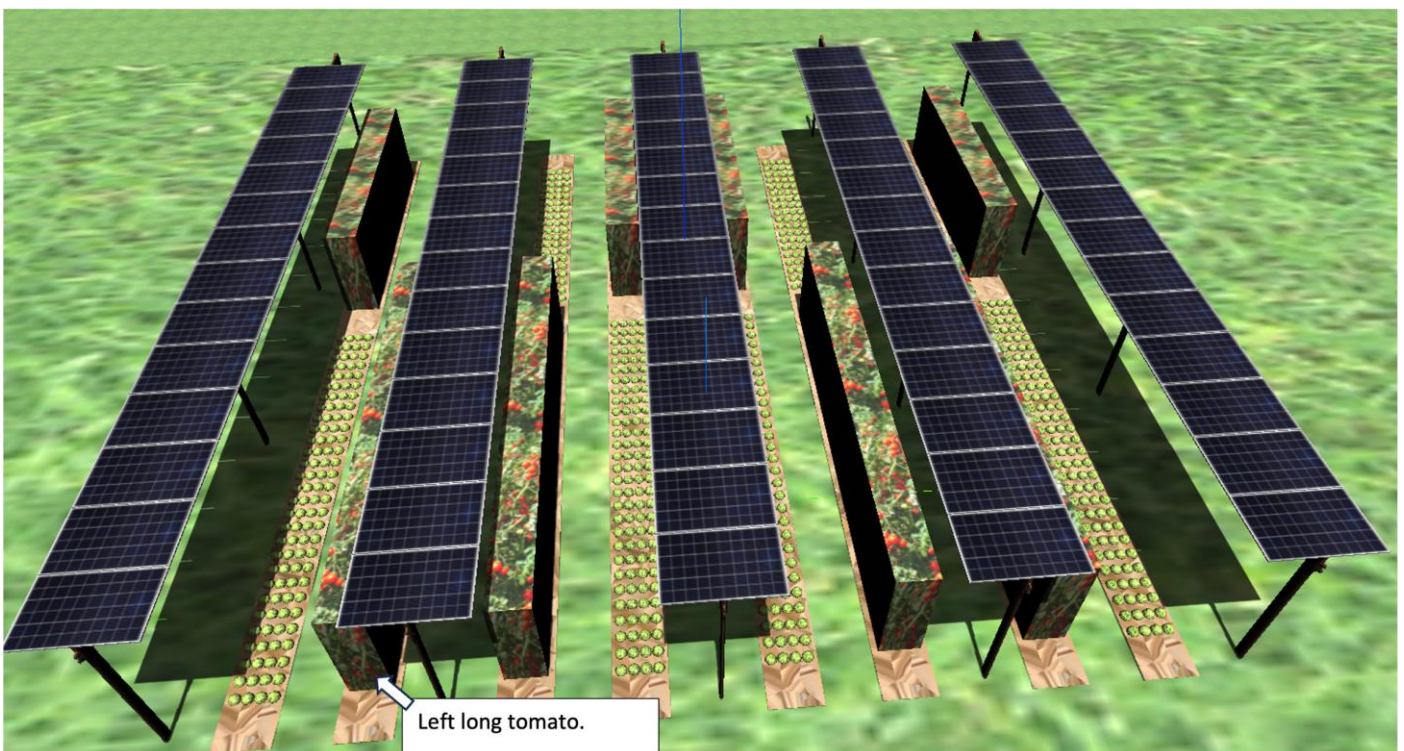


Figure 102: Base case scenario depicting proposed Agri-PV system and indicated tomato crop as the target object.

Figure 103 depicts the Centred system, wherein the crops, including the indicated target object, are positioned directly beneath the PV modules.

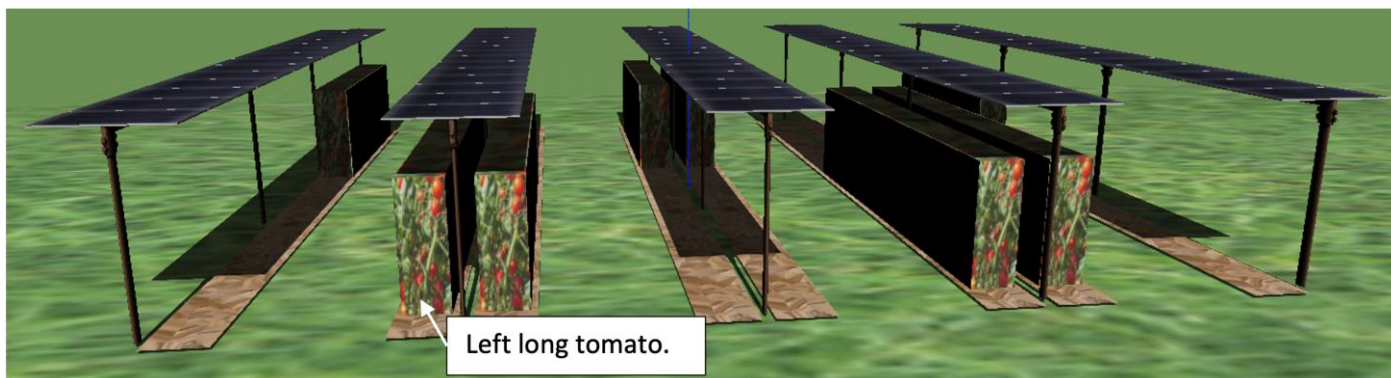


Figure 103: Crops placed at the centre.

Figure 104 depicts the reference case, that is scenario with no PV system, for the shading loss estimation.

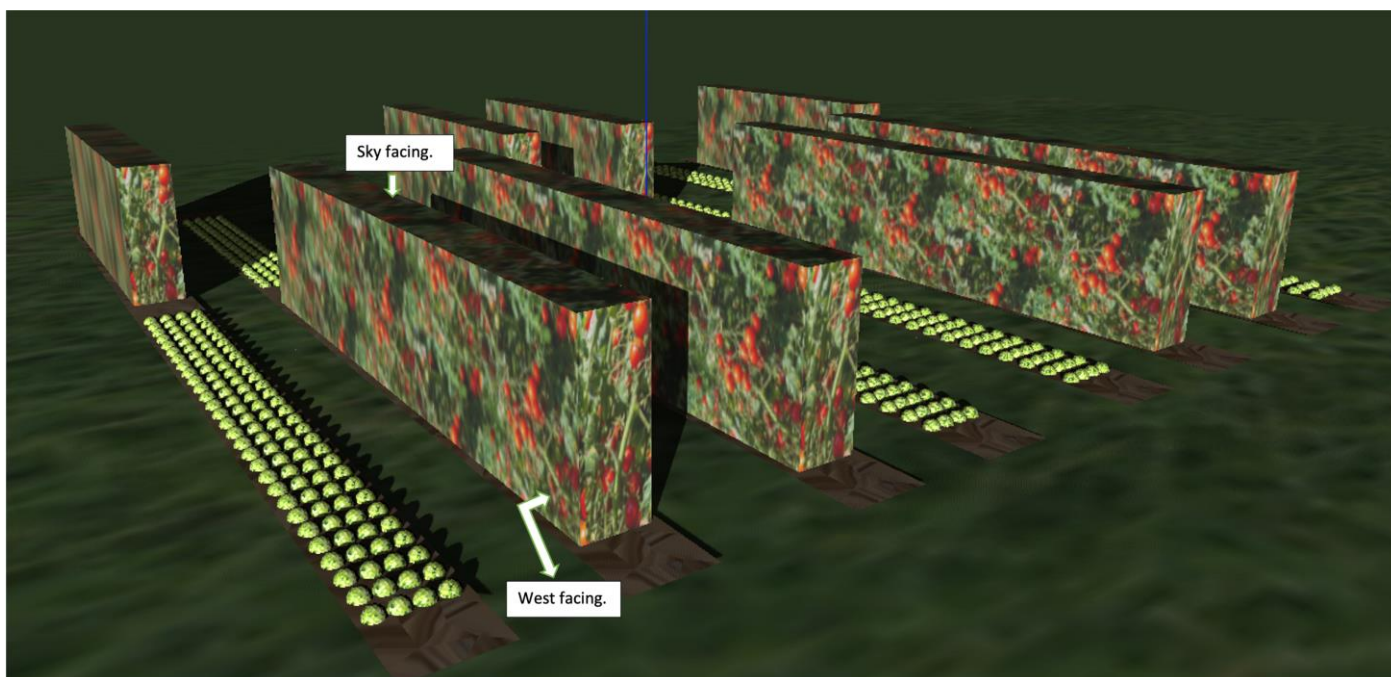


Figure 104: Reference case of the shading loss estimation.

All the vertical sides of the crop are split in three zones as a function of their height from the ground. Zone 1 being the bottom most zone, covering the height from 0.5m – 1m. Zone 2 being the middle zone covering the height from 1 m - 1.5m. Similarly, Zone 3 being the topmost zone covering the height between 1.5 m – 2 m. This zone separation is shown in Figure 105 with the west and sky-facing sides indicated.

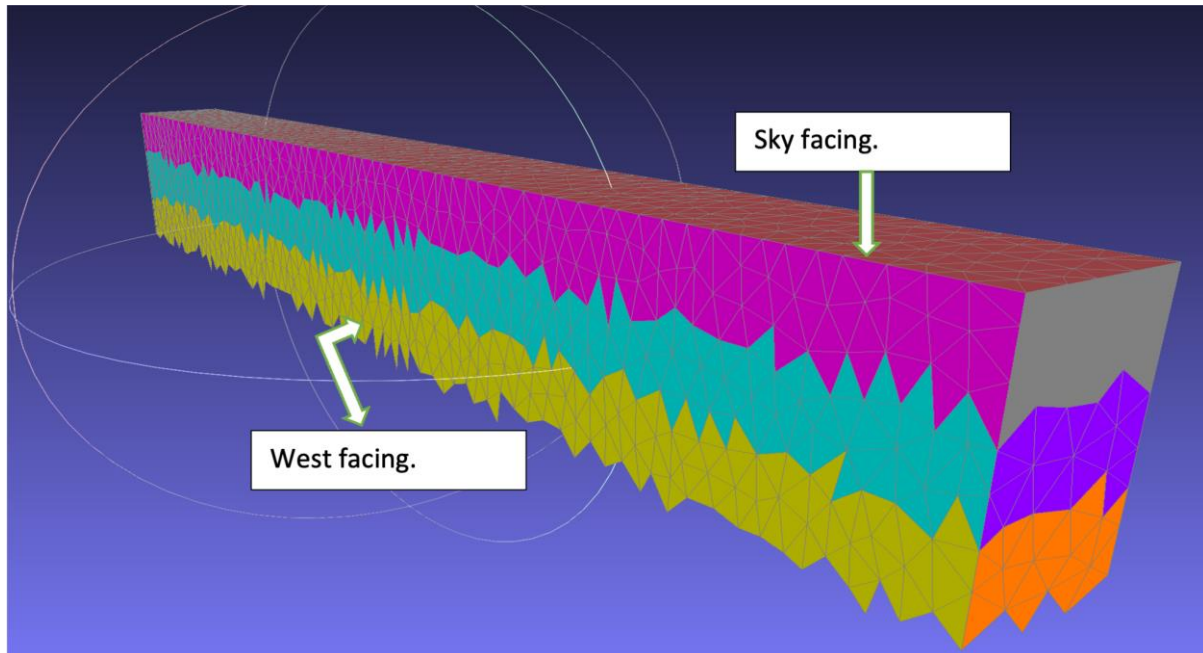


Figure 105: Zone separation for the left long tomato with the west facing side indicated.

Figure 106 and Figure 107 show the evolution of global irradiance and the corresponding shading loss percentage over all the sides of the crop and their individual respective zones.

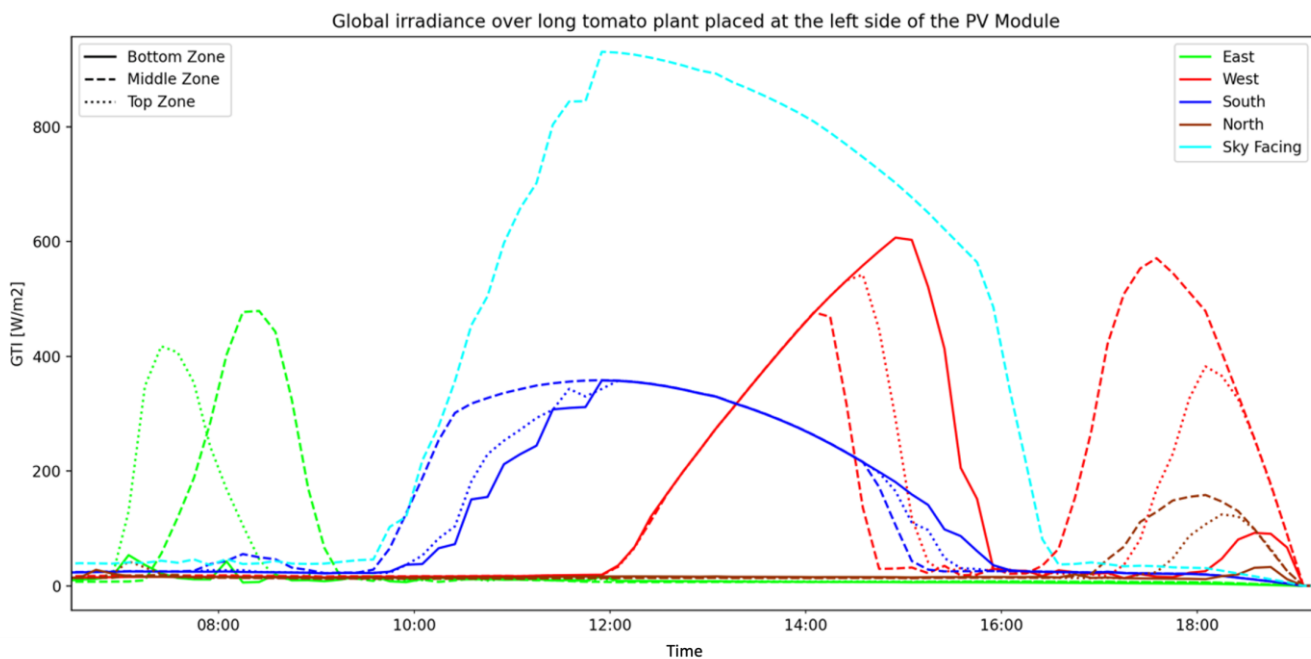


Figure 106: Global irradiance on 18th of July (TMY).

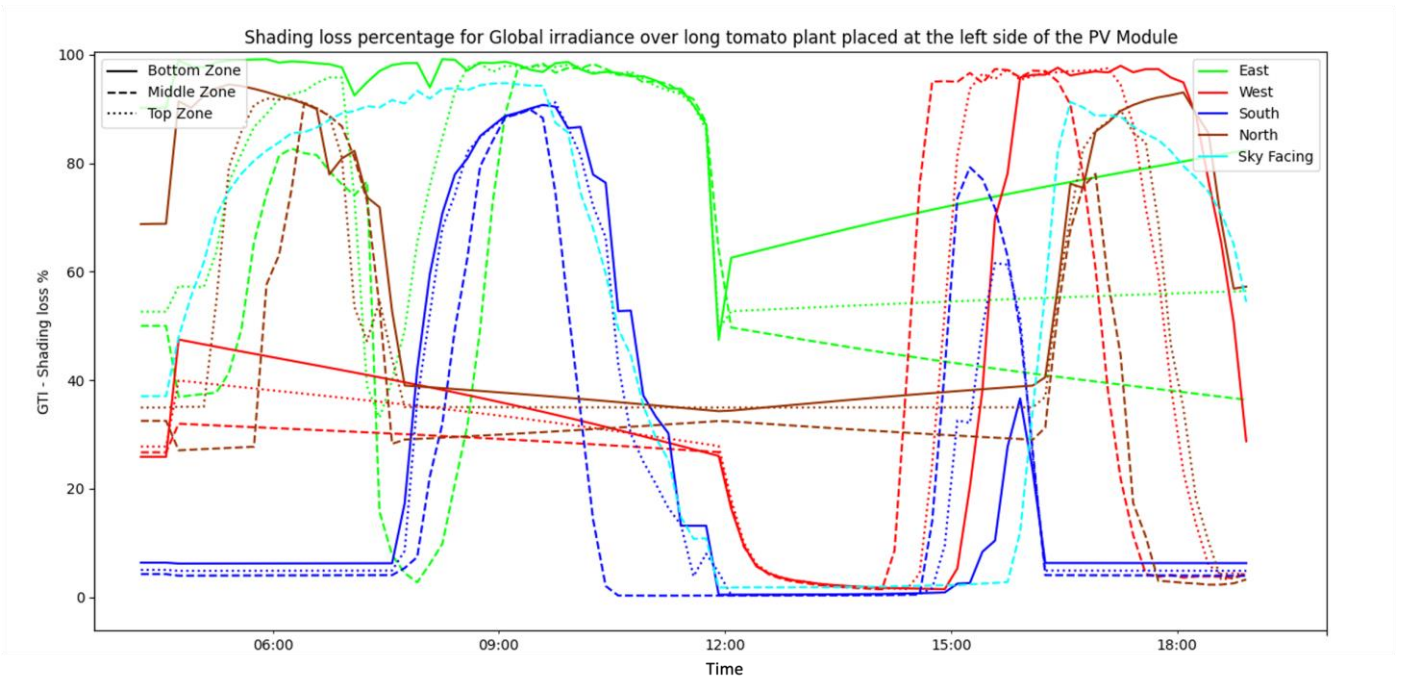


Figure 107: Global shading loss percentage on 18th of July (TMY).

Figure 108 illustrates the evolution of cumulative global irradiation on the 18th of July in the Typical Meteorological Year (TMY) time series across all zones of the west-facing side using a heatmap representation. This visualization offers insights into variations in solar exposure throughout the day and highlights areas of potential shading or reduced irradiance.

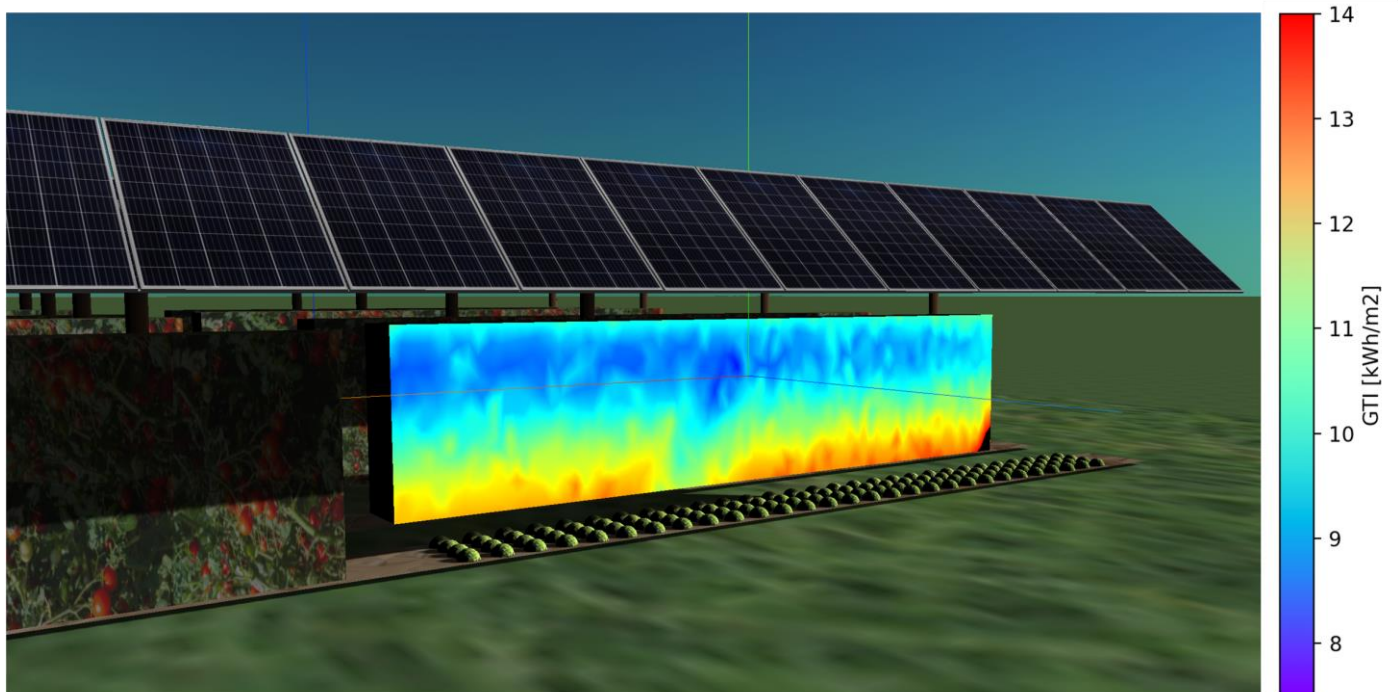


Figure 108: Heatmap for the cumulative daily global irradiation (18th July TMY) over all three zones of west facing side for the long tomato placed at the left side of the PV module.

With the west face split in three zones, hereinafter referred as bottom zone, middle zone, and the top zone are indicated by the colours yellow, cyan, and magenta respectively. For graphical representation, middle zone is compared between the base case and the centred system. Figure 109 depicts the shading loss percentage comparison for ‘base’ and ‘centred’ case on 18th of July of the TMY time series.

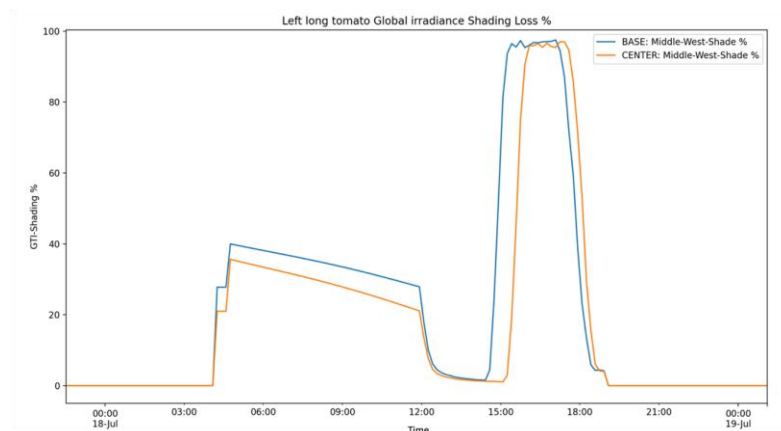


Figure 109: Shading loss percentage on 18th of July, for the middle zone of west facing side.

To better visualize the above plot and to validate the results from the plot, shading pattern for any chosen moment in time can be visualized in LuSim. For observing the stark contrast in the shading pattern for the selected target object at the specific zone, Figure 110 and Figure 111 present the shading as observed at the time stamp 15:00 via a realistic view and the corresponding heatmap for that instance for 'Base' and 'Centred' system respectively. Furthermore, the targeted zone on these crops is indicated, to highlight the difference in shading pattern.

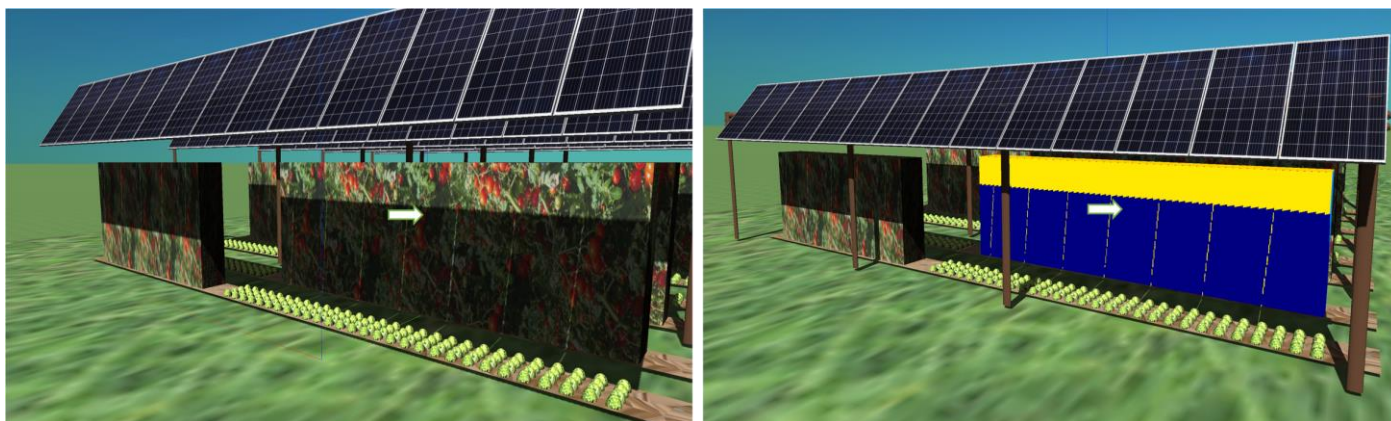


Figure 110: Realistic shading and corresponding heatmap in 3D space for the 'Base' system on its indicated west facing middle zone, at 15:00 on 18th July (TMY).

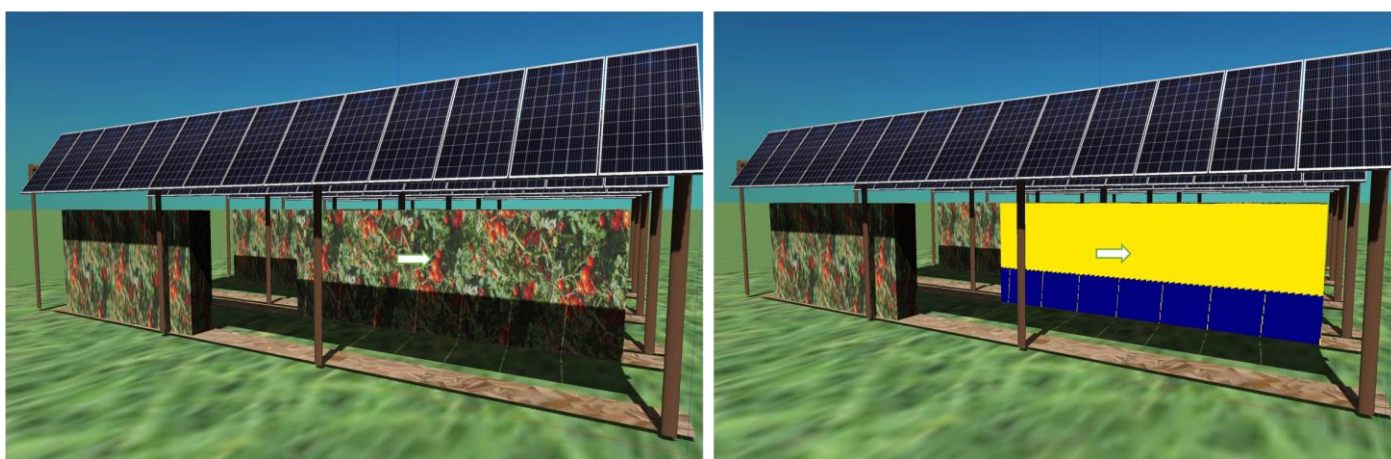


Figure 111: Realistic shading and corresponding heatmap in 3D space for the 'Centred' system on its indicated west facing middle zone, at 15:00 on 18th July (TMY).

However, the significance of the above depicted difference in shading pattern for 'base' and 'centred' system can be better brought to light when the shading losses are integrated for monthly and yearly values. Figure 112 and Figure 113 depict shading loss comparison for the west facing middle zone between the two system configurations for monthly and yearly values, respectively.

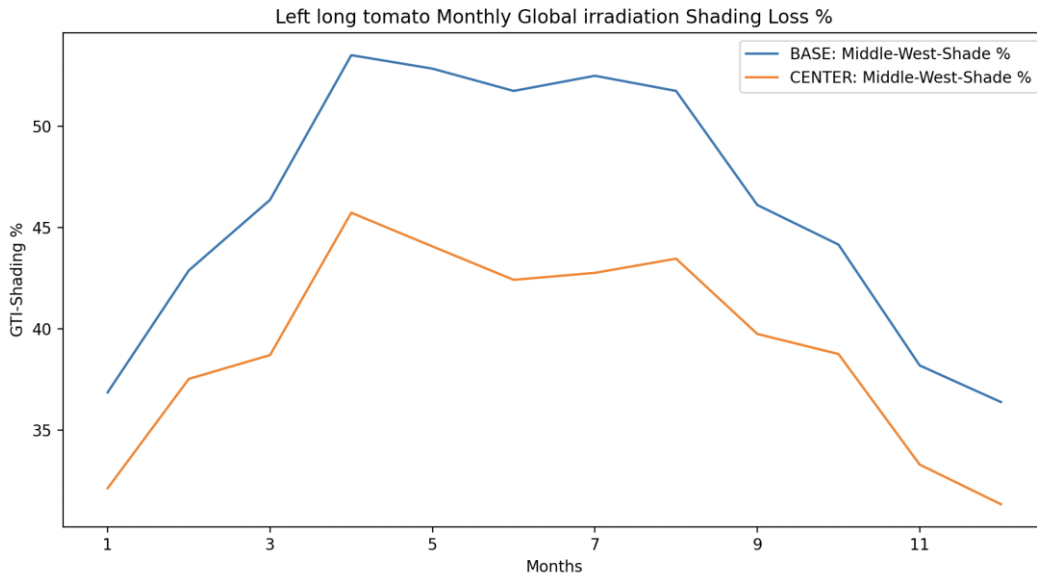


Figure 112: Monthly shading loss percentage, for the middle zone of west facing side.

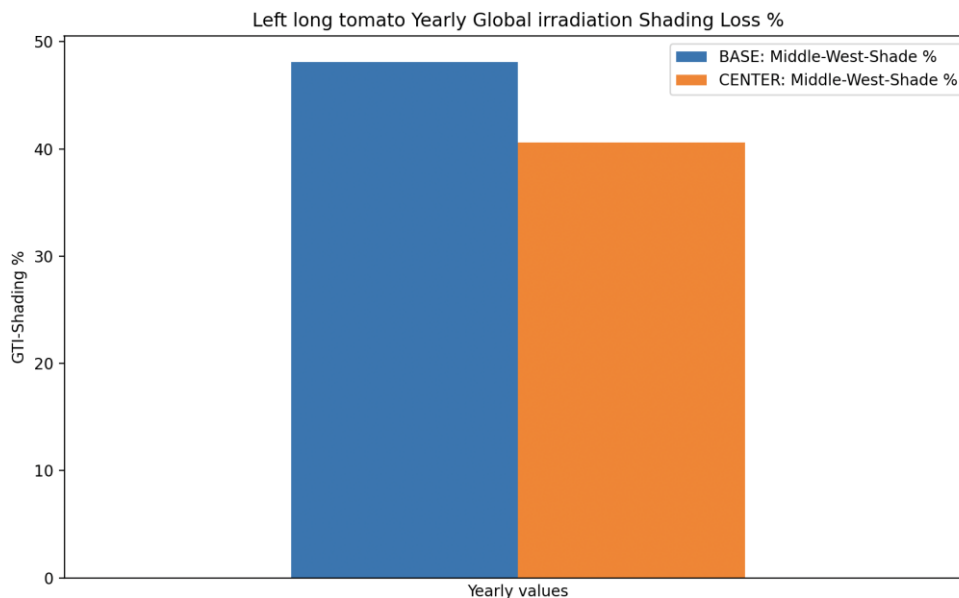


Figure 113: Yearly shading loss percentage, for the middle zone of west facing side

Similar trends are observed for all the vertical sides of the crop's envelope when comparing the 'base case' and the 'centred' case. Contrary to popular belief, it is more beneficial to place the crops directly under the PV system when the vertical sides of the crops are of interest for receiving light.

However, for the sky-facing side, the trend observed between the 'base' and 'centred' system is different. In the following section, graphs and images are produced to illustrate this comparison.

Figure 114 depicts the shading loss percentage comparison for the 'base' and 'centred' cases on a clear-sky day, specifically the 18th of July (TMY).

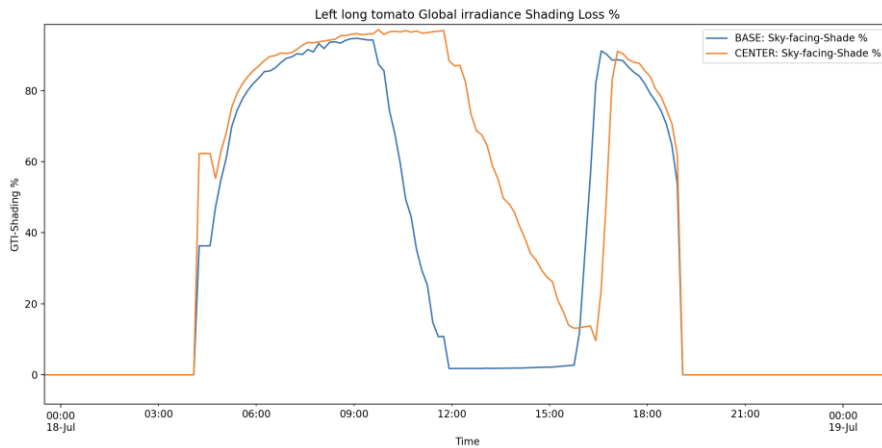


Figure 114: Shading loss percentage for 18th of July, for the sky facing side.

Similar to the approach for the vertical sides, to better visualize the stark contrast in the shading pattern for the selected target object for the sky-facing side, Figure 115 and Figure 116 present the shading as observed at the time stamp 12:00 via a realistic view and the corresponding heatmap for that instance, for the systems 'base' and 'centred', respectively. Furthermore, the targeted zone on these crops is indicated, to highlight the difference in shading pattern.

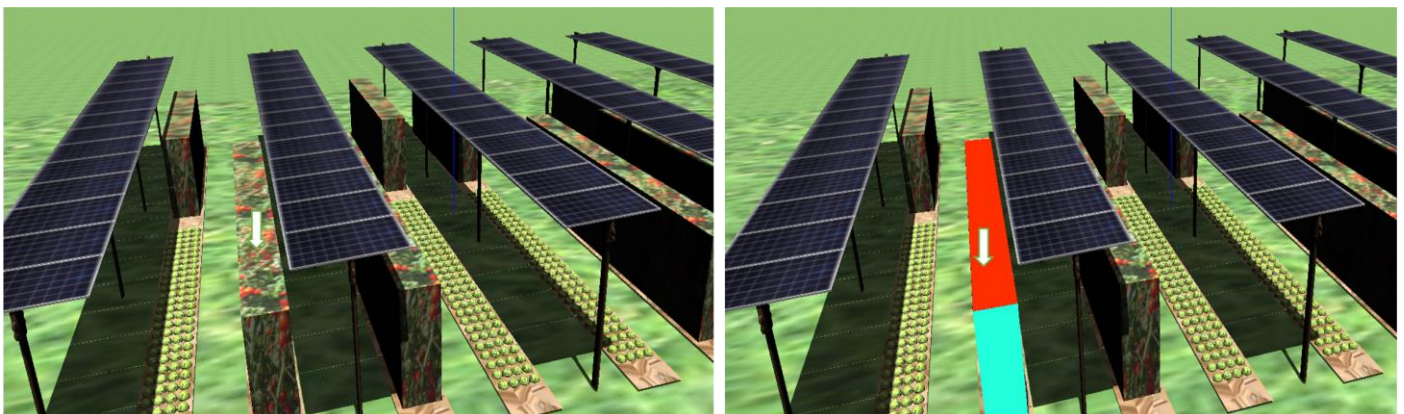


Figure 115: Realistic shading and corresponding heatmap in 3D space for the 'Base' system on its indicated sky-facing side, at 12:00 on 18th July (TMY).

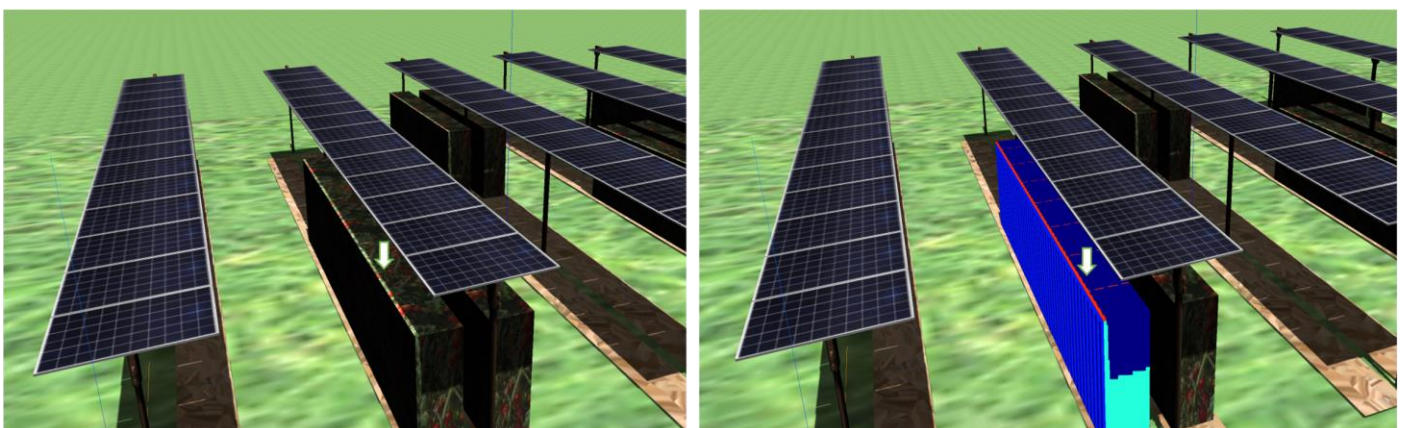


Figure 116: Realistic shading and corresponding heatmap in 3D space for the 'Centred' system on its indicated sky-facing side, at 12:00 on 18th July (TMY).

However, the significance of the above depicted difference in shading pattern for ‘base’ and ‘centred’ system can be better brought to light when the shading losses are accumulated for monthly and yearly values. Figure 117 and Figure 118 depict shading loss comparison for the sky facing side between the two system configurations for monthly and yearly values respectively.

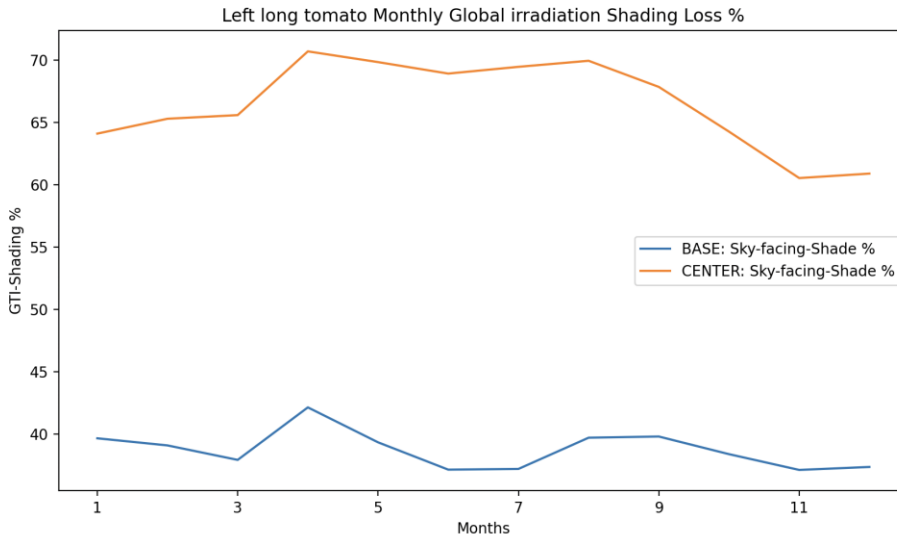


Figure 117: Monthly shading loss percentage comparison, for the sky facing side.

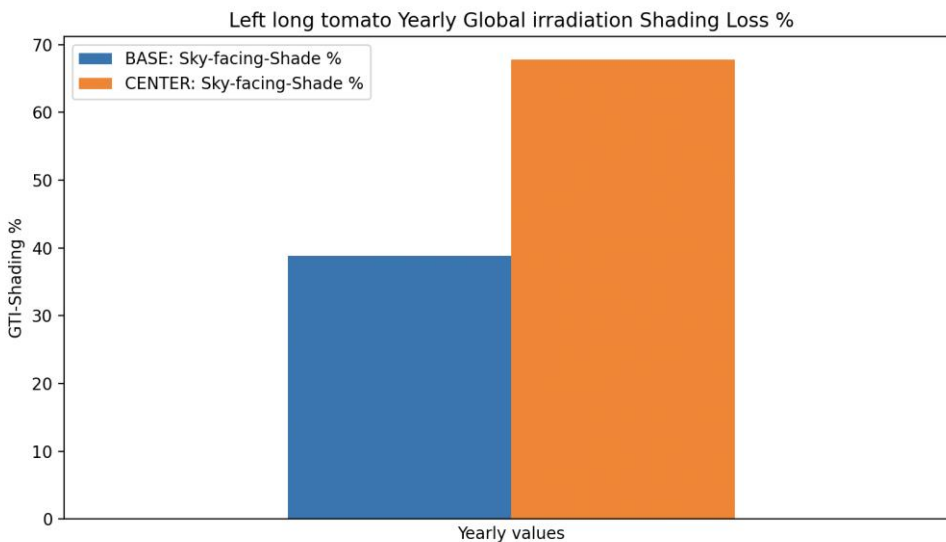


Figure 118: Yearly shading loss percentage comparison, for the sky facing side.

Contrary to the trend observed for the vertical sides, the sky-facing side shows opposite trend. That is, when horizontal sky-facing side of the crop’s envelope is of interest for the light capture, it is beneficial to not keep the crop directly under the PV module, or in other words, ‘base’ case will be preferred over the ‘centred’ system. As it can be observed from the above plots, how ‘base’ case has significantly less shading loss compared to the ‘centred’ system.

However, while the sky-facing side of the crops may receive more irradiance per surface unit, the vertical light collection surfaces of the canopy are significantly larger. As a result, photosynthesis is primarily driven by the amount of irradiance reaching the vertical sides rather than the sky-facing side. Therefore, the beneficial positioning of the crops directly under the PV system for optimal light exposure on their vertical sides remains crucial, despite potential differences in irradiance levels on the sky-facing side.

Additionally, the entire range of pitch distances between two frames has been examined for the proposed configuration to assess the impact of the PV system by analyzing the global incident irradiance and the shading pattern. This analysis involves dividing the pitch distance into five different zones, achieved by utilizing five patches of equal dimensions. Figure 119 illustrates these five patches placed adjacent to each other to cover the complete pitch distance. Subsequently, these zones will be referred to as zone 1, 2, 3, 4, and 5, respectively, progressing from left to right or from west to east.

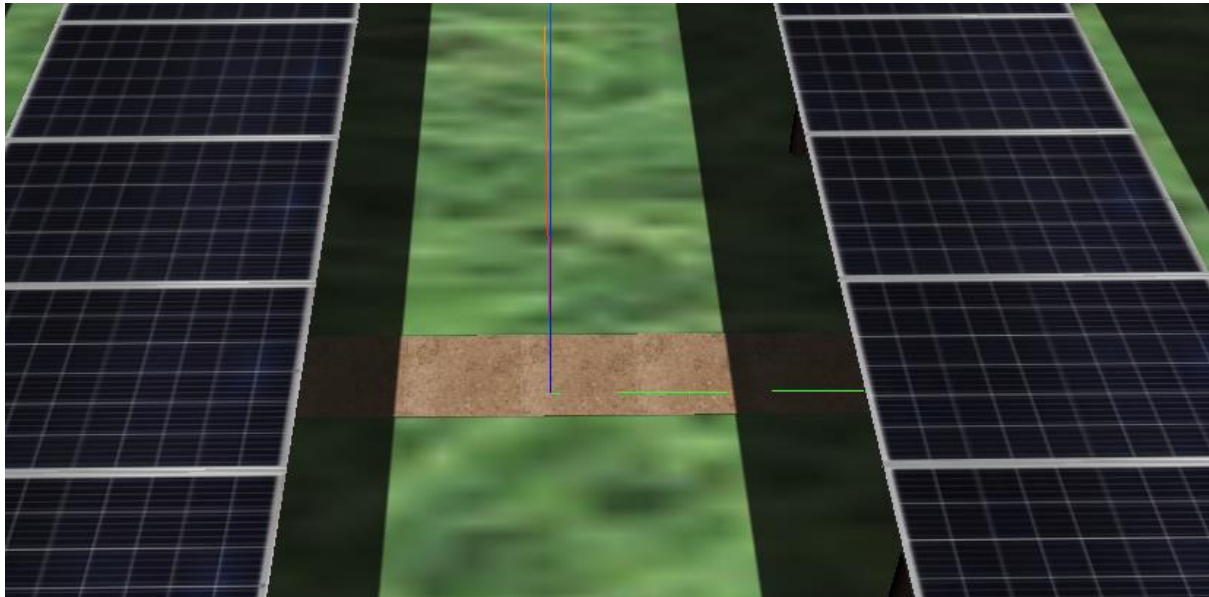


Figure 119: Five zones covering the pitch distance.

Shading losses are estimated in the same way as for the above cases, that is taking a reference case with no PV system. The intention behind analysing each of these zones is to see the evolution of incident global irradiance on them and eventually to observe the optimum situation of the crop cultivation land, in this case zone, in terms of incident global irradiance and the shading loss. Figure 120 and Figure 121 show the global incident irradiance and the corresponding shading loss percentage for 18th of July of the TMY time series, respectively.

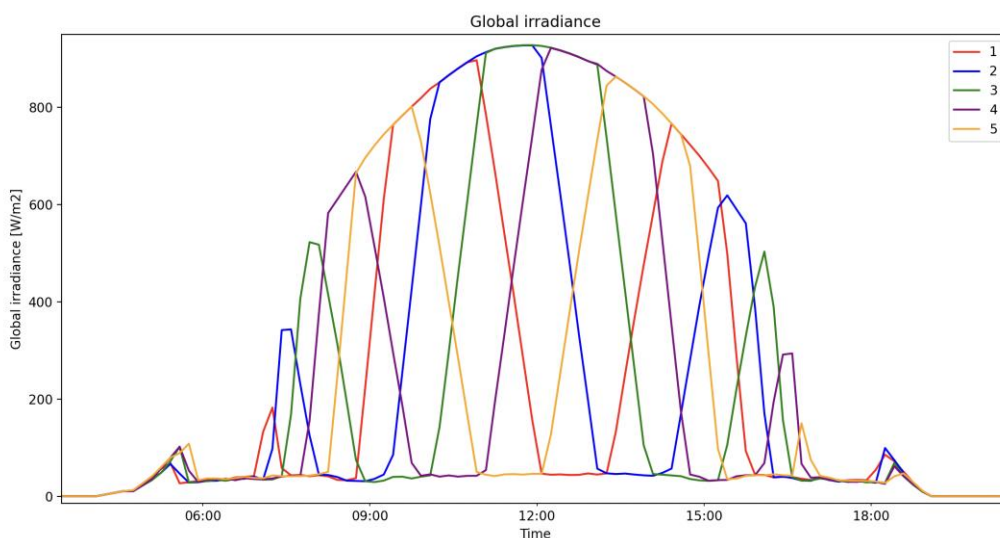


Figure 120: Global irradiance for 18th of July across the complete pitch distance using 5 zones.

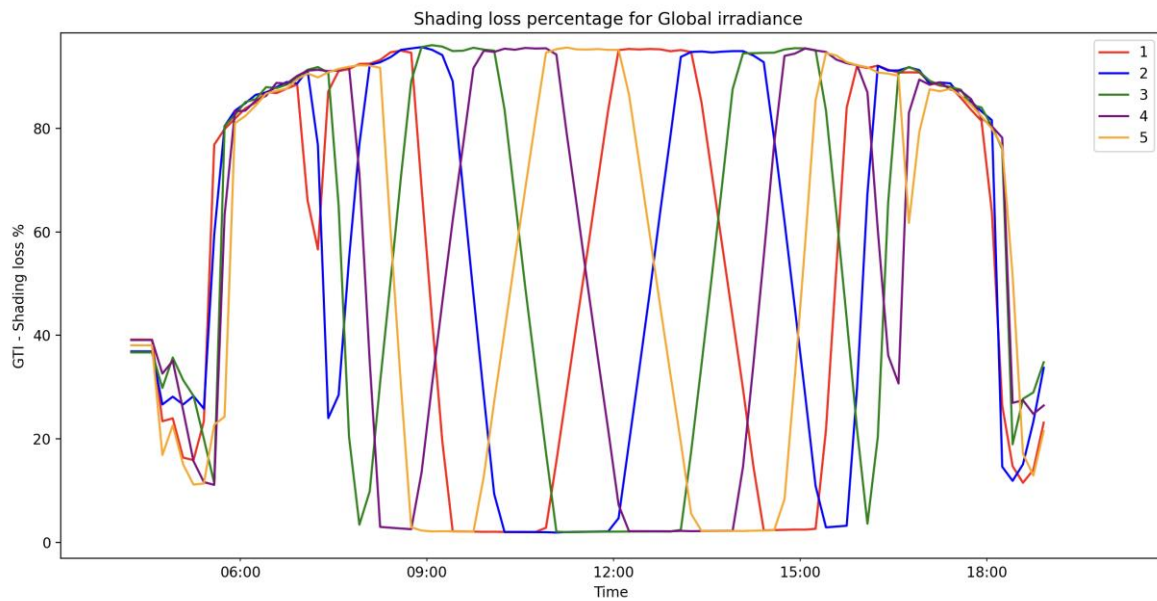


Figure 121: Shading loss percentage for 18th of July across the complete pitch distance using 5 zones.

At any given moment in time, all five zones do not uniformly receive the same global irradiance due to differences in shading patterns. While the variation in shading patterns over time for a clear-sky day is depicted through a plot above, Figure 122 provides realistic images generated in LuSim. These images showcase shading in 3D space and the corresponding heatmap at an arbitrary moment, specifically 11:45 on the 18th of July of the TMY time series. By examining these images, differences between zones in terms of shading intensity and distribution become evident, highlighting the dynamic nature of irradiance distribution across the proposed configuration.

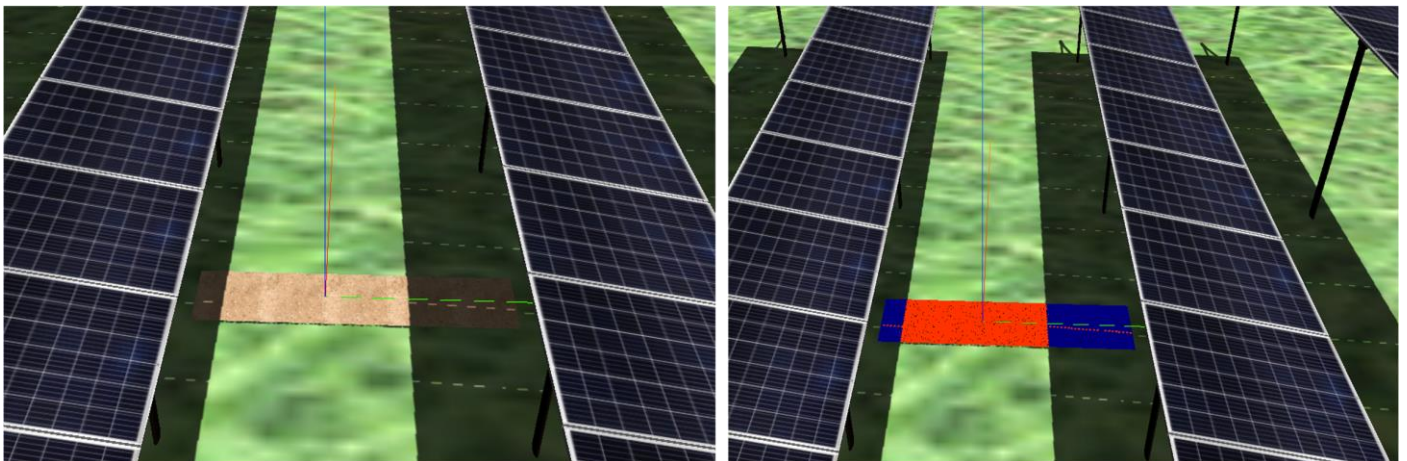


Figure 122: Shading (left) and the corresponding heatmap (right) across the pitch using 5 zones, at 11:45 on 18th July (TMY).

The significance of the placement of each of these zones can be observed when the global irradiance and the shading losses are integrated for monthly and yearly values. These differences overall can determine the placement of the crop cultivation land. Figure 123 and Figure 124 show the monthly global irradiation comparison and the corresponding shading losses.

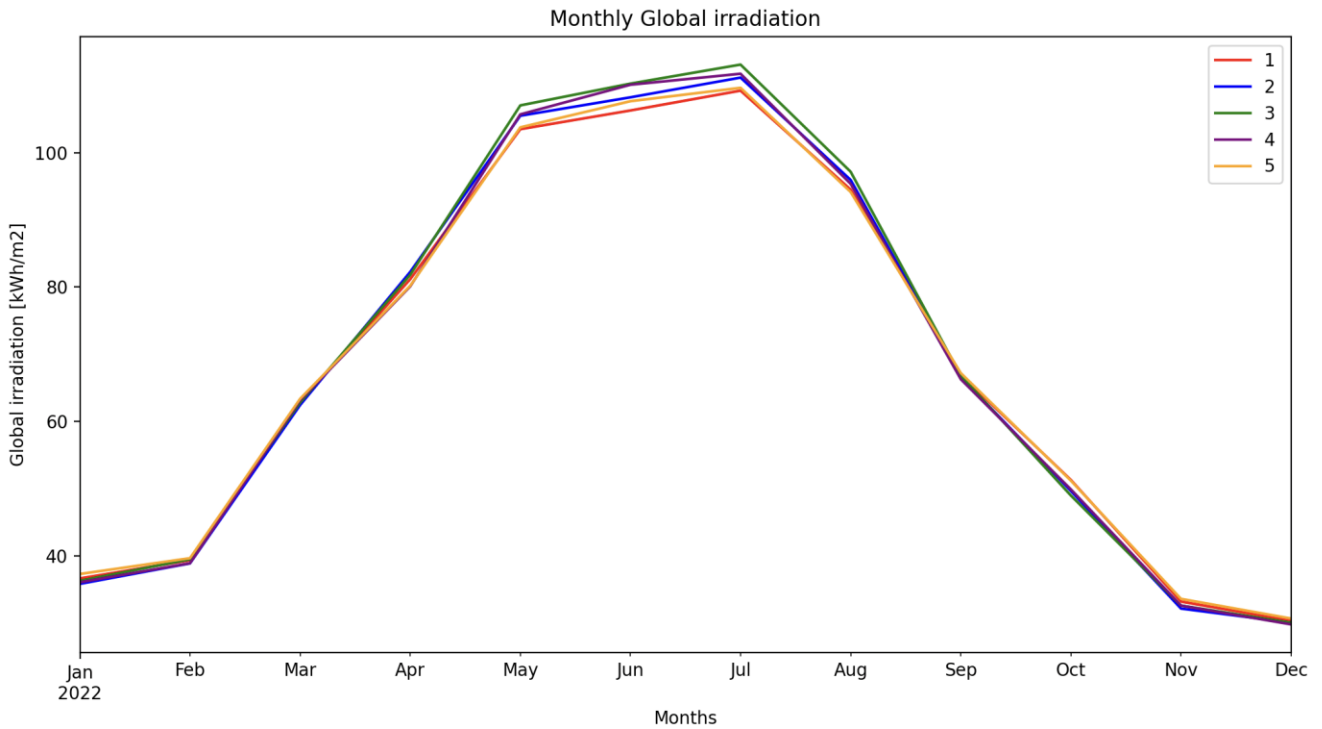


Figure 123: Monthly global irradiation across the complete pitch distance using 5 zones.

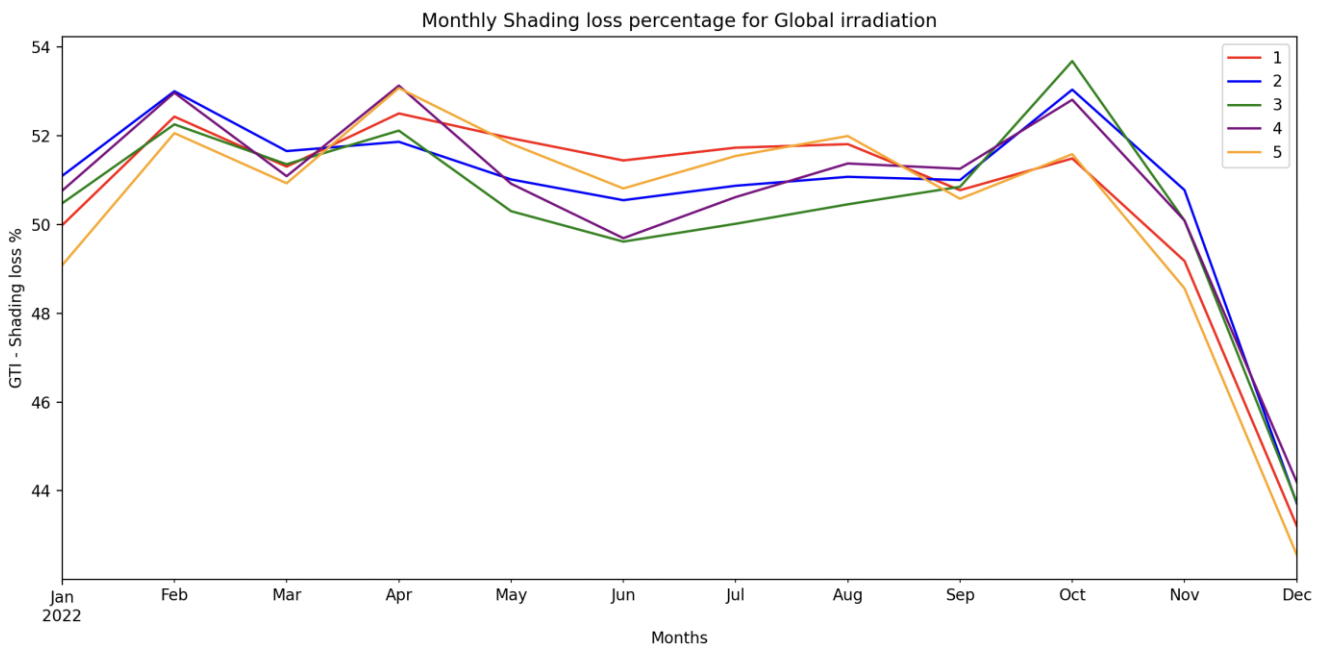


Figure 124: Monthly global irradiation shading losses across the complete pitch distance using 5 zones.

An overall effect of the placement of the five zones with respect to the PV system can be observed through yearly global irradiation and shading loss values. Notably, the zone positioned in the middle or the third zone exhibits a slight advantage compared to other zones in terms of total yearly global irradiation and shading losses. Figure 125 and Figure 126 provide yearly bar plots for the yearly global irradiation and the corresponding shading losses respectively.

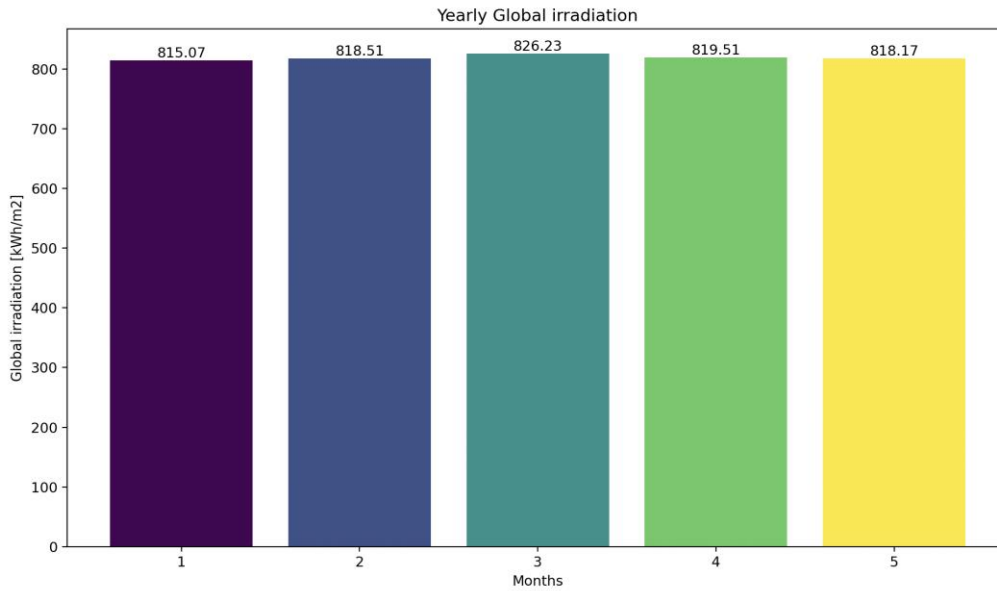


Figure 125: Yearly global irradiation across the complete pitch distance using 5 zones.

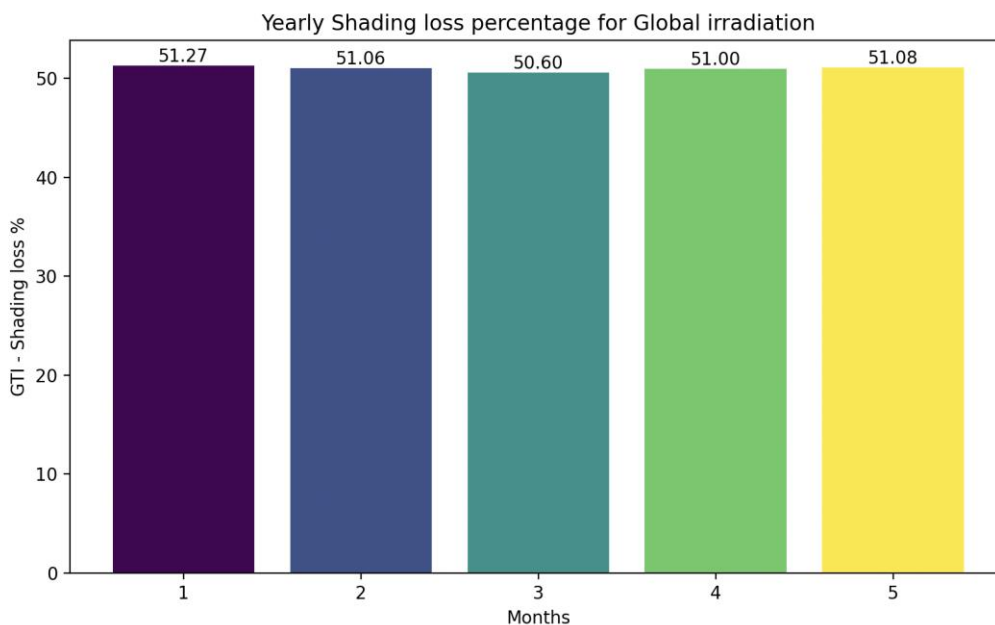


Figure 126: Yearly global irradiation shading losses across the complete pitch distance using 5 zones.

3.3. CONCLUSION AND DISCUSSION

The proposed Agri-PV system in Barcelona aims to cultivate short-stature and trellised seasonal vegetables, including tomatoes, melons, lettuce, and fava beans, between and under the trackers. This choice complements other demonstrators planned in the Bolzano area (apple trees) and Scalea (citrus), ensuring a diverse array of agricultural experiments across different regions.

The design of supporting structures for PV modules in Section 1 is detailed, depicting a 3D model integrated into LuSim's environment. Each row of the PV array is supported by a simple U-framed structure grouped in three along a North-South direction, with dimensions outlined. These dimensions are replicated in consecutive rows with a pitch along the East-West direction. Section 2B mirrors Section 1's structure but with a frame height difference. Section 2A retains the same support structure dimensions as Section 1.

Each section comprises rows of tracking PV modules with a specific pitch, housing bifacial PV modules arranged in portrait fashion with a slight gap between them.

In assessing plant growth, incident irradiance must be integrated separately for specific plant zones. Different representations of plants can be employed, ranging from simple geometric shapes to complex structures. Each approach has its advantages and computational implications. Simple shapes reduce computational complexity but may lack accuracy, while complex structures offer realistic representations but require more resources.

For the initial study phase, the crop's envelope is represented as a rectangular cuboid, enabling light distribution analysis under the PV system. This approach facilitates comparisons across different crop types while providing valuable insights into shading effects and light exposure variations.

While complex plant models offer detailed representations, basic shapes are favoured for their computational efficiency and compatibility with parametric models. These models enable the direct assessment of photosynthesis based on solar radiation reaching the canopy's outer envelope.

The study focuses on lettuce and tomato crops, modelling them in detail to analyse shading patterns and light exposure. The arrangement of crops, such as lettuce rows, is adjusted to optimize space utilization while maintaining adequate spacing for growth.

In subsequent phases, more representative crop envelopes will be modelled, reflecting the unique growth characteristics observed on-site. The findings from ground-level analysis will inform further adjustments to enhance accuracy and applicability.

The study compares different configurations, including infinite sheds, fixed-tilt systems, and centred layouts, to assess their impact on shading losses and irradiance levels. Insights from these comparisons guide the optimization of Agri-PV system designs for maximizing energy production and agricultural productivity.

The study also examines the positioning of zones relative to the PV system to identify optimal placement strategies. Yearly global irradiation and shading loss values provide comprehensive insights into the effectiveness of different configurations in harnessing solar energy while minimizing shading-induced productivity losses.

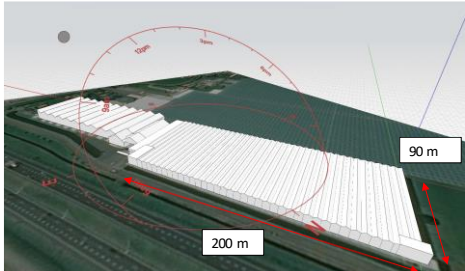
Overall, the study contributes to the development of efficient and sustainable Agri-PV systems, offering valuable insights into design considerations, crop modelling approaches, and optimization strategies for maximizing synergy between solar energy generation and agricultural production.

4. AGRIVOLTAIC DEMONSTRATOR 3 - NETHERLANDS

4.1. TECHNICAL SPECIFICATIONS

Table 12 describes the envisioned features of the demo of Bolzano and the updates in terms of Technical Specifications at M12 of the project.

Table 12: Envisioned features of the demo in the Netherlands and the updates in terms of Technical Specifications at M12 of the project

Use case 4	Greenhouse retrofit and KUBO bluelab
Unique Value Proposition	Retrofit of existing greenhouse fully equipped with sensors to correlate tomatoes yield with incident light depending on presence of uncoated and coated PV modules.
Location	Netherlands.
Replication potential	Use validated modelling to perform simulations for other countries (MEDA) and other crops (lettuce, berries) and check business models.
Crop	Tomatoes
Solutions implemented in the demo	 <p>The available area is of 200 x 90 m. The size of the SYMBIOSYST PV deployed solution will be of around 40 kWp (around 100-150 PV modules depending on semitransparency for an area of around 200-300 m²). Start with PV panel of standard size to keep cost down, make special Al profile for easy mounting. Use of semi-transparent agri-PV modules. Optimize PV module layout (cell/string spacing) and bill of materials (encapsulant, glass coating, etc.). Optimize PV system layout (horizontal/landscape orientation, rows vs chessboard pattern, etc.). Optimize PV system integration in landscape in general (visual key performance indicators to increase acceptance like with BIPV). The testing will compare the crop yield with clear glass, with PV modules, with coated PV modules.</p> <p>The Bluelab is KUBO’s facility already equipped with sensors and the possibility to compartmentalize into various volume for direct comparison. The lab will be equipped with semi-transparent uncoated and coated PV modules.</p>
Use of electricity	The PV system will be connected under the same Point of Delivery of the greenhouse. Although the size of the demonstrator will not allow for the coverage of the electrical demand, through modelling and validation with field data we will demonstrate the possibility to achieve nearly zero energy greenhouse.

This prototype is located at Lotsweg 3, 2636 JH, in the municipality of Schipluiden (near Delft), in the Netherlands.

The demo driver possesses a typical existing greenhouse structure in which vegetables such as tomatoes, cucumbers, peppers, lettuce and many other varieties, can be grown. At the moment there is a large demand for ‘extra’ energy, and same is expected from Agrivoltaic systems. However, the greenhouse market is very hesitant to install PV- panels above the vegetation area. The common idea is that all the available sunlight should be available for the maximization of crop yield. In this Demo the aim is to measure how much light is blocked by the PV-panels when they are installed in intervals above the growing area. With the DLI (Daily Light Integral) data of this test, it is of the interest to determine the number of PV panels that could be installed without losing crop yield. The coordinates of the site where the prototype will be located are 51.997963, 4.313927.

Figure 127 displays the existing greenhouse with the SYMBIOSYST test area.



Figure 127: Existing greenhouse and display of the SYMBIOSYST test area

Figure 128 shows a closer view over the VENLO greenhouses.

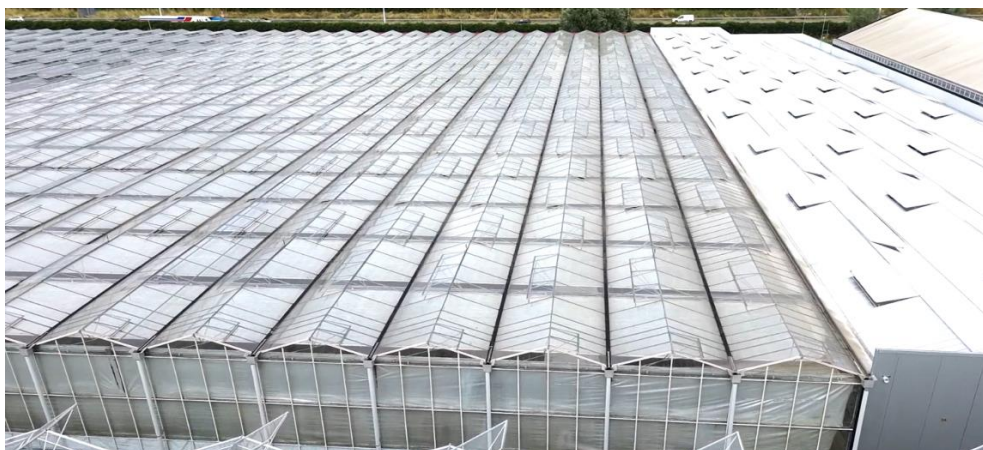


Figure 128: Closer view over the VENLO greenhouses

Figure 129 shows a view of the greenhouse with dimensions indicated. The total size of the test area is 51 m x 86 m.

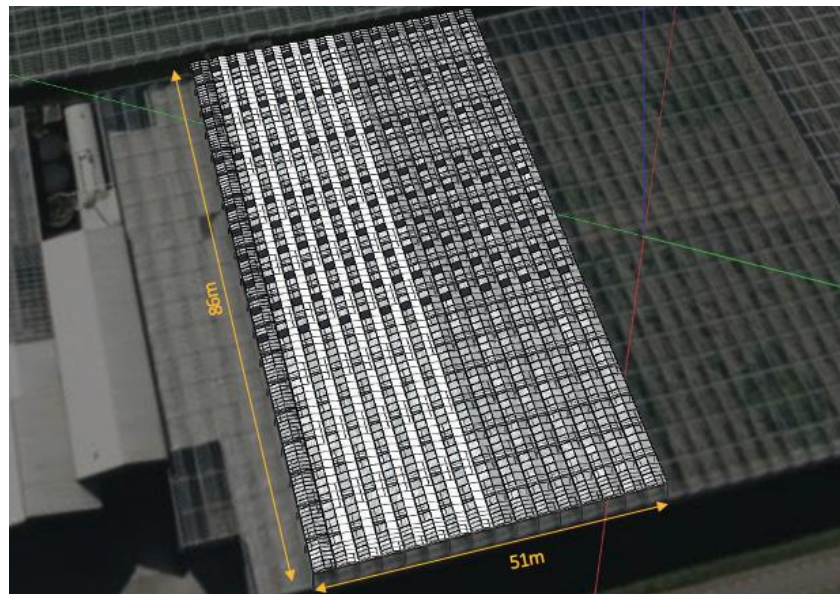


Figure 129: View of the greenhouse with dimensions indicated

The test area is distinctively divided in six zones, as seen in Figure 130, which shows the top view of the demo site with 6 distinct zones, where zones 1, 2, 3 and 4 will generate electricity. These four zones will feature south-west facing PV panels that are installed in a specific repetitive pattern covering the vegetation. More specifically zone 1 and 2 will feature 24 panels each, that are placed in intervals of 9 m, while zone 3 and 4 will showcase 48 panels each, placed in 4.5 m apart.

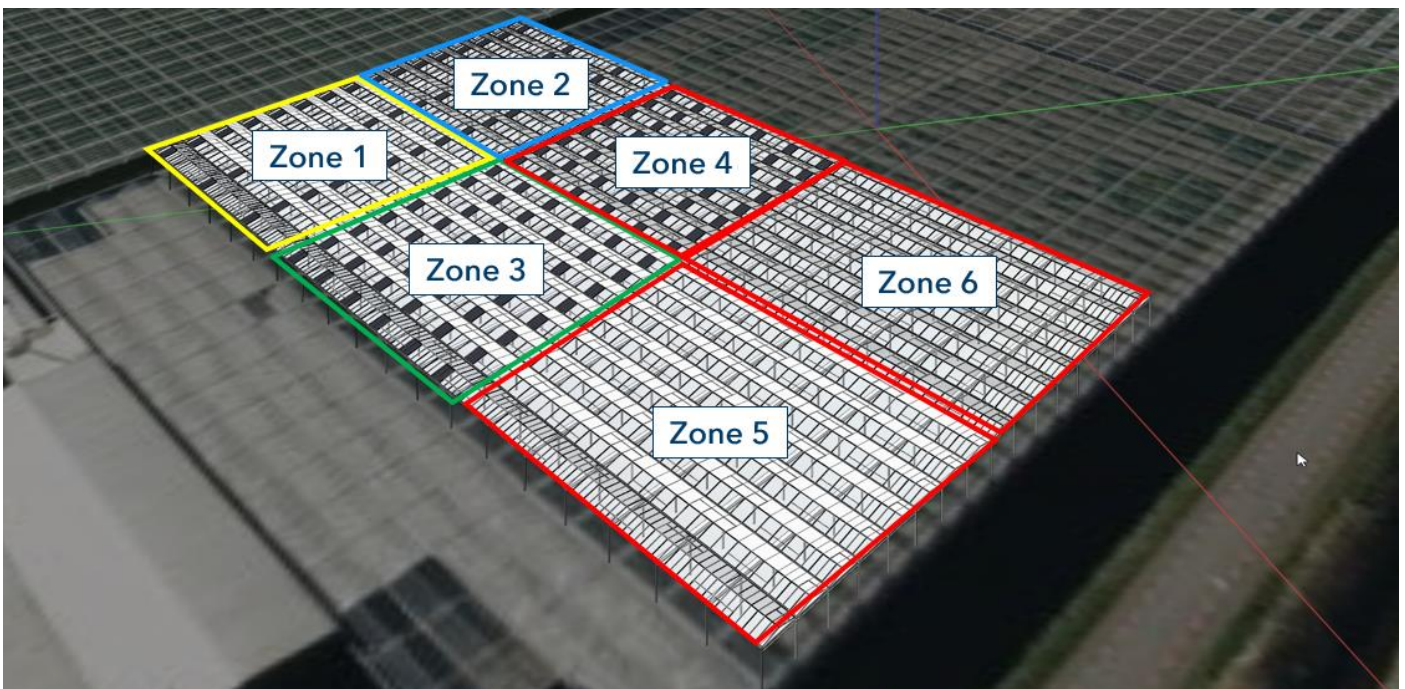


Figure 130: Top view of the demo site on the greenhouse with 6 distinct zones

To better visualise the zones, Figure 131 offers a closeup view for the four zones featuring PV panels.



Figure 131: Closeup view for the four zones featuring PV panels

Fully opaque, 365 W Aleo PV panels with dimensions 1,557 mm x 1,137 mm will be used for the Agrivoltaic prototype.

Figure 132 shows the dimensions and other related modules for the mentioned Aleo PV panel.

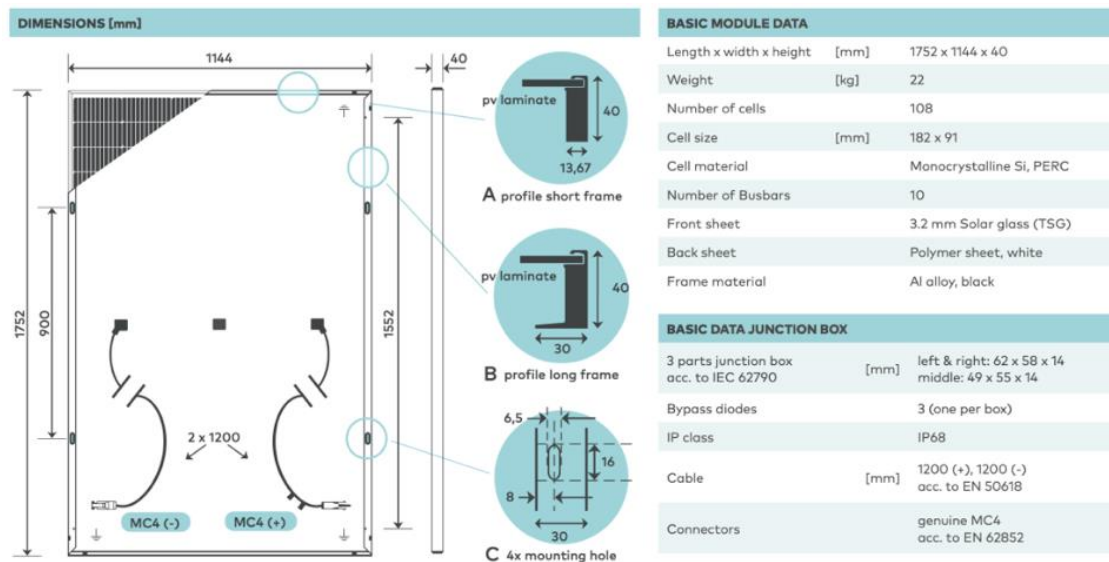


Figure 132: dimensions and other related modules for the mentioned Aleo PV panel

Furthermore, Figure 133 showcases the image of the PV panel to be installed (left) and the first PV panel being installed (right).



Figure 133: PV panel to be installed (left) and the first PV panel being installed (right)

Additionally, zone 1, 3 and 5 will have, Fotoniq diffusive PAR+ coating while the remaining zones 2, 4 and 6 will contain normal clear glass. FOTONIQ (Delft, the Netherlands) developed PAR+, a water-acrylic based, semi-permanent, retro-fit diffusive coating aimed to glass greenhouses. Figure 134 depicts the zones containing coating and clear glass, respectively. Its main attribute is to bring the benefits of light scattering while minimizing light loss to existing glass greenhouses. It is a more sustainable solution than existing seasonal coatings because of its higher durability, designed to be of 8 years.

Diffuse covering materials have proven to increase yield in many crops [12]. By scattering the light through translucent and diffusive coatings, both the vertical and horizontal light distributions is expected to be improved which results in a more homogenous light distribution over the leaves[13][14]. This promotes crop growth as it increases light use efficiency [15].

Another expected effect is the reduction of the complex shading effects introduced by the presence of multiple PV panels under direct light conditions. During light peaks an imbalance can occur between absorption and utilization of light energy. Diffuse materials decrease the amplitude and the rate of light intensity peaks on top leaves which, therefore, absorb less light. This results in less photoinhibition and lower leaf temperatures [16][13][15].

Within the context of this field test, a version of PAR+ coating will be sprayed on top of the greenhouse using conventional spraying processes known to the industry so the effects of a light diffusive material can be directly compared to clear glass under the Agri-PV context. Clearly a unique test in the field. In terms of coating application, the goal will be to spray an uniform looking film that gives to the greenhouse panels an average hemispherical transmittance of $(80 \pm 1)\%$ and a hortiscatter of $(35 \pm 5)\%$. For comparison, low iron clear glass and the common float glass have hemispherical transmittances respectively of 84% and $82 \pm 1\%$. Both with small hortiscatter values.

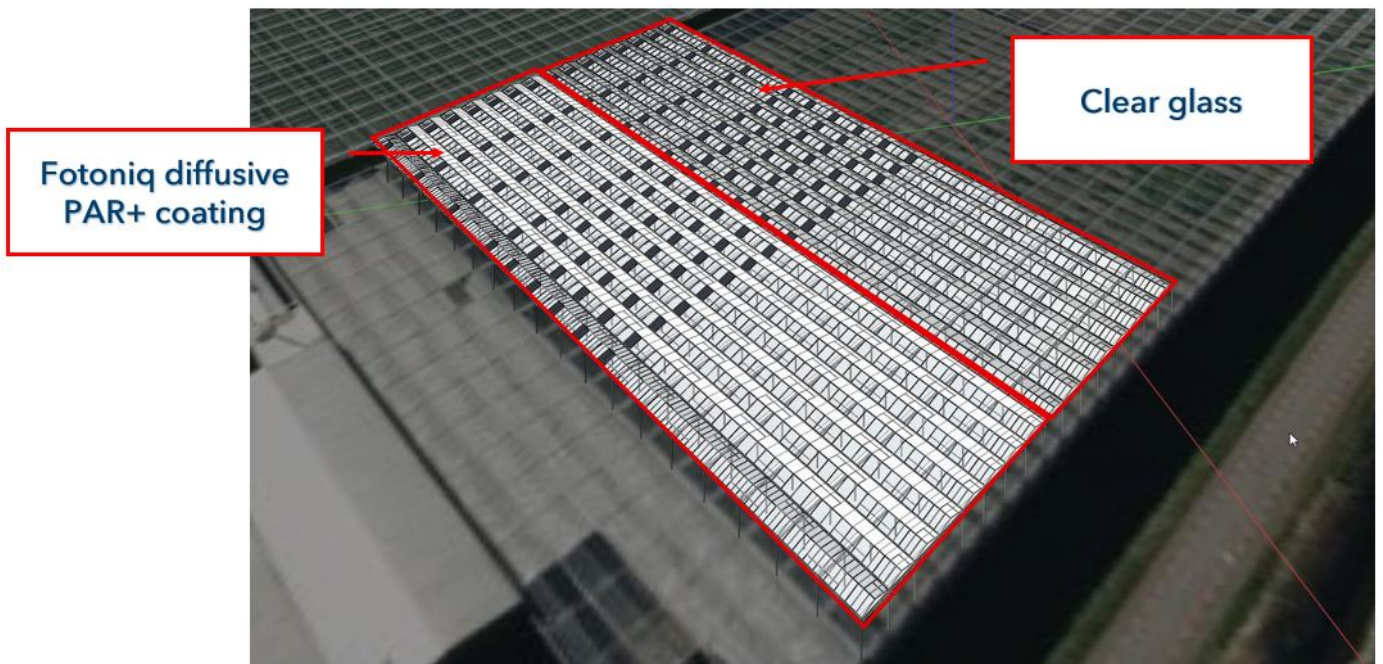


Figure 134: Layout of the zones containing coating and clear glass, respectively

Furthermore, Figure 135 depicts the detailed string arrangement and Table 13 shows the details of the envisaged wiring of the PV arrays to be installed on the greenhouse. Congruently, it is planned to have 1 inverter for every six strings containing 24 PV panels each. The specifications of the inverter are to be determined by Laborelec/Engie.

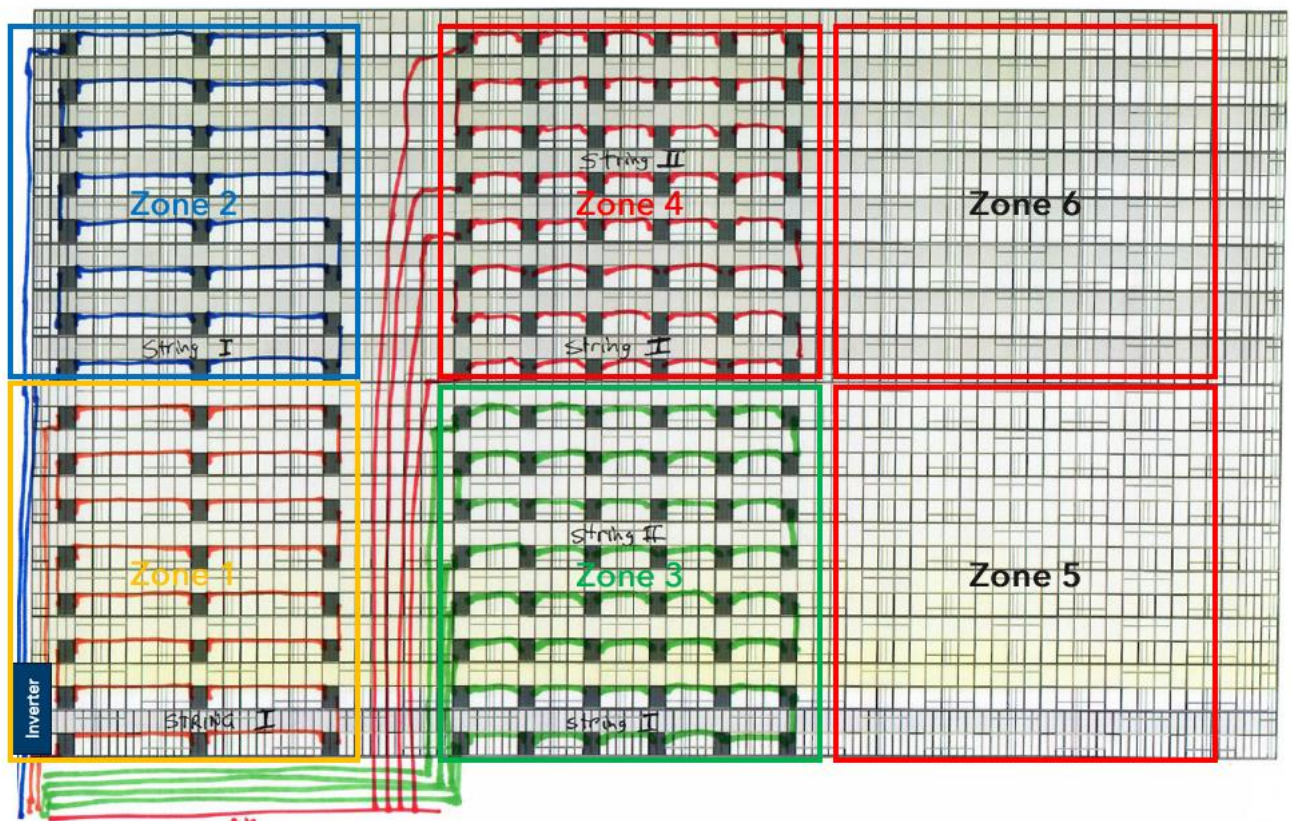


Figure 135: Detailed string arrangement for the PV arrays on the greenhouse

Table 13: Details of the envisaged wiring of the PV arrays to be installed on the greenhouse

Zone 1				Zone 2			
	Length (m)	Amount #	Totaal amount of meters		Length (m)	Amount #	Totaal amount of meters
String 1				String 2			
Post (paal)	5	2	10	Post (paal)	5	2	10
1st panel	3	1	3	1st panel	30	1	30
ridge (nok)	10	16	160	ridge (nok)	10	16	160
traverse (oversteek)	4	7	28	traverse (oversteek)	4	7	28
last panel	24	1	24	last panel	51	1	51
			225				279
Zone 3				Zone 4			
	Length (m)	Amount #	Totaal amount of meters		Length (m)	Amount #	Totaal amount of meters
String 3				String 5			
Post (paal)	5	2	10	Post (paal)	5	2	10
1st panel	30	1	30	1st panel	55	1	55
ridge (nok)	5.5	20	110	ridge (nok)	5.5	20	110
traverse (oversteek)	4	3	12	traverse (oversteek)	4	3	12
last panel	42	1	42	last panel	66	1	66
			204				253
String 4				String 6			
Post (paal)	5	2	10	Post (paal)	5	2	10
1st panel	42	1	42	1st panel	66	1	66
ridge (nok)	5.5	20	110	ridge (nok)	5.5	20	110
traverse (oversteek)	4	3	12	traverse (oversteek)	4	3	12
last panel	55	1	55	last panel	78	1	78
			229				276

For on-field Daily Light Integral (DLI) measurements, a total of 90 Quantified PAR light sensors will be employed. Figure 136 depicts a Quantified sensor attached to a tomato plant for illustration purposes. Each zone comprises 9 to 16 sensors positioned in a grid-like formation, as demonstrated in Figure 137.



Figure 136: Quantified sensor attached to a tomato plant

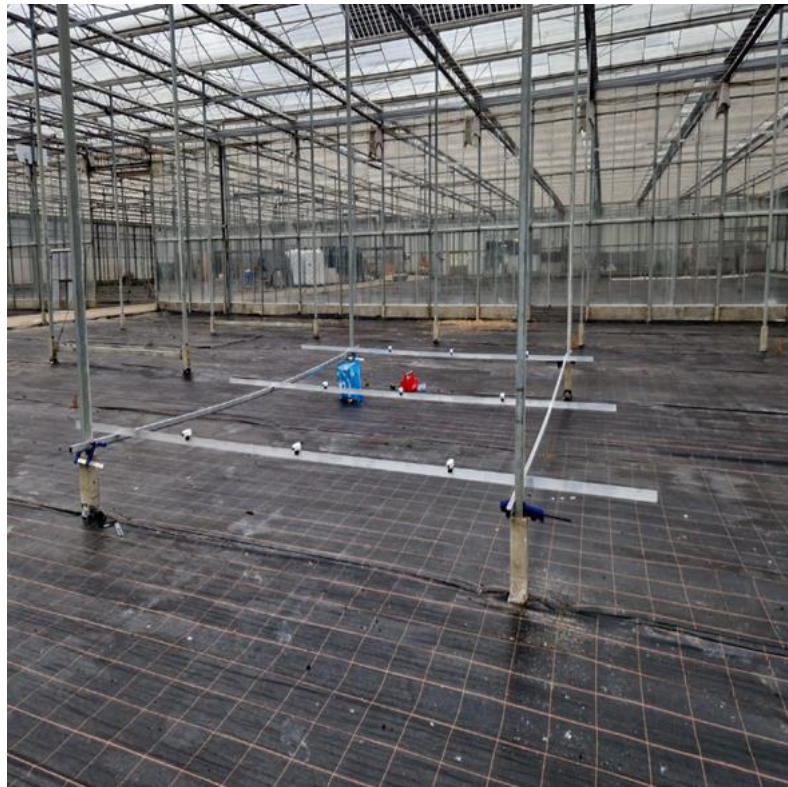


Figure 137: each zone containing 9 to 16 sensors placed in a grid-like formation

4.2. CONCLUSION AND DISCUSSION

There are several objectives identified with this demonstrator that are either ongoing or planned to be executed in the next phase of the deliverable's context.

3E will develop an user interface where the measured data of the light sensors and the electrical power generation of the PV panels can be visualized, and the object is to give access to all the partners to interact with the tool.

LuciSun and TUDelft will develop 3D calculation tool for light measurement, that will be validated with the actual measurements.

In the context of developing a tool for the light measurement, the eventual goal is for LuciSun and TUDelft to create a digital twin that corresponds with the actual measured data in the greenhouse.

5. AGRIVOLTAIC DEMONSTRATOR 4 - SCALEA

5.1. TECHNICAL SPECIFICATIONS

Table 14 describes the envisioned features of the demo of Scalea and the updates in terms of Technical Specifications at M12 of the project.

Table 14: Envisioned features of the demo in the Scalea and the updates in terms of Technical Specifications at M12 of the project

Use case 2	SCALEA
Unique Value Proposition	Innovative citrus orchard solution that can integrate irrigation, frost and snow protection, hail protection systems; together also with agronomic sensors and insect detection systems.
Location	<p>SCALEA (Cosenza) Italy.</p> <p>The coordinates where the prototype is located are as follows (nearby the existing greenhouses owned by EF Solare Italia):</p> <ul style="list-style-type: none"> 39°46'22.95"N; 15°48'23.02"E; 
Replication potential	The replicability of the solution is high, thanks to the planned renewal of plantations in south Italy, together with new plantations in the Mediterranean area.
Crop	The Scalea Demo is focused on citrus fruit trees (mainly citruses, in particular the type White Zagaria and 2KR Citrus Limon, famous for its properties such as its pleasant parfum, medium shape, and generally +30% of juiciness with respect to other varieties) in a "Classic" 3D configuration, with

	<p>trees height \leq than 2.5 m (at maximum grow), in four rows with mutual distance of 5.0m. This choice is particularly useful for the proposal, as it is complementary to the demonstrator planned in the Bolzano area (apple tree).</p>
<p>Solutions implemented in the demo</p>	 <p>The Scalea Demo involves approximately 42 m trackers designed and manufactured by CONVERT. The useful height of the trackers is 3.20 m (at rotating axis), ensuring the free movement of agricultural machinery. All four rows of the orchard (10.40m each) are covered by trackers: one tracker line N-S for each row of trees (with interspace W-E of 5.0m). Weathering steel is used to manufacture the trackers, as a low environmental and visual impact in an agri-PV field. To meet both agricultural and electricity production optimisation needs, a specific tilting and weather emergency programme will be developed and implemented within the SCADA system, aimed at the Scalea Demo. This system can be networked with the monitoring systems (digital platform) developed within the project.</p>
<p>Water catchment / irrigation</p>	<p>Precision irrigation systems are provided to increase water saving. The type tested is a drip sub-irrigation system.</p>
<p>Health & Safety</p>	<p>To overcome the lack of specific safety standards for agri-PV plants, the current electrical and fire safety standards developed for utility scale PV plants will be applied.</p>
<p>System integration</p>	<p>Approximately 70% of the crops area is covered by photovoltaic panels; to ensure complete protection of the remaining 30%, the Demo of Scalea will also be integrated by hail protection systems as nets.</p>
<p>Use of electricity</p>	<p>The complete use of the electrical PV energy produced within the Scalea Demo plant is foreseen, ensuring the power supply of the cultivation electric equipment as new tractors, pumps, compressors, etc.</p>

The Demo plant in Scalea in his first release has been realized in November 2021, for this reason it plays also a role of Demo Drivers for the SYMBIOSYST project. It has been designed with single-axis solar tracking technology in order to modulate irradiation and reduce fixed-shadowing. PV Modules are elevated up to 3.20 meters from the ground and installed in rows at a distance of 5 m, to allow the operations of agricultural machinery. Figure 138 illustrates the Demo Plant in Scalea from a lateral E-W view.

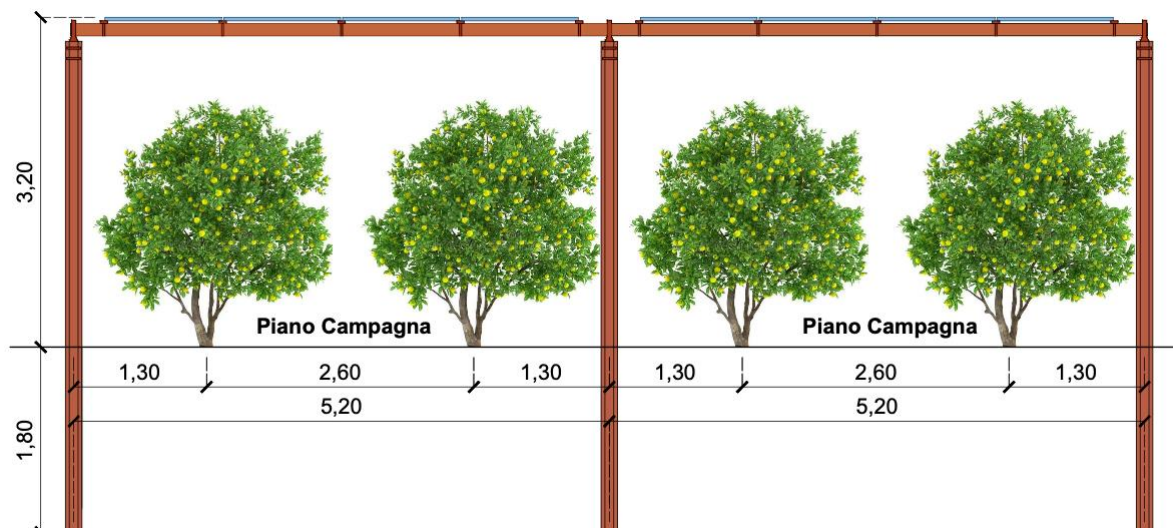


Figure 138: Demo Plant in Scalea – lateral E-W view

Figure 139 illustrates the Demo Plant in Scalea, through a top view, with the position of sensors. The weathering steel mounting structures are ground-fixed without the use of concrete. The irrigation is controlled in order to improve water consumption thanks to non-fixed shadowing and a digital watering control system, together with aerial irrigation systems. The monitoring system allows to measure temperature, humidity, crop growth, and PAR. On the Eastern side of the Agri-PV plant, a Control area is in place, with two rows of orchard in open field and PAR sensor, for comparing the results versus in-PV-plant one.

Characteristics

- PV modules: n.40 x JA Solar P6-60 Poly 240 W 1650 x 991 x 40 mm ($P_{tot} = 9.6$ kW) – to be revamped.
- Structure: single-axis tracker 1P, Height: 3.2 m, Span 5.2 m, Pitch: 5 m.
- Agri sensors: Ground Temperature (1), Humidity at -20 cm and -40 cm (2), PAR1 (3) and PAR2 (4) (Photosynthetically Active Radiation) respectively in Agri-PV plant and in Open field plant (i.e. the Control plant, at Est side of Agri-PV plant), Dendrometer (5).

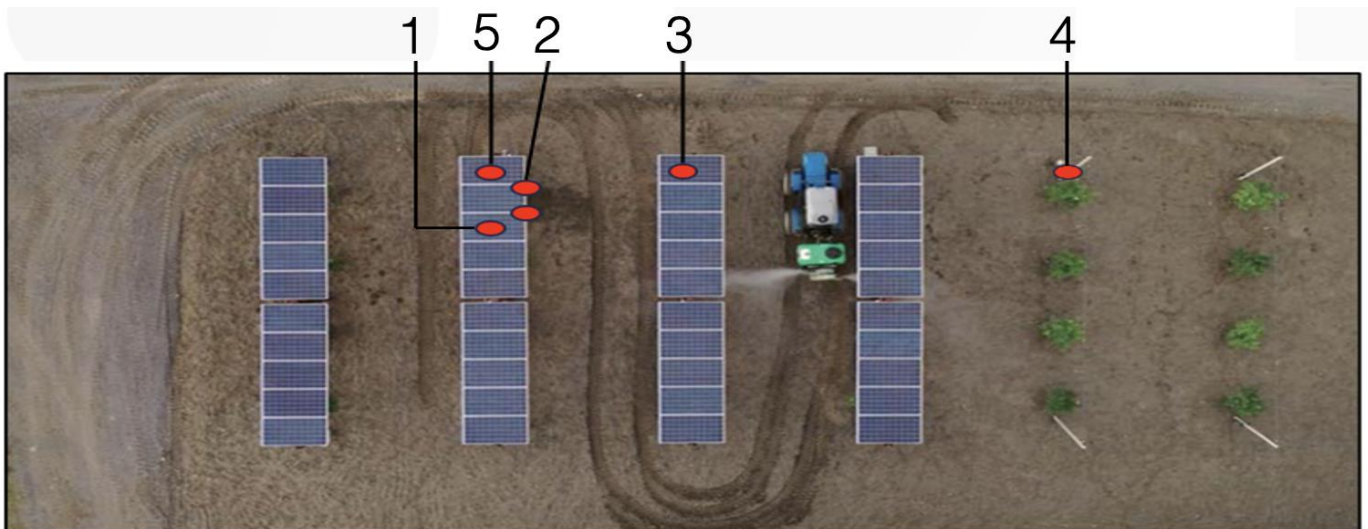


Figure 139: Demo Plant in Scalea – Top view, with the position of sensors

By Q6 2024 is planned a revamping of PV modules with more efficient ones – to be identified soon, also to allow the simulations.

Meanwhile, initial ground experiments yield the following observations:

- The plants were planted in November 2021. As such, data on agricultural yields are not yet available, given that a three-year growth period is necessary before the first harvest can be assessed.
- Comparative growth between crops situated under the Agrivoltaic (Agri-PV) system and those in open fields shows no significant difference, with an average height of 1.5 meters for both sets.

Figure 140 shows a photograph from the Demo Plant in Scalea, showing the lemon orchard within the Agri-PV system.



Figure 140: Demo Plant in Scalea – lemon orchard within the Agri-PV demo plant

The project has already accumulated over one year of data (from July 1, 2022, to June 30, 2023) using agricultural sensors installed to monitor:

- Ground Temperature (Figure 141);
- Humidity at depths of -20 cm and -40 cm (Figure 142);
- Photosynthetically Active Radiation (PAR) within the agrivoltaic (agri-PV) system and in open fields (Figure 143 and Figure 144).

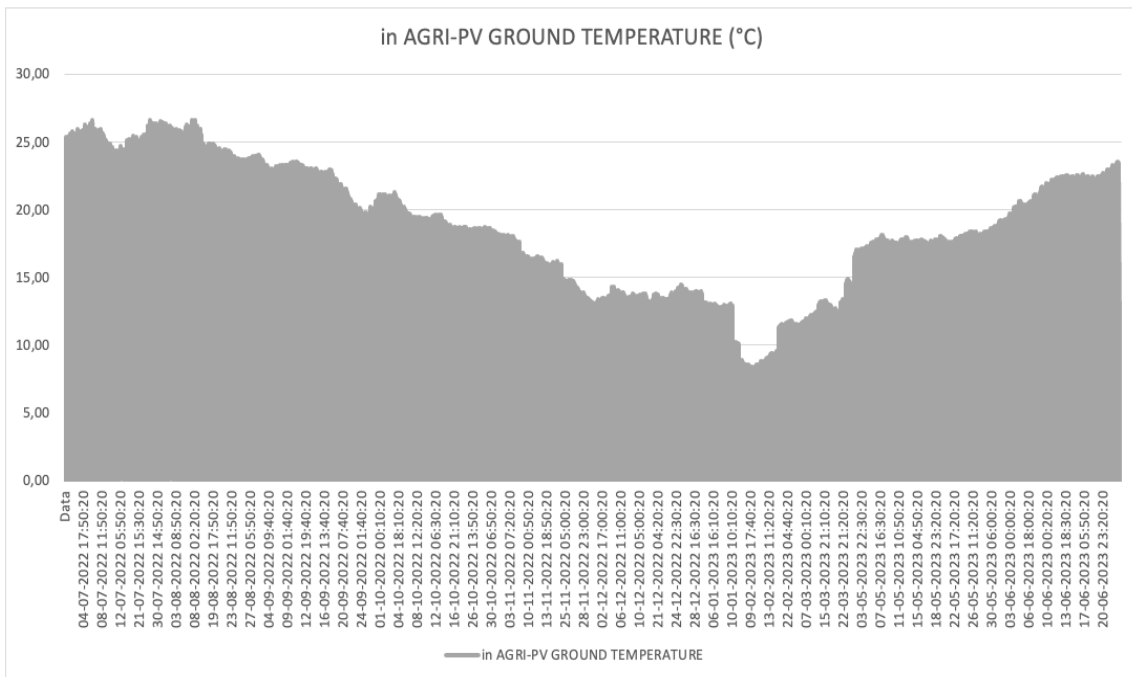


Figure 141: Ground temperature measured in the agri-PV system during one year

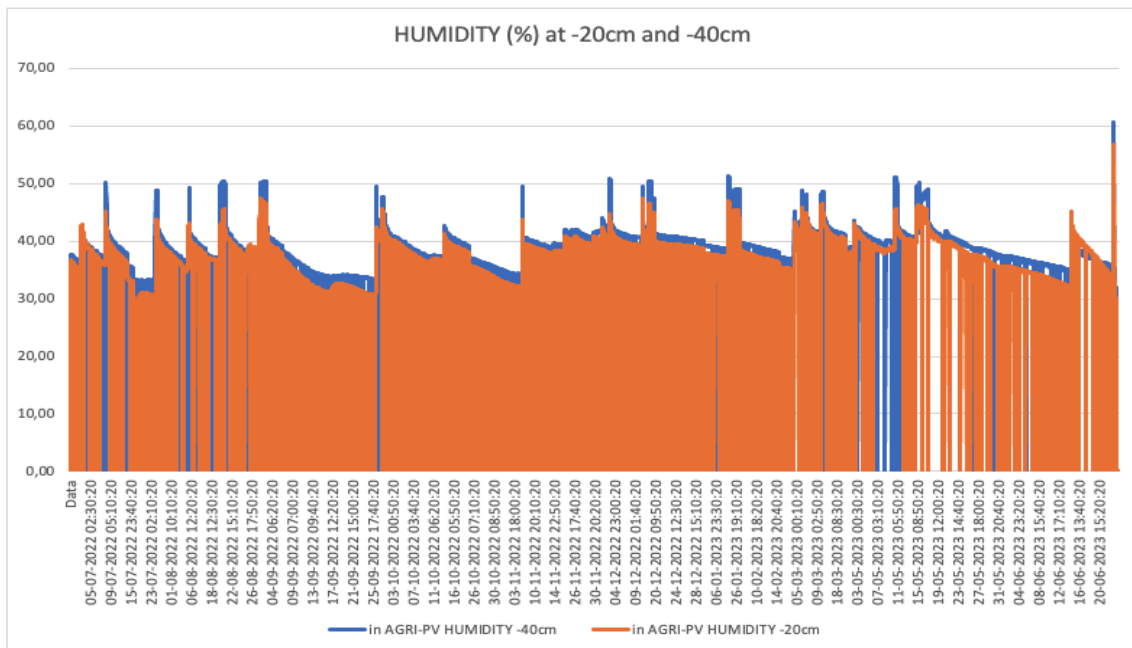


Figure 142: Air humidity measured in the agri-PV system during one year

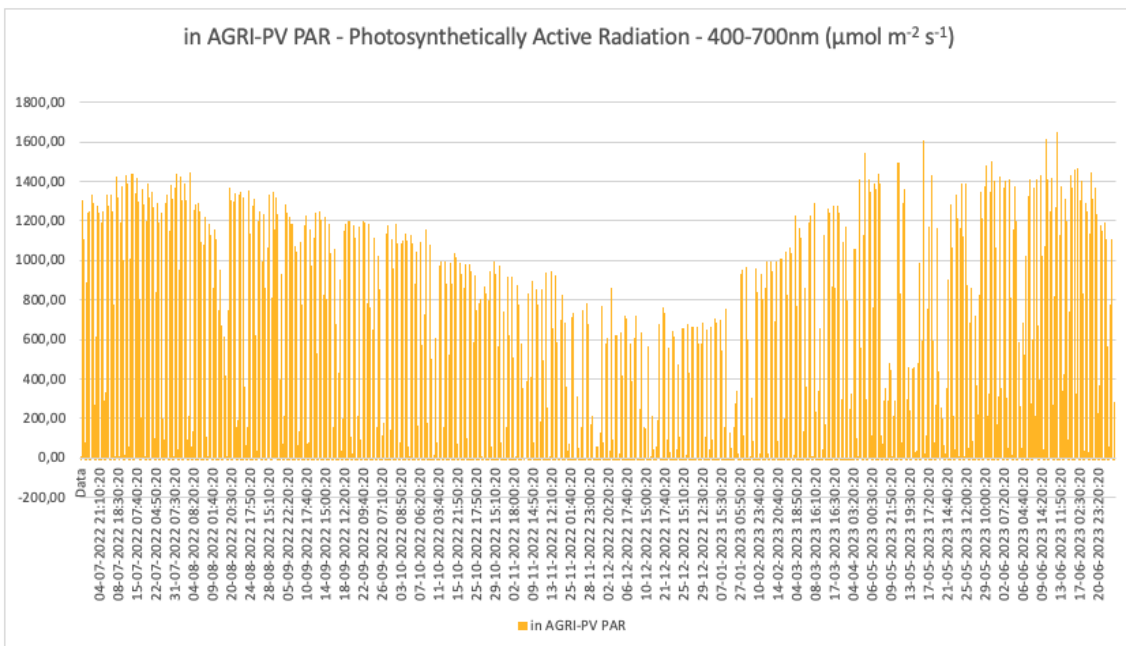


Figure 143: Photosynthetically Active Radiation (PAR) measured in the agri-PV system during one year

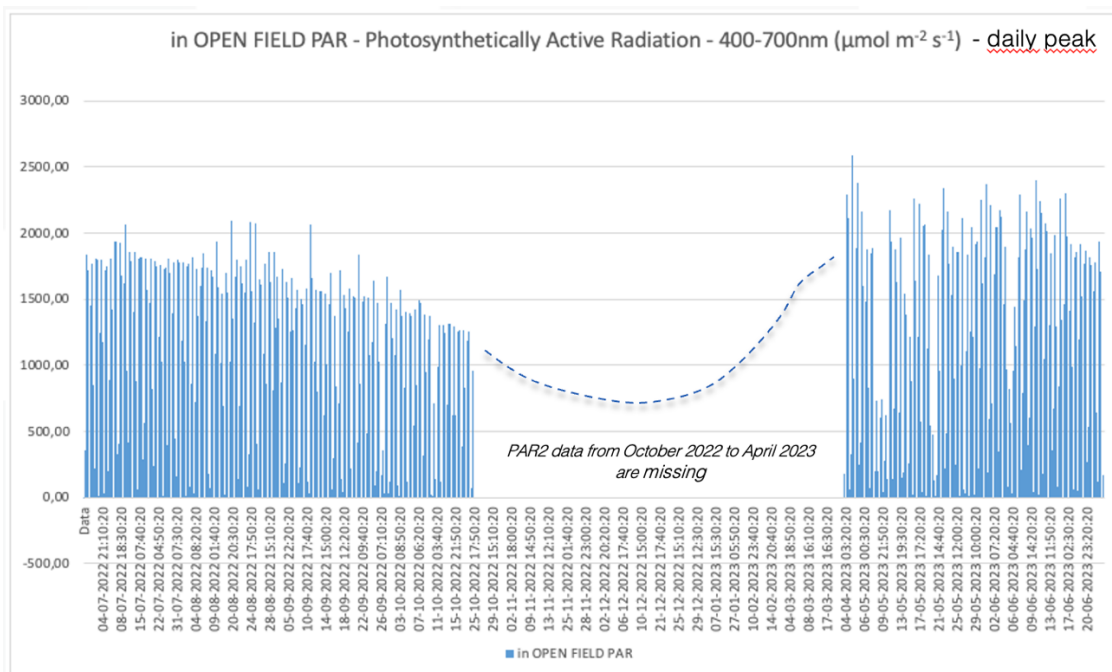


Figure 144: Ground temperature measured in the agri-PV system during one year – Daily-integrated values

To further illustrate the results of the measurements, two days of data monitoring are shown as examples of the trends observed in the open field for one day of summer (Figure 145) and winter (Figure 146).

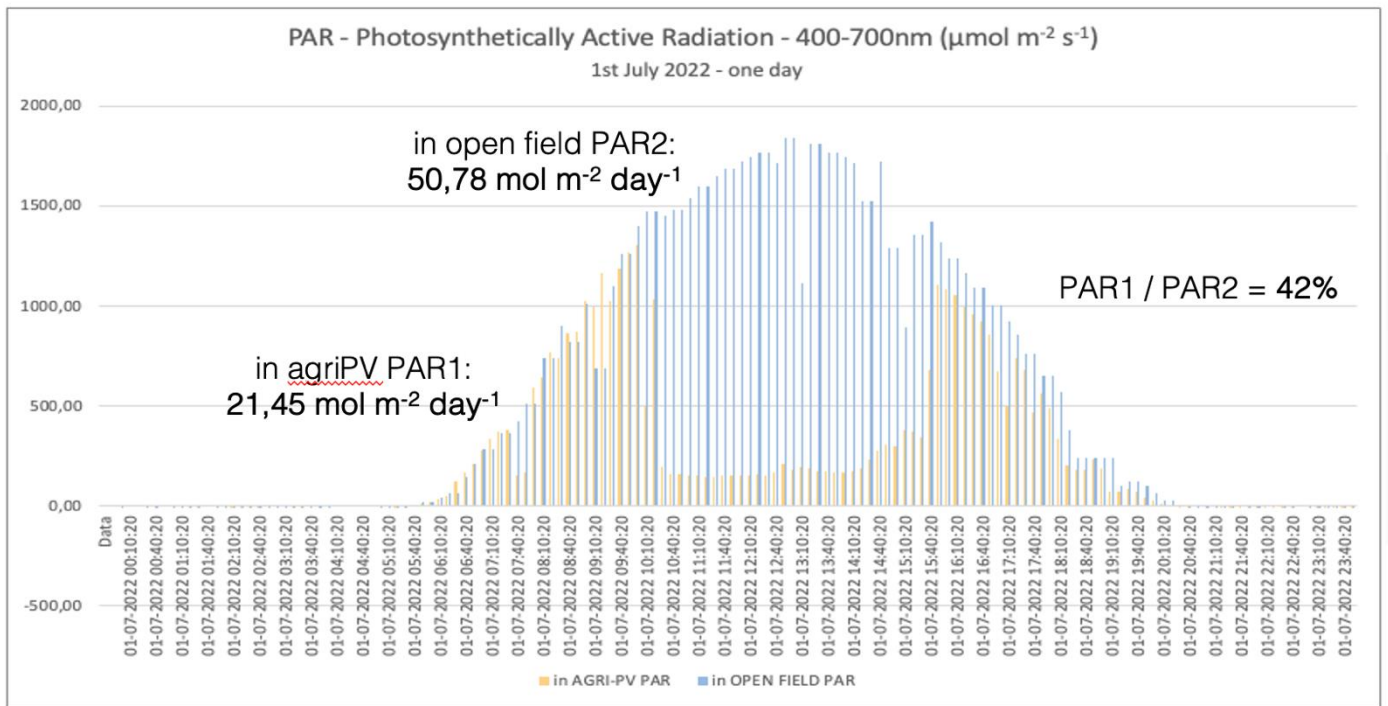


Figure 145: Results of the measurements illustrated on the data monitored for one day of summer – 1 July 2022

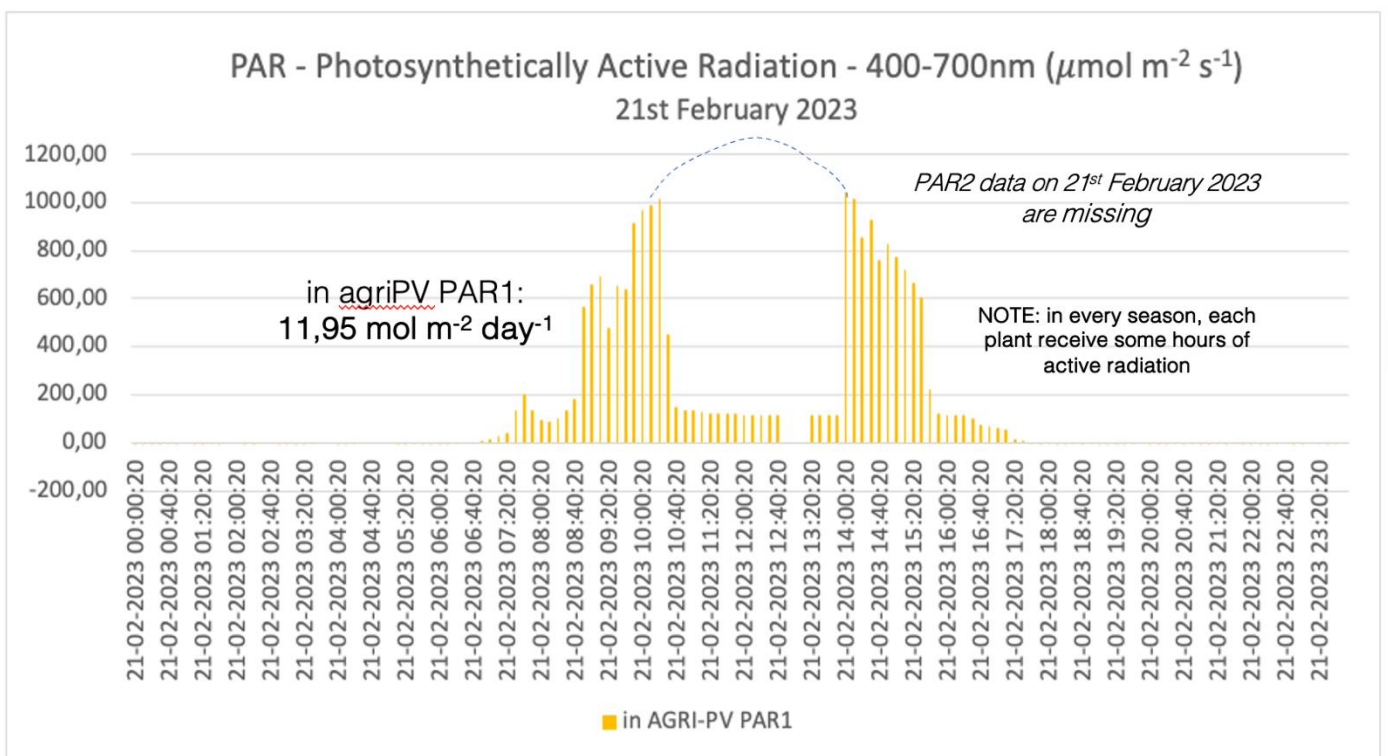


Figure 146: Results of the measurements illustrated on the data monitored for one day of winter – 21 February 2023

5.2. CONCLUSION AND DISCUSSION

Preliminary results reveal key insights into the climatic conditions and their impact on crop health within the agrivoltaic (agri-PV) system:

- The average humidity throughout the year and across the day approximately stands at 35%, which is below the critical threshold of 40%.
- Ground temperature ranges between 10°C and 25°C annually, optimal for lemon cultivation, and remains relatively stable over the course of the day.
- Despite receiving about 58% less photosynthetically active irradiance (measured in $\text{mol m}^{-2} \text{day}^{-1}$) and experiencing a 26% reduction in peak radiation ($\text{max } \mu\text{mol m}^{-2} \text{s}^{-1}$) compared to open-field plants, visual inspections of the agri-PV system plants indicate they exhibit fewer stress symptoms. Notably, there is an absence of pigmentation in the leaves and an increased presence of upward-growing small branches. This suggests that the reduction in radiation and precipitation peaks, attributed to the protective overhead PV modules, may offer a beneficial microclimate.

Comprehensive results and analyses are anticipated in the third and fourth years of the project, aligning with the planned research timeline.

6. REFERENCES

- [1] Dorigoni A., Micheli F., Guyot training: a new system for producing apples and pears, *Eur. Fruit Mag*, 2018.
- [2] Huld, T., Šúri, M. and Dunlop, E.D. (2008), Comparison of potential solar electricity output from fixed-inclined and two-axis tracking photovoltaic modules in Europe. *Prog. Photovolt: Res. Appl.*, 16: 47-59. <https://doi.org/10.1002/pip.773>
- [3] Huld, T., Cebecauer, T., Šúri, M. and Dunlop, E.D. (2010), Analysis of one-axis tracking strategies for PV systems in Europe. *Prog. Photovolt: Res. Appl.*, 18: 183-194. <https://doi.org/10.1002/pip.948>
- [4] Robledo J. et al., From video games to solar energy: 3D shading simulation for PV using GPU, *Solar Energy*, 2019, <https://doi.org/10.1016/j.solener.2019.09.041>.
- [5] Robledo J. et al., Dynamic and visual simulation of bifacial energy gain for photovoltaic plants, *European Photovoltaic Solar Energy Conference and Exhibition (EU PVSEC)*, 2021.
- [6] Robledo J. et al., Lessons learned from simulating the energy yield of an agrivoltaic project with vertical bifacial photovoltaic modules in France, *European Photovoltaic Solar Energy Conference and Exhibition (EU PVSEC)*, 2021.
- [7] Robledo J. et al., Key parameters for the simulation of agrivoltaics in greenhouses with bifacial PV modules, *WCPEC-8*, 2022.
- [8] El Boujdaini I. et al., 3D modelling of light-sharing agrivoltaic systems for orchards, vineyards and berries, *European Photovoltaic Solar Energy Conference and Exhibition (EU PVSEC)*, 2023.
- [9] Holmgren W.F., Hansen C.W., Mikofski M.A., “pvlib python: a python package for modeling solar energy systems.” *Journal of Open Source Software*, 3(29), 884, (2018). <https://doi.org/10.21105/joss.00884>
- [10] Ward, G. J. (1994). The RADIANCE lighting simulation and rendering system. In *21st Annual Conference on Computer Graphics and Interactive Techniques*, (pp. 459–472). doi:10.1145/192161.192286.
- [11] Pelaez, A., & Deline C. (2020). *bifacial_radiance*: a python package for modeling bifacial solar photovoltaic systems. *Journal of Open Source Software*, 5(50), 1865, <https://doi.org/10.21105/joss.01865>
- [12] Hemming, S., Dueck, T., Janse, J., & van Noort, F. (2007). The Effect Of Diffuse Light On Crops.
- [13] Li, T., Heuvelink, E., Dueck, T., Janse, J., Gort, G., & Marcelis, L. (2014). Enhancement of crop photosynthesis by diffuse light: quantifying the contributing factors. *Annals of Botany*, 114(1), 145-156.
- [14] Li, T., & Yang, Q. (2015). Advantages of diffuse light for horticultural production and perspectives for further research. *Frontiers in Plant Science*, 6, 704.
- [15] Kaiser, E., Morales, A., & Harbinson, J. (2018). Fluctuating light takes crop photosynthesis on a rollercoaster ride. *Plant Physiology*, 176(2), 977-989.
- [16] Urban, O., Klem, K., Ač, A., Havránková, K., Holišová, P., Navrátil, M., Zitová, M., Kozlová, K., Pokorný, R., & Šprtová, M. (2012). Impact of clear and cloudy sky conditions on the vertical distribution of photosynthetic CO₂ uptake within a spruce canopy. *Functional Ecology*, 26(1), 46-55.